REPUBLIC OF CAMEROON
Peace – Work - Fatherland

THE UNIVERSITY OF YAOUNDE I

FACULTY OF SCIENCE

POST GRADUATE SCHOOL FOR SCIENCES, TECHNOLOGY AND GEOSCIENCES

DOCTORATE RESEARCH AND TRAINING UNIT FOR GEOSCIENCES AND APPLICATIONS

REPUBLIQUE DU CAMEROUN
Paix – Travail - Patrie

UNIVERSITÉ DE YAOUNDÉ I

FACULTE DES SCIENCES

CENTRE DE RECHERCHE ET DE FORMATION DOCTORALE EN SCIENCES, TECHNOLOGIES ET GEOSCIENCES

UNITE DE RECHERCHE ET DE FORMATION DOCTOALE EN GEOSCIENCES ET APPLICATIONS

DEPARTMENT OF EARTH SCIENCES
DEPARTEMENT DES SCIENCES DE LA TERRE

Laboratory of Geosciences of Superficial Formations and Applications
Laboratoire de Géosciences des Formations Superficielles et Applications

Geological study of sapphire occurrences in Mayo Kila and Mbiame areas (North-West Region, Cameroon)

Thesis Presented in Partial Fulfilment of the Requirements for the Degree of Ph.D. in Earth Sciences

Specialty: Geoscience of Superficial Formations

Option: Mining Geology

By
MBIH Paul KEMENG
Matricule: 04X344
M.Sc. in Earth Sciences

Under the Supervision of

YONGUE FOUATEU Rose
Professor
University of Yaoundé I

Academic year 2020/2021

UNIVERSITE DE YAOUNDE I

FACULTE DES SCIENCES

DEPARTEMENT DES SCIENCES DE LA TERRE

THE UNIVERSITY OF YAOUNDE I

FACULTY OF SCIENCES

DEPARTMENTOF EARTH SCIENCES

UNITE DE RECHERCHE ET DE FORMATION DOCTORALE

« GEOSCIENCES ET APPLICATIONS »

ATTESTATION DE CORRECTION DE THESE DE DOCTORAT/Ph. D

****

Spécialité **: Géologie Minière**

Option **: Géosciences des Formations Superficielles**

Nom et Prénom du candidat : **MBIH Paul KEMENG**
Matricule: **04X344**

Titre de la thèse: Geological study of sapphire occurrences in Mayo Kila and Mbiame areas (Northwest Region, Cameroon).

Date de soutenance : vendredi, le 26 juillet 2021.

Nous, membres du jury, après avoir lu le document qui nous a été présenté, attestons que le candidat a effectué toutes les corrections, conformément aux observations formulées lors de la soutenance.

En foi de quoi, la présente **Attestation de correction** lui est délivrée, pour servir et valoir ce que de droit.

Président du jury **Examinateur**

DEDICATION

To my parents,

Nawain Ita Luoh and Bobe Amos Mbih.

ACKNOWLEDGEMENTS

This work has been realized through combined efforts made by different people at various levels. I wish to express my profuse gratitude to:

My supervisor Pr. YONGUE FOUATEU Rose for her availability and devotion to the successful realization of this work. Her valuable criticisms and suggestions have immensely added value to this work.

Dr. MEFFRE Sebastien, of the University of Tasmania for funding the geochemical analyses of corundum and zircon inclusions at the ARC Centre of Excellence in Ore Deposits, University of Tasmania, Australia.

The Rector of the University of Yaounde I, Pr. SOSSO Maurice Aurélien and the Dean of the Faculty of Science, Pr. Jean Claude TCHOUANKEU for accepting me to be one of their students.

The Head of Department, Pr. NDJIGUI Paul Désiré and the general staff of the Department of Earth Sciences, in particular, Pr. NZENTI Jean Paul, Pr. BITOM Lucien Dieudonné, Pr. NKOUMBOU Charles, Pr. KAMGANG Pierre, Pr. NJILAH Isaac KONFOR, Pr. NDAM NGOUPAYOU Jules-Remy, Pr. ONANA Vincent, Pr. EKOMANE Emile, Pr. GANNO Sylvestre and Dr. Elisé SABABA, for imparting a great deal of knowledge to me that has greatly upgraded my educational standard.

My wife CHIA Leah FUNKUIN, for her encouragement, moral supports and ceaseless prayers.

Dr. KANOUO Sylvestre, for devoting his valuable time to read and correct this work. He greatly contributed to the actual quality of the work.

My seniors and friends in the Department of Earth Sciences, particularly Dr. TESSONTSAP TEUTSONG, Dr. BANAKENG Lucien, Dr. ANABA Achille and Dr. MBANGA Nyobe Jules.

The entire staff of the Department of Geology/MINMIDT, particularly the Director of Geology, Mrs. AGBOR Kareen OJONG, for creating a conduisive working atmosphere that has permitted me to complete this thesis while working.

The experience laboratory technicians of MIPROMALO like: Mr. SUILABAYU.L. Simplicius, Mr. KEMMEGNI Dieudonné, and Mr. MEDZI N. Michel, for their assistance in particle size distribution analysis.

My family for their moral support, in particular, Pr. MBIH Jerome, Dr. MBIH Richard, Mr. YONG Francis, Mr. MBIH Henry, Miss MBIH Gladys, and the entire ATAM's family.

My friends and classmates for their constructive criticisms and moral support, I think particularly NCHIMENYI NDASHI, LAYU Donatus, Mohamad Moctar, TATA Isa, NDIMUKONG Franklin, KUNYUKUBUNDO Frankline, AMOUGOU Leonel, TSOALA Carlos, MALLA Henriette and TSOUNGUI Carine.

I am also thankful to Mr. Sale and Mr. TATA Wirba of Dumbo and Mbiame villages respectively, my field guides who devotedly assisted me during the field phases of this work.

ABSTRACT

Mayo Kila and Mbiame as well as other parts of Mount Oku are known to host alluvial sapphire occurrences. These deposits have been characterized in order to trace the source rock(s) of their host materials within geological formations in the local and regional settings. Alluvial and geological prospections were carried out in the areas, followed by laboratory analyses such as particle size distribution for alluvial materials, LA-ICP-MS for sapphire grains, and ICP-AES and ICP-MS for surrounding rocks.

Alluvial prospection showed that, the Bewende and Mbven Rivers in Mayo Kila and Mbiame respectively are the main alluvial sapphire concentration areas. These sapphires occur in association with other minerals such as zircon, apatite, tourmaline, hornblende and magnetite. Particle size distribution analysis show that the detrital materials are made up of fine to coarse sand and cobble, pebble gravel sizes. The sediments are poorly to very poorly sorted, indicative of a close source. Sapphires from these placers are mostly blue, with sizes that range from 2 to 5 mm. They are dominantly euhedral to sub-hedral with angular to sub rounded grains. Those from Mbiame are euhedral with few sub-rounded to rounded polished lustrous grains, features acquired during moderate to short distance transport from a proximal source. Primary relicts of some crystals are displayed by platy and barrel shaped grains. Their surfaces show irregular corrosion patterns, indicative of disequilibrium with their carrier magma.

Geochemical analyses of the sapphires by LA-ICP-MS show trace element concentrations such as Fe (2,208 - 14,473 ppm), Ti (82 - 1,783 ppm), Ga (77- 512 ppm), Mg (upto 264.9 ppm), Cr (upto 168 ppm) and V (upto 82 ppm). Calculated ratios show extreme variations, with Fe/Mg (43 - 3,043), Fe/Ti (2 - 76), Ti/Mg (1 - 328), and Ga/Mg (0.4 - 363) values that express affinity to magmatic corundum. Solid inclusions in these sapphires are limited to rutile and zircon. Their zircon inclusions are characterized by hafnium (13,354 – 26,238 ppm), thurium (4,018 – 45,584 ppm), uranium (7,825 – 17,175 ppm) and Th/U ratios between 0.39 and 2.65. These values are similar to those of zircons crystallized in a crustal environment, in highly evolved melts close to syenitic or granitic compositions. Cenozoic age (mean of 30.78 ± 0.28 Ma) obtained from these zircon inclusions is within the range of ages obtained from Mount Oku volcanic rocks.

Both areas are characterized by plutonic and volcanic rocks. The plutonic rocks in Mayo Kila are two mica granites, biotite granites, diorites and monzonite. Their composition is typical of High-K calc-alkaline to shoshonitic and an alkali-calc to calc-alkalic series. Most of the samples are metaluminous with affinity to I-type granites while only one biotite granites sample is peraluminous with affinity to S-type granite. They are formed by partial melting from different protoliths at crustal level. These protoliths are metapelites, metagreywacks and metatonalites to metaamphibolites. These rocks were formed in a syn- to post-collisional tectonic setting. The mafic volcanic rocks in both areas express an alkaline affinity with magmas that portray a residual mantle source, formed from the partial melting of garnet peridotite, and are similar to alkaline basalts from an intracontinental rift.

The above data show that the sapphires of the study area are magmatic, with parent rock close to syenitic or monzonitic compositions, probably the Ntumbaw syenites, formed at crustal level. They were transported to the surface by mantle formed alkaline basaltic magma through the numerous fractures that characterize the Cameroon Line and the Central Cameroon Shear Zone.

Key words: NW Cameroon, Sapphire, Geochemistry, geochronology, Geotectonic context.

RESUME

Dans la Région du Nord-Ouest Cameroun, les localités de Mayo Kila et Mbiame ainsi que d'autres parties du Mount Oku regorgent des indices importants de saphir. Le présent travail avait pour objectif principal de caractériser les indices de saphirs et ses dépôts alluviaux avec pour but de définir leur provenance au sein du contexte géologique local et régional. Afin d'atteindre cet objectif, des prospections alluvionnaires et géologiques ont été effectuées dans ces zones, suivies des analyses en laboratoire tels que la granulométrie pour les matériaux alluvionnaires, la LA-ICP-MS pour les grains de saphirs, et ICP-AES et ICP-MS pour les roches encaissantes.

Les principaux résultats obtenus révèlent que les rivières Bewende dans le Mayo Kila et Mbven à Mbiame sont les principales zones de concentration du saphir. L'analyse morphologique montre un matériau détritique constitué en majorité de sables et graviers, de formes variables. La granulométrie révèle que ces alluvions sont mal à très mal classées. L'association des minéraux lourds est constituée de zircon, apatite, tourmaline, hornblende et magnétite. Les saphirs provenant de ces placers sont de couleur bleue et de taille variant entre 2 et 5 mm. Ils sont majoritairement automorphes à sub-automorphes avec des grains anguleux à sub-arrondis. Ceux de Mbiame sont automorphe avec quelques grains arrondis, polis et brillants, caractéristiques d'un transport assez court et d'une source proximale. Les reliques primaires de certains grains sont représentées pas des grains aplatis et barillet. Leurs surfaces présentent des corrosions irrégulières, indiquant ainsi le déséquilibre avec le magma vecteur.

Les analyses géochimiques présentent des teneurs en éléments trace tels que le fer (2208-14473 ppm), le titaniun (82-1783 ppm), le galium (77-512 ppm), le magnésium (jusqu'à 264.9 ppm), le chrome (jusqu'à 168 ppm) et le vanadium (jusqu'à 82 ppm). Les rapports Fe/Mg (43-3043), Fe/Ti (2-76), Ti/Mg (1-328) et, Ga/Mg (0.4-363), dont les valeurs montrent une affinité avec les corindons magmatiques. Les inclusions solides de zircon sont caractérisées par des teneurs élevées en Hf (13354 - 26238 ppm), Th (4018 - 45584 ppm), U (7825-17175 ppm), et d'un rapport Th/U compris entre 0.39 et 2.65, traduisant une cristallisation dans un environnement crustal. Ces teneurs élevées montrent une corrélation significative avec les zircons cristallisés dans les magmas bien évoluées, proche des compositions syénitique et granitique. L'âge cénozoïque (en moyenne de 30.78 ± 0.28 Ma) obtenu de ces inclusions de zircon se rapproche de l'âge des roches volcaniques du Mont Oku (Ligne Volcanique du Cameroun).

Les deux zones d'etude présentent des roches plutoniques et volcaniques. Ces deux types de roches ont été échantillonnés à Mayo Kila, tandis que seules les roches volcaniques ont été échantillonnées à Mbiame. Les roches plutoniques du Mayo Kila sont des granites à deux micas, des granites à biotite, des diorites et des monzonites. Leur composition est typiquement calco-alcaline hyperpotassique à shoshonitique. Ils sont principalement métalumineuses avec des affinités des granites de type I. Seule un echantillon de granites à biotite est peralumineux, présentant une affinité avec les granitoïdes de type S. Ils sont formés par fusion partielle des différents protolites au niveau de la croûte. Ces protolites sont les méta-pelites, les méta-grauwakes et les méta-tonalites à méta-amphibolites. Ces roches sont formées dans un contexte tectonique syn - à post-collision. Les roches volcaniques mafiques des deux zones d'étude ont une source mantellique et constitués des roches de la série alcaline, résultant de la fusion partielle des péridotites à grenat similaires à certains basaltes alcalins provenant d'un rift intracontinental.

Ces données montrent que les saphirs de cette zone d'étude sont d'origine magmatique, dont la roche mère a une composition assez proche de celle des syénites ou des monzonites, probablement les syénites de Ntumbaw, qui s'est formée au niveau de la croûte. Ces saphires sont transportée vers la surface par un magma basaltique alcaline provenant du manteau. Ledit transport s'est effectué à travers les nombreuses fractures qui caractérisent la Ligne du Cameroun et la zone de cisaillement Centre Cameroun.

Mots clés: Nord-Ouest Cameroun, saphir, Géochimie, Géochronologie, Contexte géotectonique.

TABLE OF CONTENTS

LIST OF FIGURES

LIST OF TABLES

LIST OF ABBREVIATIONS

Bt: Biotite

Hb: Hornblende

Mc: Microcline

Mu: Muscovite

Ol: Olivine

Or: orthoclase

Ox: Opaque oxides

Pl: Plagioclase

Px: Pyroxenes

Qtz: Quartz

Sa: Sanidine

OIB: Ocean Island Basalt

MSWD: Mean Squared Weighted Deviation

TBSZ: Tcholliré-Banyo Shear Zone

Il: Ilmenite

Mag: Magnetite

Sp: Sapphire

TP: Topaz

Tm: Tourmaline

Zr: Zircon

ALS: Australian Laboratory Services

CAFB: Central African Fold Belt

CCSZ: Central Cameroon Shear Zone

CHIME: Chemical Th-U total Pb Isochron Method

CL: Cameroon Line

MALI: Modified Alkali-Lime Index

OVG: Oku Volcanic Group

GENERAL INTRODUCTION

1- PROBLEM STATEMENT

Corundum is a crystallized aluminum oxide (Al_2O_3 with ≈53% of Al and ≈47% of O), made up of two varieties (ruby and sapphire). Ruby is red and sapphire represents all other colours of corundum. They are mostly mined in placers accumulated nearby or very far from their host rocks (Limtrakun et al., 2001; Zaw et al., 2014). They can also be found in paleo-placers, formed from the lithification of unconsolidated corundum-bearing sediments (Garnier et al., 2004; Giuliani et al., 2007). Corundum is also found as xenocrysts (Sutherland et al., 2002; Graham et al., 2008) and/or in xenoliths (Guo et al., 1996; Upton et al., 1999) in some basaltic flows. In primary deposits, corundum is an accessory mineral associated with magmatic (syenite, monzonite, lamprophyre) or metamorphic (marble, granulite, mica-schist, cordieritite, gneiss, migmatite, mafic-ultramafic metamorphite, and metabauxite) rocks (e.g. Graham et al., 2008; Sutherland et al., 2009, 2015a; Aydogan and Moazzen, 2012). During their crystallization, they trap fluids, melts, and other minerals that fingerprint their conditions of formation (Sutherland et al., 1998, 2015a, b; Pakhomova et al., 2006; Zaw et al., 2006, 2014). Precious to semi precious stones are mainly used in the jewelry industry (Limtrakun et al., 2001, Abdulrahman, 2017).

Generally, most corundum occurrences in the world are being exploited in secondary deposits of alluvial and eluvial placers (Hauzenberger et al., 2003), due to their high weathering resistance, hardness (Moh's scale of hardness= 9) and high specific gravity (3.9 – 4.1) that facilitates their concentration in these placers (Garnier et al., 2004) of proximal or distal sources. Information concerning the geological context of their primary deposits remains rare (Mercier et al., 1999) and attributing the primary origin of these alluvial corundum deposits to either a magmatic or metamorphic rock or their ages is often a difficult task.

Important sapphire deposits of metamorphic and magmatic origins have been described around the world in countries like the United States of America, Thailand, Vietnam, Australia and China, and in African countries such as Madagascar, Tanzania, Mozambique, Kenya, Nigeria and Cameroon (Hughes, 1997).

In Madagascar, primary deposits have been grouped into three geological settings: magmatic settings in syenite and granite, metamorphic settings and associated alkaline metasomatics in rocks like desilicated gneiss, acidic and mafic to ultramafic granulites (Rakotondrazafy et al., 2008).

In Cameroon, sapphire mineralization has been associated to CCSZ and CL (Boaka à Koul et al., 2011) magmatic occurrences have been described in Nsanaragati (SW Region) (Kanouo et al., 2012) and Mayo Kewol (Adamawa Region) (Boaka à Koul et al., 2011).

Gem quality corundum (sapphire and ruby) was discovered in Cameroon since 1966 in the Cretaceous Mamfe basin (Laplaine, 1969). Its deposits are being artisanally exploited in detrital alluvial deposits in the Adamawa and South-West Regions of Cameroon. In Adamawa Region, concentrations of blue sapphires are being exploited in placers in Mayo Kewol, Paro Lawel, Mayo Dankali, Karange, Tignere and Tibati (Boaka et al., 2010). In the South-West Region, blue sapphires are being mined in Nsanaragati and Tinto in the western part of the Mamfe basin (Kanouo et al., 2012 a). In the North-West Region, Mayo Kila and Mbiame are the latest occurrences discovered in Cameroon. In Mayo Kila, corundum grains occur in low concentration within alluvial materials partly covering granitic bedrocks and rare basaltic dykes while in Mbiame, very high concentrations of blue sapphires are mined in alluvial material within basalts and conglomerates.

The high demand for corundum in the jewelry industry for its beauty (colour, clarity and scarcity) raises the need to prospect and discover new deposits. For scientific and economic interests, the occurrence of undocumented alluvial sapphires in the localities of Mayo Kila and Mbiame is the focus of this study. These corundum occurrences have not been characterized, the history of their genesis is still not understood, and the nature of their source rocks is still to be determined.

2- OBJECTIVES

The main objective of this research is to characterize the existing sapphire occurrences, trace the source rock(s) of their host materials within the local and regional geologic settings and to propose a genetic model for their formation.

The specific objectives of this research are as follows:

- to define the morphological characteristics of the gem placers;
- to determine the petrographic and geochemical characteristics of the surrounding host rocks;
- to determine the geochemical characteristics of the sapphire grains;
- to determine the age of the sapphire occurrence;
- and to define the possible relationship that exists between these sapphire occurrences and the Cameroon Line.

3- LAY OUT OF WORK

After the general introduction with a problem statement and principal objectives, this work is divided into three parts, with six chapters.

PART I: Geography, literature review and research methodology

The chapters of this part present the geography and geological settings of the study areas as well as the research methodology. It is divided into four chapters as follow:

Chapter I: Geography and geological settings

In this chapter, the locations of the study areas are presented as well as their climatic conditions, hydrology, relief, vegetation and human and economic activities. As far as the geological settings are concerned, the regional and local geology are also highlighted.

Chapter II: Literature review

This chapter presents a review of the Cameroon Line (the geology, ages of the different volcanic massifs and the different anorogenic complexes) and the Cameroon Fold Belt. It also presents a background review on corundums and their deposits.

Chapter III: Materials and research methods

This chapter deals with the materials and methods used to attain the objectives of this study. These materials are the bibliographic review of the study areas and sapphire deposits as well as field equipments. The methods are mainly field trips and laboratory analyses.

PART II: Results

This part treats on the one hand the field results of the morphology of alluvial materials, soil and alluvial profiles and on the other hand, the morphological, geochemical and geochronological characteristics of the sapphire grains. Also, the petrography and geochemistry of the surrounding rocks are presented. The results are further divided into two chapters as follows:

Chapter IV: Morphological, geochemical and geochronological characteristics of Mayo Kila and Mbiame gem placers

In this chapter, morphologies of alluvial profiles and alluvial materials in Mayo Kila and Mbiame are presented. It also presents the morphological, geochemical and geochronological results of analysed sapphire grains obtained from the gravels.

Chapter V: Petrographic and geochemical characterizations of surrounding rocks in Mayo Kila and Mbiame

This chapter looks at the petrology and geochemical characteristics of the surrounding rocks in Mayo Kila and Mbiame.

PART III: Discussion

In this part, the results are discussed in order to establish a possible relationship between the surrounding rocks and the sapphire occurrences.

Chapter VI: Characteristics and provenance of clastic materials forming the Mayo-Kila and Mbiame gem-bearing placers and rocks of the surrounding

In this chapter, the main results from field investigations and laboratory analyses are discussed. This includes the interpretation of sedimentological, geochemical, geochronology and some gemological aspects of sapphire grains. It also presents the characteristics of the surrounding rocks and their relation to the sapphire occurrences.

PART I

GEOGRAPHY, GEOLOGICAL SETTINGS AND RESEARCH METHODOLOGY

CHAPTER I

GEOGRAPHY AND GEOLOGICAL SETTINGS

The study areas (Mayo Kila and Mbiame) are found in the North-West Region of Cameroon. They are bordered to the north by Nigeria, to the west by the South-West Region and to the east and south east by the Adamawa plateau and the West Region respectively (Fig.1). This chapter presents both their geography and geological settings. The geographical setting situates the study areas within the North-West Region and presents their climate, geomorphology, vegetation, drainage systems and human and economic activities, while geological setting presents the brief geology of Mayo Kila situated in Nkambe area and Mbiame within the center of the Oku massif.

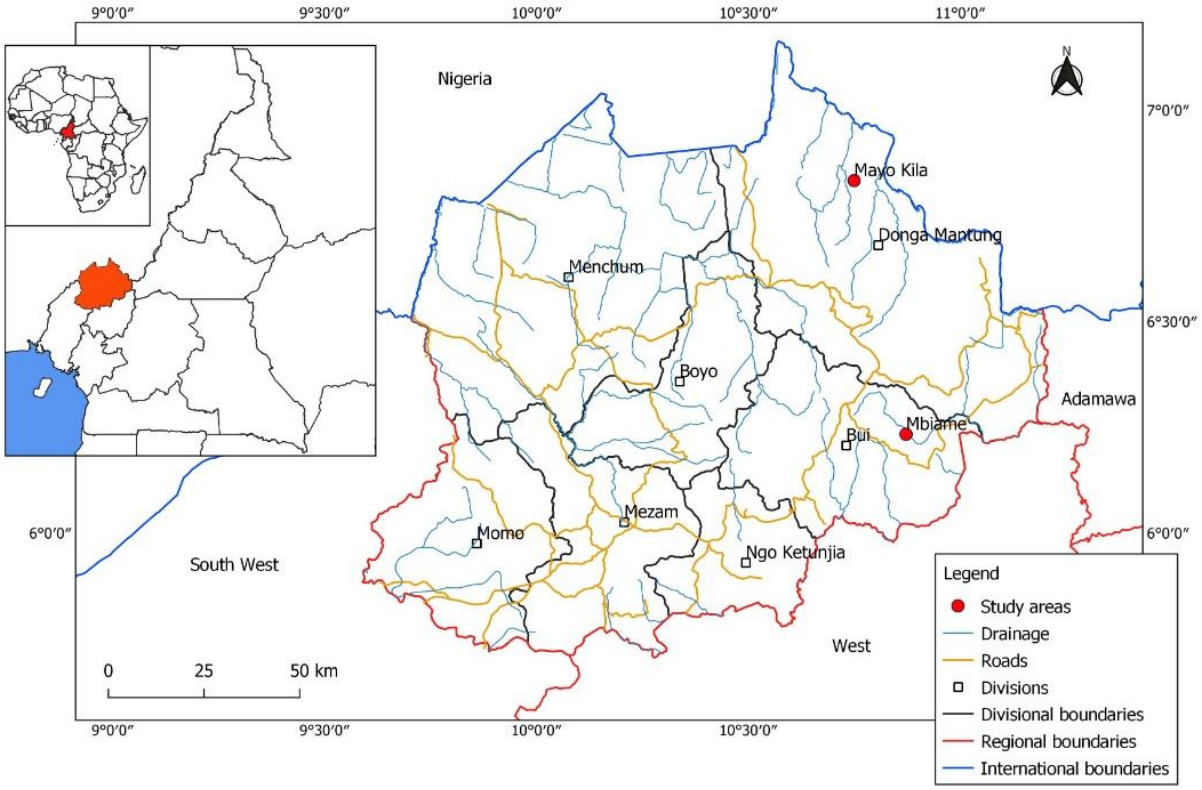

Figure 1: Location of study areas within the North-West Region

I.1- Geographical setting

I.1.1- Location and accessibility

I.1.1.1- Mayo Kila

Mayo kila is situated about 22 km NW of Nkambe, and about 16 km N of Misaje. Administratively, it belongs to the Misaje Sub-Division in the Donga Mantung Division, North-

West Region. Geographically, it stretches between latitudes N 06°35' to N 06°50', and longitudes E 010°30' to E 010° 45' (Fig. 2). It is bordered to the north by Nigeria and access to Mayo Kila village is mostly by foot or motorcycle via Dumbo.

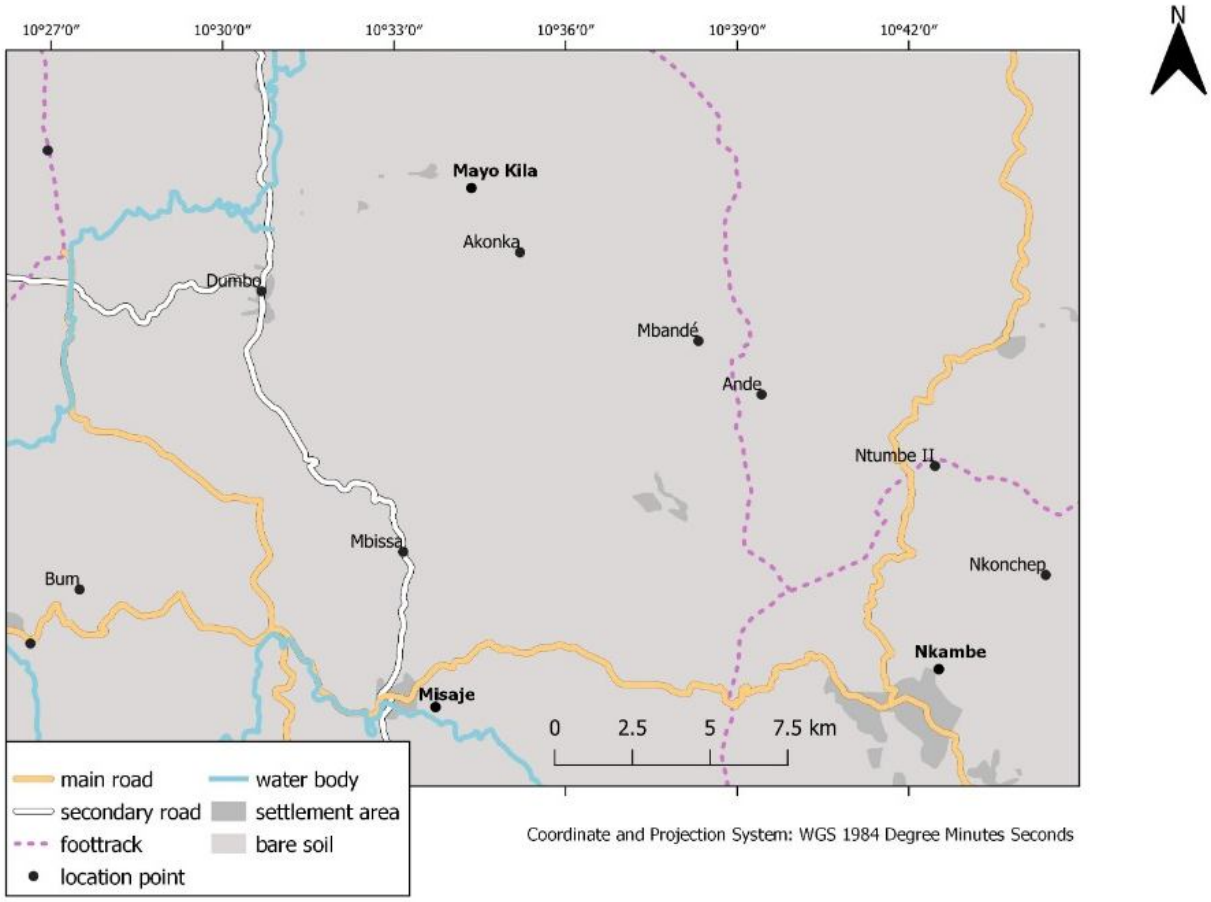

Figure 2: Location map of Mayo Kila.

I.1.1.2- Mbiame

Mbiame is situated about 11.7 km east of Kumbo. Administratively, it is the headquarters of Mbven Sub-Division in Bui Division, North-West Region. Its geographic coordinates run from latitudes N06°10'24" to N06°14'00" and longitudes E010°48'00" to E010°52'21". It is easily accessed by an earth road from Kumbo (Fig. 3).

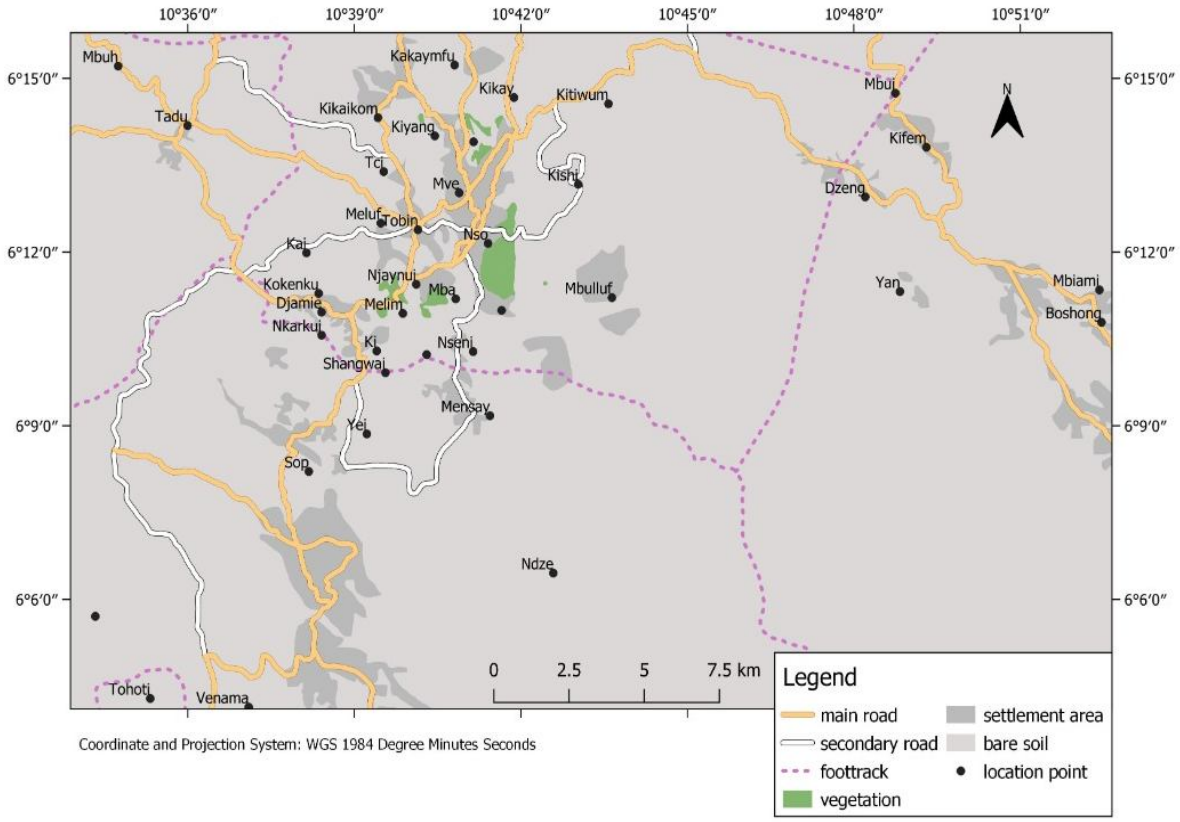

Figure 3: Location map of Mbiame.

I.1.2- Climate

These areas experience a humid tropical climate of the Western Cameroonian Mountains, characterized by two seasons (Sighomnou, 2004). These two seasons (rainy and dry seasons) have unequal durations (Fig. 4):

- a rainy season from mid-March to mid-November;
- a dry season from mid-November to mid-March;

It has an annual rainfall of about 2007.3 mm of water per year (Tabel 1) and an annual average temperature of about 17.1°C.

Table 1 : Temperatures and precipitations of Nkambe area from 1991 to 2011 (Cameroon Tea Estate meteorological station).

months	Jan	Feb	Mar	Apr	May	Jun	Jul	Aug	Sep	Oct	Nov	Dec	average
P (mm)	4.21	19.71	82.77	167.22	217.53	228.25	296.99	316.51	316.16	307.22	50.57	2.23	2007.3
T (^{0}C)	16.9	17.75	18.33	18.24	17.6	16.81	16.17	16.07	16.4	16.77	17.06	16.78	17.1
2T(°C)	33.8	35.5	36.66	36.48	35.2	33.62	32.34	32.14	32.8	33.54	34.12	33.56	

P= Mean monthly rainfall T= Mean monthly temperatures

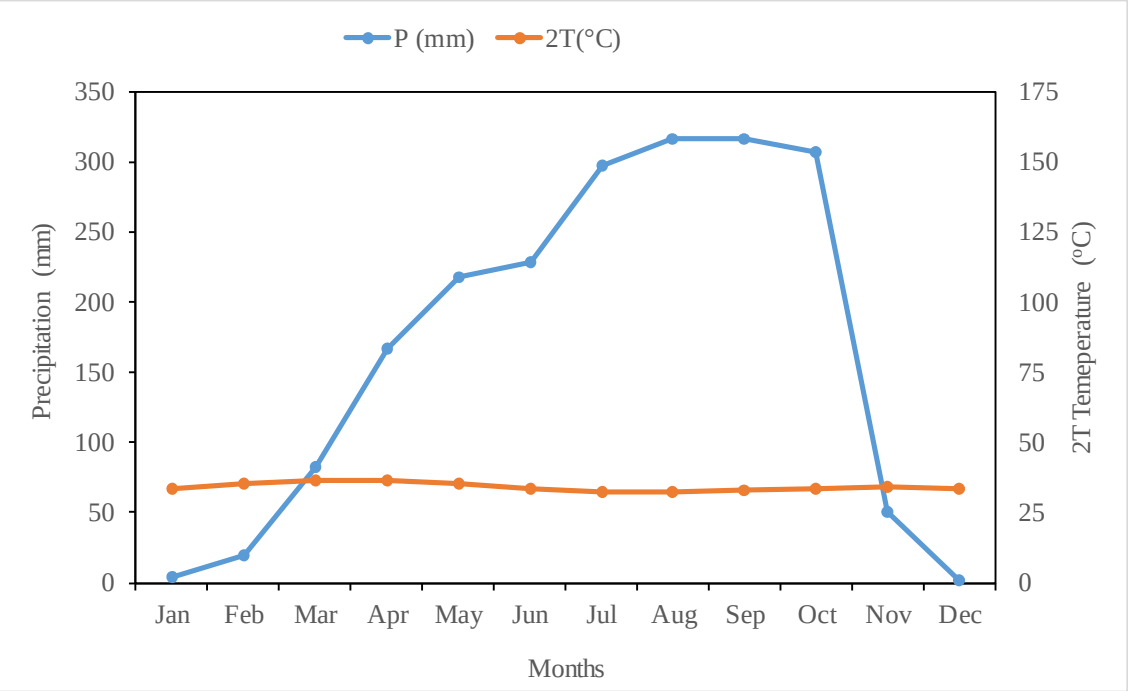

Figure 4: Ombrothermic diagram of Bagnouls and Gaussen (1957), for Nkambe area from 1991 to 2011.

I.1.3- Hydrology

The Menchum, Donga and Katsina Ala are the major rivers that drain the Northwest Region of Cameroon (Fig. 5).

The Menchum flows about 20 km south of Wum and 30 km north of Bafut. It drains the Oku-Kom highlands and flow from an altitude of about 2,400 m around Lake Oku to the west of Fundong with elevation of about 800 m. Its upper basin includes two main branches, which meets near Mbengwi. The Abi that drains Bali and the northern slopes of the Bamboutos Mountains and has its source frm an altitude of about 2,168 m, and the other, the Mezam or Machu. This second name suggests that the Mezam constitutes the upper Menchum with its source at the foot of Mt Neshele (2,621 m) and its two crater lakes, the Bambili Lakes in the Lefo massif. It then receives three main tributaries on the right bank, the Movum, the Mugom and the Joaka amplified by the Mete River. These rivers drain the western part of the Oku Massif, from the Bamenda Mountains north of Sabga and the Kom Plateau, from Bambui to Njinikom and Fundong. The Menchum then serves as a common border between the two countries before joining the Katsena.

The Donga River arises from the Mambilla Plateau in Eastern Nigeria and forms part of the international border between Nigeria and Cameroon. It flows northwest to merge with the Benue River in Nigeria.

The Katsina Ala is a river with source from the Bamenda highlands in northwestern Cameroon. It is a major tributary of the Benue River in Nigeria, it flows about 320 km northwest in Cameroon passing through the Eastern Nigerian-Cameroon border into Nigeria Neba, 1999).

In Mayo kila, the drainage system is mainly dentritic with many seasonal streams and rapids, generated from the high altitudes that characterize the area. The main river is the Akon, which is supplied by River Donga, and drains the eatern part of the study area. Many other unidentified streams supplying from the northwest, center and southwestern parts of the study area.

The drainage partern is dendritic in Mbiame, with main rivers in the north such as the Nsang, Marin, Manakan, Maka, Moba, Mbam, Sunka and Kumbi. In the southwestern part, Lake Oku and its highlands supply Rivers Mintua, Mugom, Mankon and the Nun plain. Rivers Nze, Nza, Nka, Nuot, Bibi and the Ndudu drain the southeastern part. Most of these rivers take their rise from the numerous highlands in the area.

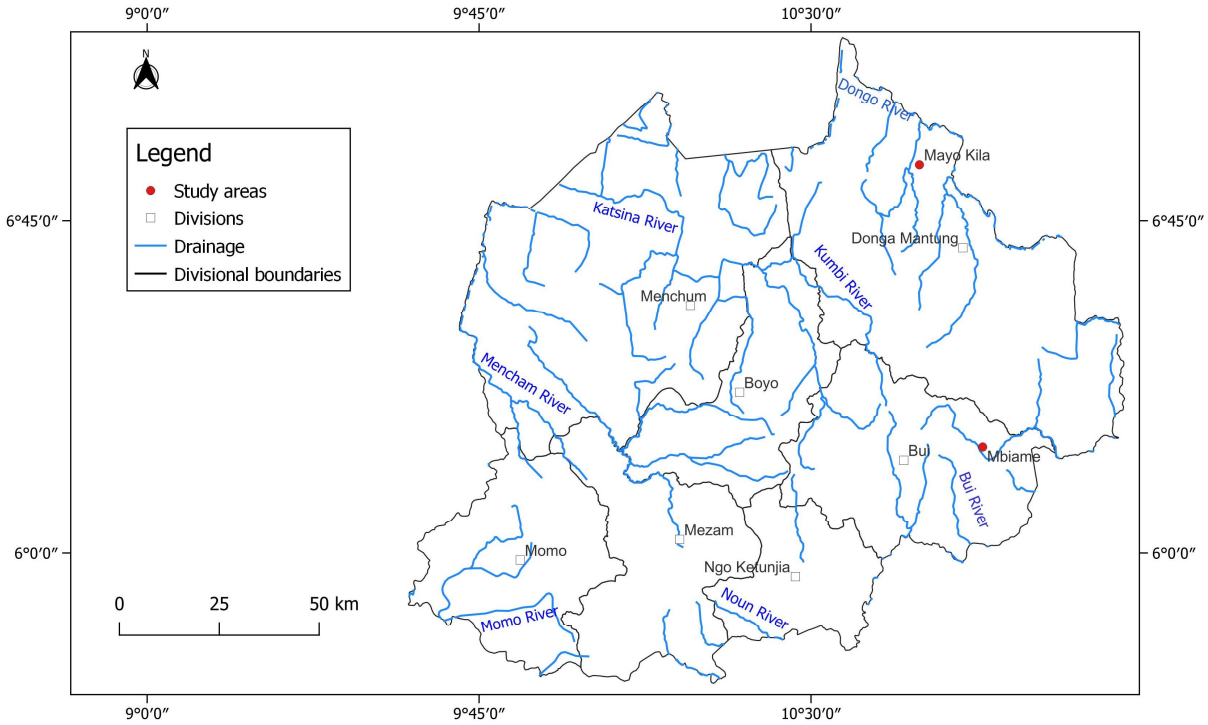

Figure 5: Drainage map of the study area.

I.1.4- Geomorphology

The study areas are found in the West Cameroon Highlands and represent one of the continental volcanic massifs of the Cameroon Line (CL). Mayo Kila and Mbiame are found in the Nkambe plateau and Mount Oku stratovolcano areas respectively. The area is bordered to the north by the Adamawa plateau, to the west by the Bamoun plateau and to the Southwest by the Bamenda mountains.

I.1.4.1- Mayo Kila

Mayo Kila is built on a mountainous relief and is characterized by high volcanic massifs and steep V-shaped valleys with altitudes that show three main topographic units (Fig. 6).

- the first unit ranges in height between 400 - 800 m and represents low area such as valleys. This unit can be observed in the north eastern part of the study area;
- the second unit that ranges between 800 - 1200 m characterizes the average elevated areas and covers the west and the central part of the study area;
- the third unit ranges between 1200 – 1600 m with a peak of 1761 m and represents the highest relief. It occupies the south eastern part.

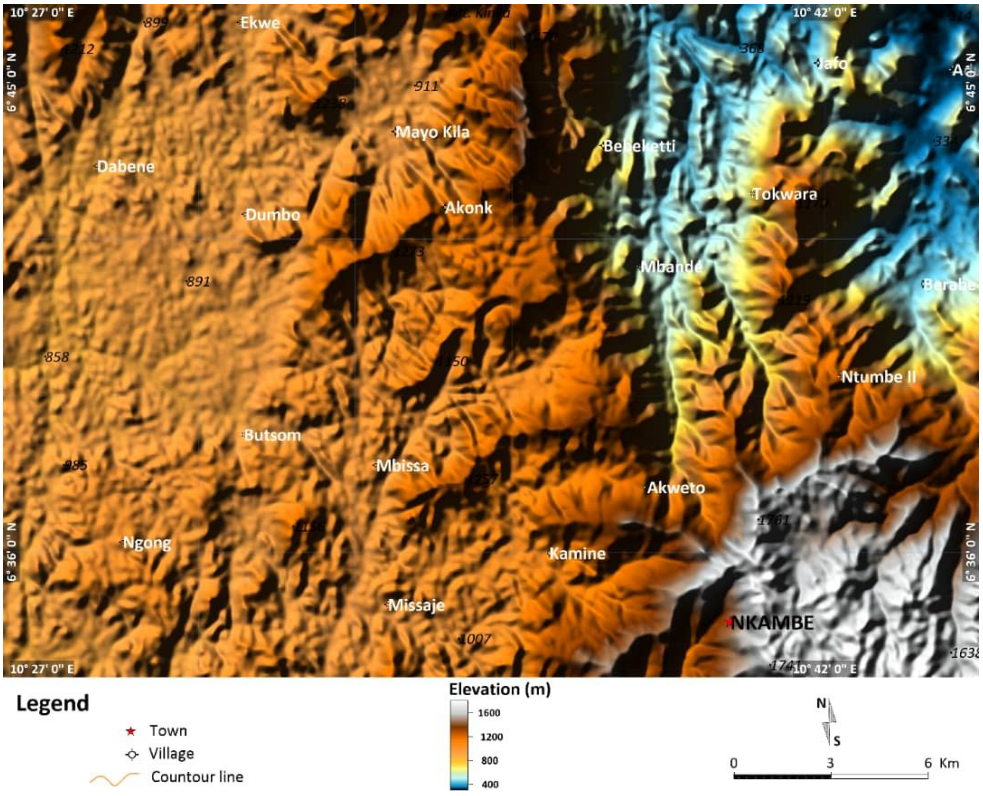

Figure 6: Geomorphological map of Mayo Kila.

I.1.4.2- Mbiame

Mbiame is situated at the west of Mount Oku and is characterized by a mountainous relief. Three main topographic units can be distinguished in the area (Fig. 7).

- the first unit has altitudes between 900 - 1150 m and represents the low areas and valleys, it occurs in the south eastern part of the study area;
- the second unit is between 1150 - 1950 m, medium elevated areas which are represented by mountains with V-shaped valleys although few U-shaped valleys could also be seen in some places;
- the third unit has the highest altitudes within the Mount Oku area and range between 1950 - 2300 m. According to Njilah et al. (2007), the peak of Mount Oku is situated at altitude of 3011 m. These altitudes occur mostly in the western part of the study area.

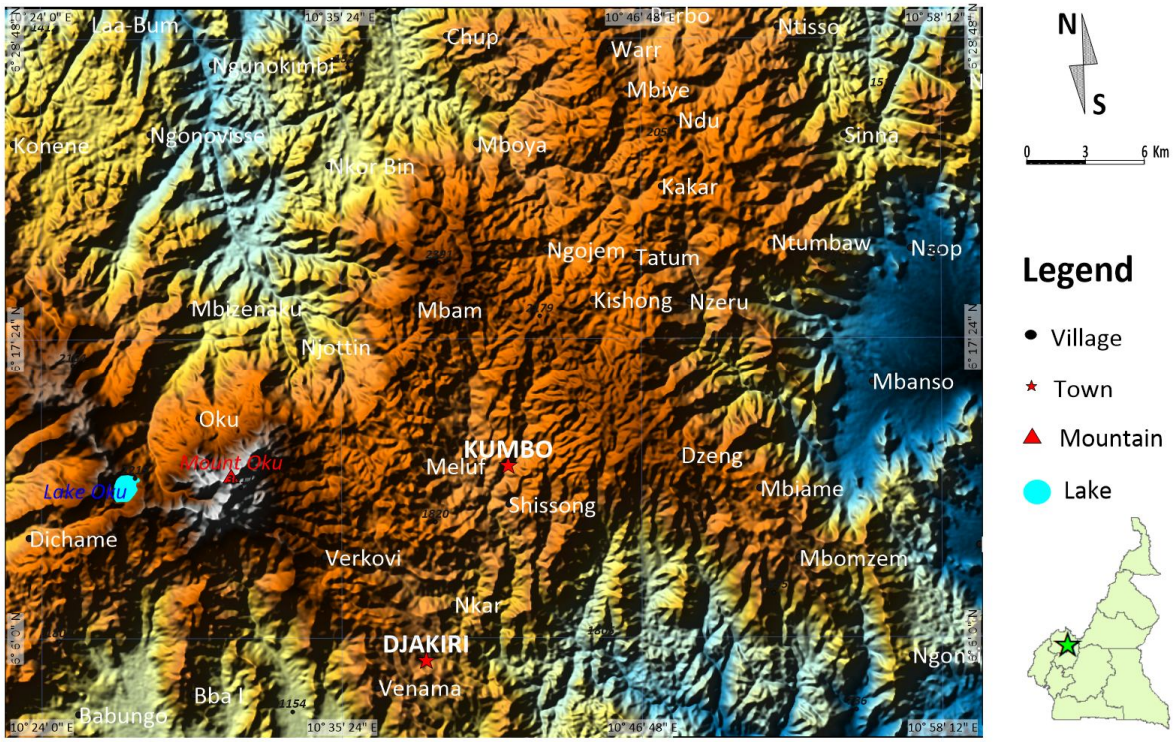

Figure 7: Geomorphological map of Mount Oku area.

I.1.5- Vegetation

The vegetation of Mayo Kila and Mbiame areas are dominated by a peri-forest savanna. It is strongly related to the drainage system of the region as forests are clustered along rivers. Pins (*Abies pectinata*) and eucalyptus (*Eucalyptus grandis*) are observed around habitation zones while lowlands and swampy valleys are dominated by raffias *(Raphia mamillensis*). Fruit bearing

trees like mangoes, pears, plum, guavas and relicts of coffee (*Coffea arabica*) plantations are also observed. The common cultivated crops include maize (*Zea mays*), cassava (*Manihot esculenta*), beans (*Phaseolus vulgaris*), groundnuts (*Arachis hypogea*) and cocoa yams (*Colocasia esculenta*).

I.1.6- Human and economic activities

The ethnic groups in both areas are mostly the Mfumte, Yamba, Mbaw, Wimbum, Nso, Noni, Mbororos and Bamunka. Agriculture is the major activity of the population. The agro-pastoral sector is mostly represented by livestock farming practiced by the Fulani nomads through their cattle-rearing activity. The area also hosts the Dumbo Cattle Ranch. Industrial agriculture is characterized by tea cultivation at the Ndu Tea Estate, while traditional agriculture involves the cultivation of crops like maize, cocoyam, cassava, beans, irish potatoes, banana, and plantain. Okra, tomatoes, groundnuts, sweet potatoes, and palm oil are roduced in this region. The commercial sector is essentially animated by the buying and selling of livestock and associated products by business men from urban areas and neighboring Nigeria, while most farm products are sold locally.

I.1.7- Soils

The soils in both areas are humic ferralitic and hydromorphic. In Mayo Kila, the soils are reddish brown and were developed from the deep weathering of the existing granito-gneissic substratum and. While in Mbiame area, they mostly developed from volcanic rocks. These soils have a high organic matter content favored by the humid climate, and have a silty clayey texture. Hydromorphic soils on their part occur in swampy areas and are dark grey to black, due to their high content in organic matter. Those around the lake Oku area are mostly developed from volcanis ashes (Godwill, 2019).

I. 2- Geological context

Mayo Kila and Mbiame are part of the Oku Volcanic Group (OVG), situated west of the Central African Fold Belt in Cameroon. This volcanic group represents one of the continental volcanic massifs of the Cameroon Line (CL). It is composed of four major adjacent stratovolcanoes: Mount Oku, Mount Babanki, Nyos and Nkambe (Njilah et al., 2013). The Oku massif occupies a central position along the continental sector of the CL (Fig. 8) and has been described as a stratovolcanic edifice of approximately 90 km in diameter and 3011 m high (Njilah et al., 2007, 2013). The volcanic products are basanites, picrobasalts, hawaiites, mugearites, benmorites, ignimbrites, trachy-andesites and trachy-basalts (Asaah et al., 2014; Chenyi et al., 2017; Wotchoko et al., 2017; Tedonkenfack et al., 2019). This volcanism of Mt Oku has ages of 31-22 Ma (Rankenburg et al., 2004, 2005).

The Mayo Kila placers from which the studied corundums were sampled are situated within the Nkambe granitoids. Nkambe is built on granitoids, banded gneisses, porphyroblastic gneisses and amphibolites (Tetsopgang et al., 2008). The granitoids include foliated and massive biotite monzogranite, hornblende-biotite granite, magnetite-free and magnetite-bearing two-mica granites (Fig. 9) (Tetsopgang et al., 1999, 2008). Intruded granites, monzogranites, and tonalites in this area are locally covered by Cenozoic basaltic and andesitic exposures, extruded by trachyte-rhyolite (Tetsopgang et al., 2011). CHIME (Chemical Th-U total Pb Isochron Method) zircon and monazite dating of magnetite-free and magnetite-bearing two-mica granites gave an age of 530 ± 9 and 510 ± 25 Ma respectively (Tetsopgang et al., 1999). Obtained ages for foliated and massive biotite granitoids range from 569 ± 12 to 558 ± 15 Ma and 533 ± 12 to 524 ± 28 Ma, respectively. Allanite CHIME dating of quartz-rich hydrothermal cross-cutting veins gave an age of 436 ± 13 and 420 ± 16 Ma (Tetsopgang et al., 2008).

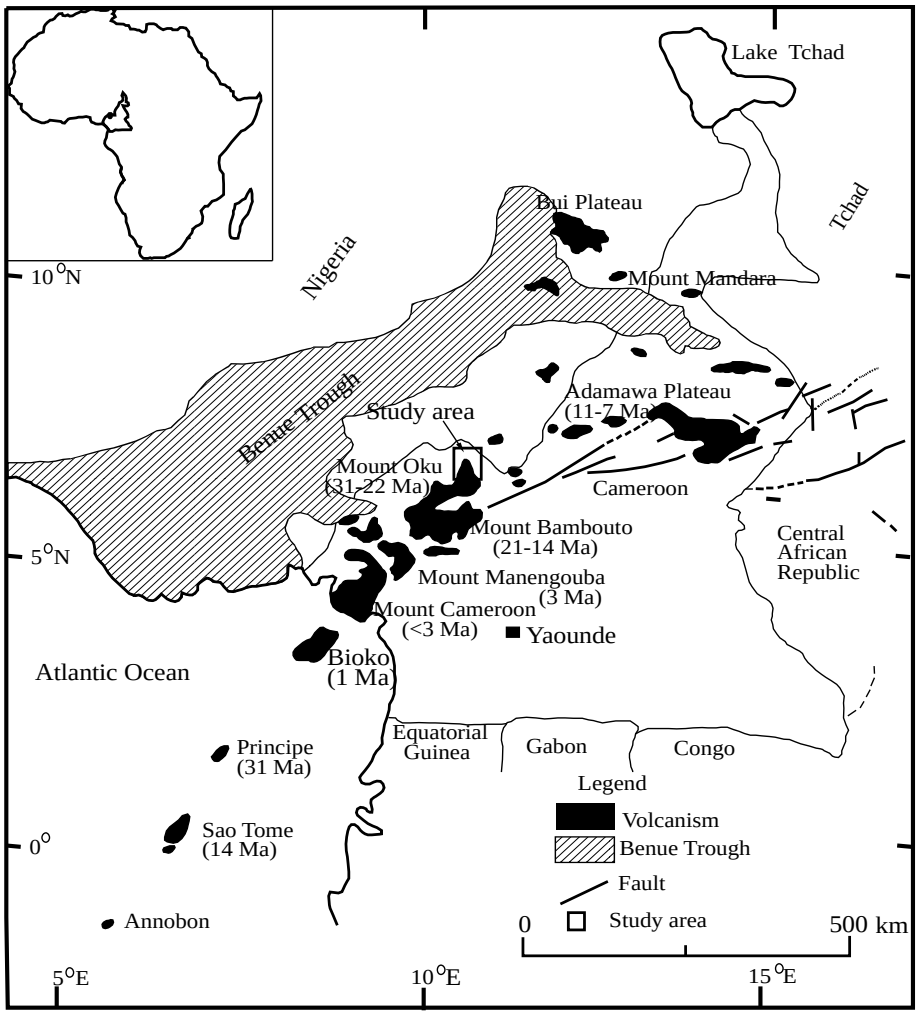

Figure 8: Location of study area on the Cameroon Line (Ateba et al., 2009) and ages of volcanoes from Rankenburg et al. (2005).

Two-mica granites found in Nkambe occur as elongated plutons parallel to the regional structures SW-NE (Tetsopgang et al., 2006). These SW-NE regional structures tie with the overall linear SW-NE trending chain of alkaline magmatism which defines the Cameroon Line (CL) (Njonfang et al., 2011). These granites are High-K calc-alkali types, corundum normative, and display peraluminum to metaluminum affinities (Tetsopgang et al., 2006). Foliated biotite granites lie parallel to the regional sub-vertical N-S to NNE-SSW trending structures. These foliated granites are essentially synchronous with the regional metamorphism that produced migmatite gneiss, amphibolites and anatectic granites in the area (Tetsopgang et al., 1999).

The volcanic rocks of Mount Oku show a compositional gap with mafic lavas on the one hand and acid lava on the other hand (Njilah et al., 2007). Volcanic materials of Oku massif range from basalts, trachytes, rhyolite (Fig. 9) and layered pyroclastites (Njilah et al., 2007, 2013). This massif, like other volcanic massifs of the West Cameroon Highlands is underlined by a granite-gneissic substratum of Pan-African age (Njilah et al., 2007, 2013, Njonfang et al., 2011, Kamgang et al., 2013), migmatites, and biotite diorites said to be uplifted during the general doming that accompanied the eruption of the CL (Njilah et al., 2007, 2013).

Njilah et al. (2007) point out three volcanic series: a lower series, made up of basic lava flows with fragments of basement granite. The trachytes and rhyolites of this series outcrop in the forms of flows and plugs; a middle series, made up of basaltic flows overlain by trachyte and rhyolite intercalated with pyroclastic flows; an upper series, constituted of a series of recent cinder cones and a crater occupied by Lake Oku.

The rare granitic outcrops of Mount Oku occur in very low altitudes, like river beds and swamps while basalts crop out as huge blocks, columns and disjointed blocks. In Mbiame, deeply weathered basaltic outcrops are accompanied by conglomerates with grey, yellowish and brownish clastic materials of mostly basaltic fragments. The conglomerate fragments vary from millimetric sizes up to 4 cm and are cemented by a brown to grayey matrix. These conglomerates are hosts to light and dark magnetic and non-magnetic heavy minerals.

Mbiame is located within the main massif of the Oku Volcanic Group. It is made up of a well exposed volcanic assemblage predominantly characterized by basalts, trachytes, and rhyolites (Fig. 9). The Ntumbaw pluton is exposed about 20 km NNE of Mbiame. This pluton with surface area of about 12 km^2 is mainly composed of intermediate rocks distributed within two centers (C1 and CII). CI is composed of monzodiorite, monzonite and quartz monzonite while CII is made up of quartz syenite and syenogranite (Déruelle et al., 1991). The two juxtaposed centres are intrusive into the Pan-African basement and are partly covered by recent basaltic lava flows (Ghogomu et al., 1989).

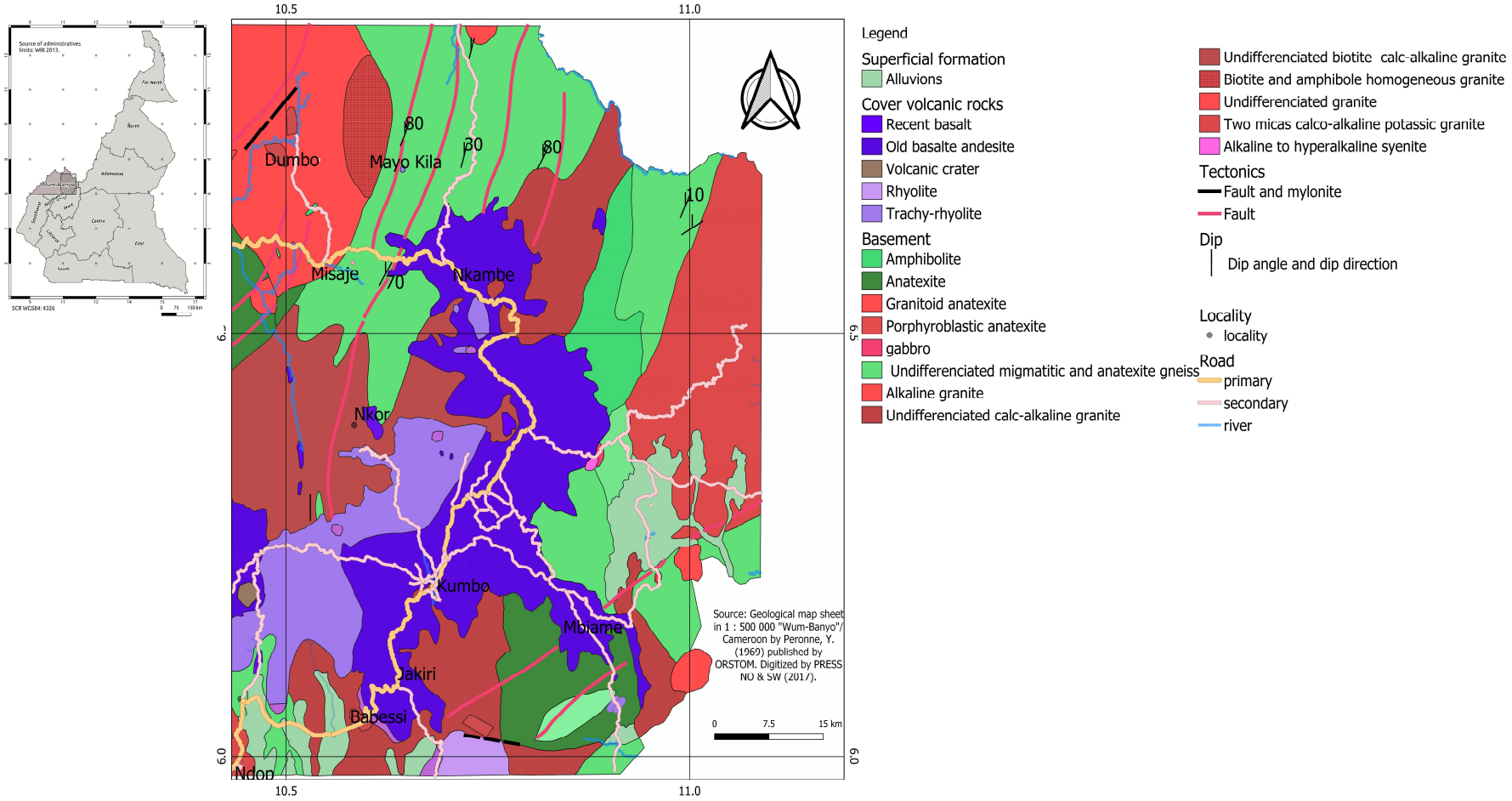

Figure 9: Geological map of study areas (after Peronne, 1969), using the 2007 INSPIRE (Infrastructure for Spatial Information in Europe) code and specification on Geology -Technical Guidelines.

Conclusion

The study areas, Mayo Kila and Mbiame are found in the West Cameroon Highlands and are situated within the Oku Volcanic Group, one of the continental volcanic massifs of the Cameroon Line. They are characterized by a humid tropical climate with an annual rainfall of about 2009.5 mm of water per year and an annual average temperature of about 17.1°C. The area is drained by the Donga and the Katsena-Ala rivers. The vegetation is dominated by a peri-forest savanna. Its geology is typically that of the Cameroon Line with volcanic rocks like basanites, picrobasalts, hawaiites, mugearites, benmorites, ignimbrites, trachy-andesites and trachy-basalts underlined by a granite-gneissic substratum of Pan-African age. The granite basement has been dated between 569 ± 12 and 524 ± 28 Ma while the volcanic cover is mostly Cenozoic.

CHAPTER II

LITERATURE REVIEW

This chapter presents a literature review on the Cameroon Line, the petrography, geochemistry and ages of the different volcanic massifs, the anorogenic ring complexes of the CL as well as some proposed models for its formation. The second part presents the fold belt in Cameroon, with attention to the main geotectonic units that define the mobile belt in Cameroon. The third part presents the general characteristics of corundum such as their morphology, physical and geochemical properties, geochronology, and economic aspects as well as corundum producing countries. It also presents information on the different types of deposits (primary and secondary), corundum occurrences in Cameroon and their characteristics (petrography, mineralogy, geochemistry and geochronology).

II.1- Cameroon Line

The Cameroon Line (CL) is a linear chain of Cenozoic volcanoes stretching for about 1600 km from the Gulf of Guinea into continental Africa (Aka et al., 2004) and characterized by a series of genetically related intraplate volcanoes (Rankenburg et al., 2005; Ngako et al., 2006) (Fig.10). It is made up of oceanic and continental volcanic sectors. The volcanic islands of the oceanic sector are: Annobon (or Pagalu), São Tome, Principe and Bioko, while the continental sector is made up of plutonic anorogenic complexes (Njonfang et al., 2011) and volcanic massifs of Mount Cameroon (4095 m), Mount Manengouba (2420 m), Mount Bambouto (2679 m), Mount Bamenda and Mount Oku (3011 m).

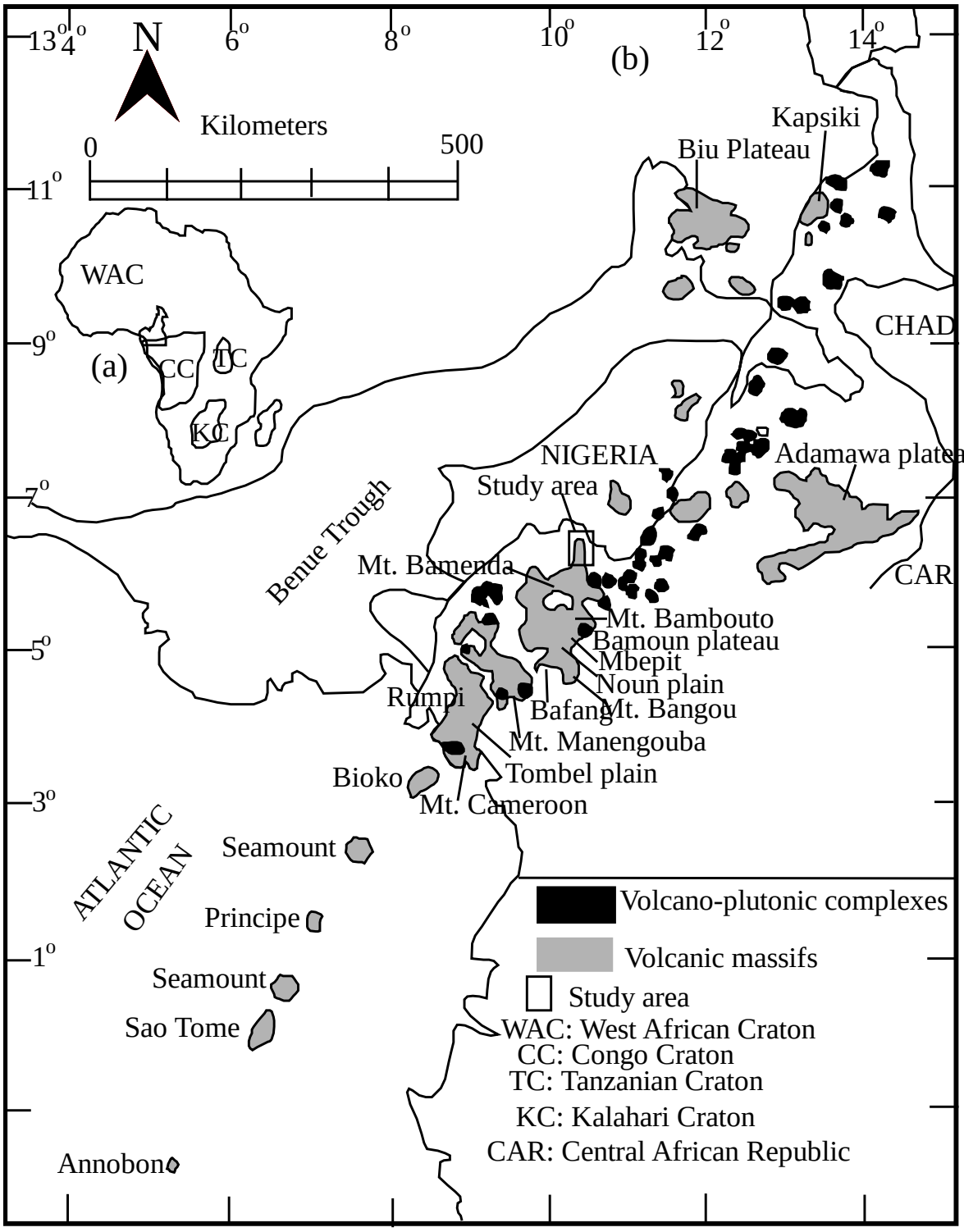

Figure 10: a: Inset, bottom right African cratons (after Njonfang et al., 2011); **b:** Location of study area along the Cameroon Line (adapted after Njonfang et al., 2011). Location of seamounts after Burke (2001).

II.1.1- Oceanic massifs

The oceanic sector of the CL is made up of six major volcanoes: the Annabon, São Tomé Principe Islands, Bioko (Déruelle et al., 2007) and two seamounts (Burke, 2001). The Annobon and São Tomé are stratovolcanoes while Principe is a lava flow. They are made up of volcanic rocks that range from nephelinite, basanite and basalt to trachyte and phonolite (Fitton and Dunlop, 1985; Deruelle et al., 1991).

Annobon (Pagalu) is situated to the south of the CL and represents the smallest island (Fig. 10). According to Cornen and Maury (1980), the volcano was progressively built on: a first stage of submarine palagonitic breccia volcanism that was later intruded by basaltic dikes; a second stage, represented by layered basanitic flows which were intersected and fed by dikes dated at 5.35 Ma; and a third stage characterized by the emplacement of tristanitic and trachytic plugs of 3.9 Ma and ankaramitic basanite flow.

São Tomé is a roughly conical stratovolcano of about 2024 m above sea level. The volcanism of the island is made up of a submarine eruptive phase represented by palagonite tuffs and pillow lavas of unknown age (Aka et al., 2001). The island is composed of basaltic lava flows with a landscape of cinder cones in the northeast and phonolitic and trachytic plugs in the southeast quadrant (Barfod and Fitton, 2014).

Principe is built on the oceanic floor at a depth of about 3000 m and culminates at 948 m above sea level. Basaltic rocks occur in the north, while phonolites and tephrites are common in the south (Deruelle et al., 1991). These volcanic rocks are divided into two stratigraphic units:
a younger lava series made up of basanite and nephelinite overlying an older lava series of transitional to mildly alkaline basalt and hawaiite (Fitton and Hughes, 1977).

Bioko Island is located in the Gulf of Guinea, about 35 km SW of the continental Mount Cameroon. It consists of three volcanoes, the Pico Santa Isabel occupies the northern part of the island and the Pico Biao and San Carlos volcanoes (Deruelle et al., 1991). Two types of volcanic products are found on the Bioko Island: pyroclastic ejections (spheroid bombs, cognate blocks, lapilli, coarse and fine ash, and shiny and black scoriae) and lava flows (Yamgouot et al., 2016).

II.1.2- Continental volcanic massifs

The continental massifs are built upon horsts that alternate with grabens, with predominance of monogenic cones (Déruelle et al., 1991, 2007). It is oriented N30°E and segmented by N70°E shear zones that developed during Pan-African (Deruelle et al., 2007). This continental extension is divided into two branches: one of which stretches to the Biu Plateau in north-eastern Nigeria, while the other passes through the Adamawa Plateau. These continenetal volcanic massifs are Mount Cameroon, Mount Manengouba, Mount Bambouto, Mount Bamenda and Mount Oku.

II.1.2.1- Mount Cameroon

Mount Cameroon is a large stratovolcano with an estimated volume of ~1200 km^3. It is found in the South-West Region and represents the only current active volcano along the Cameroon Line (CL) with its last eruption history dated back to 2000 (Ateba et al., 2009). It is also the first continental volcanic massif on the CL. The lavas are picrites, alkali basalts, hawaiites, mugearites (Déruelle et al., 1987, 1991) and basanites (Tsafack et al., 2009). These lavas and pyroclastites are built on a crystalline basement of Paleozoic age (Njonfang et al., 2011).

Using the ^{40}K-^{40}Ar dating method, the ages of five whole rocks yielded a range of 2.83±0.11 (Late Pliocene) to 0.00±0.09 Ma. The groundmass dating shows very recent ages of 29±2 ka, 20±3 ka, and 0 ka.

II.1.2.2- Mount Manengouba

Mount Manengouba is located about 120 Km north-east of Mount Cameroon. It is mainly consists of a shield volcano overlain by a stratovolcano that culminates at 2411 m and covers 500 km^2. It is set up on a volcano-tectonic height trending N30°E above the uplifted granite basement and crosscut by N 0°, N 30° to 50°E and N 140°E faults (Pouclet et al., 2014). Its lithologic units are made up of basalts, hawaiites, mugearites, benmoreites, trachytes, dolerites and pyroclastic materials (Pouclet et al., 2014). The volcanic history of this mountain can be presented in four chronological stages: an early Manengouba shield volcano between 1.55 and 0.94 Ma; the Eboga strato-cone between 0.94 and 0.89 Ma; a caldera collapse and silicic extrusions of the Elengoum Complex between 0.89 and 0.70 Ma; and an intra-caldera and flank activity between 0.45 and 0.11 Ma (Pouclet et al., 2014).

II.1.2.3- Mount Bambouto

Mount Bambouto is found in the West Region of Cameroon and represents one of the principal relief features of the Western Cameroon Highland and a major volcano along the CL. It is mainly composed of basanitic-basaltic to trachytic-rhyolitic lava flows, which overlie granitic and rare dioritic basement of Pan-African age (Kwekam et al., 2010; Merle et al., 2017). It is a stratovolcano (Nkouathio et al., 2008) in which trachytes and rhyolite compositions of ignimbrite with scoria fragments have also been found (Nono et al., 2004). According to Kagou et al. (2010), the volcanic history of Mount Bambouto can be summarized as follows: a first stage of 21 Ma, which corresponds to the building of the initial basaltic shield volcano; a second stage from 18.5 to 15.3 Ma, marked by the collapse of the caldera related to the pouring out of ignimbritic rhyolites and trachytes; a third stage, from 15 to 4.5 Ma, renewed with basaltic

effusive activity, together with post-caldera extrusions of trachytes and phonolites. The 0.5 Ma Totap activity is said to be the fourth stage, characterized by recent Quaternary basaltic activities.

II.1.2.4- Mount Oku

Mount Oku is situated to the North of the Bambouto mountain and form one of the central volcanic massifs of the Western Cameroon Highlands. It plays host to an important depression where the Oku Crater Lake is formed. This crater is probably the source of Bambili, Sabga and Big Babanki ignimbrites. Its rocks are basanite, alkali basalts, hawaiite, mugearites and trachyte-rhyolite flows with intercalations of pyroclastic materials, upon Pan African basement rocks of granites, migmatites and biotite diorites (Njilah et al., 2007). Major, trace and REEs analyses of the Mount Oku lavas indicate that they are under-saturated and are characterized by high contents in alkalis ($Na_2O + K_2O$) of mostly more than 5. K-Ar age dating showed that volcanic activity in Mount Oku started about 31 Ma ago around Ndu (Marzoli et al., 2000). Njilah (1991) in Marzoli et al. (2000) further precise that this activity lasts up to 23 Ma in the Ndu area and progressed SW to Mount Bamenda 25-15Ma.

II.1.3- Anorogenic ring complexes

More than 60 anorogenic ring-complexes crop out along the continental sector of the Cameroon Line from Mount Cameroon to Lake Chad (Déruelle et al., 1991, 2007). Their distribution shows that they are abundant in the Tikar Plain (Njonfang et al., 2013). All the complexes have a typical alkaline character with trachytes and rhyolites commonly associated to plutonic rocks like syenite and granite (Déruelle et al., 2007).

Amongst these complexes, only a few have been well documented on the basis of their petrography and spatial distribution, these representative complexes are the Nda Ali, Pandé, Nigo, Mboutou, Kokoumi, and Ntumbaw (Njonfang et al., 2011).

The Nda Ali subvolcanic complex is situated in the South-West Region of Cameroon, precisely in the Mamfe basin and rises up to 1000 m. It is structurally controlled by NW- and NE-trending fracture systems (Déruelle et al., 1991; Njonfang et al., 2011). The plutonic rocks form a gabbro-diorite- monzonite-syenite alkaline suite, while volcanic rocks are made up of tephri-phonolite, nepheline phonolite, and dikes of phonolite and basanite with a predominance of alkali trachytes (Déruelle et al., 1991; Njonfang and Moreau, 1996; Njonfang et al., 2011).

The Pandé subvolcanic complex is a small (4.9 × 3.4 km), egg-shaped complex striking W-E and rising to 1231 m. It is also composed of both plutonic and volcanic rocks. Plutonic rocks form a syenite-granite peralkaline suite with syenites predominating over granite. Two

volcanic sequences are rhyolite and trachyte which respectively occupy the eastern border and the central parts of the pluton (Njonfang et al., 2011).

The Nigo complex is a large anorogenic plutonic complex, located in the north-eastern segment of the CL close to the Y-shaped split west of Ngaoundere (Kamdem et al., 2002). It has a height of 900 m above the surrounding surface of Panafrican basement and has a diameter of 7 km. It forms a gabbroic ring complex with hypersthene bearing monzonite to syenite intrusions in the center and is cut by basaltic and trachytic dikes.

The Mboutou complex is situated north of Cameroon and has a diameter of 5.5 km. It forms a gabbro-syenite-granite, suite where gabbros are dominant. Three types are recognized: titanomagnetite and ilmenite cumulates (melagabbros), layered olivine and clinopyroxene gabbros, and plagioclase cumulates (noritic leucogabbros) (Déruelle et al., 1991; Njonfang et al., 2011).

The Kokoumi anorogenic pluton belongs to the E-W Garoua rift structure, which represents the easternmost extension of the Benue trough (Ngounouno et al., 2001) and is composed of a plutonic gabbro-nepheline monzosyenite-nepheline syenite series and of lamprophyric (monchiquites and camptonites) and trachyte dykes. Gabbros include olivine-nepheline- and kaersutite-bearing gabbros. Monchiquites contain carbonate ocelli, and trachyte lacks ferromagnesian minerals. Nepheline syenites contain aegirine-augite, F-arfvedsonite and aenigmatite. With the exception of trachytes, all the rocks are nepheline normative (Ngounouno et al., 2001; Njonfang et al., 2011).

The Ntumbaw complex is situated in the NW Region of Cameroon and occupies a surface area of about 12 km^2. The complex is unique in the fact that it is mainly composed of intermediate rocks distributed within two centers (C1 and CII). The two juxtaposed centres are intrusive into the Pan-African basement and are partly covered by recent basaltic lava flows (Ghogomu et al., 1989). CI is composed of monzodiorite, monzonite and quartz monzonite while CII is made up of quartz syenite and syenogranite (Déruelle et al., 1991).

The Sabongari complex also known as Mba (Mount) Namboé culminates at 1595 m above sea level, with a height of 590 m above the Tikar plain. It is mainly made up of peralkaline granites in which riebeckite and aegirine constitute the mafic phases. The plutonic rocks are amphibole–biotite granite, pyroxene granite, diorite and monzodiorites, and subordinate syenites, while rhyolite is the dominant volcanic rocks of the complex, followed by trachytes and basalts. Undocumented basaltic and microgabbro dykes cross-cut orthogneiss and granite basements resepectively (Njonfang et al., 2013).

II.1.4- Origin of the Cameroon line

The origin of the CL is still under debate. Several models have been proposed, but there is no unique model that can singly explain the complex traits of the CL. Most of these proposed models are based on the geology, geochemical, structural, geophysical, and geochronological data.

II.1.4.1- Structural interpretations

The Cameroon Line is a complex volcanotectonic feature. Its magmatic evolution has been interpreted to be in relation with the development of tectonic structures, including the reactivation of structures in the Cenozoic (Moreau et al., 1987; Deruelle et al., 1991). However, if this were the case, the Central African Fold Belt (CAFB) which stretches from the Gulf of Guinea through Cameroon and extends to the Central African Republic would have formed a complete alignment of volcanoes without any gap between massifs of Mount Bambouto and those of the Ngaounderé Plateau. Thus, the existence of this gap between these two volcanic centers could be that, the basement tectonic structures only played the role of channeling magmas to the surface than in the generation of these magmas (Asaah et al., 2015). Given the similarity in the structural alignment of the Benue Trough, CL and the East African Rift System with its NE-SW extension in South Africa, a mechanism of episodic emplacement of alkaline magmas through the entire African continent could be presented in terms of the alignment of magmatic complexes, resulting from a complex interaction between hot spots and lithospheric fractures, including Precambrian faults during African plate motion (Ngako et al., 2006; Njonfang et al., 2011).

II.1.4.2- Displacement of the African plate

This model is fundamentally founded upon the fact that the Benue Trough and the continental sector of the Cameroon Line are similar in shape and size (Fitton, 1980; Deruelle et al., 1991). Both structures are Y-shaped and have been termed the "Y"-shaped hot zone (Fitton, 1980). According to Fitton (1980), there was a displacement of the African plate with respect to the asthenosphere, such that the hot asthenosphere which would have underlined the Benue Trough became displaced and was oriented beneath Cameroon and the Gulf of Guinea. This model suggests that, at about 70 Ma ago, the motion of the African plate over asthenosphere may have temporarily stopped before Africa resumed its anticlockwise motion, thus allowing the hot zone in the asthenosphere to establish itself as the developing Cameroon Line.

II.1.4.3- Hot spot, hot line

This model is based on the hypothesis that a fossil hot spot exists at the continent-ocean boundary (Halliday et al., 1990), and according to this "hot spot'' hypothesis, the magmatic activity along the CL could be related to an active plume with signature initiated in the deep mantle (Halliday et al., 1990; Deruelle et al., 2007), as the African plate movement over a stationary sub-lithospheric hot spot that was periodically fed and melted by a deep mantle plume head (Lee et al., 1994). The hot spot model cannot be retained as the possible origin of the CL due to the fact that, there is no systematic progression in the ages of volcanism for the rest of the Cameroon Line (Lee et al., 1994; Deruelle et al., 2007). Also, the youngest and only active volcano of the continental sector is Mount Cameroon, and is located at the south of the continental sector (Asaah et al., 2015).

For these reasons, an alternative model to explain volcanic alignments along the CL has been proposed and named the 'hot line'. This model supported by seismic and gravimetric data in the oceanic sector suggests that the CL may be the result of a linear mantle upwelling zone, or hot line, extending from NE to SW (Lee et al., 1994) independently supplying each volcano of the CL (Deruelle et al., 1991; Meyers et al., 1998).

II.1.4.4- Plate-wide swells

Burke (2001) suggested that a mantle plume (711 plume), which is located at latitude 7°N and longitude 11.5°E, could be responsible for the development of the CL. According to Burke (2001), this model generated the CL in three stages: (1) a position over the 711 plume for the past about 140 Ma; (2) a location adjacent to a right-angled bend of the continental margin for about 125 Ma; (3) and the establishment of a new platewide pattern of shallow-mantle convection at about 30 Ma when the African plate came to rest.

II.1.4.5- Edge convection and lithospheric instability

Recently, a new geophysical model based on seismic wave behavior has been developed to constrain the origin of the CL (Reusch et al., 2010). This model proposes an 'edge convection' model that is driven by lateral variations of lithospheric thickness. According to this model, lower temperatures in thick continental roots compared to those of the adjacent thinner lithosphere generate an edge 'down welling' which feeds an 'up-welling' beneath the thinner region (King and Ritsema, 2000). The structure of the CL, which includes the alternating horsts (main volcanic massifs) and grabens (plains), may support this model. In an attempt to improve upon the work of Reusch et al. (2010), a laboratory-based model called 'lithospheric instability', designed by Milelli et al. (2012), indicates that there may be instability within the sub-continental lithospheric mantle at the edge of a continent.

II.2- Characteristics of corundum and their deposits

This sub-chapter presents the general characteristics of corundum such as their morphology, physical and geochemical properties as well as economic aspects. It also presents information on the different types of deposits (primary and secondary), corundum occurrences in Cameroon and their characteristics (petrography, mineralogy, geochemistry and geochronology).

II.2.1- Characteristics of corundum

Corundum is a crystallized aluminum oxide (Al_2O_3) with 52.93% of Al and 47.07% of O) (Kündig et al., 2012). It is represented by sapphire and ruby varieties (Hughes, 1997). The oxygen atoms are organized in hexagonal closed packing with Al cations filling the interstitial octahedral sites (Fig.11). It crystalizes in the rhombohedral system, can take the forms of a rhombohedron, bipiramidal hexagonal or tabular crystals, and can be prismatic (Delaunay, 2004).

Corundum is mostly characterized by two common morphologies (Figs. 12a and b):

- a flat, tabular crystal habit with a hexagonal prism terminated at both ends by a basal plane with well-developed rhombohedral faces (Fig. 12a);
- a barrel shape displaying hexagonal bipyramidal faces terminated at both ends by a basal plane (Fig. 12b).

The former crystal habit is metamorphic dominant, while the latter occurs in both magmatic and metamorphic sapphires, but remains dominant in corundum of magmatic origin. The latter is also found to be common for corundum megacrysts, derived from host alkali basaltic rocks (Limtrakun, 2003; McGee, 2005).

Corundum is a gemstone used mostly in the jewelry industry for its beauty, durability, and stability. Beauty, a quality that varies among individuals, can be based on one or any combination of colour or lack of colour, luster and transparency. The beauty of the gemstone can also be enhanced by optical properties through cutting and fashioning by the lapidary. Durability is the resistance of the gemstone to damage and dependent upon physical properties, such as hardness and tenacity. Tenacity is the resistance to bending and breaking, while hardness is the resistance to scratch (corundum has a hardness of 9 on the Moh scale of hardness). Stability refers to the gem's ability to retain colour in spite of heat, light, or chemical assaults. The physical and optical properties of corundum have been summarized in Tables 2 and 3.

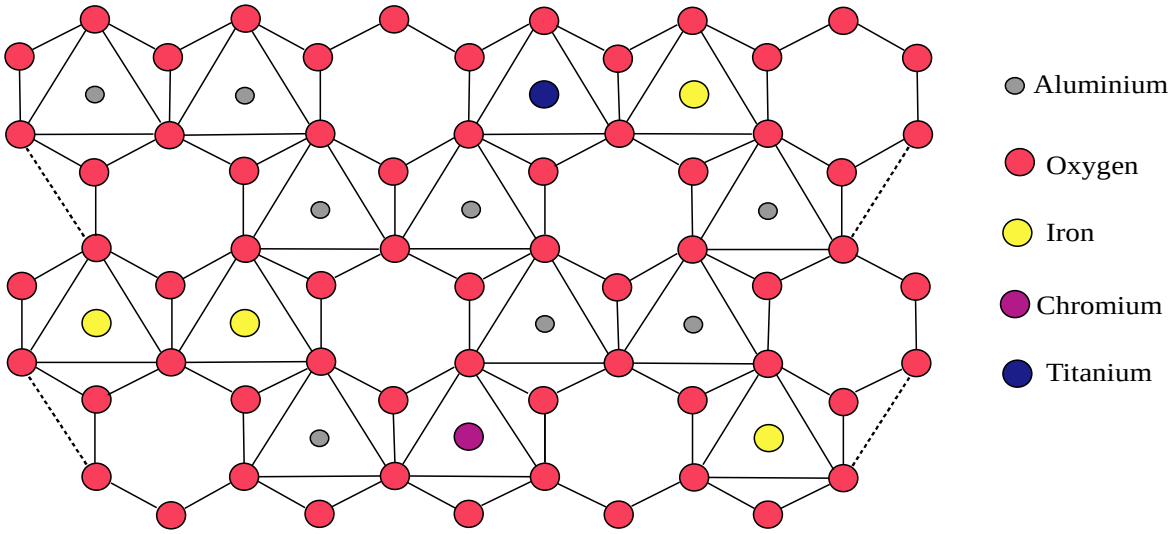

Figure 11: Crystal structure of corundum with the incorporation of chromophore cations (Natori, 1996 in Delaunay, 2004)

.

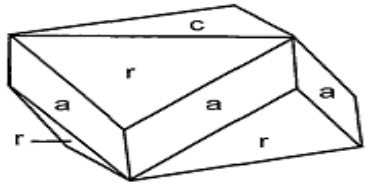

(a) Flat-shaped

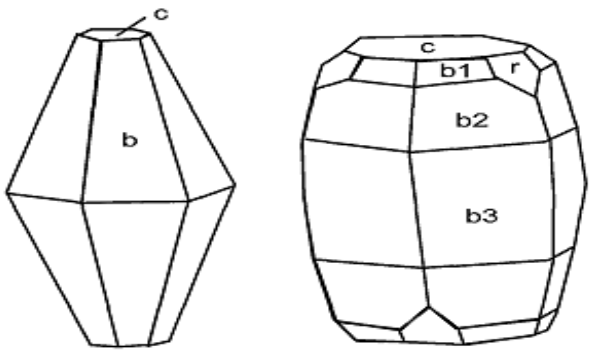

(b) Barrel-shaped

Figure 12: Crystal habit of corundum; (**a**) flat-shaped: is the metamorphic dominated habit, (**b**) barrel-shaped: is the magmatic dominated habit. *c*- pinacoid, *r*- rhombohedron, *a*- prism, *b*- bipyramidal. After Guo (1993) in Limtrakun et al. (2003).

Table 2: Physical properties of corundum (Walton, 2004).

Colour	Ruby: Red Sapphire: All other colours, frequently blue, but also, grey, yellow, green white and brown.
Streak	Corundum is harder than the streak plate. When scratched across a streak plate a white powder is produced (powdered streak plate).
Luster	Adamantine to vitreous.
Diaphaneity	Transparent to translucent
Cleavage	None. Corundum does display parting perpendicular to the c-axis.
Moh's hardness	9
Specific Gravity	3.9 - 4.1
Distinguishing characteristics	Hardness, high specific gravity, often found as six-sided hexagonal crystals that sometimes tapers into a pyramid, often with parting, high luster and conchoidal fracture.
Chemical composition	Al_2O_3
Crystal system	Rhombohedral system

Table 3: Optical properties of corundum (Walton, 2004).

Relief	Strong
Pleochroism	Strong showing thick blue to greenish blue
Refraction index	1.766 – 1.774.
Birefringence	-0.008 low compared to that of diamond.
Dispersion	0.018
Luminescence	Variable
Specific gravity	3.94 - 4.08

II.2.2- Trace element chemistry

Trace element chemistry is used to constrain the genetic environment of sapphires crystallization. It determines the elemental compositions and correlations between elements. It helps to classify corundum derived from basaltic terrains into metamorphic and magmatic suites in conjunction with mineral inclusions. The most contraining elements are Mg, Ga and Fe, due to their ablity to substitutions in the Al_2O_3 structure (Peucat et al.,2007).

Sutherland et al. (1998) suggested that metamorphic suites are characterized by high Cr and low Ga contents with Cr_2O_3/Ga_2O_3 ratios above 3, while magmatic suites display high Ga and low Cr contents with Cr_2O_3/Ga_2O_3 ratios below 1.

Peucat et al. (2007) used Ga/Mg ratio in conjunction with Fe concentration of 112 sapphires samples collected from 19 deposits of different geologic background throughout the world as a tool to discriminate between metamorphic and magmatic blue sapphires. Their study showed that Ga/Mg ratio is generally high (>10) for magmatic sapphires and low (<10) for metamorphic and metasomatic sapphires.

These discriminations are based on the fractionation of the Ga/Al ratio and of Mg in sapphires during crystallization. Magmatic sapphires usually have higher Ga/Al ratios than metamorphic sapphires. The low Ga/Al ratio for metamorphic sapphires is explained by the extraction of Ga from metamorphic rocks by circulating F-rich fluids during partial melting of granulites. During fluid circulation, F would complex with Ga to form GaF_6^{3-} ions that are extracted, leaving a restitic granulite depleted in Ga over Al (Whalen et al., 1987). Magnesium on its part is low in magmatic sapphires (<20 ppm) and high in metamorphic sapphires (>60 ppm).

Syngenetic mineral inclusions in sapphires can provide important information on the origin of their host corundum. For instance, mineral inclusions associated with magmatic sapphires are those of the columbite-group, zircon, spinel, rutile, and feldspar. These Nb, Ta, Zr, and Ti bearing mineral inclusions have been suggested to be derived from highly evolved felsic melts such as syenites (Sutherland et al., 1998; Coenraads et al., 1990; Pakhomova et al., 2006). On the other hand, undersaturated alkaline melts are usually characterized by mineral inclusions like plagioclase, nepheline, or calcite (Baldwine et al., 2016), olivine and pyroxene (Pakhomova et al., 2006).

Also, zircon inclusions sapphire can be dated to determine the ages of the host sapphires. For example, from the dating of zircon inclusions in sapphires, it has been demonstrated that the time of sapphire crystallization coincides with the time of basaltic volcanism in the area, thus suggesting a strong genetic relation between both events (Coenraads et al., 1990; Sutherland et al., 1998; McGee, 2005; Sutherland et al., 2009).

II.2.3- Colour variation

Colour variation in sapphirse has been attributed to the substitution of Al in its structure by trace elements like Fe, Ti, Cr, V and Ga. Amongst these elements, iron and titanium (Fe^{2+} and Ti^{2+}) are responsible for the blue colour of sapphire while chromium (Cr^{3+}) and minor vanadium (V^{3+}) are responsible for the red colour of ruby (Fléchet, 2007; Peucat et al., 2007). The substitution of Fe^{3+} into the lattice produces a yellow tint and combinations of the other impurities are responsible for the other colours like orange, green and purple.

II.2.4- Corundum genesis and deposits

II.2.4.1- Corundum genesis

Corundum is formed deep in the lithosphere in a regime of extremely high pressure and temperature. They are originally torn from the earth's crust by a magma generated from the mantle before being transported to the surface (Fléchet, 2007). It also crystalize in crustal magmatic, metamorphic and metasomatic regimes (Hauzenberger et al., 2003; Giuliani et al., 2007; Peucat et al., 2007; Simonet et al., 2008). Corundum is a very rare oxide which is only stable in alumina-rich and silica-poor rocks (Hauzenberger et al., 2003; Simonet et al., 2008), although a few exceptions have been reported in the corundum-quartz assemblages in hydrothermally altered quartziferous porphyry in the Bond Range (Tasmania) (Bottrill, 1998). In the presence of silica, Al is preferentially incorporated into aluminosilicate minerals such as feldspars and micas (Giuliani et al., 2014). Generally, factors that will allow or prevent the appearance of corundum are P, T, the protolith mineralogy and chemistry, the presence or absence of fluids, and their chemical characteristics (Simonet et al., 2008). Most corundum deposits are mined in alluvial and eluvial placers. Their occurrence as placers is due to their resistance to weathering, high hardness and specific gravity (Gerhard and Pat, 2006), which facilitates its concentration in surface environments Sutherland et al., 2002).

II.2.4.2- Geologic context of corundum mineralization

Corundum is rare because it requires an environment enriched in alumina and impoverished in silica. The presence of Cr, V, Fe, and Ti is necessary to substitute for Al in the structure (Giuliani et al., 2014). They can be hosted in different rocks type but two major geological environments are favorable for their formation (Peucat et al., 2007; Simonet et al., 2008; Graham et al., 2008):

- amphibolite to medium pressure granulite-facies metamorphic belts;
- alkaline basaltic volcanism in continental rifting environments.

In the amphibolite to medium pressure granulite facies metamorphic belts, P-T conditions to correspond to pressures above 3 kbar and to temperatures above 450 °C for 3 kbar and 550 °C for 7 kbar (Simonet et al., 2008). Favorable lithologies are alumina-rich and/or silica-poor rocks such as marbles, aluminous gneisses, mafic and ultramafic rocks, giving rise to deposits such as desilicated pegmatite, gneiss and skarn (Simonet et al., 2008; Giuliani et al., 2014). In the processes, the circulation of fluids and transfer of heat is favoured by the proximity of the rock to tectonic structures. Such deposits are encountered in the Pan African metamorphic belts such as

the Mozambique Belt, thus explaining the occurrence of a wide corundum province covering East Africa, Madagascar, and Sri Lanka (Giuliani et al., 2014).

The hosting of sapphires in alkaline basaltic volcanism of continental rifting environments is to be a two-stage process: the first stage involves the magmatic/metamorphic generation of corundum at crustal/mantle depths; and a second stage of alkaline intraplate basaltic incorporation and transport of the sapphire xenocrysts to the earth's surface (Sutherland et al., 1998). This indicates that the generation of corundum has to occur at levels higher than the magma generation. These processes are connected to the existence of a deep fracture system hat allows a rapid transfer of the melt from the mantle to the surface.

II.2.4.3- Geologic context

According to Giuliani et al. (2014), the distribution of corundum deposits worldwide is closely linked to collision, rift and subduction geodynamics. Three main periods of corundum formation are recognized. These periods include: the Pan-African orogeny (750 - 450 Ma), the Cenozoic alkali basalt extrusions (65 Ma - Quaternary) and the Cenozoic Himalayan orogeny (45 Ma - Quaternary).

In the Pan-African orogeny (750 - 450 Ma), primary ruby and sapphire deposits found in the gemstone belt of Eastern Africa, Madagascar, India and Sri Lanka are linked to the collisional processes between East and West Gondwana, during Pan-African tectonometamorphic events. The U-Pb zircon ages of deposits in these areas are between 612 to 510 Ma and 494 to 487 Ma, confirming corundum mineralization episode during the late Pan-African orogenic cycle.

In the Cenozoic alkali basalt extrusions (65 Ma -Quaternary), gem corundum occurs worldwide as xenocrysts incorporated in basaltic magmas during their ascent. Such sapphire and ruby deposits occur from Tasmania, Australia, in the South, through Eastern Australia, Southeast Asia and Eastern China to Far Eastern Russia. They are also found in Nigeria and Cameroon.

In the Cenozoic Himalayan orogeny (45 Ma - Quaternary), the marble-hosted ruby deposits in Central and Eastern Asia occur in metamorphic blocks that were affected by major tectonic events during the Cenozoic Indo-Asian collision. The Oligocene to Pliocene ages (40-5 Ma) obtained from ion probe U-Pb analyses of zircon inclusions in corundum are consistent with extensional tectonic events that were active from Afghanistan to Vietnam, in the ruby-bearing metamorphic belt.

II.2.4.4- Corundum type deposits

Corundum deposits can either be primary or secondary. Primary corundum deposits are those where the corundum is entrained inside the same rock where it crystallized. While in secondary deposits, corundum is an inherited mineral that formed in a petrogenetic setting different from where it is deposited either in clasts or as xenocryts.

Simonet et al. (2008) proposed a classification of gem corundum deposits, according to shared petrographic and genetic characteristics, taking into consideration primary and secondary deposits. This classification follows the principal rock classification into sedimentary, metamorphic and igneous types as illustrated in Fig. 13.

Primary deposits

In these deposits, corundum can crystalize from magmatic, metamorphic or metasomatic rocks with characteristic low silica and high alumina contents.

Magmatic deposits

Magmatic corundum has been described in plutonic rocks like syenite and rare monzonite to syenogranite compositions (Pakhomova et al., 2006). In these rocks, corundum occurs as an accessory mineral phase in the magmatic melt (Giuliani et al., 2014).

In syenite, blue sapphires have been reported in Mg-low and Ga-rich melt in Garba Tula (Central Kenya) (Simonet et al., 2004; Peucat et al., 2007). In this deposit, sapphire crystalizes in a syenite dyke of several metres thick. The dyke is composed of scattered black mica crystals in a coarse feldspathic matrix. It is cut by pegmatite veins consisting of feldspar, quartz, biotite and muscovite. Corundum and zircon are the main accesory minerals in the syenite dyke (Simonet et al., 2004, 2008). U–Pb geochronology on zircon crystals dated the dyke at 579 ±6 Ma, corresponding to the Barsaloian episode of the Mozambique Belt in Kenya (Simonet et al., 2004). This deposit is within ages of the Pan-African orogeny (750 - 450 Ma) deposits.

In the alkali-basaltoid volcanism of Central Vietnam, sapphires crystallized from a more fractionated iron-rich syenitic melt with the participation of CO_2 and CO_2-H_2O fluids in shallow crustal levels. The subsequent eruptions of alkali basalts favored the transport of garnet and pyroxene megacrysts as well as sapphire and zircon xenocrysts to the surface (Izokh et al., 2010).

Sapphires from Cerová Highlands, Western Carpathians (southern Slovakia) are secondary and occur as xenoliths in alkaline basalts. Its primary deposit is associated to well evolved melt of syenite/anorthoclasite composition (Uher et al., 2012).

Metamorphic deposits

Metamorphic rocks are a major source of high-quality corundum. In these rocks, it is relatively common and appears in a wide range of pressure and temperatures (Fléchet, 2007; Simonet et al., 2008). Three types of metamorphic deposits are considered: metamorphic deposits s.s, metasomatism deposits and anatectic deposits.

In metamorphic deposits s.s, corundum crystalizes as a result of isochemical metamorphic reaction in silica-poor or alumina-rich rocks. Deposits of this type include:

- gem corundum-bearing aluminous gneisses and granulites;
- ruby- bearing meta-limestones (marble);
- ruby-bearing mafic granulites.

An example of gem corundum-bearing aluminous gneisses and granulite exists in the Highland complex of Sri Lanka where corundum occurs in a biotite-silimanite gneiss. This deposit results from recrystallization and metamorphic differentiation which led to the formation of aluminium-rich, silica-poor bands in a semi-pelitic gneiss (Dissanayake et al., 2000). In the Mangari ruby deposit of SE Kenya, ruby is enclosed within a metasedimentary sequence dominated by sillimanite-graphitic gneisses associated with ultrabasic bodies. In this deposit, ruby occurs in lenses on the inner side of the contacts between the ultrabasites and the surrounding metasediments, and in veins within the ultrabasic bodies (Mercier et al., 2007).

Ruby-bearing meta-limestones (marble) can be exemplified with the marble-hosted rubies of Central Southeast Asia, located in the Himalayan Mountain Belt. These deposits present excellent quality ruby with intense colour and high transparency. They occur in Afghanistan, Pakistan, Azad-Kashmir, Tajikistan, Nepal, Myanmar, Northern Vietnam and Southern China (Garnier et al., 2008). Amongst other genetic models, Okrusch et al. (1876) in (Garnier et al., 2008), proposed the ruby formation to be a consequence of regional metamorphism in the amphibolite facies grade of calcareous rocks enriched in aluminum relative to silica, chromium and titanium. Such bulk rock chemistry may have resulted from lateritic weathering of an impure limestone, formed in a karst environment, before metamorphism (Garnier et al., 2008). Ruby hosted in grey marble has been reported in the Nangimali formation in Nanga Parbat Himaliya, Pakistan (Pêcher et al., 2002).

Ruby-bearing mafic granulites is described in Chantel, Central France (Forestier and Lasnier, 1969). In Northern Mozambique, corundum-bearing amphibolites associated with pargasite, spinel, and anorthite have been described in the Montepuez Complex within the Neoproterozoic Mozambique Belt (Fanka and Sutthirat, 2018).

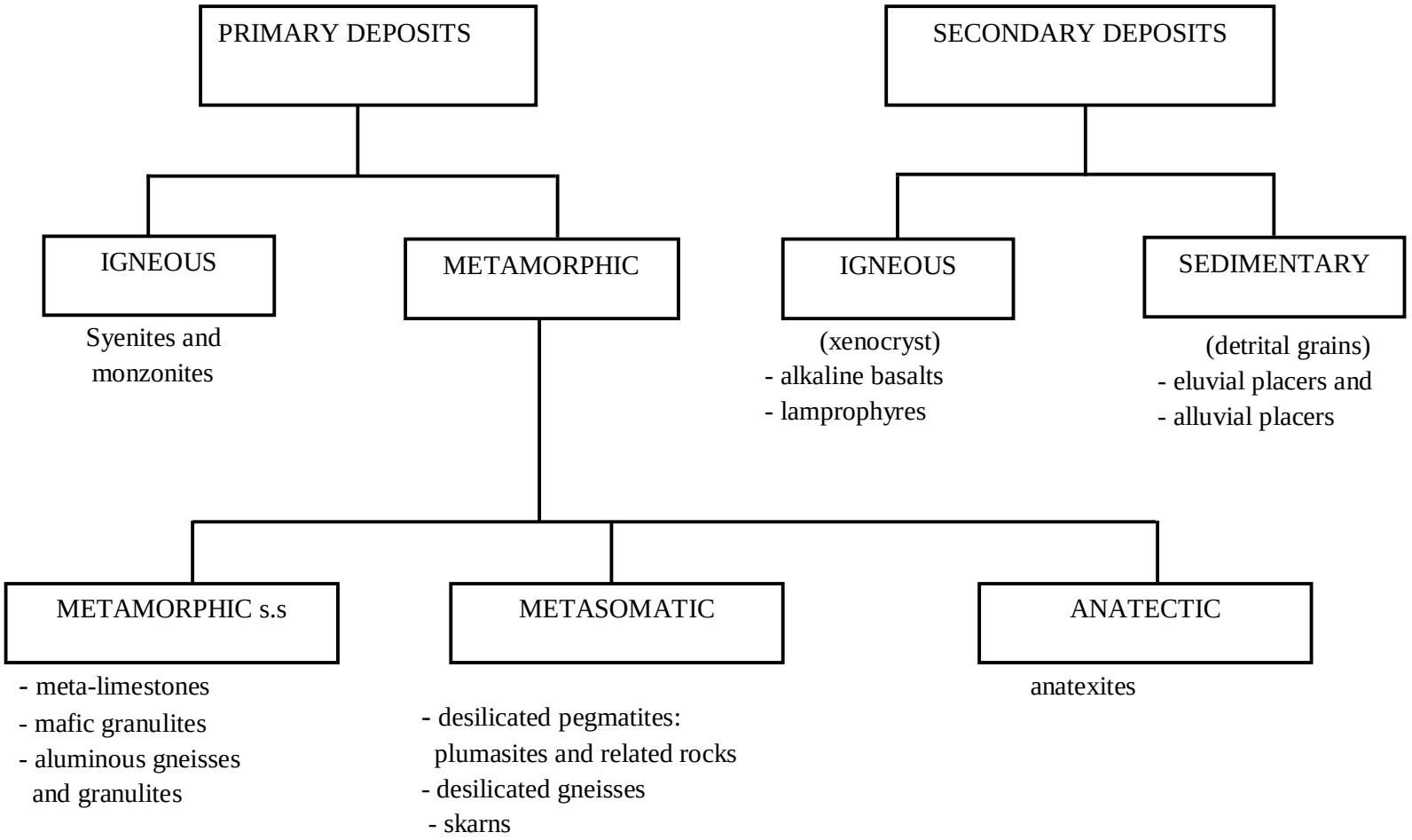

Figure 13: Classification scheme for gem corundum deposits (after Simonet et al., 2008).

In metasomatic corundum deposit formation (Figure 14), fluids are required for large scale metasomatic processes because they transport solutes by diffusion and more importantly by infiltration. In such systems, the dissolution and precipitation of minerals by crustal fluids control the location and size of ore deposits and other metasomatic rocks (Rohan, 2001). In the case of metasomatic corundum deposits, the silica-aluminous component undergoes a desilication. The silica is being pumped out by the silica-deficient unit leaving in place alumina which is less mobile to remain in the protolith and recrystallize as corundum. These deposits are formed through the introduction of fluids into tectonic structures or via contact metamorphism and are limited to restricted areas that can only extend to few meters (Baldwin, 2016). Deposits of this type include:

- desilicated pegamites, plumasites and related rocks (Fig. 14a);
- desilicated gneisses (Fig. 14b);
- corundum-bearing skarns (Fig. 14c).

Desilicated pegmatite corundum deposits have been described at the Meetiyagoda gem corundum deposit in Sri Lanka. They are associated with large pegmatites veins that crosscut metamorphic rocks (Dissanayake et al., 2000). In Greece, the central Naxos Island sapphire deposit is associated with desilicated granite pegmatites intruding ultramafic rocks. Sapphire occurs either within the pegmatites themselves or associated metasomatic reaction zones. Inclusions in corundums are: spinel and pargasite, margarite, zircon, apatite, diaspore, phlogopite and chlorite and chloritoid, ilmenite, hematite, ulvospinel and rutile (Voudouris et al., 2019).

Desilicated gneisses result from metasomatic alteration, including desilication, which affects felsic rocks that have been tectonically put in contact within ultramafites (Simonet et al., 2008). In the Sahambano deposit of Madagascar, sapphires occur in lenses of felspathic gneisses (Rakotondrazafy et al., 2008). In the North Atlantic Craton of Greenland, ruby is hosted by kyanite paragneiss and sillimanite gneiss in the Maniitsoq and Nuuk regions respectively. They are both associated with ultramafic rocks (amphibole-peridotite) that occur in direct contact with the ruby-bearing zones, which have been transformed to mica schist by metasomatic reactions (Yakymchuk and Szilas, 2018).

Skarns are contact metamorphic rocks composed of calcium, magnesium and iron silicate. They are derived from limestone or dolomite by the metasomatic introduction of large amounts of silicon, aluminium, iron and magnesium from a nearby igneous intrusion,

usually granitic. Desilication in skarns is initiated by the silica-deficient host rock. Corundum-bearing skarns have been reported at the Bakamuna deposit in Sri Lanka (Dissanayake et al., 2000).

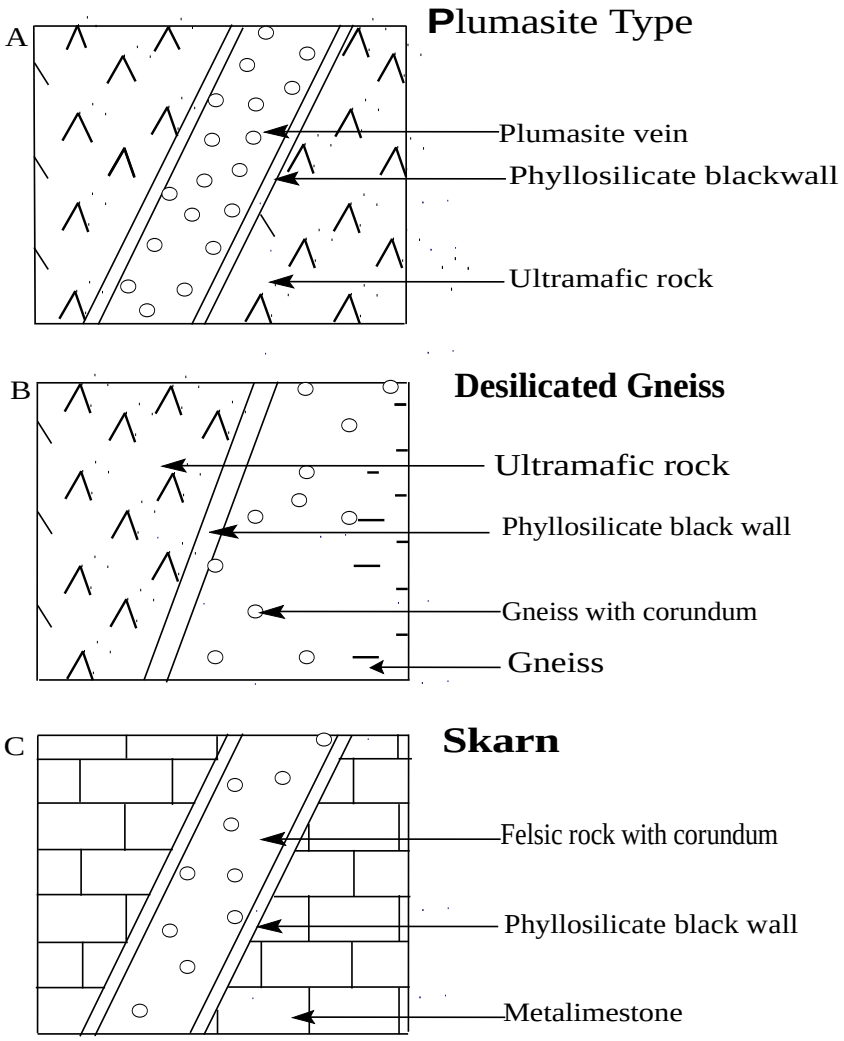

Figure 14: Schematic illustration of the main categories of metasomatic deposits (after Simonet et al., 2008).

Anatectic deposits result from anatexis process which indicates the partial melting of crustal rocks. During anatexis, differentiation as well as desilication processes may occur especially in alumina-rich rocks where corundum appears in the anatexis residues. During the melting of metapelitic rocks, silica enters the first melt, leaving an alumina-rich residue that may crystallize corundum (Baldwin et al., 2016). Deposits of this type are rare and are not mined in the hard rock for gem corundum, but likely contribute in supplying alluvial corundum deposits (Simonet et al., 2008). Corundum-bearing anatectic aluminous rocks

occur in the deeply subducted North Dabie complex zone of Central China. In this deposit, the rocks consist of corundum, biotite, K-feldspar and plagioclase. These rocks show clear macro- and micro-structural evidence of anatexis by dehydration melting of muscovite in the absence of quartz (Li et al., 2020).

Secondary deposits

In these deposits, corundum is present as an inherited mineral, either as a clast or a xenocryst, for which its primary origin is a rock different from its host. Thus, in sedimentary deposits, corundum is a clast of detrital origin, and in basaltic deposits, corundum is a xenocryst in the lava (Coenraads et al., 1990).

Sedimentary deposits

Sedimentary gem corundum deposits are the most represented and are formed from the weathering of pre-existing corundum-bearing rocks. Since corundum is resistant to weathering and has a high density, it turns to be concentrated in association with other heavy minerals by mechanical action of the transporting river or stream. They are concentrated in hydrographic traps and are either found as pebbles in gravel lenses or in lithified conglomerate (paleo-placer) (Giuliani et al., 2014). These deposits are either:

- alluvial corundum deposits;
- eluvial placer corundum deposits;
- paleo-placer corundum deposits.

Alluvial placer corundum deposits are the most widely represented in Australia, Thailand, Vietnam (Mercier et al., 1999), Sri Lanka (Dissanayake et al., 2000), Cameroon (Boaka et al., 2010; Kanouo et al., 2012a) and elsewhere in the world. Deposits of this type occur mostly in old stream terraces and flood plains and are characterized by well-rounded grains (Dissanayake et al., 2000).

Eluvial placer deposits are found on hill slopes and flat areas between valleys. Generally, eluvial deposits are usually not far from the source rock and often grade into alluvial deposit, rendering identification difficult. They are often characterized by the presence of rock fragments and the angular to sub-rounded nature of the corundum minerals are typical of eluvial beds.

Paleo-placer deposits are reworked sedimentary corundum deposits; they are characterized by different cemented mineral phases. In the Ilakaka-Sakaraha area of Madagascar, paleo-placers of corundum are known from alkali basalt deposits and is made up of facies like ferruginous pisoliths, limonite nodules, hematite and calcareous fragments cemented by carbonates (Rakotondrazafy et al., 2008).

Igneous deposits

The occurrence of corundum inside basalts is highly unexpected from a chemical point of view, reasons being that alkali basalts are undersaturated with respect to corundum, and alkali basalts are too rich in FeO and MgO for corundum to be stable (Baldwin and Ballhaus, 2018). Thus, in most basaltic fields, corundum is found as xenocrysts (Sutherland et al., 2002; Graham et al., 2008; Guo et al., 1996; Upton et al., 1999). In some basaltic flows, it is often characterized by corroded surfaces, indicative of disequilibrium with its transporting basaltic magmas (Coenraads et al., 1990).

Corundum in alkaline basalts

Corundum described as xenocryst in alkaline basalts has been reported in many deposits around the world (Levinson and Cook, 1994; Sutherland et al., 1998). It is suggested to be xenogenic and that alkaline basalts serve as transporters from different crustal and mantle sources (Izokh et al., 2010). Yui et al. (2006) demonstrated using oxygen isotopes that the sapphires from the Chanthaburi-Trat of Thailand are xenocrysts, brought up to the surface by nearby alkali basalts.

Corundum megacrysts come from placer deposits and represent eroded xenocrysts that were initially transported from underlying lithosphere by intraplate eruptives (Sutherland et al., 2009). The corundum crystal occurs in alkaline basalts which did not crystallize from the basaltic melt but were introduced into the melt from an external magmatic or metamorphic source. Deposits of this type exist in Eastern Australia and are linked to Cenozoic basaltic fields that erupted through granite-intruded Palaeozoic to Early Mesozoic fold belts (Zaw et al., 2006; Sutherland et al., 2009).

Lamprophyres deposits

A dark-coloured, strongly porphyritic, intrusive igneous rock, containing abundant euhedral phenocrysts of biotite and/or amphibole, accompanied by phenocrysts of olivine,

diopside, apatite, or opaque oxides, set in a mafic, felsic, or glassy groundmass. Lamprophyres corundum deposits are quite rare. They have been reported in the Yogo Gulch sapphire deposit in Montana, USA (Meyer and Mitchell, 1988). Sapphires are believed to be xenocrysts that were inherited from the metamorphic basement.

II.2.5- Corundum producing countries

Ruby and sapphire are perhaps the world's most widely sold coloured gemstones, accounting for approximately one-third of sales by value (BUZ Consulting, 2009, in Shor and Weldon, 2009). Shor and Weldon (2009) grouped corundum producing countries into:

- traditional or historic sources, made up of India (Kashmir), Burma (Myanmar), Sri Lanka and Thailand;

- newer major sources, made up of Australia, Madagascar and Vietnam;

- lesser producers, made up of Cambodia and Laos, China, Greenland, Kenya, Malawi, Tanzania, Pakistan, Afghanistan, elswhere in central Asia and the United States. Yager et al (2008) mentioned Cameroon, Nigeria and Nepal.

II.2.6- Corundum deposits in Cameroon

In Adamawa and South west regions, corundum is artisanally exploited in alluvial deposits in Mayo Kewol and Nsanaragati in (Boaka et al., 2010; Kanouo et al., 2008, 2012). While in the Northwest Region, new deposits have been discovered in Mayo Kila and Mbiame (Mbih et al., 2016).

Generally, corundum mineralizations in Cameroon has been attached to the general Pan-African tectono-metamorphic and tectono-magmatic events, characterized by the Central Cameroon Shear Zone and the Cameroon Line (Boaka et al., 2011). This is partly due to the fact that most identified corundum deposits are clustered along these major geologic structures (Fig. 15).

II.2.6.1- Mamfe corundum deposits

The Mamfe sedimentary basin has been described as a WNW-ESE trending half-graben in Southeastern Nigeria that extends into Southwestern Cameroon. It forms the southern-most part of the West and Central African rift system that resulted from the breakup and subsequent separation of South America from Africa during the Early Cretaceous

(Ajonina, 2016). It is also described as a small intra-continental basin that forms an arm of the Benue Trough of Nigeria (Ndip et al., 2018). This basin is believed to be composed predominantly of continental sediments with marine deposits, consisting mainly of conglomerate, arkosic sandstone, mudstone, limestone, and evaporites (Dumort, 1968).

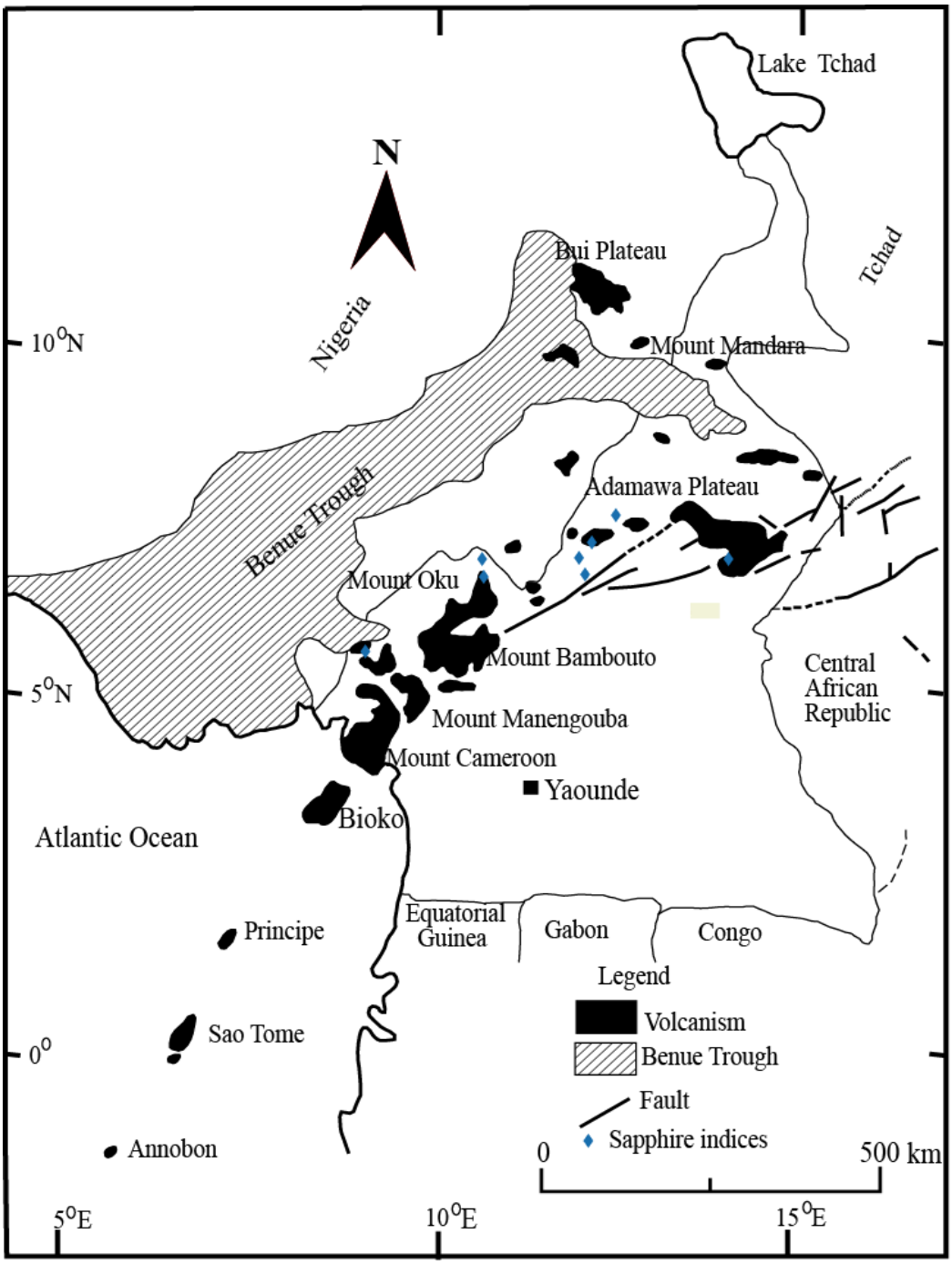

Figure 15: Sapphire deposits in Cameroon with data from Kanouo (2014) and Boaka (2018).

The basin is underlined by a Precambrian basement complex composed of granites, gneisses, syenites and migmatites (Dumort, 1968; Njonfang and Moreau, 1996), and extruded by basic and intermediate rocks of Tertiary age, composed of trachytes, phonolites, basalts, basanites and picro-basalts, (Dumort, 1968; Njonfang and Moreau, 1996; Kanouo, 2014). Important mineral indices in the basin are lead, zinc, rutile and sapphire (Kanouo et al., 2012b, c; Kanouo, 2014).

The sapphires are mostly pale to dark blue colour and occur in association with Zircon, tourmaline, kyanite, spinel and garnet (Kanouo et al., 2012c; Kanouo, 2014). The largest corundum sampled from its placers was 8 mm and weighed 4.5 carats. The estimated sapphire concentration in the deposits was 460 g/m^3 of the excavated gravel with 0.878 g of gem quality sapphire (Laplaine and Soba, 1967). The magmatic origin of these sapphires is indicated by their trace element contents: Fe (2496 - 4643 ppm), Ga (149 - 307 ppm), with low V (4 - 41 ppm) and Mg (2 - 42 ppm) (Kanouo et al., 2012c; Kanouo, 2014). Calculated trace element ratios show the following high ranges in Fe/Mg (96.8 - 1106.8), Fe/Ti (0.5 - 81.5), Ti/Mg (14.5 - 174.1) and Ga/Mg (6.2 - 89.3), and very low values in Cr/Ga (<0.01) (Kanouo et al., 2012c). The U-Pb analysis of detrital zircons from this placer yielded Th/U ratio range from 0.6 to 3, and $^{206}Pb/^{238}U$ corrected mean age gave 12.39 ±0.55 Ma, thus, characterizing an upper Cenozoic magmatic event.

II.2.6.2- Mayo Kewol corundum deposits

Mayo Kewol is situated between Mayo Banyo and Djerem Divisions. According to Baoka à Koul. (2018), the local geology is made up of plutonic and volcanic rocks. The plutonic rocks are granites, granodiorites, quartz monzonites, diorites, quartz diorites and gabbro, while the volcanic rocks are mostly alkaline basalts. The plutonic assembly is cut by basic and quartzo-felsparthic dykes, with part of the assembly presenting a gneissic and mylonitic structure underlying the deformation zone.

Sapphire mineralization is essentally alluvial and is associated with ruby, topaz, beryl, zircon, monazite, cassiterite, magnetite and ferrocolumbite (Baoka à Koul et al., 2010, 2011). The sapphires are mostly blue and their trace element analysis shows high concentrations in Fe (up to 4140 ppm), Ga (up to 420 ppm) and Ti (1960 ppm) and very low Mg (0 – 80 ppm), V (0 – 90 ppm) and Cr (0 - 130 ppm) (Baoka à Koul et al., 2011; Baoka à Koul, 2018). Most of these values are those of magmatic sapphires (Peucat et al., 2007; Sutherland et al.,1998). Their oxygen isotopic signatures $\delta^{18}O$ present values between 4.7 and 5.4‰, within the range

suggested by Giuliani et al. (2007) for sapphire from basaltic environment and magmas of syenitic composition.

II.2.6.3- Artisanal exploitation of sapphire in the study areas

Artisanal mining of sapphires in the localities of Mayo Kila and Mbiame is less developed compared to those of Adamawa plateau and the Mamfe basin, where this ativity has been identified as one of the key revenue generation tools. Contrary to these new deposits in the North-West Region, a clear value chain has been identified around the deposits of Adamawa plateau and the Mamfe basin. This value chain is made up of local artisanal miners, local retailers, retailers from other towns and Regions and foreign buyers from Sri lanka, Thailand, Nigeria and China.

In Mayo Kila, the low concentration of sapphires in the placers as well as lack of buyers has hindered the development of this activity as a key revenue generation tool. In this area, agriculture is preferred over sapphire exploitation and only few locals practice sapphire exploitation during breaks in farming seasons and during the arrival of a potential buyer. Figure 16 illustrates the digging and panning for sapphires in a river bed in Mayo Kila.

The intensity of this activity can be seen on figure 17, which shows a large surface area of abandoned pits. Before the outbreak of the Anglophone crisis, sapphire artisanal mining was gradually becoming a major revenue generation activity in Mbiame as most artisanal miners in this locality testified the selling of sapphires for up to 250 000 FCFA during their first week of exploitation. Due to the recent discovery of Mbiame sapphire placers, the area was gradually becoming a new destination for sapphire marketing in Cameroon, due to the high sapphire concentration in the placers. As a result of the ongoing crisis, most artisanal miners are stock with their products due to lack of buyers. The main problem of these artisans was the lack of best exploitation techniques to maximise production, the inadequate knowledge on sapphire grain evaluation and pricing and environmental issues due to abandoned pits. Exploition is mostly done in low land areas also used for cattle grasing, hence causing conflicts between cattle farmers and the artisanal miners. If this activity is well organized in this area, it can represent a major revenue generation tool.

Figure 16: A: Sapphire pitting, and **B**: panning in river beds in Mayo Kila.

Figure 17: Sapphire exploitation in Mbiame along the Mbven Placer. **A:** Pitting and water removal from pit, **B**: abandoned pits, **C**: Hand picking of sapphire, **D:** panned sapphire grains

II.2.7- Applications of corundum

Corundum is a raw material that is exploited for its optical, mechanical and chemical qualities and in jewelry for its gem properties like beauty, stability and durability.

- iIn antiquity, natural corundum was mined as emery (a mechanical mixture of corundum and magnetite), used in the manufacture of grinding and polishing compounds (Abdulrahman, 2017).
- Natural corundum abrasive is used in the fabrication of watche glasses and manufacture ceramics.

- Alumina powder is used as a refractory mineral for traditional, composite ceramics and for neoceramics due to its high temperature of fusion (T> 2000°C).
- Alumina has a high resistance to chemical attack and abrasion, high electric and mechanical resistance, is inert in reductive and oxidative atmospheres.
- Ruby and sapphire are highly used in the jewellery industry.
- Corundum as well as other gemstones are of special monetary significance in a number of developing economies in SE Asia and Africa where they account for a significant proportion of the gross domestic product, both in terms of mined rough and manufactured product (Graham et al., 2008).

Conclusion

The Cameroon Line (CL) is a linear chain of Cenozoic genetically related intraplate volcanoes and plutonic complexes. Its volcanic rocks are mostly basalts, basanites, trachytes and phonolites. More than 60 anorogenic ring-complexes out crop along the continental sector of the CL with compositions typical of alkaline magmas. Its origin can be drawn from a series of connected events, including mantle plumes and lithospheric structures.

The Cameroon Mobile Belt (Central African Fold Belt) is a megatectonic structure formed during the Neoproterozoic collision between the West African Craton and the Congo craton. In Cameroon, it is defined in three main geotectonic units: the Poli Group in the northern part, the Adamawa domain in the central part, and the Yaoundé Group that occupies the southern part.

In Cameroon, sapphire deposits are found in the Adamawa plateau, Mamfe Cretaceous basin, and in the North-West Region, new deposits are seen in Mayo Kila and Mbiame. These deposits are known to be aligned along the Cameroon Line. Sapphire mineralization in Cameroon occurs within the West Cameroon Domain characterized by Precambrian terrains.

The chapter that follows presents the materials and methods used in this study.

CHAPTER III

MATERIAL AND METHODS

This chapter presents a literature review, the materials and methods used to obtain field and laboratory data. The acquisition of field data includes field survey using field equipments and the acquisition of laboratory data with the aid of laboratory equipments as well as analytical techniques.

III.1- Literature review

A literature review was initially carried out from previous works on sapphire deposits, geology, and geographical setting of the study areas using maps of these areas. This was to better understand the geological and geographical settings of the areas. Amongst these documents, topographic and geologic maps of Mayo Kila (Nkambe) and Mbiame (Mount Oku area), obtained from the National Institute of Cartography (NIC), were exploited.

III.2- Field survey

Field surveys were carried out to observe the distribution of the corundum occurences and to understand the relationship between the mineralization and its surrounding host-rocks. It involved three main stages: explore the drainage system and the valley morphologies in Mayo Kila and Mbiame in order to identify the best zones of alluvial accumulation; detailed alluvial prospection; and geological reconnaissance in both areas.

Field works were carried out in the study areas between 2013 and 2016. After the drainage systems and relief features of the area were also closely observed, field work proceeded with alluvial prospection and geologic prospection, where outcrops of the different rock types were observed, described and sampled.

III.2.1- Geological prospection

Geological prospection was carried out in the study areas with particular attention to locate the primary source of corundum and other minerals within the igneous and metamorphic rocks that outcrops in the areas.

The method used in this field survey is similar to that described by Compton (2016), which consisted of exploring rock outcrops along road cuttings, footpaths, river beds, valleys and hill slops with the aid of GPS, compass-clinometers and geologic hammers. Rock outcrops were observed and their texture, mineralogy, structure, mode of occurrence and any

possible mineralization described. Rock samples were collected and their geographic coordinates recorded, this was later used to produce sampling maps of the study areas.

III.2.2- Alluvial prospection

Detailed alluvial prospection was done along rivers in the areas, the Bewende River in Mayo Kila and the Mbven River in Mbiame. During this phase, test pits were dug in point of high detrital materials accumulation along plains and meandering river valleys. Each pit was mapped and characterized based on the morphological properties of each horizon such as colour, structure, texture, particle size, thickness, depth and the nature of the bed rock. Each horizon was carefully sampled and stratigraphic profiles constructed and described. Parts of the samples from each horizon were washed and observed with the naked eye and hand lens for possible mineral identification. The mapped pits and other random sample points were later plotted on the drainage maps of the areas.

The pitting and sampling procedure were as follows, with the aid of a spade, gravel was dug from the river banks and active river beds, away from collapsed soil material. Before obtaining the gravel, the sterile part (clay, silt, sand and the pebble fractions) was removed and thrown on the bank about five (05) meters away from the digging point. Sufficient wet sediments were collected to yield the required amount of sediment, from several places along the length of the stream channel.

The gravel samples collected from these points were washed in a manner similar to that described by Lapworth et al. (2012) as follows:

- mud was removed from the gravel samples in the pan by successive washing. Washing was done through a 5 mm nylon sieve until the complete elimination of the fine (clay and silt) and very course (>5 mm) fractions;
- the washed wet gravel was passed through a coarse upper nylon sieve (2 mm gauge), and corundum and other minerals grains larger than 2 mm were isolated by hand picking;
- the <2 mm sediment fraction was passed through a lower nylon sieve with a 150 µm nylon mesh. The >150 µm fraction was retained and a portion panned to collect the heavy mineral concentrate;
- the <150 µm fraction of stream sediment was left to settle out and water decanted prior to collection. The collected sample was transferred into a nylon sample bag and allowed to air dry and was later packaged and labeled for further laboratory analyses.

In this study, about 5 kg per horizon of unwashed gravel (fresh gravel) was also collected, packaged and labeled for laboratory analyses.

III.3- Laboratory analyses

In the laboratory, stream sediment samples were analyzed for their particle size distribution (granulometry), heavy mineral occurrences and morphology, petrography, geochemistry and geochronology of sapphires grains. Surrounding rock samples of the study areas on their part were subjected to petrographic and geochemical analyses.

III.3.1- Analyses of host rocks outcropping in Mayo Kila and Mbiame

III.3.1.1- Petrography

Fresh rock samples collected in Mayo Kila and Mbiame were described and thin sectioned in the Institute of Geological and Mining Research, Nkolbisson, Yaoundé, Cameroon. The description of hand specimens was based on colour, structure, grain size, and mineralogical composition. The prepared thin sections were characterized under a polarizing microscope at the laboratory of Internal and Applied Geodynamics in the Department of Earth Science, University of Yaoundé I, Yaoundé, Cameroon. In this study, only one volcanic rock was encountered and sampled in Mayo Kila area, and the sampling of exclusively volcanic rocks in Mbiame area was simply due to their similarity with the U-Pb zircon inclusion age obtained for the Mayo Kila sapphires.

III.3.1.2- Geochemical analyses of fresh rock samples

Sixteen (16) fresh rock samples from the two study areas were analyzed for their major, trace and rare earth element contents at the Australian Laboratory Services (ALS) in South Africa. These analyses were performed on prepared rock powders of each rock type using two different analytical techniques. The Inductively Coupled Plasma-Atomic Emission Spectrometry (ICP-AES) was used to determine major elemental contents. The trace and rare earth element abundances were determined using Inductively Coupled Plasma-Mass Spectrometry (ICP-MS).

Fresh rock samples were cleaned with deionized water and subsequently crushed and powdered with an agate mill. 0.2g of each powdered rock was mixed with 0.9g of lithium metaborate ($LiBO_2$) and 0.6 g of boric acid (H_3BO_3). The obtained mixture was well stirred and fused in 1000°C furnace. The resulted solution was cooled and dissolved in 100 ml of 5% nitric acid (HNO_3). The obtained solution was analyzed with ICP-AES to determine the

major elemental contents (in wt.%). The trace and rare earth elements contents (in ppm) were obtained by analyzing the dissolved solution with ICP-MS.

III.3.2- Analyses of the placer materials

This presents aspects of sedimentological analyses which include particle size distribution and heavy mineral separation and the analyses of sapphire grains.

III.3.2.1- Sedimentological analyses

This consists mainly of the technique used to obtain the different particle fractions from gravelly layers and that was used for heavy mineral separation.

III.3.2.1.1- Grain size distribution analyses

The washed samples from the field were oven dried at a temperature of 110°C for 24 hours, after which a precision electric scale was used to weigh 350 to 1950g of the different samples. Each weighed sample was passed through a series of AFNOR standardized sieves columns, with diameters of: 50 mm, 40 mm, 35 mm, 20 mm, 15 mm, 10 mm, 6.5 mm, 4 mm, 2.5 mm, 2 mm, 1.6 mm, 1mm, 0.8 mm, 0.5 mm, 0.4 mm, 0.135 mm, 0.2 mm and 0.1 mm. The sieves were mounted in column on an electromagnetic shaker. The refuse retained by each sieve was weighed, packaged and labeled. The simple and cumulative weights of these refuse were used to plot their representative cumulative curves. The cumulative percentages permitted the calculations of deviation quartile and the Trask Sorting Index (So). This analysis was done in the «Laboratoire d'Analyse des Materiaux» (LAM), of the Local Materials Promotion Authority (MIPROMALO), Yaoundé, and the laboratory of metallogeny, Department of Earth Sciences, University of Yaoundé I, Cameroon.

III.3.2.1.2- Analyses of heavy mineral concentrates

The study of heavy minerals was done in the Laboratory of Geosciences of Superficial Formations and Applications, Department of Earth Science, University of Yaoundé I, Cameroon.

Sample preparation

Sample preparation and separation followed standard procedures as described by Mange and Maurer (1992). Before separation, sample treatment involved: acid digestion to eliminate carbonates, and washing with water to dissolve soluble salts; removal of organic

substances; freeing the grains from adhering clays or iron oxide coating, and sieving to extract the required grain size. After particle size separation using sieves of different mesh diameters, fractions of >315 µm were used for heavy mineral analysis. The <315 - 200 µm and 100 - 63 µm fractions were subjected to heavy mineral separation.

Separation

Two methods were used to separate heavy minerals in this study, namely the gravity separation method and the magnetic separation method.

Through gravity separation, the <315 - 200 µm and 100 - 63 µm fractions together with the panned concentrates were used for heavy mineral analysis by gravitational settling in bromoform (density 2.89g/cm^3), using the funnel technique. By this method, 10g of each dried and weighed sample was carefully introduced into a separating funnel, filled with the heavy liquid (bromoform). The pouring of these samples was often accompanied by continuously stirring to avoid thorough wetting of the grains. Heavy minerals sink to the bottom of the funnel, just above the pinch clip. This mixture was allowed for 6-8 hours, until complete sinking of all the heavy mineral grains, after which the pinch clip was slowly opened to pour the settled heavy fraction into a lower funnel equipped with a filter paper. The collected heavy fraction was further washed with alcohol at 95% to eliminate traces of bromoform. After separation, the heavy minerals were mounted on a glass slide using Canada balsam. The solidified slides were used to prepare polished thin sections for microscopic observation.

Magnetic separation was done by the use of a bar magnet that was passed over the concentrate to separate magnetic heavy minerals from non-magnetic minerals.

III.3.2.1.3- Macroscopic and microscopic description of heavy minerals

The coarse grain heavy minerals were observed, characterized and quantified under a binocular loupe and microscope. Each grain was characterized using parameters such as colour, degree of transparency, grain size, fracture, shape, luster, degree of roundness. These observations were done following methods similar to those described by Mange and Maurer. (1992). These observations were done in the Department of Earth Sciences of the University of Yaoundé I, Cameroon.

The separated fine grain fraction of the heavy minerals was used to prepare thin sections which were characterized under the polarizing microscope, based on parameters such as colour, shape, pleochroism, relief, extension angles and grain size.

III.3.3- Sapphire analyses

Grain morphologies were observed and described as well as the geochemical analyses and the U-Pb dating of zircons inclusions in the studied sapphires. Only sapphire grains from Mayo Kila were analyzed for trace elements and zircon inclusion dating. This was due to the fact that this study was initially planned only for the Mayo Kila sapphires discovered in 2008. The age obtained from the zircon inclusion in the sapphires were similar to those of mafic volcanic rocks found in the Oku Massif. Hence, with the aim to study the mafic volcanic rocks and compare them with other sapphire hosted mafic volcanic rocks around the world, an interesting placer sapphire occurrence was discovered in Mbiame, west of the Oku Massif. Nonetheless, at the time of this discovery, the finances of the project were not enough to carry out other analyses on the sapphires.

III.3.3.1- Analyses of sapphire external morphology

Sapphire grains were observed under a binocular microscope and classified with respect to their colour, degree of transparency, grain size, fracture, shape, form (degree of roundness), lustre, wearing and brightness. These observation and classification were done in the Department of Earth Science of the University of Yaoundé I, Cameroon.

III.3.3.2-Trace element geochemistry

A total of nineteen (19) sapphire grains from the Mayo Kila gem bearing alluvial materials were analyzed for trace elements quantification at the ARC Centre of Excellence in Ore Deposits, University of Tasmania, Australia using the LA-ICP-MS (Laser Ablation-Inductively Coupled Plasma Mass Spectrometry). The analytical procedures were similar to those described in Zaw et al. (2006), Kanouo et al. (2012c, 2016), with each grain being spotted in core and rim. Polished and mounted corundum was analyzed under standard procedures, using a New Wave UP-213Nd: YAG Q-switched Laser Ablation system coupled with the Agilent HP 4500 Quadrupole ICP-MS. The international standard NIST 612 was used as the primary standard to calculate concentrations and correct for ablation depth. The basaltic glass BCR-2 was used as the secondary standard. Figure 18 shows the locations of trace element analyses on the sapphire grains.

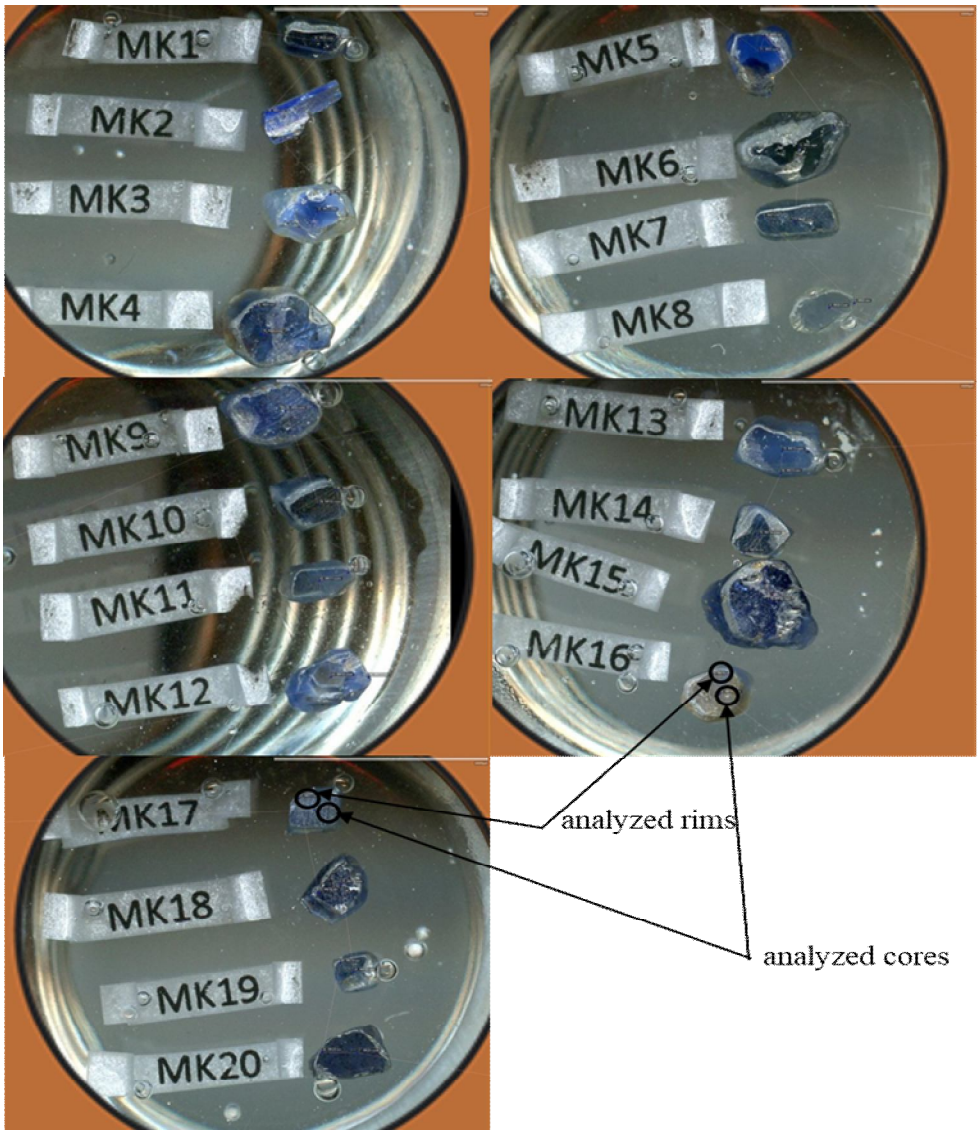

Figure 18: Samples analyzed for trace elements and their analysis locations.

III.3.3.3- U-Pb Zircon dating

Six trace elements (U, Th, Hf, Ti, Fe and Pb) were quantified in zircon inclusions found in two sapphire grains (MK6 and MK11). The analysis was carried out by LA-ICP-MS at the ARC Centre of Excellence in Ore Deposits. This same technique was used to date these inclusions. Corundum mounts were polished to expose the inclusions before the trace element quantification and U-Pb dating. They were then cleaned in distilled water in an ultrasonic bath and mounted on a double sided sticky tape on an epoxy block for analysis.

Zircon inclusion analyses were performed on an Agilent 7500cs quadrupole ICPMS with a 193 nm Coherent Ar-F gas laser and the Resonetics S155 ablation cell. The down hole fractionation, instrument drift and mass bias correction factors for Pb/U ratios on zircons

were calculated using two analyses on the primary (91500 standard of Wiendenbeck et al., 1995) and one analysis on each of the secondary standard zircons (Temora standard of Black et al., 2003 and JG1 of Jackson et al., 2004), analyzed at the beginning of the session and every 15 unknown zircons (roughly every 1/2 hour) using the same spot size and conditions as used on the samples. Additional secondary standards such as The Mud Tank Zircon of Black and Gulson (1978), Penglai zircons of Li et al. (2010), and the Plesovice zircon of Slama et al. (2008) were also analyzed. The correction factor for the $^{207}Pb/^{206}Pb$ ratio was calculated using large spots of NIST610 analyzed every 30 unknowns and corrected using the values recommended by Baker et al. (2004).

Each analysis on the zircons began with a 30 seconds blank gas measurement followed by a further 30 seconds of analysis time when the laser was switched on. Zircons were sampled on 32 micron spots using the laser at 5 Hz and a density of approximately 2 J/cm^2. A flow of He carrier gas at a rate of 0.35 litres/minute carried particles ablated by the laser out of the chamber to be mixed with Ar gas and carried to the plasma torch. Isotopes measured were ^{49}Ti,^{56}Fe, ^{90}Zr, ^{178}Hf, ^{202}Hg, ^{204}Pb, ^{206}Pb, ^{207}Pb, ^{208}Pb, ^{232}Th and ^{238}U with each element being measured every 0.16 s with longer counting time on the Pb isotopes compared to the other elements. The data reduction used was based on the method outlined in detail in Meffre et al. (2008); and Sack et al. (2011) similar to that outlined in Black et al. (2004) and Paton et al. (2010). Element abundance on zircons were calculated using the method outlined by Kosler (2001). Zircon was used as the internal standard element, assuming stoichiometric proportions and using the NIST610 to standard correct for mass bias and drift. Figure 19 shows the locations of zircon Pb/U age analyses on the sapphire grains.

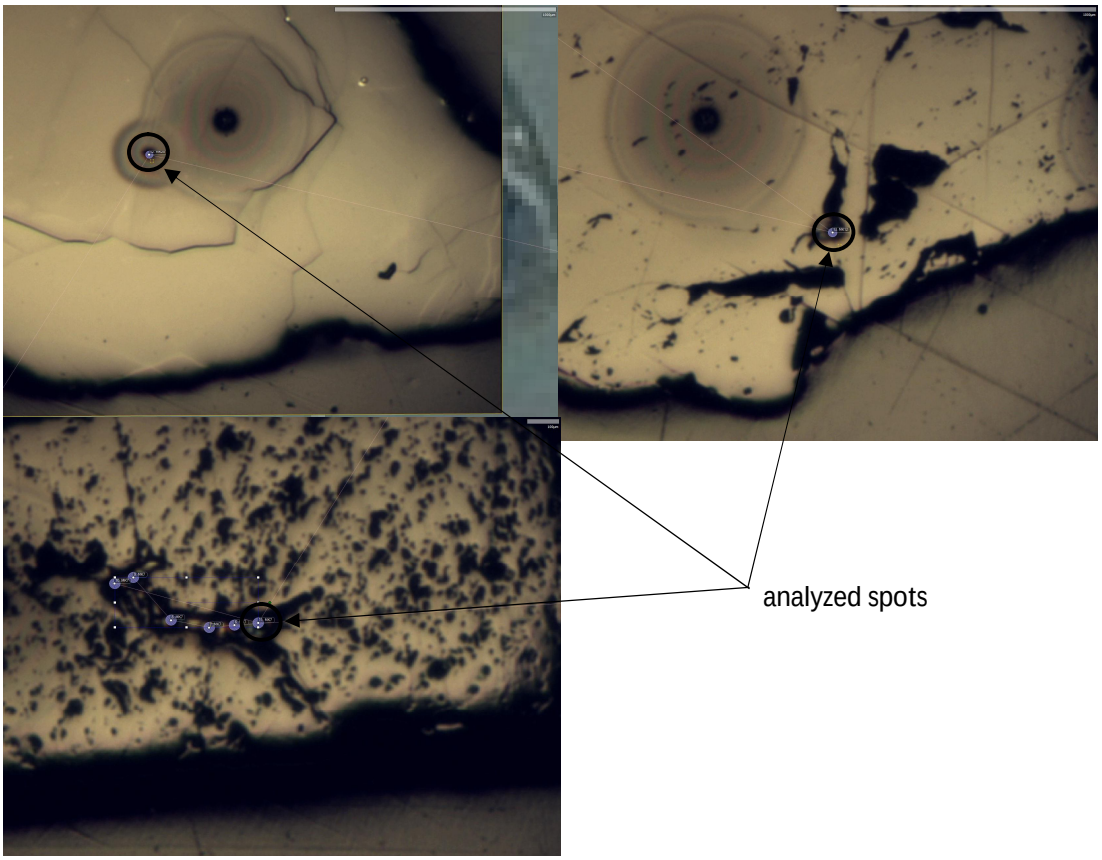

Figure 19: Zircon Pb/U age analysis locations.

Conclusion

The geological study of sapphire occurrences in Mayo Kila and Mbiame was done both in the field and in the laboratory.

On the field, alluvial prospection was done along the Bewende and Mbven rivers in Mayo Kila and Mbiame respectively. Stream sediments and lithified clastic materials were sampled in both areas. The search for the primary source of sapphires was done through geological prospection of host rocks outcropping in the areas.

In the laboratory, research works consisted of the analyses of the placer materials and sapphire grains. The placer materials were analyzed for their particle sizes, heavy mineral contents, macroscopic and microscopic characteristics. Sapphire grains were analyzed for its trace element contents and its zircon inclusion age using LA-ICP-MS. Outcropping host rocks were analyzed for their major, trace and rare earth element contents using ICP-AES and ICP-MS.

The next chapter presents the morphological, geochemical and geochronological characteristics of Mayo Kila and Mbiame gem placers materials as well as those of the surrounding rocks.

PART II

RESULTS

CHAPTER IV

PETROGRAPHIC AND GEOCHEMICAL CHARACTERISTICS OF ROCKS IN MAYO KILA AND MBIAME

This chapter presents field relationships and petrographic results for sedimentary, volcanic and plutonic rocks outcropping in Mayo Kila and Mbiame. To these data, are added complete geochemical results of targeted volcanic and plutonic rocks in the study areas.

IV.1- Field description and petrographic features of rocks

IV.1.1- Rocks in Mayo Kila

The area is characterized by high volcanic mountains with altitudes that range from 900 m to 1556 m. Generally, field observations present magmatic rocks and detritic materials of cobble and pebble size fragments that represent the alluvial materials. The magmatic rocks are made up of a dominant plutonic unit represented by granitoids (≈95 %) and a volcanic unit represented by mafic lavas (≈5%). Twelve (12) rock samples were collected at different points and labeled MK for petrographic and geochemical analyses. The sample points are plotted on the geologic map (Fig. 20).

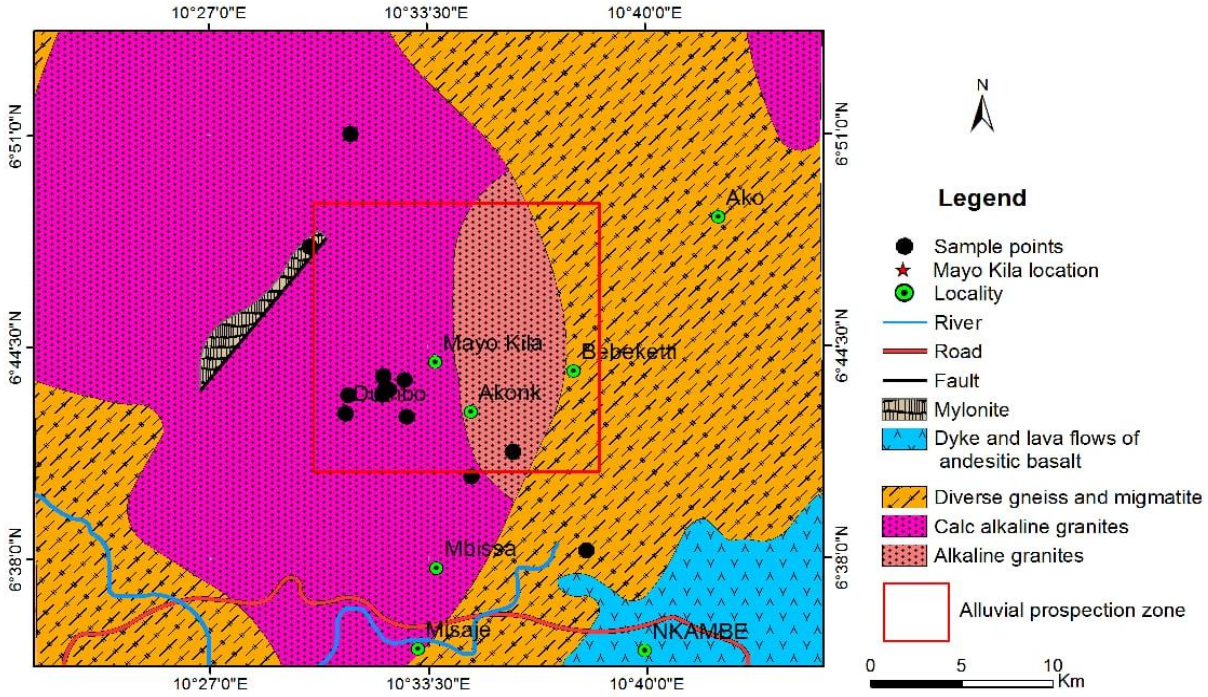

Figure 20: Sampling map of Mayo Kila (after Peronne, 1969).

IV.1.1.1- Alluvial materials

These clastic materials are made up of rock fragments of mostly cobble and pebble sizes, observed in almost all river beds and flats in the area. They are dominantly composed of granite and quartz (Fig. 21), and very few mafic rock fragments. These rock fragments vary in size from few millimeters to more than fifteen centimeters. Their colour varies with the different rock types. Granites are the most represented (about 85%) and vary from white, pink to grey. They are highly weathered and present granular porphyritic textures. Quartz fragments are also represented (about 10%) and vary in colour from white, grey, pink to violet with very smooth surfaces. Basaltic fragments are very rare (less than 5%). They are dark and massive and mostly seen as floats. The rock fragments have various shapes from well rounded, rounded to angular. With the exception of quartz fragments, most of the rock fragments show deeply weathered surfaces.

Figure 21: Cobble and pebble size clastic materials on river beds.

IV.1.1.2- Volcanic unit

Field relationships

This is represented by a massive dark coloured mafic volcanic rock that occupies less than 5% of the entire lithological units of the area. It outcrops as a dyke within granite on hill top at latitude N06°42' 313" and longitude E010°32' 531" with an altitude of 1224 m.

Classification

The unique mafic volcanic rock sample (MK07) collected in Mayo Kila was plotted in basanite domain on the igneous rock classification diagram of Le Maitre et al. (2002), figure not included.

Petrography

This paragraph describes the hand specimen and thin section of the basanite sample identified from the Total Alkaline Silica classification diagram of Le Maitre et al. (2002).

Basanite

On hand specimen, the basanite sample is a dark massive rock with a microlitic texture. Under the microscope, the sample (MK07) presents a fluidal structure characterized by the orientation of plagioclase (Figure 22). The mineralogical composition is made up of plagioclase (≈70 vol.%), olivine (≈14 vol.%), clinopyroxene (≈11 vol.%), opaque oxides (≈4 vol.%) and less than 1% of volcanic glass.

Olivine occurs both as microcrystals and microphenocrystals. Its crystals are mostly euhedral to sub hedral with sizes up to 0.3 mm. It has a high relief and most of the crystals are weathered to idingsite and are characterized by a brownish coating along cracks.

Plagioclase also occurs as microlites and microphenocrystals, with its euhedral crystals that form well oriented elongated laths of up to 1 mm long. Its relief is low.

Clinopyroxene crystals are light brown and occur mostly as microcrystals with sizes of about 0.2 mm. They are mostly subhedral with a high relief.

Opaque oxides have sizes of about 0.08 mm. They mostly occur in contacts with olivine and pyroxene crystals.

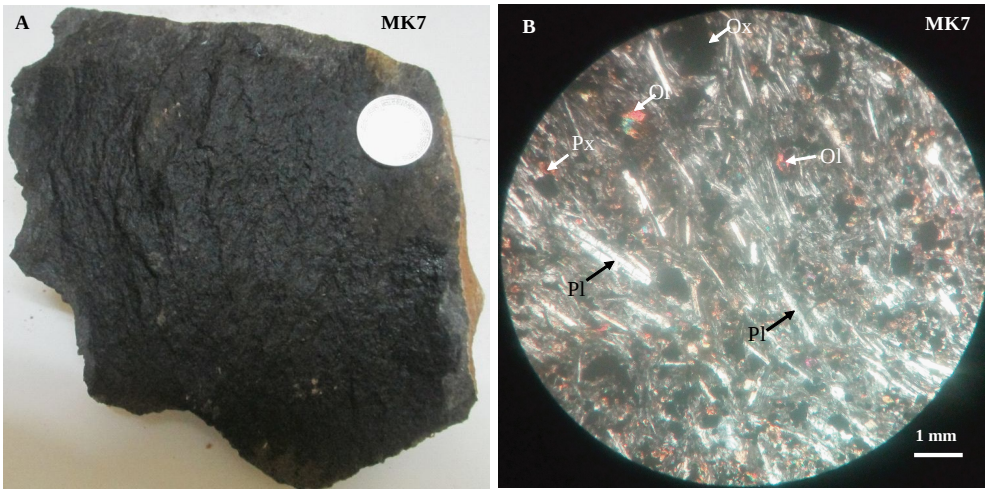

Figure 22: Macroscopic and microscopic aspects of Mayo Kila basanite. A: hand specimen of basanite (MK7), B: photomicrographs (XPL) of basanite (MK7). Pl: plagioclase, Ol: olivine, Px: pyroxene, Ox: oxide.

IV.1.1.3- Plutonic unit

Field relationships

Plutonic rocks in Mayo Kila are mainly made up of different facies of granitic rocks, followed by quartz veins. On the basis of mineral grain size and colour, medium to coarse grained facies were observed in the field, with colours that vary from pink to grey. The rocks outcrop mostly on hills and hill slopes and along river beds. These granitic rocks outcrop as domes, tors, slabs, ball and block-like forms (Fig. 23). Some of the tors can go as tall as three meters high (Fig. 23 B) and the blocks vary between 0.5 meters to 2.5 meters (Fig. 23 D).

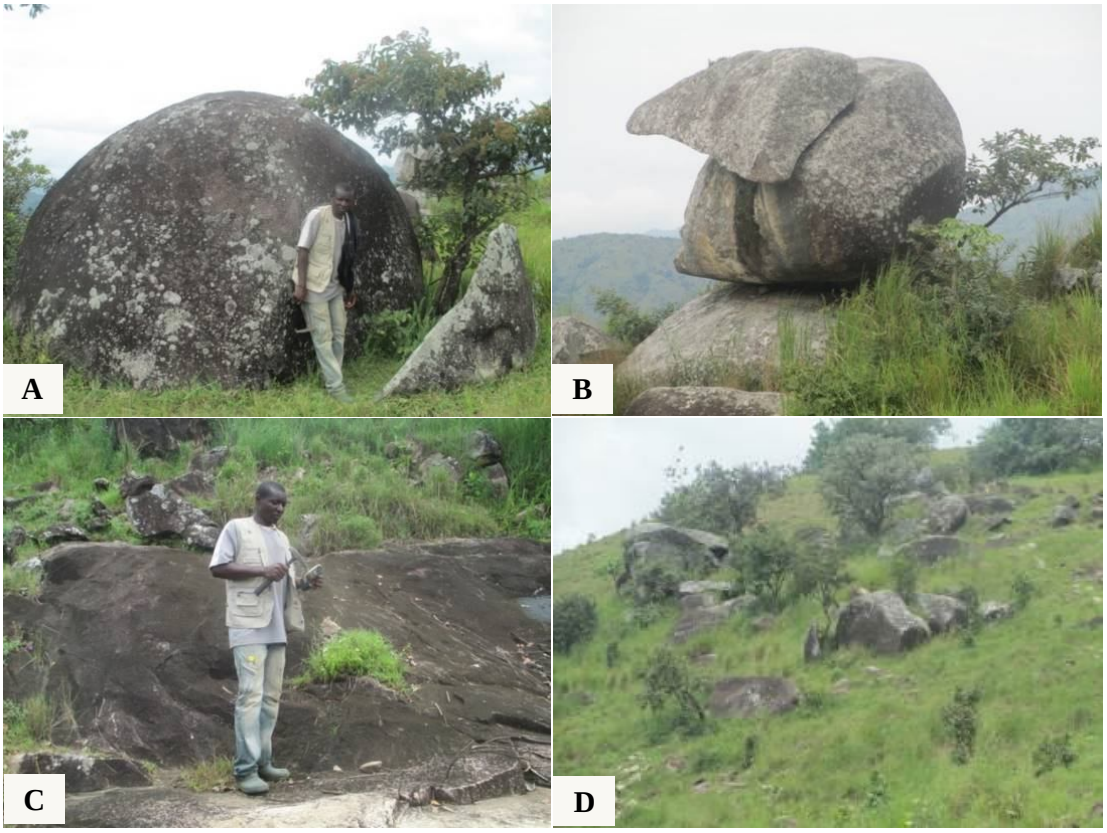

A: Dome - like granitic outcrop **B**: Granitic tors

C: Slab - like granitic outcrop **D**: Granitic blocks

Figure 23: Different modes of occurrence of plutonic rocks in Mayo Kila area.

Classification

The rock samples collected from the plutonic unit in Mayo Kila were plotted on the Total Alkaline Silica (TAS) classification diagram of Cox et al. (1979). They correspond to granite (MK01, MK03, MK04, MK08 and MK09), diorite (MK11 and MK12) and monzonite (MK10) (Figure 24).

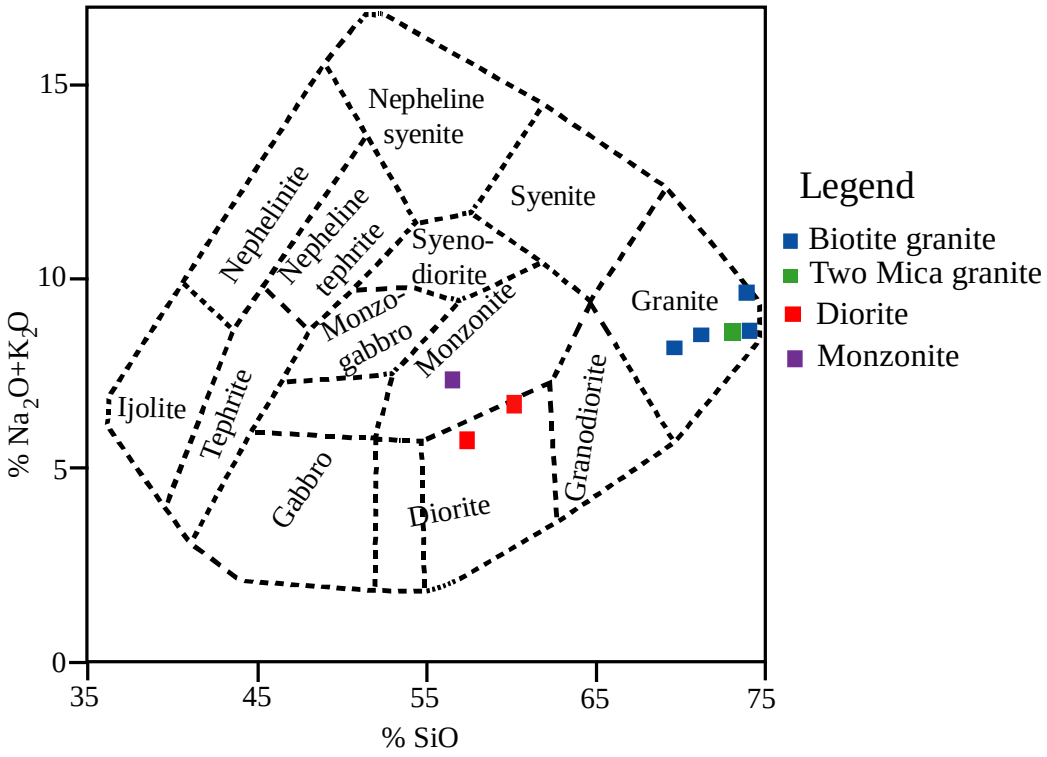

Figure 24: Classification of Mayo Kila plutonic rocks using the Total Alkali Silica (TAS) diagram of Cox et al. (1979).

Petrography

Fine grained diorite

The rock out crops mostly as domes on hills and hill slopes and as slabs along seasonal river beds. The rock shows alternations of light and dark bands (sample MK12). The light bands are quartzofelpathic while the dark bans are ferromagnesian (Figure 25).

Under the microscope, it is made up of plagioclase (40 vol.%), biotite (30 vol.%), hornblende (25 vol.%), quartz (5 vol.%), and opaque minerals (less than 1%) of the entire rock. They are slightly deformed and presents a preferred orientation of minerals.

Plagioclase occurs as euhedral rectangular laths, with lengths of approximately 0.5 mm and widths of about 0.2 mm. It is characterized by pronounced polysynthetic twining. It occurs mostly as phenocrysts and presents a weak to moderate relief.

Biotite occurs as elongated euhedral flakes, with microphenocrystals of up to 1mm long. In some places, biotite flakes contain inclusions of opaque oxides and are replaced by greenish chlorite along cleavage planes.

Hornblende occurs as euhedral crystals of about 0.6 mm, characterized by two cleavages on their basal sections. It has a high relief.

Quartz occurs as large anhedral crystals with sizes of about 0.5 mm. Most grains display an undulating extinction with a weak relief and sometimes occur as small inclusions in plagioclase (myrmekites).

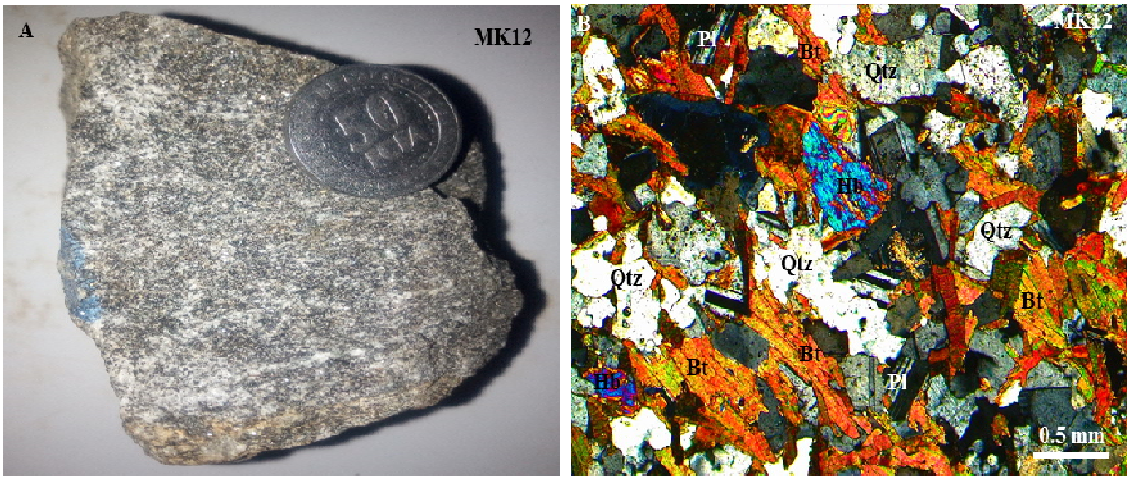

Figure 25: Macroscopic and microscopic aspects of Mayo Kila fine grained diorite. A: Hand specimens of fine-grained diorite, B: Granular texture (XPL) and minerals composition, Qtz: quartz, Pl: plagioclase, Bt: biotite, Hb: Hornblende.

Coarse grained diorite

These rock crop out in a dome form about 3 km NE of Dumbo village, between latitudes N06°43'36" and N06°42'27" and longitudes E010°32'06" and E010°31'03", at an altitude of 912 m. They portray a granular to granular porphyritic texture (Fig. 26).

Under the microscope, it is made up of plagioclase (25 - 35 vol.%), amphiboles (15 - 30 vol.%), biotite (≈20 vol.%), quartz (5 - 10 vol.%), microcline (2 - 5 vol.%), secondary muscovite (≈1 vol.%). Opaque minerals in all the samples are less than 1%.

Plagioclase occurs as euhedral crystals of rectangular laths. Its sizes vary in length between 0.9 and 2.5 mm, with widths between 0.3 to 06 mm. They are marked by polysynthetic twining. They mostly occur as phenocrysts and host quartz inclusions. Some grains are sericitized, with secondary muscovite replacements in few crystals (Fig. 26 B).

Hornblende occurs as euhedral to sub hedral crystals with sizes of about 2 to 5 mm and are characterized by their two cleavage basal sections. It has a strong relief.

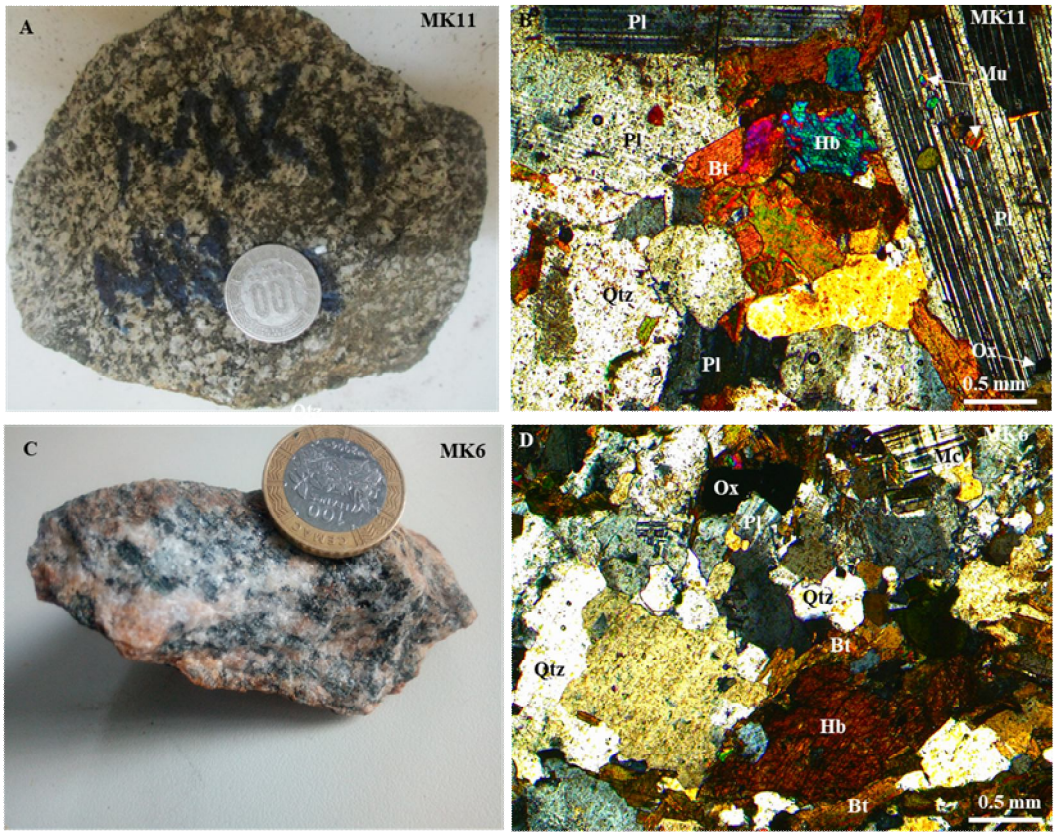

Figure 26: Macroscopic and microscopic aspects of Mayo Kila coarse grained diorite. A: coarse grained diorite hand specimen (MK11) B: Granular texture of coarse grained diorite (MK11), C: coarse grained diorite (MK6), D: Granular porphyritic texture of coarse grained diorite (MK6), Qtz: quartz, Pl: plagioclase, Bt: biotite, Hb: hornblende, Mu: muscovite, Mc: microcline, Ox: opaque oxide.

Biotite crystals occur as euhedral flakes with microphenocrystals to phenocrystals of about 1 to 1.5 mm long, and contain inclusions of opaque oxides. It has a moderate relief, in some places, biotite is partly replaced by chlorite.

Quartz occurs as large anhedral crystals with sizes of up to 1 mm or more. Its crystals also display an undulating extinction.

Microcline mostly occurs as phenocrysts with sizes of up to 0.5 mm. It has a weak relief and, in some sections, the occurrence of myrmekite is observed with quartz inclusions.

Muscovite is secondary and occurs only in sample MK11 (Fig. 26 B). They form flakes of anhedral crystals of about 0.1 mm. It mostly occurs with the large plagioclase crystals and displays a low to moderate relief.

Monzonite

Its outcrops are rare and occur at latitude N06°43'1" and longitude E010°32'2". The hand specimens are grey to dark grey, medium to coarse-grained and present slight foliation characterized by light felsic bands alternating with dark mafic bands. Its minerals include quartz, microcline, plagioclase, biotite, and horndblende.

Under the microscope, the rock (MK10) is approximately made up of quartz (≈8 vol.%), plagioclase (≈15 vol.%), microcline (≈12 vol.%), biotite (≈40 vol.%) and hornblende (25 vol.%) in a granular texture. Rutile and opaque minerals form accessory minerals and are less than 1% (Fig. 27).

Quartzo-felsparthic light band

Quartz crystals are anhedral and elongated with length of about 0.5 mm, display an undulating extinction.

Microcline crystals are mostly euhedral to sub hedral with sizes of up to 0.7 mm and low relief. Inclusions of quartz are observed in some places.

Plagioclase crystals are sub hedral and have sizes of about 0.3 mm.

Ferromagnesian band

Biotite has a preferred orientation, defining the foliation. The crystals show average sizes of more than 1 mm long, and display a moderate relief.

Hornblende is found as euhedral to sub hedral crystals of about 0.5 mm. The crystals show a moderate relief.

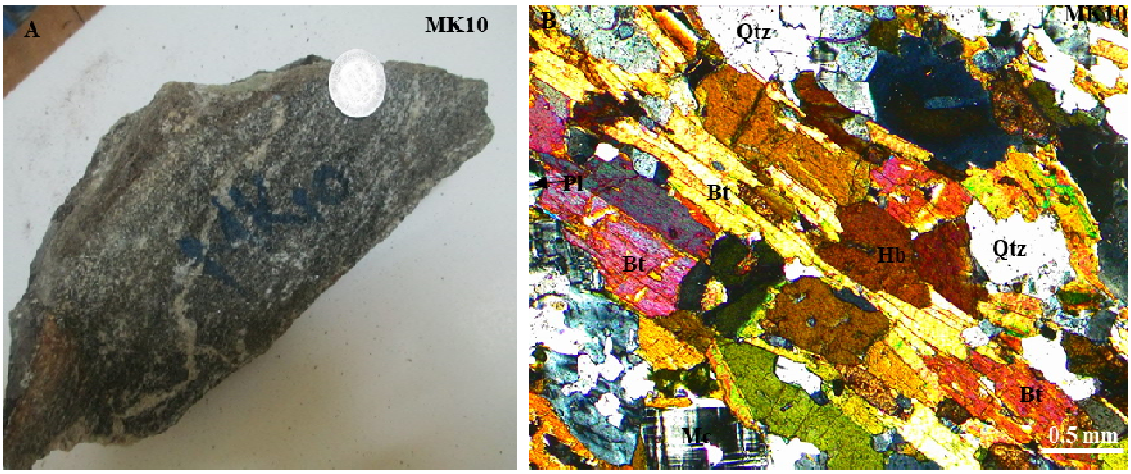

Figure 27: Macroscopic (A) and microscopic (B) aspects of Mayo Kila monzonite. Qtz: quartz, Pl: plagioclase, Bt: biotite, Hb: hornblende, Mc: microcline.

Pink biotite granite

These rocks crop out midway between Dumbo and Mayo Kila villages. The rocks are medium-grained (Fig. 28), and display a granular texture (samples MK04 and MK08).

Under the microscope, its mineralogy is made up of quartz (30 - 35 vol.%), plagioclase (15 - 25 vol.%), microcline (20 - 30 vol.%), biotite (8 - 10 vol.%) and opaque minerals.

Quartz occurs as anhedral crystals with sizes that range from 1 to 2 mm. It also displays undulating extinction and occurs as small inclusions in plagioclase and microcline.

Plagioclase is seen as sub automorphic laths with sizes of up to 4 mm and are characterized by distinct polysynthetic twining. Crystals mostly occur as phenocrysts and some of them host quartz inclusions (Fig. 28 B).

Microcline mostly occurs as phenocrysts with automorphic crystals of up to 3 mm, with a low relief.

Biotite occurs as euhedral flakes with phenocrystals of about 0.3 mm. Most biotite crystals are transformrd to chlorite.

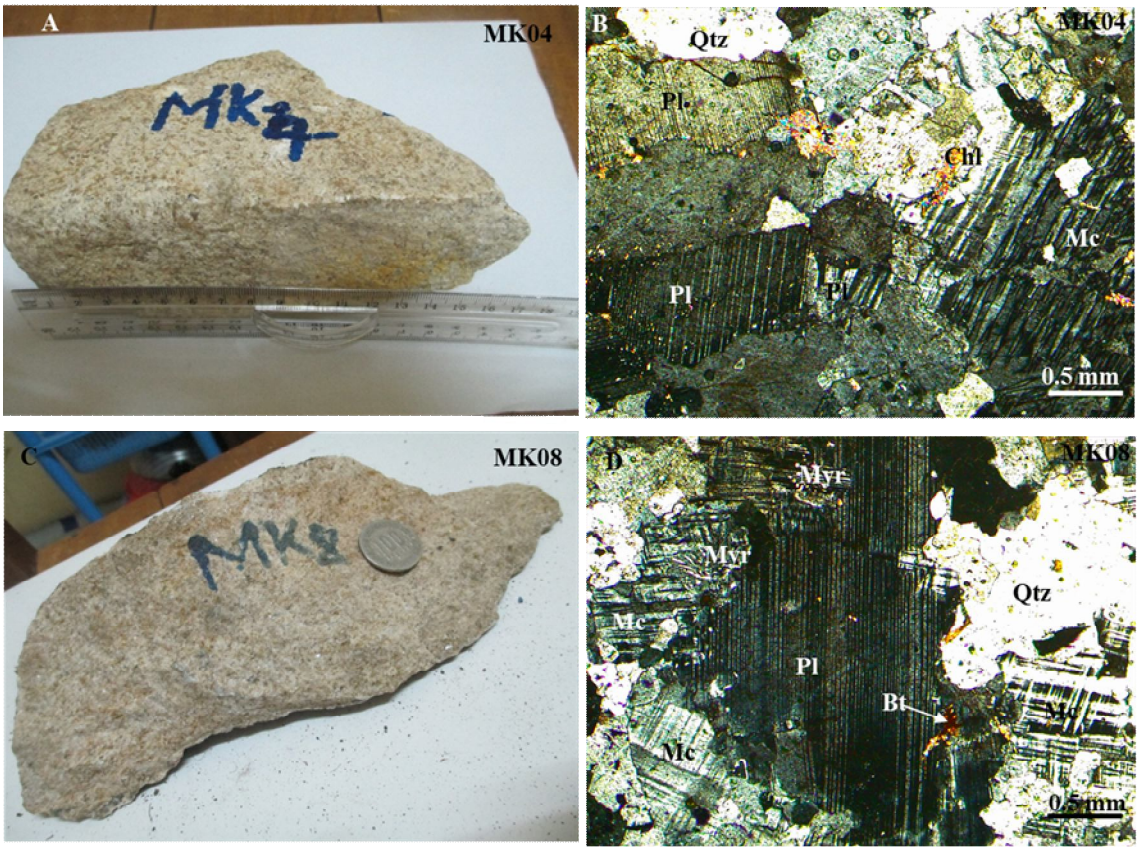

Figure 28: Macroscopic and microscopic aspects of Mayo Kila pink biotite granite. A: hand specimen of MK04, B: Granular texture of MK04, C: hand specimen of MK08, D: Granular texture of MK08. Qtz: quartz, Pl: plagioclase, Bt: biotite, Mc: Microcline, Myr: Myrmekite, Chl: choritized biotite, Or: Orthoclase.

Grey biotite granite

The rock is medium to coarse-grained (Fig. 29). The samples collected (MK01 and MK09) are mostly grey with visible minerals such as quartz, plagioclase and biotite. The rock displays a granular to granular porphyritic texture.

Under the microscope, it is made up of quartz (40 - 45 vol.%), plagioclase (20 - 25 vol.%), biotite (8 - 10 vol.%) and microcline (20 - 22 vol.%). Opaque minerals in all the samples are less than 1%. In very weathered samples, chlorite occurs as a secondary phase along biotite boundaries.

Quartz occurs as anhedral crystals with sizes of up to 4 mm. Its relief is low and it displays an undulating extinction. Its crystals also occur as small inclusions in plagioclase and microcline (myrmekites) (Fig. 29 B).

Plagioclase occurs as sub euhedral to anhedral rectangular laths. Its sizes are between 0.8 and 2.5 mm and crystals are characterized by their pronounced polysynthetic twining. Their phenocrysts host inclusions of quartz (Fig. 29 B).

Microcline mostly occur as phenocrysts with lengths of up to 2 mm. They show a low relief and, in most sections, the occurrence of myrmekite is observed with quartz inclusions in the pericline twinned crystals.

Biotite occurs as euhedral flakes with microphenocrystals of about 0.4 mm. Chlorite crystals are seen along biotite borders. The crystals show a moderate relief.

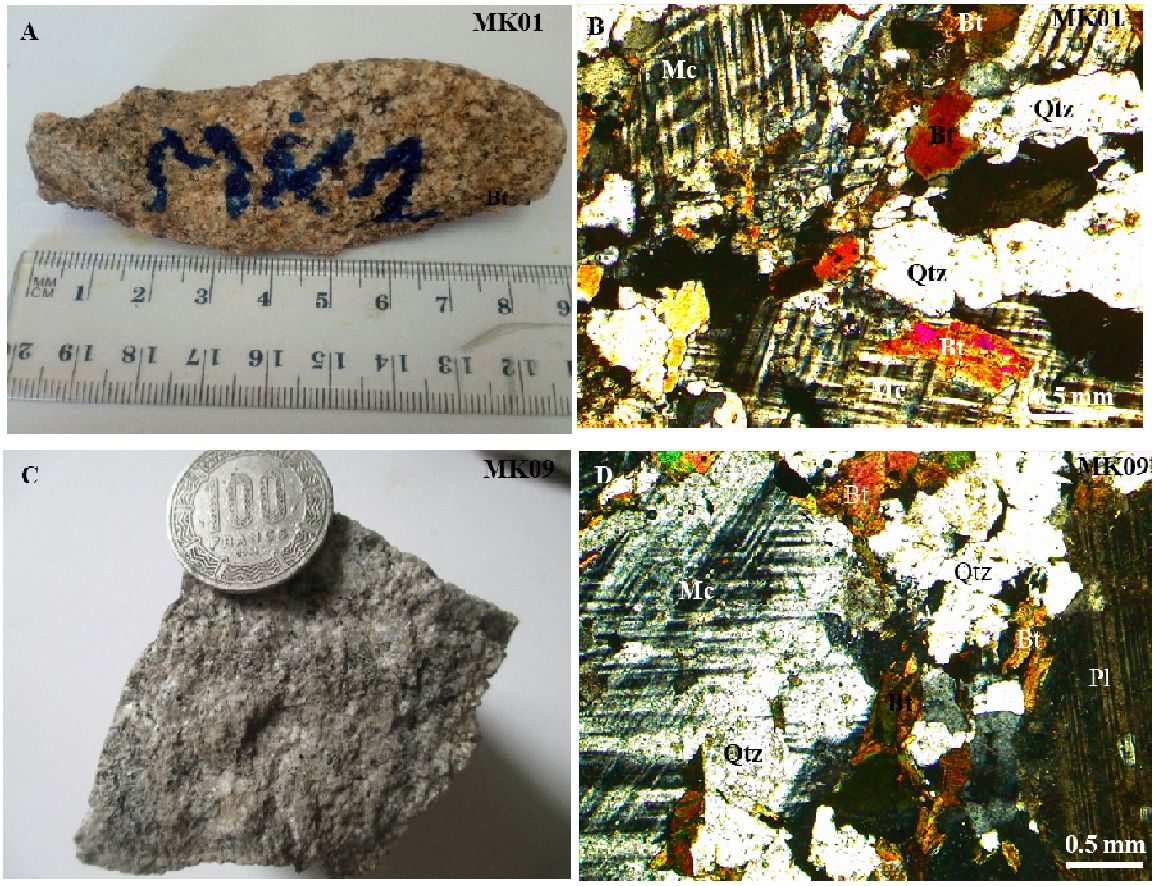

Figure 29: Macroscopic and microscopic aspects of Mayo Kila grey biotite granite. A: hand specimen of sample MK01, B: Granular porphyritic texture of MK01, C: hand specimen of sample MK09, D: Granular porphyritic texture of MK09. Qtz: quartz, Pl: plagioclase, Bt: biotite, Mc: microcline.

Two mica granite

It crops out between latitudes N06°43'01" and N06°43'13" and longitudes E010°32'08" and E010°32'13" at an altitude of about 949 m. It is generally pink to grey, medium grained. In the two samples collected (MK02 and MK03), visible minerals are quartz, plagioclase and biotite. The rocks display a granular texture.

Under the microscope, its mineralogy is made up of quartz (30 - 35%), plagioclase (15 - 25 vol.%), microcline (10 - 15 vol.%), biotite (5 - 10 vol.%), muscovite (≈10 vol.%), orthoclase (≈4 vol.%) and opaque minerals in all the samples are less than 1% (Fig. 30).

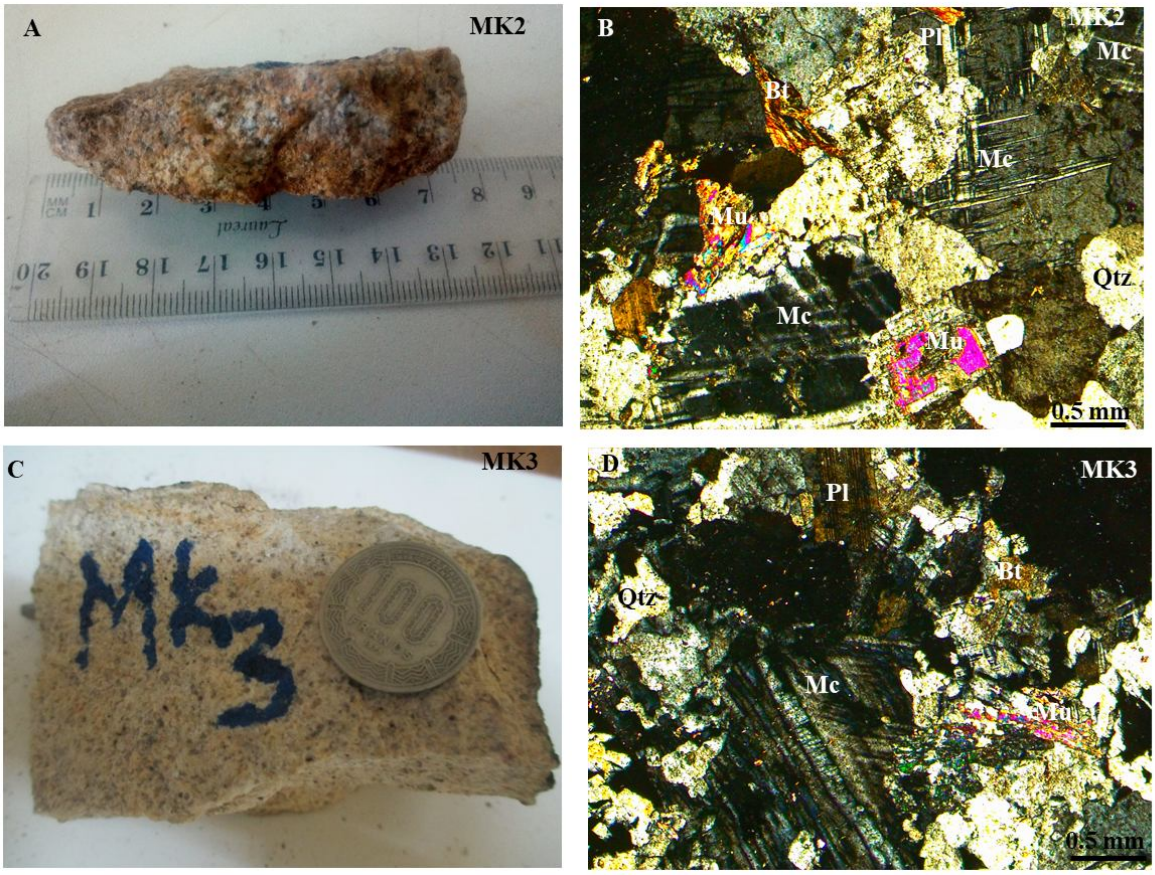

Figure 30: Macroscopic and microscopic aspects of Mayo Kila two mica granites. A and C: hand specimen of samplesMK2 and MK3, B and D: are microphotographs showing the granular textures of the two mica granites. Qtz: quartz, Pl: plagioclase, Bt: biotite, Mu: muscovite, Mc: microcline.

Quartz occurs as anhedral crystals with sizes up to 2 mm. It also displays an undulating extinction and occurs as small inclusions in microcline (myrmekites) in places.

Plagioclase occurs as sub automorphic to automauphic crystals with rectangular laths. Its crystals are characterized by typical polysynthetic twinning. Their sizes are less than 0.5 mm and some crystals host quartz inclusions (myrmekites).

Biotite occurs as euhedral flakes with phenocrystals of about 0.5 mm. Some crystals contain inclusions of opaque oxides and chlorite crystals.

Muscovite flakes represent about 10% of the entire rock and show euhedral to sub hedral flakes of about 0.6 mm and a low relief.

Quartz veins

They crop out as veins (Fig. 31) with a white to grey colour. They crosscut granitic outcrops and are more visible in highly weathered granites and soils. The veins mostly follow a NW - SE direction.

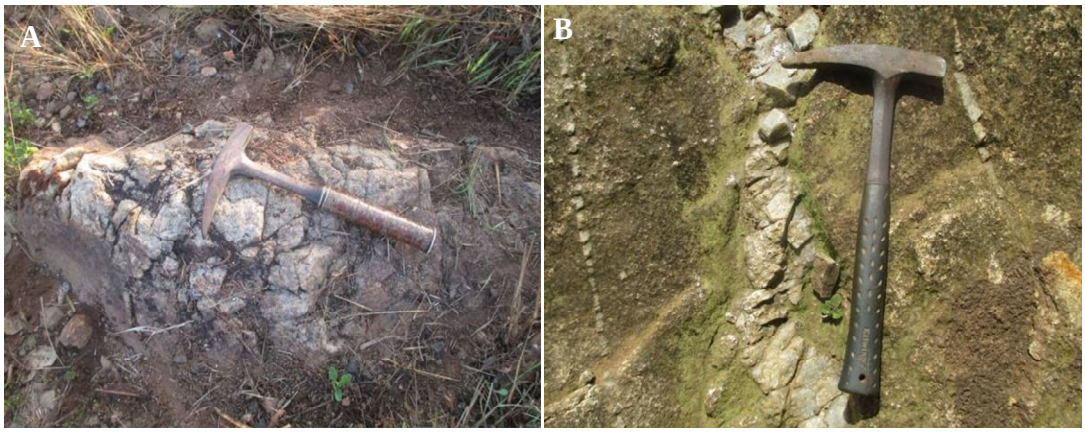

Figure 31: Outcroping quartz veins.

IV.1.2- Rocks in Mbiame

Mbiame is situated in the west of Mount Oku about 70 km south of Mayo Kila. It is characterized by two main lithological units: a superficial unit made up of conglomerates composed of clastic materials of mafic rock fragments and detrital materials along river beds. A predominant mafic unit that occurs as huge blocks, columns or disjointed blocks. As far as sampling is concerned, rock samples were collected in Mbiame and other parts of Mount Oku (Fig. 32).

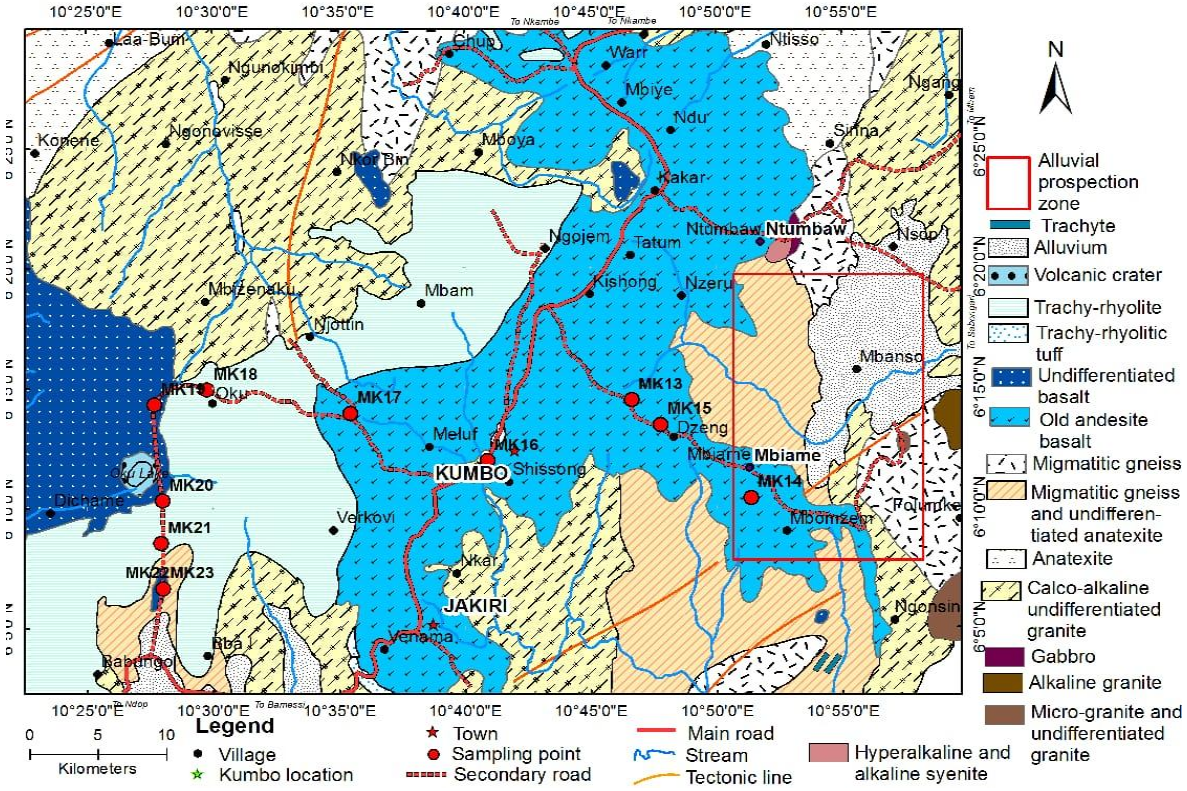

Figure 32: Sampling map of Mbiame and its environs (after Peronne, 1969)**.**

IV.1.2.1- Alluvial materials

They consist of gravel sized clastic materials and conglomerates.

Gravel sized clastic materials

These alluvial materials were observed along the Mbven River and are constituted of cobble and pebble sized clastic rock fragments from mostly mafic volcanics, rhyolites, few fragments from the granite-gneiss basement and quartz fragments (Fig. 33). These rock fragments vary in size from few millimeters to more than sixteen 16 cm. They are mostly sub to well-rounded with rough to smooth surfaces. The fragments occur in different percentages: mafic volcanic clasts (≈70%), granitic fragments (≈15%), rhyolite fragments (≈8%) and quartz fragments (<7%) (Fig. 34).

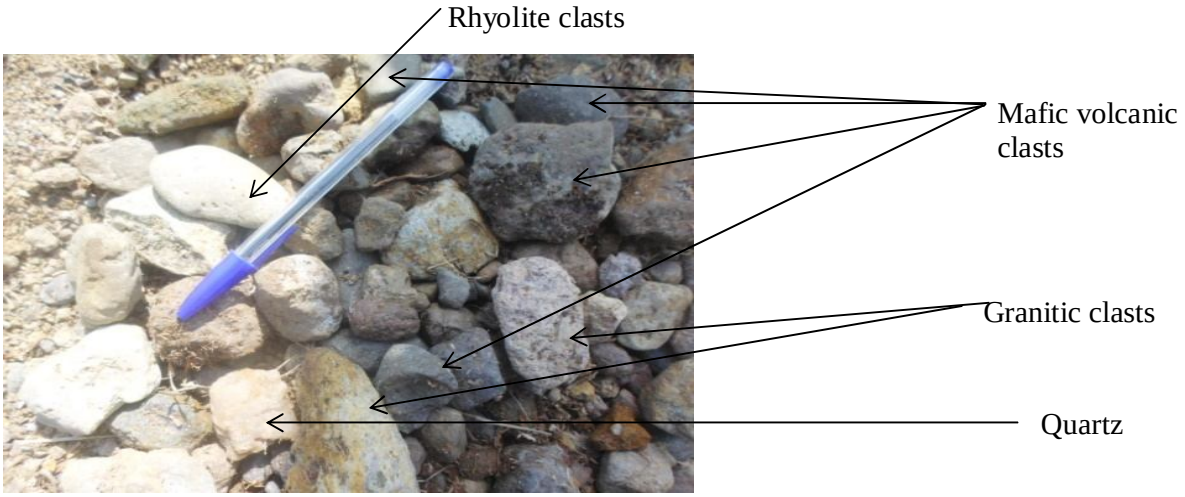

Figure 33: Cobble and pebble sized clastic rock fragments.

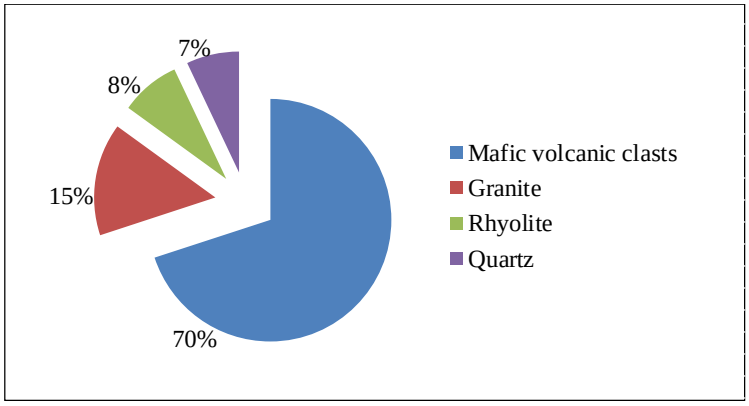

Figure 34: Proportion of rock-type clasts in alluvial material from the Mbven River.

The smaller gravel sized clastic materials are mostly granules, with particle sizes ranging from millimeters to few centimeters. These particles are sub angular, rounded to well-rounded (Fig. 35). They vary in colour from grey, pink and brown, and are associated with sapphire, zircon and tourmaline mineralization.

Figure 35: Gravel sized alluvial materials.

Conglomerates

Conglomerates crop out as slabs with hard pan-like surfaces (Fig. 36 A), some few meters on the northern side of the Mbven River. The cemented materials (rhyolite and basalt fragments) range from millimetric to up to 10 cm. They are made up of sub-rounded, rounded to well-rounded rock fragments with mostly smooth surfaces. The clasts are grey to brown and are cemented by a brown groundmass (Figure 37 B and C). They also host incrustation of light and dark coloured minerals (Fig. 36 D).

Figure 36: Conglomerate outcrops. A**:** Mode of occurrence of conglomerates, B: Conglomerate block, C: Hand specimens of conglomerate, D: Heavy mineral incrustations in conglomerates.

IV.1.2.2-Volcanic unit

It consists of different mafic lava flows, pyroclastites of scoria and pumice and other volcanic projections.

Field occurrences

Volcanic rocks in Mbiame occur as huge blocks, sub-rounded to well-rounded boulders on hill slopes and streams, columnar sections along road cuttings and disjointed

blocks in savanna areas (Figure 37 A-D). Most of the rocks are dark and massive, few samples display amygdaloidal texture and are characterized by whitish incrustations of quartz. They show thin to very thick weathered surfaces.

Figure 37: The different modes of mafic lava occurrences. A: blocky outcrop, B: Rounded boulders in streams, C: Columnar basalt outcrop, D: Disjointed blocks.

Classification

The rock samples collected from the volcanic units in Mbiame were plotted in the Total Alkaline Silica (TAS) classification diagram of Le Maitre (2002). The volcanic rock samples MK13, MK17, MK04, MK18, MK19 and MK21 fall in the basanite domain, and samples MK14 and MK20 fall in the domain of foidite (Fig. 38).

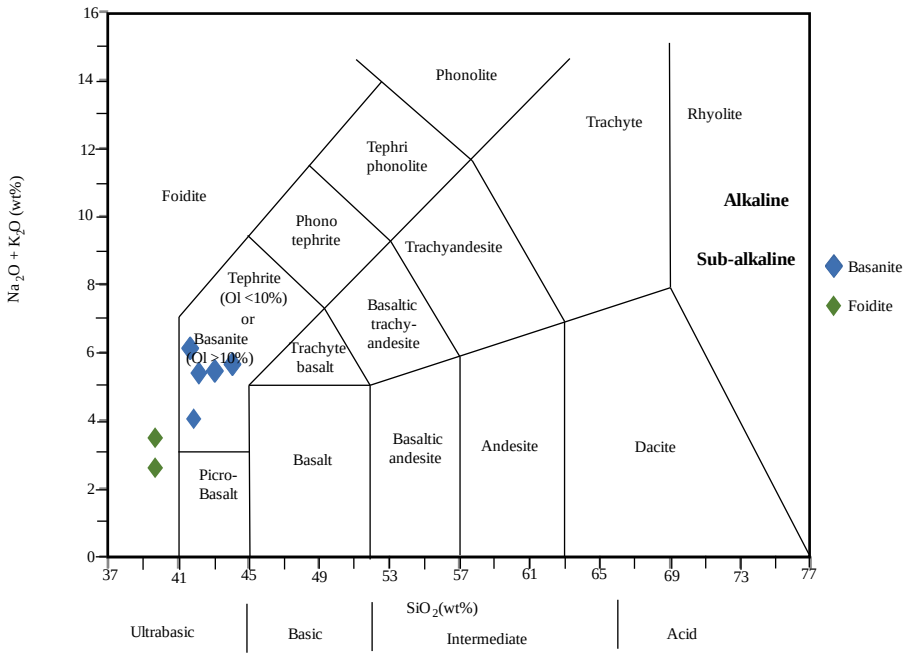

Figure 38: Classification of Mbiame mafic volcanic rocks using the Total Alkaline Silica variation (TAS) classification of Le Maitre (2002).

Macroscopic and microscopic descriptions

Basanite

This rock was sampled at Belem, Tadu, Elak Oku and Mbok Jikejem. It is a dark and massive rock with yellowish brown patches.

Under the microscope, the basanites display microlitic to microlitic porphyric textures with mineralogical compositions made up of plagioclase (40 - 60 vol.%), olivine (20 - 50 vol.%), clinopyroxene (10 - 15 vol.%), quartz agmydales (≈3 vol.%), opaque oxides (2 - 17 vol.%) and less than 1% of volcanic glass. Olivine and pyroxene mostly occur as phenocryst and are embedded in a groundmass made up mostly of plagioclase microlits, although in some samples, olivine and pyroxene also occur in the groundmass (Fig. 39 A-H).

Plagioclase is euhedral to sub hedral range from less than 0.2 to 0.6 mm long. It occurs mostly in the groundmass and in some cases as microphenocrysts and phenocrysts.
Olivine crystals range from sub hedral to euhedral. They show sizes of 0.2 to 0.5 mm and mostly occur as phenocrysts although they also occur as microphenocrysts. Some olivine crystals present evidence of iddingsitization, characterized by a brown to reddish brown alteration product along the borders and cracks (Fig. 39 B). The crystals show high relief.

Clinopyroxene occurs in most samples as sub hedral to euhedral crystals of up to 0.8 mm phenocrysts, with a high relief.

Opaque minerals are sub rounded in shape with size range from less than 0.4 mm. They also occur as inclusions within olivine and clinopyroxene crystals (Fig. 39 D).

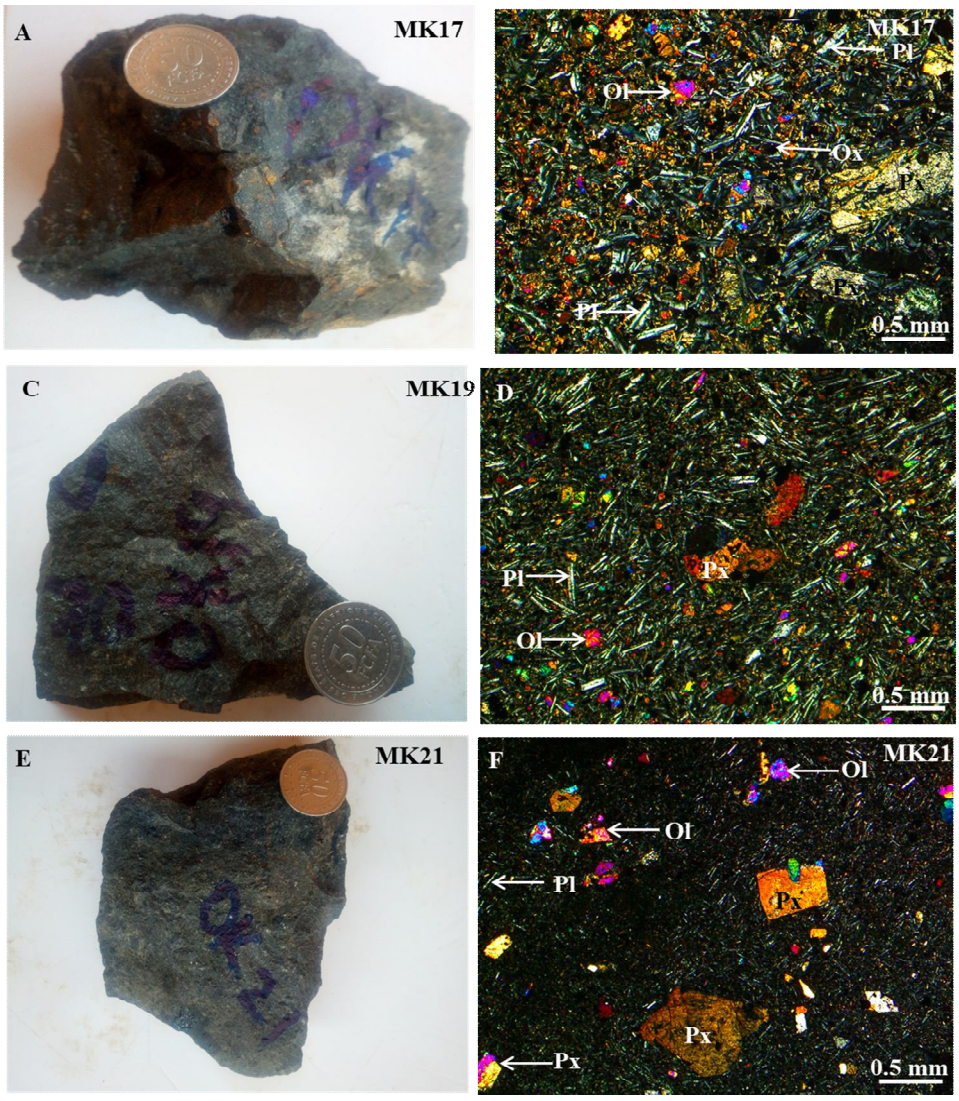

Figure 39: Macroscopic and microscopic aspects of Mbiame basanites. A, C and E: hand specimens of basanite samples. B, D and F are microphotographs of the basanites. Pl: plagioclase, Ol: olivine, Px: pyroxene, Sn: sanidine and Ox: oxide.

Foidites

On hand specimen, the rocks are dark grey, with rough surfaces and are characterized by a microlitic porphyric textures (Fig. 40 A).

Under the microscope, it is made up of plagioclase (60 - 65 vol.%), olivine (15 - 25 vol.%), clinopyroxene (5 - 10 vol.%), opaque oxides (3 - 13 vol.%) and less than 1 vol.% of volcanic glass. Olivine and pyroxene form phenocrysts and are embedded in a groundmass made of plagioclase microliths (Fig. 40 B, C).

Plagioclase crystals are euhedral to subhedral of up to 0.3 mm. They mostly form the groundmass.

Olivine is euhedral. It mostly occurs as phenocrysts of more than 1 mm. Most of its crystals have undergone iddingsitization characterized by a brown to reddish brown alteration deposit along its borders and cracks.

Clinopyroxene is mostly euhedral with sizes up to 0.7 mm in most samples where it occurs as phenocrysts. Very few crystals are seen in the groundmass.

Opaque minerals are mostly sub rounded with sizes up to 0.2 mm in some samples. They also occur as inclusions within olivine and clinopyroxene crystals.

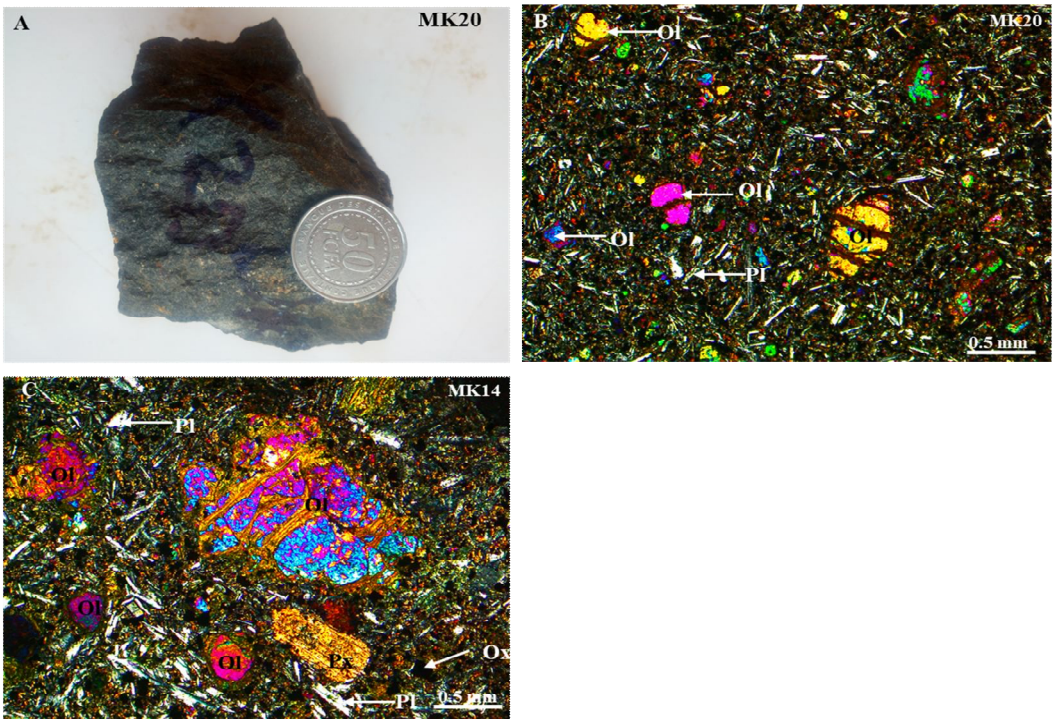

Figure 40: Macroscopic and microscopic aspects of Mbiame foidite. A: hand specimen of Mbiame foidite, B and C are microphotographs of the foidites (MK20 and MK14 respectively). Mineral abbreviations as in Figure 39.

Pyroclastic materials

These are made up of ash flows, scoria and volcanic blocks (Fig. 41). The ash flows profiles can range from 2 to 8 m high and are layered with levels that can vary from 1 to 3.5 m thick. Their colours range from light to dark grey (Fig. 41A). In some places, the ashflows lay on thick reddish brown lateritic soils (Fig. 41 B). The scoria blocks range widely in sizes, and have a light, foamy texture full of vesicles. They are mostly grey in colour with some being oxidized to reddish brown (Fig. 41 C), while the blocks are grey with sub rounded sizes that can attain up to 1 m in diameter (Fig. 41 D).

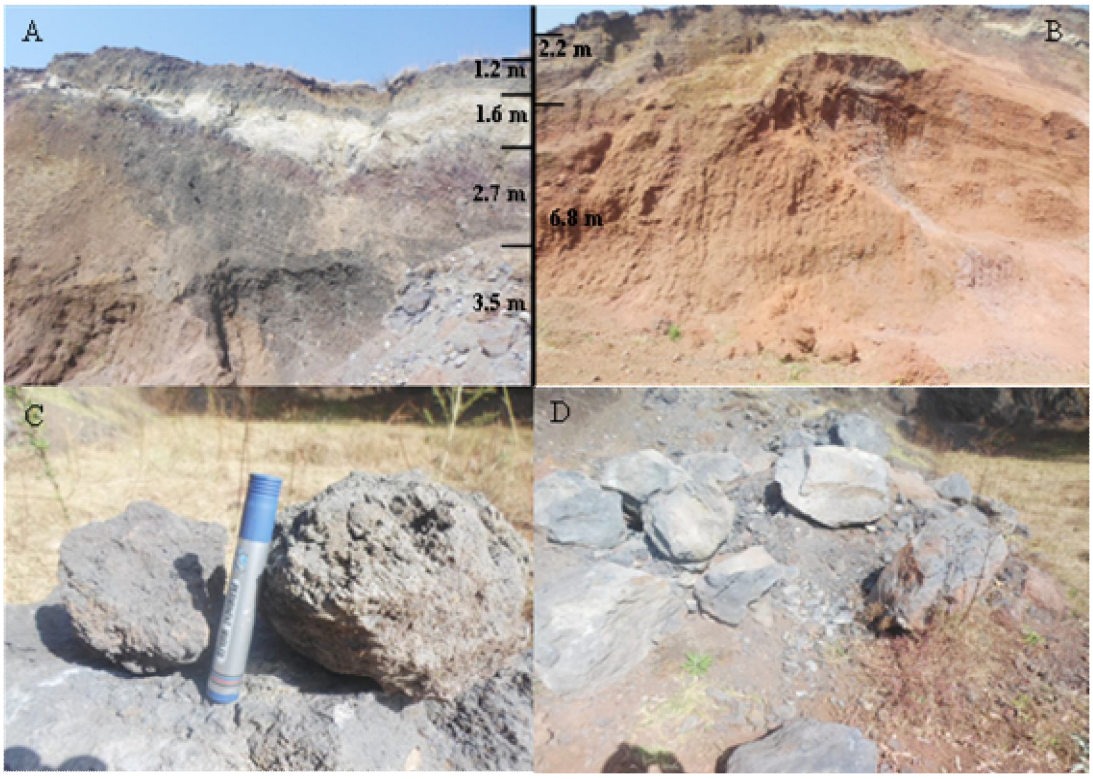

Figure 41: Pyroclastic materials along the Ketoh - Ibal Oku road. A and B: ashflows, C: Scoria, D: volcanic blocks.

Table 4 presents the different lithological units observed and sampled in the study areas.

Table 4: Major petrographic features of rocks in the study areas.

Study area	Lithological units	Rock types	Mineralogical assemblages	Textures
Mayo Kila	Plutonic unit	Biotite granite	Pink biote granite Qtz + Pl + Bt + Or + Mc + Ox Grey biotite granite Qtz + Pl + Bt + Mc + Ox	- Granular texture - Granular porphyritic texture
		Two mica granite	Qtz + Pl + Bt + Or + Mu + Mc	- Granular texture
		Diorite	Fine grained diorite Qtz + Pl + Bt + Hb Coarse grained diorite Qtz + Pl + Bt + Hb + Mu + Mc + Or	- Granular texture - Granular porphyritic texture
		Monzonite	Qtz + Pl + Bt + Px + Hb + Mc	- Granular texture
	Volcanic unit	Basanite	Ol + Pl + Px + Ox	- Microlitic fluidal texture
Mbiame and its environs	Volcanic unit	Basanite	Ol + Pl + Px + Ox + Qtz	- Microlitic - Microlitic fluidal - Microlitic porphyric - Amygdaliodal texture
		Foidite	Ol + Pl + Px + Ox	- Microlitic - Microlitic fluidal - Microlitic porphyric
		Pyroclastic materials		

IV.2- Geochemistry of the different lithological units in Mayo Kila and Mbiame

In both areas, magmatic (plutonic and volcanic) rocks were sampled. This sub chapter presents the geochemical characteristics observed in some selected analyzed samples.

IV.2.1- Geochemistry of lithological units in Mayo Kila

In this area, nine samples of the magmatic unit (eight plutonic and one volcanic) were analyzed for their geochemical characteristics. The plutonic unit is made up of four (04) samples of biotite granites, one (01) sample of two mica granite, two (02) samples of diorites and one (01) sample of monzonites. One mafic lava flow from this area represents the volcanic unit.

IV.2.1.1- Geochemistry of the plutonic assemblage in Mayo Kila

Table 5 present results of major and minor element geochemical characteristics as well as CIPW norms of Mayo Kila rocks.

Table 5: Major, minor and CIPW norms of Mayo Kila rocks.

	Plutonic unit								Volcanic unit
	Biotite granite				Two mica granite	Diorite		Monzonite	Basanite
Sample	MK 01	MK 04	MK 08	MK 09	MK 03	MK 11	MK12	MK10	MK07
SiO_2 (wt.%)	69.8	74.5	74.1	71.4	73.3	60.7	58	57.2	45.5
TiO_2	0.33	0.04	0.02	0.32	0.02	0.8	0.88	1.19	3.28
$Al2O_3$	14.45	13.35	13.8	14.05	13.8	15.85	15.8	15	16.85
$Fe2O_3$	2.74	0.79	1.09	2.25	1.5	6.22	8.94	6.94	12.85
MnO	0.03	0.01	0.01	0.04	0.08	0.09	0.16	0.13	0.2
MgO	0.35	0.02	0.02	0.71	0.01	5.17	5.41	4.03	4.59
CaO	1.01	0.51	0.59	1.51	0.45	4.67	4.73	4.61	7.82
Na_2O	3.01	3.87	3.52	3.39	4.76	3.8	2.69	3.8	3.7
K_2O	5.23	4.74	6.17	5.15	3.79	2.84	3.14	3.61	2.45
P_2O_5	0.12	0.01	<0.01	0.07	0.04	0.34	0.24	0.42	0.95
Cr_2O_3	0.002	0.002	0.002	0.004	0.002	0.035	0.02	0.02	0.003
SrO	0.05	0.01	<0.01	0.04	<0.01	0.07	0.01	0.07	0.11
BaO	0.15	0.04	0.02	0.19	<0.01	0.12	0.1	0.16	0.07
LOI	1.54	0.46	0.25	0.42	0.65	0.79	0.89	0.82	1.29
Total	98.81	98.35	99.59	99.54	98.4	101.5	101.01	98	99.66
Na_2O+K_2O	8.24	8.61	9.69	8.54	8.55	6.64	5.83	6.25	6.15
K_2O/Na_2O	1.73	1.22	1.75	1.52	0.79	0.75	1.17	7.41	0.66
FeOt	2.47	0.71	0.98	2.03	1.35	5.6	8.05	0.95	11.56
A/NK	1.36	1.16	1.11	1.26	1.16	1.7	2.02	1.48	1.93
A/CNK	1.16	1.07	1.02	1.01	1.08	0.89	0.96	0.81	0.73
CIPW norms									
Quartz %	26.46	32.16	26.84	26.79	28.63	3.97	1.91	0	-
Orthoclase	31.59	28.55	36.9	29.85	22.63	16.23	17.63	21.28	13.5
Albite	25.6	33.24	29.67	27.61	40.69	30.4	21.17	31.26	10.99
Anorthite	4.41	2.56	3.03	6.94	1.99	16.65	20.06	12.58	20.21
Nepheline	-	-	-	-	-	-	-	-	9.63
Diopside	-	-	-	-	-	2.83	0.36	6.08	8.58
Hypersthene	7.86	2.17	2.98	7.14	4.25	25.62	33.84	22.9	-
Olivine	-	-	-	-	-	-	-	-	25.17
Hematite	-	-	-	-		-	-	-	-
Magnetite	0.96	0.28	0.38	0.75	0.53	2.05	2.89	2.35	4.1
Ilmenite	0.63	0.08	0.04	0.58	0.04	1.44	1.55	2.2	5.72
Corundum	2.15	0.92	0.11	0.14	1.16	-	0	-	-
Apatite	0.28	0.02	0.02	0.16	0.09	0.74	0.52	0.95	2.02
Zircon	0.06	0.01	0.03	0.03	0.01	0.05	0.04	0.08	0.08
Perovskite	-	-	-	-	-	-	-	-	-
Chromite	-	-	0.01	0.01	-	0.03	0.02	0.03	-
Rutile	-	-	-	-	-	-	-	-	-
Total	100	99.99	100.01	100	100.02	100.01	99.99	100.01	100

IV.2.1.1.1- Major and minor element concentration

Diorite and monzonite

The major element contents of these samples are presented in Table 5. The rocks are moderate in silica and predominantly exhibit an intermediate character with SiO_2 content between 57.2 and 60.7 wt.%. In the TAS (Total Alkali Silica) diagram of Cox et al. (1979), these rocks plot in the diorite and monzonite domains (Fig. 24). Other major elements show variable concentrations with Al_2O_3 contents between 15 wt.% in monzonite and 15.85 wt.% in the diorites, Fe_2O_3 is average and varies from 6.22 to 8.94, while MgO (4.03 – 5.41 wt.%), MnO (0.09 - 0.16 wt.%), CaO (4.61 - 4.73 wt.%), Na_2O (2.69 - 3.8 wt.%), K_2O (2.84 – 3.61 wt.%), TiO_2 (0.8 – 1.19 wt.%) and P_2O_5 (0.24 - 0.42 wt.%) contents are low to moderate. The

Loss On Ignition (L.O.I = 0.79 – 0.89 wt.%) values are low, attesting to the freshness of the rocks or the low proportion of fluid in the magma. This content is justified by the rarity of secondary minerals in the rock. All the rocks are hypersthene-normative with values from 22.9 to 33.84.

Biotite granite and two mica granite

Major element concentrations of the analyzed samples are presented in Table 5. The rocks are silica-rich and predominantly exhibit a felsic character with SiO_2 content between 74.5 and 69.8 wt.%. Highest silica content is observed in sample MK04 (74.5 wt.%), while lowest concentration occurs in sample MK01 (69.8 wt.%). In the TAS (Total Alkali Silica) diagram of Cox et al. (1979), these rocks plot in the granite domains (Fig. 25). Other major elements show variable concentrations with Al_2O_3 contents between 13.35 wt.% to 14.45 wt. Fe_2O_3 is low and varies from 1.5 to 2.74 wt.%, MgO contents vary from 0.01 to 0.71 wt.%, MnO varies from 0.01 - 0.08 wt.%, CaO (0.45 – 1.51 wt.%), Na_2O (3.01 - 4.76 wt.%), K_2O (3.79 - 6.17 wt.%), TiO_2 (0.02 – 0.33 wt.%) and P_2O_5 (<0.01 - 0.12 wt.%). The Loss On Ignition (L.O.I = 0.25 - 1.54 wt. %) values are low, attesting to the freshness of the rocks or the low proportion of fluid in the magma. This content is justified by the rarity of secondary minerals in the rock. Most of these rocks are generally hypersthene and corundum-normative with values between 2.17 to 7.86 and 0.11 to 2.15 respectively (Table 5).

In the Harker diagrams (Fig. 42), the abundances of TiO_2, Al_2O_3, MnO, Fe_2O_3, CaO, P_2O_5, and SrO show a negative correlation with increasing SiO_2, BaO and Cr_2O_3 show no correlation with silica while K_2O and Na_2O (Figure 66 g, h), show only a slight positive correlation as SiO_2 increases. This slight positive correlation of Na_2O and K_2O with SiO_2, suggests that alkali feldspar to some extent, persisted in the melt phase until the later stages of magmatic evolution. Using the Al saturation index A/CNK (Fig. 43) of Chappell and White (1992), most of the samples plot in the metaluminous domain and only one biotite granites sample (MK01) is slightly paraluminous with A/CNK ratios <1.1. The total alkali contents ($Na_2O + K_2O$) range from 6.64 to 9.69 and are average in potassium with K_2O/Na_2O ratios ranging from 0.75 to 1.1.73. The studied granites also display a high-K calc-alkaline series to shoshonitic affinity on the Peccerillo and Taylor (1976) diagram (Figure 44). On the MALI (Modified Alkali-Lime Index) silica diagram of Frost et al. (2001), all samples fall in the alkaline series and show strong affinity to alkali-calcic series with only the two diorite samples falling on the line separating the calc-alkalic and alkali-calcic serieses (Fig. 45). In

the classification scheme of Frost et al (2001), to discriminate between ferroan granitoids and magnesian granitoids (Fig. 46), most of the rocks fall on the ferroan domain while the diorite and one biotite granite sample (MK9) falls in the magnesian domain.

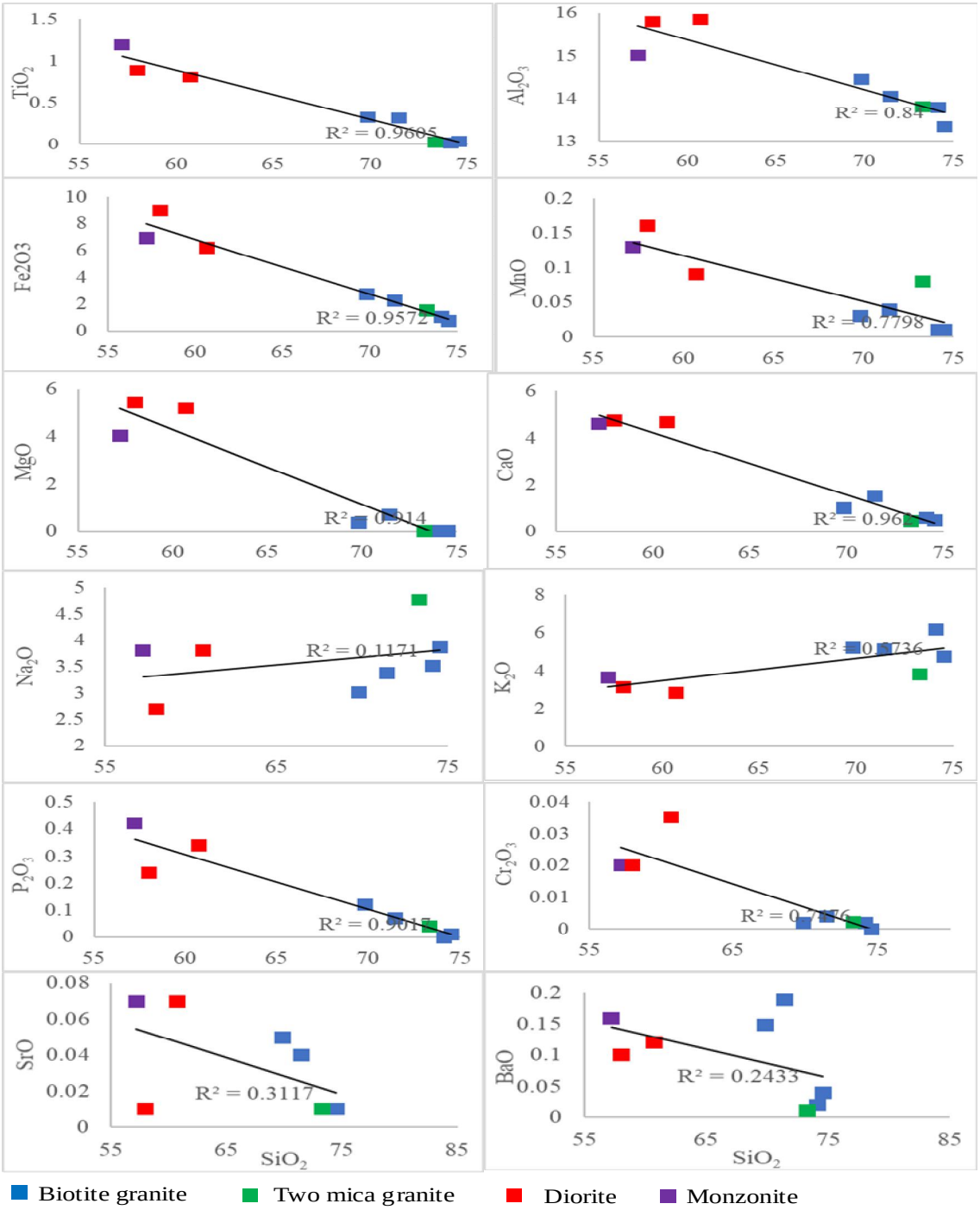

Figure 42: Harker variation diagrams of selected major elements plotted against SiO_2 for the studied plutonic rocks.

Correlation coefficients for major elements in the plutonic rocks

Correlation matrice displays the positive or negative correlations that exists between the major and trace elements of the studied rocks. Correlation is said to be positive when an absolute value of above 0.70 is obtained. Positive correlation is an indication that the elements are associated in the same processes or in the same mineral phases. On the other hand, a negative correlation is an expression of incompatibility between the elements.

Amongst the major elements in the Mayo Kila plutonic rocks (Table 6), positive correlations are seen between SiO_2 and Na_2O (0.80), SiO_2 and K_2O (0.90), TiO_2 and MnO (0.99), TiO_2 and Cr_2O_3 (0.94), Al_2O_3 and Na_2O (0.90), Al_2O_3 and K_2O (0.73), Fe_2O_3 and MgO (0.96), Fe_2O_3 and CaO (0.97), Fe_2O_3 and P_2O_5 (0.93), MnO and Cr_2O_3 (0.88), MgO and CaO (0.99), MgO and P_2O_5 (0.89), MgO and SrO (0.70), CaO and P_2O_5 (0.89), Na_2O and K_2O (0.75) and SrO and BaO (0.75).

Negative correlations are seen between SiO_2 and TiO_2 (-0.83), SiO_2 and Fe_2O_3 (-0.92), SiO_2 and MnO (-0.80), SiO_2 and MgO (-0.89), SiO_2 and CaO (-0.92), SiO_2 and P_2O_5 (-0.73) and SiO_2 and Cr_2O_3 (-0.82).

Table 6: Correlation matrix between major elements for Mayo Kila plutonic rocks. Green boxes represent negative correlations and yellow boxes indicate positive correlation

SiO_2	1.00												
TiO_2	**-0.83**	1.00											
Al_2O_3	0.64	**-0.94**	1.00										
Fe_2O_3	**-0.92**	0.55	-0.29	1.00									
MnO	**-0.80**	**0.99**	**-0.91**	0.53	1.00								
MgO	**-0.89**	0.53	-0.31	**0.96**	0.48	1.00							
CaO	**-0.92**	0.57	-0.34	**0.97**	0.53	**0.99**	1.00						
Na_2O	**0.80**	**-0.96**	**0.90**	-0.54	**-0.94**	-0.49	-0.54	1.00					
K_2O	**0.90**	**-0.87**	**0.73**	**-0.75**	**-0.86**	**-0.74**	**-0.76**	**0.75**	1.00				
P_2O_5	**-0.73**	0.24	0.06	**0.93**	0.22	**0.89**	**0.89**	-0.22	-0.53	1.00			
Cr_2O_3	**-0.82**	**0.94**	**-0.94**	0.55	**0.88**	0.58	0.60	**-0.91**	**-0.83**	0.23	1.00		
SrO	-0.56	0.15	-0.06	0.69	0.05	**0.70**	0.69	-0.24	-0.29	0.69	0.36	1.00	
BaO	-0.49	0.30	-0.21	0.53	0.24	0.44	0.51	-0.45	-0.24	0.44	0.36	**0.75**	1.00
	SiO_2	**TiO_2**	**Al_2O_3**	**Fe_2O_3**	**MnO**	**MgO**	**CaO**	**Na_2O**	**K_2O**	**P_2O_5**	**Cr_2O_3**	**SrO**	**BaO**

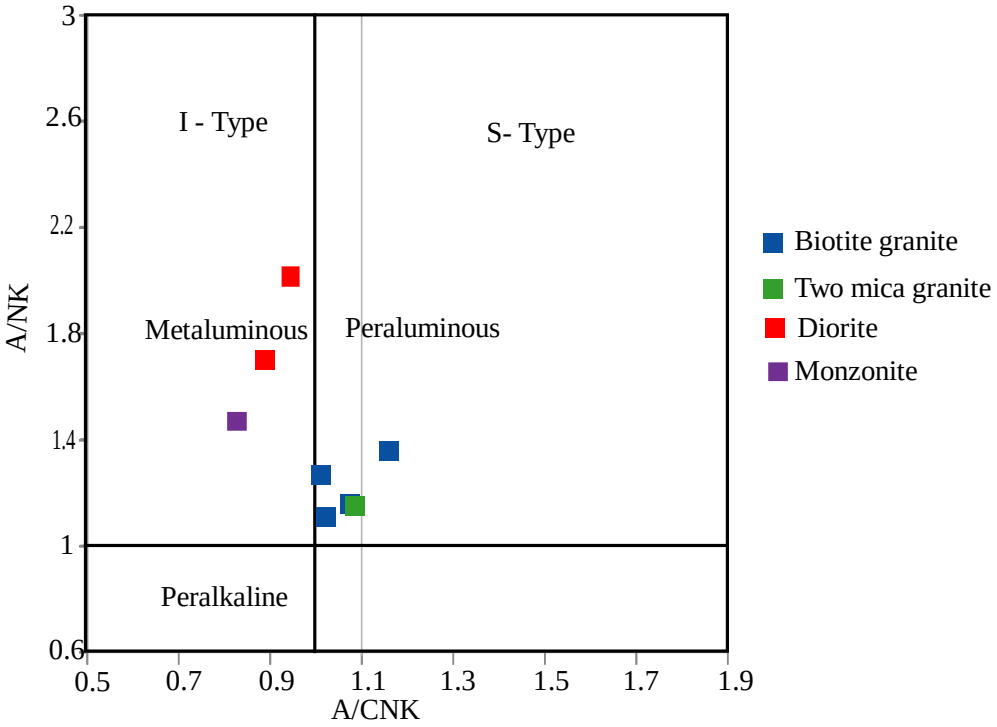

Figure 43: A/CNK versus A/NK diagram with the Shand's Index (Maniar and Piccolli 1989), showing mainly metaluminous composition for diorite and monzonite and peraluminous compositions for biotite granites and two mica granite**.**

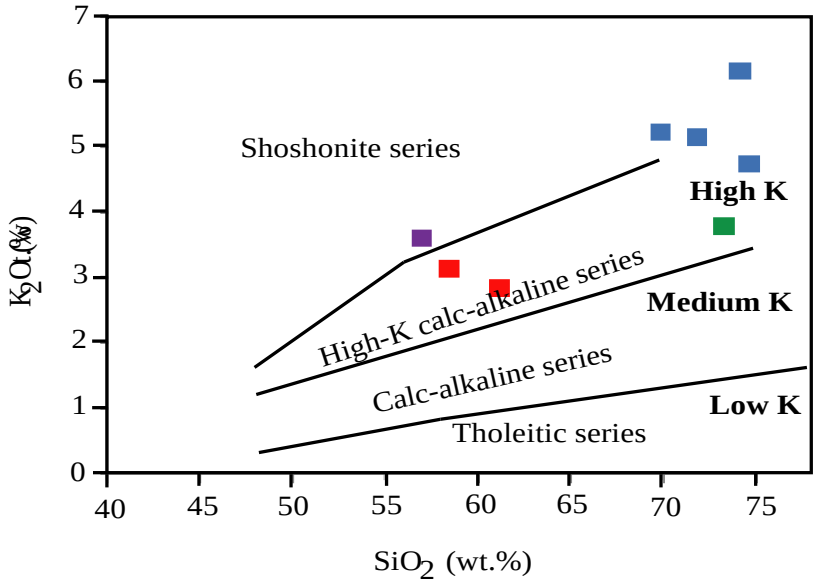

Figure 44: K_2O versus SiO_2 plot of Peccerillo and Taylor (1976) showing the shoshonitic to high potassic-calco alkaline affinity of Mayo Kila granitoids. The same legend as Figure 44.

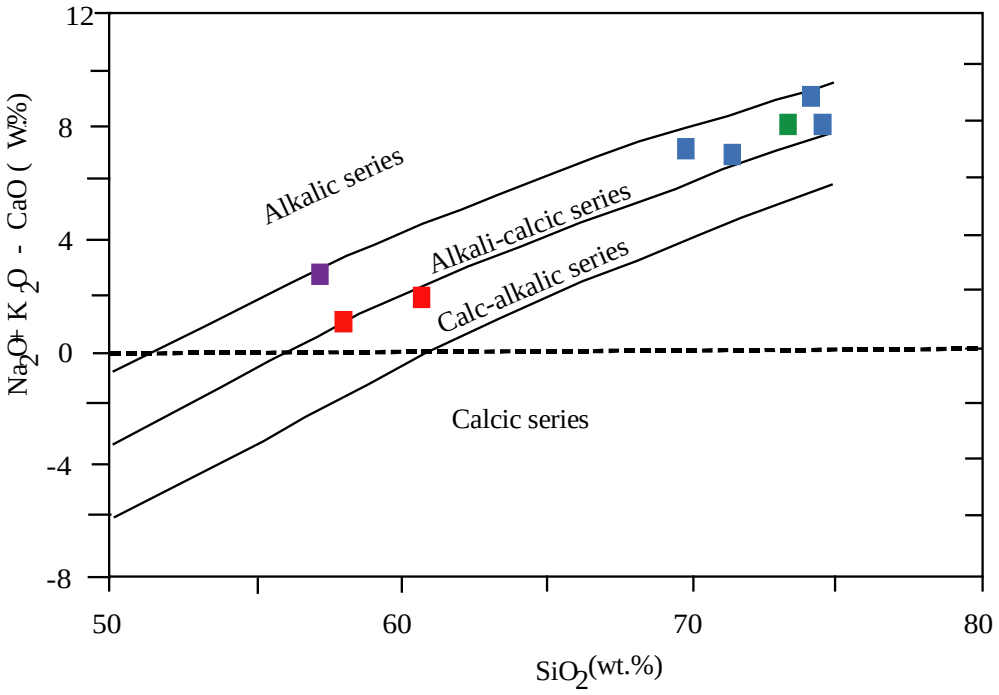

Figure 45: Position of Mayo Kila granitoids on the MALI (Modified Alkali-Lime Index) silica diagram (adapted from Frost et al., 2001). The same legend as Figure 44.

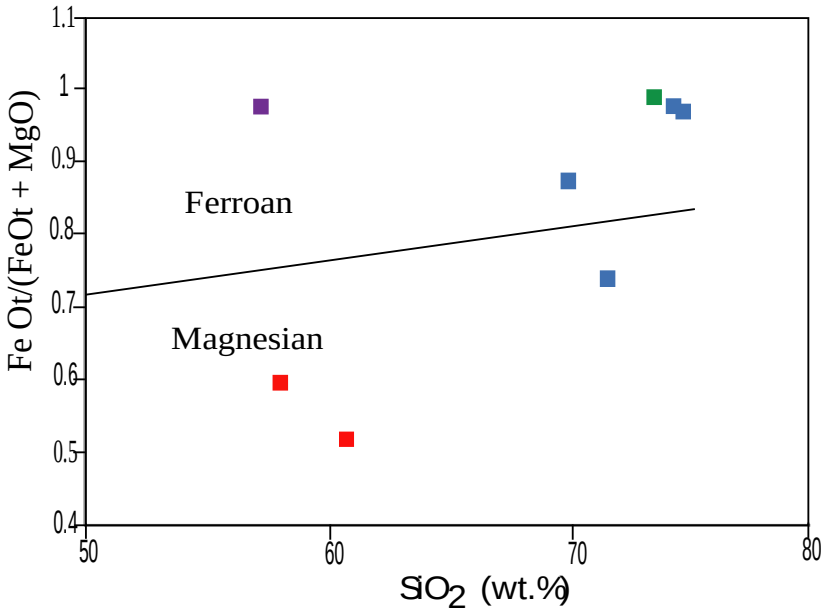

Figure 46: Position of Mayo Kila granitoids on the SiO_2 versus FeOt/(FeOt + MgO) diagram (adapted from Frost et al., 2001). The same legend as Figure 44.

IV.2.1.1.2- Trace element concentrations

Diorite and monzonite

The trace element geochemistry of these rocks is presented in Table 7. The rocks present high contents in Ba (878 - 1,355 ppm), the diorite samples have concentrations of up to 953 ppm, while monzonite show the highest concentration of 1,355 ppm. Other elements with high concentrations are Sr (298 - 813 ppm), Zr (189 - 400ppm), Rb (90.6 - 212 ppm), V (104 - 165 ppm). Elements with low to average concentrations are Pb (22 - 29 ppm), Zn (63 - 138 ppm), Y (17.5 - 32.3 ppm), Th (8.29 - 20.5 ppm), Ga (18.2 - 23.8 ppm) and Nb (- 6.7 - 20.7 ppm) while very low concentrations are observed in U and Ta with values as low as 1.57- 4.51 ppm and 0.4 - 1.2 ppm respectively. The ratio of Ba/Sr varies from 1.17 to 141.36, those of Rb/Ba and K/Rb range from 0.1 to 0.29 and 260.2 to 17.97 respectively.

Biotite granite and two mica granite

The trace element data from whole rock geochemistry of these rocks are presented in Table 7. Most of the samples present high contents in Ba (3 - 1,420 ppm**)**. Other elements with high concentrations are Sr (3.6 - 495 ppm), Zr (44 - 288 ppm), and Rb (107 - 186 ppm). Elements with low to average concentrations are Pb (34 - 79 ppm), Zn (5 - 47 ppm), V (5 - 40 ppm), Y (3 - 36.8 ppm), Th (1.81 - 36 ppm), Ga (16.7 - 31.4 ppm) and Nb (1.2 - 25.3 ppm). The concentration of U and Ta are very low with values of 0.76 - 5.57 ppm and 0.1 - 1.4 ppm respectively. The ratio of Ba/Sr varies from 0.83 to 2.59, those of Rb/Ba and K/Rb range from 0.1 to 59.33 and 367.74 to 176.75 respectively.

As SiO_2 content increases, these elements present three correlation trends (Fig. 47). Strontium, Zr and Nb correlates negatively, an absence of correlation is seen with Ba, Ga, Rb, Ta, Y, Yb, U and Th, while only Pb show positive correlations.

Table 7: Trace and rare earth elements geochemistry of Mayo Kila magmatic rocks.

	Plutonic unit								Volcanic unit	
	Biotite granite				Two mica granite	Diorite		Monzonite	Basanite	
Sample	MK 01	MK 04	MK 08	MK 09	MK 03	MK 11	MK12	MK10	MK07	
Ba (ppm)	1280	302	168.5	1420	3	953	878	1355	571	
Cd	<0.5	<0.5	<0.5	<0.5	<0.5	<0.5	<0.5	<0.5	0.7	
Co	4	1	1	4	2	26	28	20	29	
Cu	11	7	6	5	9	18	47	5	9	
Cr	10	10	10	30	10	230	140	140	20	
Cs	1.55	0.87	2.45	4.69	0.56	3.9	10.45	11.8	0.77	
Ga	22.7	16.7	21.2	19.3	31.4	18.2	20.6	23.8	21.4	
Hf	6.7	1.8	3.2	4.9	4.1	5.5	4.7	10	11.1	
Li	20	10	10	30	<10	20	30	100	10	
Mo	2	1	1	1	2	1	2	1	3	
Nb	10.3	3.5	1.2	11.6	25.3	6.7	13.7	20.7	91.8	
Ni	9	4	3	10	6	117	85	37	4	
Pb	34	52	54	37	79	23	22	29	8	
Rb	186	107	177	150.5	178	90.6	125.5	212	49.4	
Sc	2	1	<1	3	6	14	20	15	12	
Sn	3	1	1	3	3	1	2	5	3	
Sr	495	187	102	572	3.6	813	298	728	1170	
Ta	1.1	0.2	0.1	1.4	1.2	0.4	0.7	1.2	4.9	
Tl	<10	<10	<10	10	<10	<10	<10	<10	<10	
Th	30.5	1.81	5.19	36	6.61	17.8	8.29	20.5	6.13	
U	3.3	0.76	2.75	5.26	5.57	2.06	1.57	4.51	1.82	
V	30	5	13	40	6	104	165	145	205	
W	1	<1	<1	<1	1	1	1	2	2	
Y	11	3	18.8	29.2	36.8	17.5	28.9	32.3	31.3	
Zn	47	5	11	43	22	63	125	138	134	
Zr	288	47	39	140	44	238	189	400	455	
Ba/Sr	2.59	1.61	1.65	2.48	0.83	1.17	2.95	141.36	K/Nb	221.55
Rb/Ba	0.15	0.35	1.05	0.11	59.33	0.1	0.14	0.29	Y/Nb	0.34
k/Rb	233.42	367.74	289.37	284.06	176.75	260.22	207.69	17.97	Zr/Nb	4.95
La ppm	52.5	5.3	14.1	52.7	5.6	89.4	25.4	0.16	62.5	
Ce	116.5	7.7	9.3	83.4	15	171	53.8	79.4	136.5	
Pr	10.6	0.97	3.19	8.94	1.63	17.45	6.62	161.5	15.65	
Nd	37.3	3.9	14.9	32.2	8.7	63.8	27.7	19.3	69.1	
Sm	6.69	0.8	3.23	5.99	3.14	8.51	6.88	73.8	13.35	
Eu	1.11	0.26	0.52	1.12	<0.03	1.62	1.39	12.8	3.54	
Gd	3.33	0.68	3.91	5.73	3.03	5.35	5.09	2.73	9.65	
Tb	0.52	0.06	0.66	0.95	0.7	0.73	0.99	8.74	1.19	
Dy	2.22	0.54	3.58	4.95	5.53	3.88	5.48	0.99	7.32	
Ho	0.36	0.07	0.73	0.97	1.34	0.66	1.08	5.6	1.28	
Er	1.03	0.33	2.11	2.67	4.18	1.79	3.4	0.92	3.15	
Tm	0.15	0.06	0.31	0.28	0.59	0.2	0.35	2.45	0.34	
Yb	1.18	0.1	1.38	2	4.3	1.13	3.05	0.39	2.48	
Lu	0.16	0.04	0.26	0.33	0.5	0.24	0.4	2.29	0.34	
∑REE	233.65	20.81	58.18	202.23	54.27	365.76	141.63	370.91	∑REE	326.39
(La/Yb)N	30.22	36	6.94	17.9	0.88	53.74	5.66	371.27	(La/Yb)N	17.12
(Ce/Sm)N	4.2	2.32	0.69	3.36	1.15	4.85	1.88	23.55	(La/Sm)N	2.92
(Gd/Yb)N	2.28	5.5	2.29	2.32	0.57	3.83	1.35	3.04	(Ce/Yb)N	14.45
Eu/Eu*	0.72	1.07	0.45	0.58	0.03	0.73	0.72	3.08	Eu/Eu*	0.95

Eu/Eu* ($Eu/Eu^* = Eu_N/(Sm_N * Gd_N)^{0.5}$)

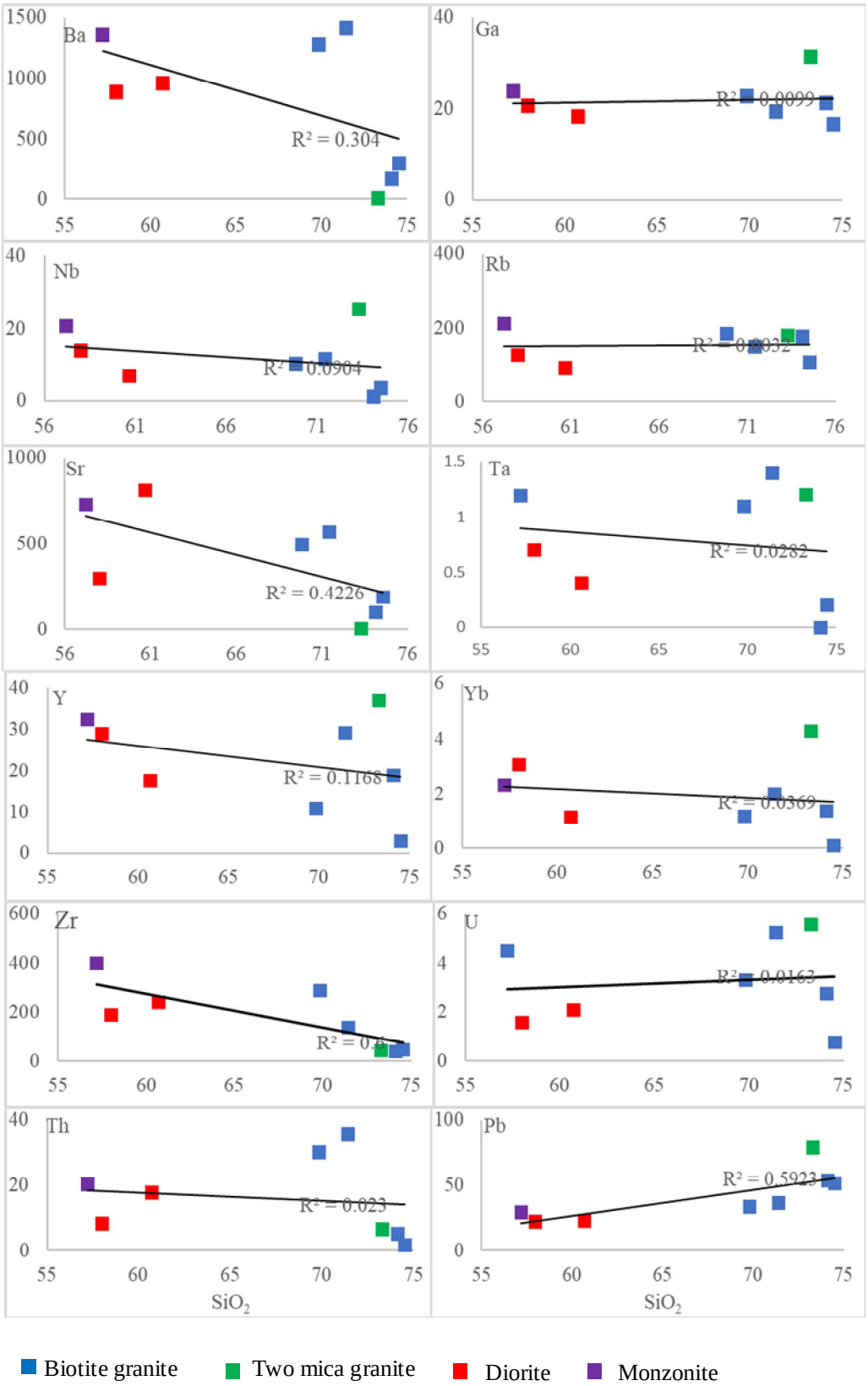

Figure 47: Variation diagrams of selected trace elements plotted against SiO_2 for the studied plutonic rocks

Correlation coefficients for trace elements in the plutonic rocks

Trace elements in the Mayo Kila plutonic rock samples show positive correlations between Ba and Sr (0.85), Ba and Th (0.87), Ba and Zr (0.81), Ga and Nb (0.81), Ga and U (0.70), Ga and Yb (0.82), Nb and Ta (0.78), Nb and U (0.70), Nb and Y (0.80), Nb and Yb (0.85), Sr and Zr (0.82), Ta and U (0.82), U and Y (0.73) and Y and Yb (0.91) (Table 8).

Negative correlations are noticed between Ba and Pb (-0.79), Pb and Sr (-0.80) and Pb and Zr (-0.72) (Table 8).

Table 8: Correlation matrix between some trace elements for Mayo Kila plutonic rocks. Green boxes indicate negative correlation and yellow boxes indicate positive correlation.

Ba	1.00											
Ga	-0.30	1.00										
Nb	0.11	**0.81**	1.00									
Pb	**-0.79**	0.60	0.22	1.00								
Rb	0.14	0.65	0.50	0.26	1.00							
Sr	**0.85**	-0.38	0.00	**-0.80**	-0.09	1.00						
Ta	0.55	0.53	**0.78**	-0.01	0.54	0.27	1.00					
Th	**0.87**	-0.09	0.13	-0.46	0.26	0.68	0.69	1.00				
U	0.20	**0.70**	**0.70**	0.35	0.67	0.06	**0.82**	0.49	1.00			
Y	0.10	0.66	**0.80**	0.12	0.43	0.01	0.63	0.13	**0.73**	1.00		
Yb	-0.15	**0.82**	**0.85**	0.32	0.38	-0.28	0.56	-0.07	0.62	**0.91**	1.00	
Zr	**0.81**	-0.03	0.30	**-0.72**	0.31	**0.82**	0.42	0.56	0.13	0.15	-0.04	1.00
	Ba	**Ga**	**Nb**	**Pb**	**Rb**	**Sr**	**Ta**	**Th**	**U**	**Y**	**Yb**	**Zr**

IV.2.1.1.3- Rare earth elements distribution

Diorite and monzonite

Rare earth elements (∑REE) vary between 141.63 and 370.91 ppm with highest values in the monzonite (sample MK10) and the lowest value in diorite (sample MK12). Chondrite normalised (Mcdonough and Sun, 1995) rare earth element (REE) abundance show low to high enrichment in LREE compared to HREE, with $(La/Yb)_N$ values that vary from 5.66 to 371.27. They show moderate HREE fractionation with $(Gd/Yb)_N$ values between 1.35 and 3.83 (Table 7). In monzonite (sample MK10), $(La/Yb)_N$ value is high (371.27), while

those of diorites are low to average (5.66 to 53.74). As for $(Gd/Yb)_N$ values, they vary from 1.35 to 3.83 in diorite and 3.04 in monzonite. The rocks show a variation in the ratios of light rare earth elements $(Ce/Sm)_N$ from 1.88 to 23.55, with highest value in monzonite (MK10 = 23.55).

Biotite granite and two mica granite

Rare earth element data is presented in table 7. Total rare earth element values (∑REE) vary between 20.81 and 233.65 ppm, with highest value in sample MK01 and lowest value in sample MK04. Chondrite normalized (McDonough and Sun, 1995) rare earth element (REE) patterns show low to high enrichment in LREE compared to HREE, with $(La/Yb)_N$ values from 0.88 to 36. They show moderately HREE fractionation with $(Gd/Yb)_N$ values between 0.57 and 5.5 (Table 7). In biotite granites, the $(La/Yb)_N$ values are moderate to high (6.94 to 36), while those in two mica granite (MK03) are very low (0.88). As for $(Gd/Yb)_N$ values of 3.83 in two mica granite (MK03) and in biotite granites, the values are low to moderate (2.28 to 5.5). The rocks show a variation in the ratios of light rare earth elements $(Ce/Sm)_N$ from 0.69 to 4.2, two mica granite (MK03) show a value of 1.15 and those of biotite granite vary from 0.69 to 4.2 with most values >2.

Most of these granitoids show prominent negative Eu anomalies (Eu/Eu^*=0.03 - 0.73), except for the monzonite sample with a stong positive anomalie (MK10 =3.08), while almost no anomalie (1.07) is observed in one biotite granite sample (MK04). Stongest negative Eu anomalie is observed in two mica granite (MK03 = 0.03). The negative Eu anomalies observed in biotite granites are strong in samples Mk08 = 0.45 and MK09 = 0.58. Also, negative anomalies are observed in diorites (MK11 = 0.73 and MK12 = 0.72) (Fig. 48).

Primitive mantle (Sun and McDonough, 1995) normalized multi-element plots (Fig. 49) display negative anomalies in Ba, Nb, Ta and Zr, and positive anomalies are observed in Rb, U and K. Also, P shows positive anomalies in samples MK03 and MK11. For Th and Yb, samples MK04 and MK08 show negative anomalies while the other samples show positive anomalies.

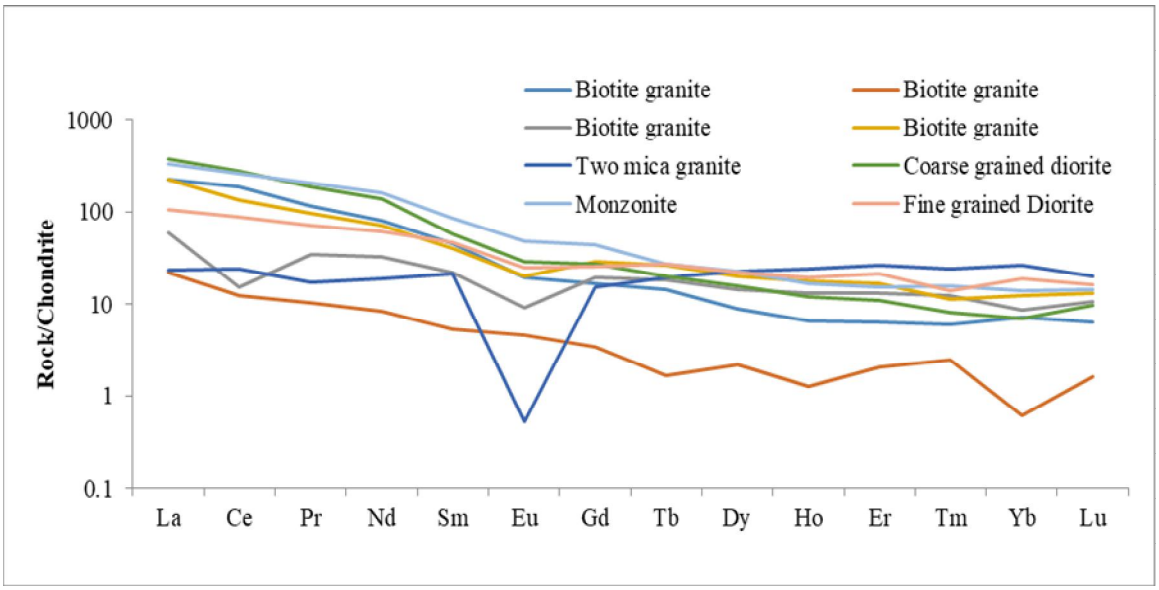

Figure 48: Chondrite normalized REE patterns of Mayo Kila plutonic rocks, normalizing values are from McDonough and Sun (1995).

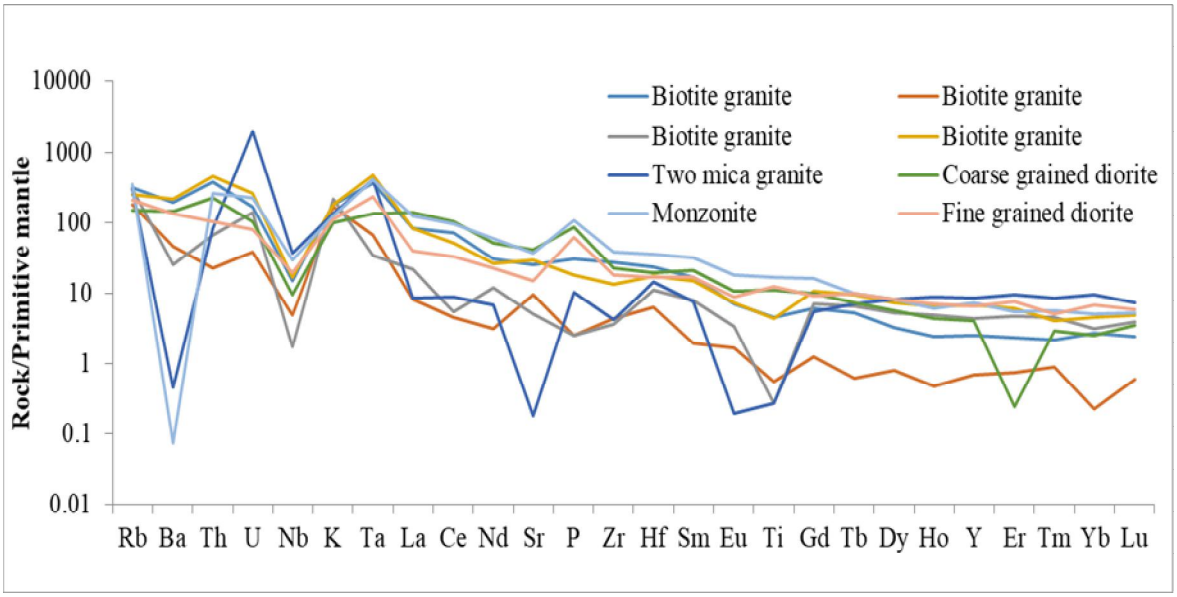

Figure 49: Primitive mantle-normalized multi-element patterns of Mayo Kila plutonic rocks, normalizing values are from McDonough and Sun (1995).

IV.2.2- Geochemistry of mafic volcanic rocks from Mayo Kila and Mbiame

Table 9 presents results of geochemical analyses of eight mafic volcanic rock samples; seven samples (five (05) basanitees (MK13, MK17, MK18, MK19, MK20) and two (02) foidites (MK14 and MK21)) from Mbiame and one basanite sample (MK07) from Mayo Kila.

Table 9: Major and minor element contents and CIPW norms of Mayo Kila and Mbiame area mafic volcanic rocks.

	Mayo Kila Basanite	Basanites from Mbiame and its environs					Foidite	
SAMPLES	MK07	MK 13	MK 17	MK 18	MK 19	MK 21	MK 14	MK 20
SiO_2 (wt.%)	45.5	44.1	41.9	42.2	43.1	41.7	39.7	39.7
TiO_2	3.28	3.7	4.93	3.54	4.25	3.68	4.96	5.86
Al_2O_3	16.85	17	13.6	14.35	15.8	14	13	12.85
Fe_2O_3	12.85	13.3	15.3	14.15	13.25	14.75	15.1	17.15
MnO	0.2	0.2	0.19	0.22	0.19	0.21	0.19	0.19
MgO	4.59	5.4	8.65	9.12	5.62	7.95	10.25	9.38
CaO	7.82	7.77	10	11.1	9.32	9.04	10	10.2
Na_2O	3.7	3.8	2.85	3.87	3.73	4.33	1.93	2.57
K2O	2.45	1.85	1.19	1.52	1.72	1.79	0.68	0.92
P_2O_5	0.95	1.4	0.78	0.86	0.94	1.14	0.58	0.52
Cr_2O_3	0.003	0.005	0.053	0.042	0.008	0.022	0.046	0.045
SrO	0.11	0.26	0.12	0.08	0.14	0.12	0.07	0.1
BaO	0.07	0.08	0.06	0.06	0.08	0.08	0.04	0.04
LOI	1.29	1.79	1.59	-0.44	0.74	-0.28	2.6	0.32
Total	99.66	100.66	101.21	100.67	98.89	98.53	99.15	99.85
FeOt	11.565	11.97	13.77	12.735	11.925	13.275	13.59	15.435
Mg#	28.41	31.09	38.58	41.73	32.03	37.46	42.99	37.8
Na_2O+k_2O	6.15	5.65	4.04	5.39	5.45	6.12	2.61	3.49
k_2O/Na_2O	0.66	0.49	0.42	0.39	0.46	0.41	0.35	0.36
A/CNK	0.73	0.76	0.56	0.51	0.63	0.55	0.59	0.54
A/NK	1.93	2.06	2.28	1.79	1.98	1.55	3.32	2.46
CIPW norms								
Quartz %		-		-	-	-	-	-
Orthoclase		10.25	6.44	-	9.55	4.92	3.82	-
Albite		12.66	1.53	-	5.69	-	0.94	-
Anorthite		21.72	18.46	15.24	19.42	12.03	22.69	18.26
Nepheline		9.08	10.82	15.73	12.61	17.9	7.61	10.37
Leucite		-	-	6.4	-	3.81	-	3.83
Diopside		4.95	18.08	18.79	15.04	18.54	16.35	17.06
Hypersthene		-	-	-	-	-	-	-
Olivine		27.72	29.87	29.64	24.01	29.4	33.81	33.29
Larnite		-	-	1.99	-	-	-	1
Hematite		-	-	-	-	-	-	-
Magnetite		4.16	4.75	4.37	4.23	4.63	4.82	5.25
Ilmenite		6.43	8.35	5.96	7.41	6.3	8.64	9.79
Corundum		-	-	-	-	-	-	-
Apatite		2.97	1.61	1.77	2	2.38	1.23	1.06
Zircon		0.05	0.04	0.05	0.04	0.06	0.03	0.03
Perovskite		-	-	-	-	-	-	-
Chromite		0.01	0.07	0.05	0.01	0.03	0.06	0.06
Rutile		-	-	-	-	-	-	-
Total		100.00	100.02	99.99	100.01	100.00	100.00	100.00

Mg# (=100 × MgO/(MgO + FeO))

IV.2.2.1- Major and minor element contents

In the total alkaline silica (TAS) classification diagram of Le Maitre et al. (2002) all the samples show alkaline affinity with samples MK13, MK17, MK18, MK19 and MK21 from Mbiame and sample MK07 from Mayo Kila ploting in the basanite domain while samples MK14 and MK20 from Mbiame plots in the foidite domain.

Basanite

The rocks are silica-poor and predominantly exhibit an ultra-basic character with SiO_2 content between 41.7 and 44.1 wt.% for Mbiame rocks and of 45.5 wt.% for the Mayo kila sample (Table 9). The total alkali content ($Na_2O + K_2O$) range from 4.04 to 6.15 and the K_2O/Na_2O ratios range from 0.39 to 0.66. Other major elements show variable concentrations with Al_2O_3 content (14 - 17 wt.%), Fe_2O_3 (13 - 15.3 wt.%), CaO (7.8 - 11.1 wt.%), MgO (4.59 - 9.12 wt.%), TiO_2 (3.28 - 4.93 wt.%), Na_2O (2.85 - 4.33 wt.%), K_2O (1.2 – 2.45 wt.%), P_2O_5 (0.78 - 1.4 wt.%), MnO (0.2 wt.%), Cr_2O_5 (0.003 - 0.053 wt.%), SrO (0.08 - 0.26 wt.%) and BaO (0.06 - 0.08 wt %). The Loss On Ignition (L.O.I = -0.44 to 1.79 wt.%) values are low.

Foidites

The rocks are silica-poor and exhibit an ultra-basic character with both samples having similar SiO_2 content of 39.7 wt.% (Table 9). On the total alkaline silica (TAS) classification diagram of Le Maitre, the samples show alkaline affinity and plot in the foidite domain (Figure 39). Other major elements show variable concentrations with Al_2O_3 content (12.85 - 13 wt.%), Fe_2O_3 (15 - 17.15 wt.%), CaO (10 - 10.2 wt.%), MgO (9.38 - 10.25 wt.%), TiO_2 (4.96 - 5.86 wt.%), Na_2O (1.93 - 2.57 wt.%), K_2O (0.68 - 0.92 wt.%), P_2O_5 (0.52 - 0.58 wt.%) and MnO (0.2 wt.%). The Loss On Ignition (L.O.I = 0.32 - 2.6 wt.%) values are low.

The total alkali content ($Na_2O + K_2O$) ranges from 2.61 to 3.49 wt.%, while the K_2O/Na_2O ratio ranges from 0.35 to 0.36.

The Harker diagrams (Fig. 50) show variation of a range of major oxides, with TiO_2, Fe_2O_3, MgO and CaO showing a negative correlation as SiO_2 (Fig. 50 a,c,d,e), increases while Na_2O, K_2O, Al_2O_3 and P_2O_5 correlates positively with increasing SiO_2 (Figure 51 b,f,g,h).

The Mg# ranges from 31.09 to 42.99, for Mbiame samples and 28.41 for the Mayo Kila sample but generally falls within the range (1 - 65) obtained for other samples of the Oku Volcanic Group (Asaah et al., 2015). On the Na_2O versus K_2O diagram of Middlemost (1975) (Fig. 51), most samples plot in the Na_2O series while the Mayo Kila sample plots in the K_2O series. One Mbiame foidite sample plots on the line separating the Na_2O and the K_2O series.

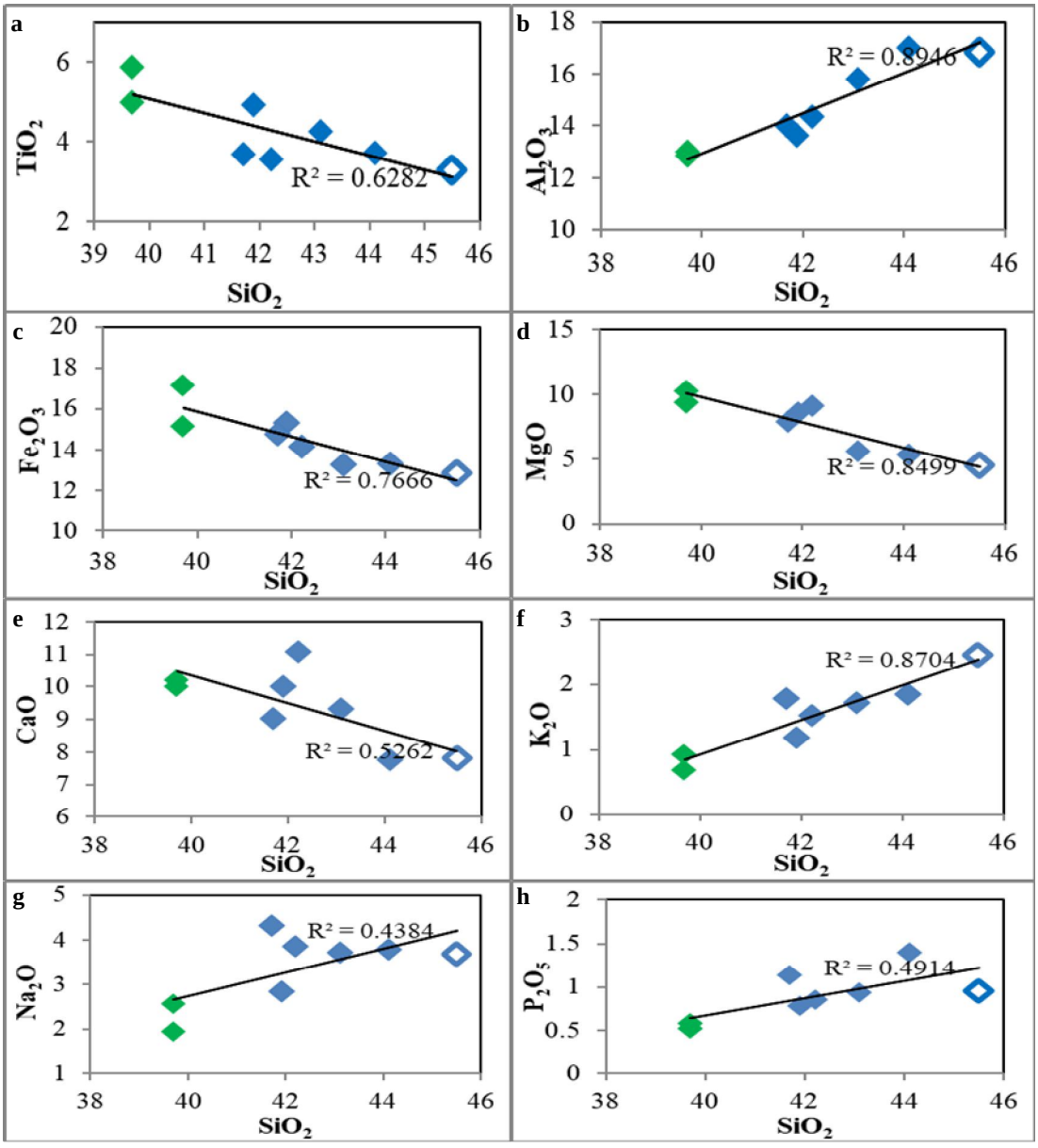

Figure 50: Harker variation diagrams of major elements for Mbiame and Mayo Kila volcanic rocks.

Correlation coefficients for major elements in the lavas

Major elements in Mayo Kila and Mbiame lavas show positive correlations (Table 10) between SiO_2 and Al_2O_3 (0.95), SiO_2 and K_2O (0.93), SiO_2 and P_2O_5 (0.70), SiO_2 and BaO

(0.75), TiO_2 and Fe_2O_3 (0.86), Al_2O_3 and K_2O (0.86), Al_2O_3 and P_2O_5 (0.76), Al_2O_3 and BaO (0.75), Fe_2O_3 and MgO (0.80), Fe_2O_3 and Cr_2O_3 (0.80), MgO and CaO (0.84), MgO and Cr_2O_3 (0.94), CaO and Cr_2O_3 (0.85), Na_2O and K_2O (0.82), Na_2O and P_2O_5 (0.79), NaO and BaO (0.88), K_2O and P_2O_5 (0.72) K_2O and BaO (0.81), P_2O_5 and SrO (0.81) and P_2O_5 and BaO (0.89).

Negative correlations on their part are observed between SiO_2 and TiO_2 (-0.79), SiO_2 and Fe_2O_3 (-0.88), SiO_2 and MgO (-0.92), SiO_2 and CaO (-0.73), SiO_2 and Cr_2O_3 (-0.81), TiO_2 and Al_2O_3 (-0.73), TiO_2 and MnO (-070), TiO_2 and Na_2O (-0.81), TiO_2 and K_2O (-0.85), TiO_2 and P_2O_5 (-0.75), TiO_2 and BaO (-0.75), Al_2O_3 and Fe_2O_3 (-0.89), Al_2O_3 and MgO (-0.95), Al_2O_3 and CaO (-079), Al_2O_3 and Cr_2O_3 (-0.91), Fe_2O_3 and BaO (-0.75), MgO and K_2O (-0.88), MgO and (-0.78), CaO and K_2O (-0.71), K_2O and Cr_2O_3 (-0.85), P_2O_5 and Cr_2O_3 (-0.74), Cr_2O_3 and BaO (-0.79) (Table 10).

Table 10 : Correlation matrix between major elements for Mayo Kila and Mbiame volcanic rocks. Green boxes indicate negative correlation and yellow boxes indicate positive correlation.

SiO_2	1.00												
TiO_2	**-0.79**	1.00											
Al_2O_3	**0.95**	**-0.73**	1.00										
Fe_2O_3	**-0.88**	**0.86**	**-0.89**	1.00									
MnO	0.25	**-0.70**	0.16	-0.29	1.00								
MgO	**-0.92**	0.62	**-0.95**	**0.80**	-0.01	1.00							
CaO	**-0.73**	0.48	**-0.79**	0.60	0.12	**0.84**	1.00						
Na_2O	0.66	**-0.81**	0.61	-0.61	0.68	-0.61	-0.39	1.00					
K_2O	**0.93**	**-0.85**	**0.86**	-0.80	0.41	**-0.88**	**-0.71**	**0.82**	1.00				
P_2O_5	**0.70**	**-0.75**	**0.76**	-0.69	0.41	-0.69	-0.69	**0.79**	**0.72**	1.00			
Cr_2O_3	**-0.81**	0.67	**-0.91**	**0.80**	-0.11	**0.94**	**0.85**	-0.65	**-0.85**	**-0.74**	1.00		
SrO	0.51	-0.29	0.67	-0.42	-0.05	-0.62	-0.68	0.40	0.40	**0.81**	-0.60	1.00	
BaO	**0.75**	**-0.75**	**0.75**	**-0.75**	0.33	**-0.78**	-0.62	**0.88**	**0.81**	**0.89**	**-0.79**	0.62	1.00
	SiO_2	**TiO_2**	**Al_2O_3**	**Fe_2O_3**	**MnO**	**MgO**	**CaO**	**Na_2O**	**K_2O**	**P_2O_5**	**Cr_2O_3**	**SrO**	**BaO**

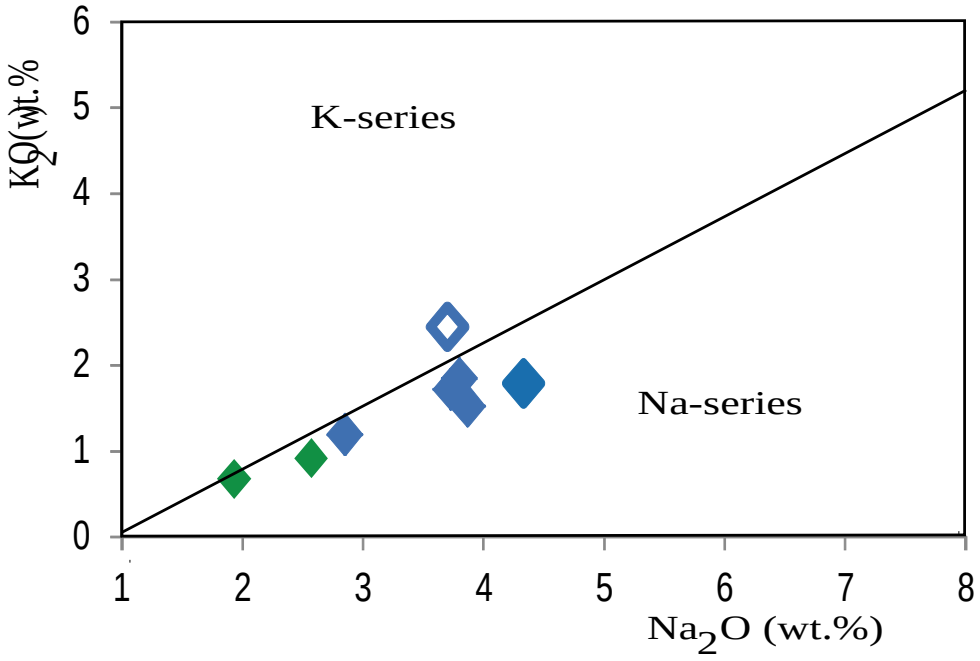

Figure 51: Na_2O versus K_2O subdivision diagram of the alkaline series (Middlemost, 1975) of Mbiame and Mayo Kila volcanic rocks. Same smboles as in Figure 50.

IV.2.2.2- Trace elements distribution

Basanites

Trace element data for lavas from Mbiame and Mayo Kila are presented in Table 11. The concentrations of compatible elements like Ni, Co, Cr, Sc and V in the samples range from 4 -184 ppm, 29 - 56 ppm, 20 - 340 ppm, 12-25 ppm and 173 - 302 ppm respectively. Some of these values remain lower than those assumed for primary magmas while others overlap with values obtained from primary derived magmas (Ni: 300–400 ppm; Cr: 300–500 ppm; Co: 50–70 ppm; e.g., Frey et al., 1978; Jung and Masberg, 1998), thus, indicating slight crystal fractionation with the removal of olivine + pyroxene ± spinel assemblage (Kamgang et al., 2013). Its trace element ratios of K/Nb, Y/Nb and Zr/Nb range between 194.12 - 237, 0.39 - 0.45 and 3.69 - 4.62 respectively.

Foidites

Trace element data for foidite lava from Mbiame are presented in Table 11. The concentrations of compatible elements like Ni, Co, Cr, Sc and V in Mbiame samples range from 171-354 ppm, 59-74 ppm, 300 ppm, 25-26 ppm and 324-327 ppm respectively. These values slightly overlap with those obtained from primary derived magmas (Ni: 300–400 ppm;

Cr: 300–500 ppm; Co: 50–70 ppm; e.g., Frey et al., 1978; Jung and Masberg, 1998). Thus, signifying slight crystal fractionation with the removal of olivine + pyroxene ± spinel assemblage (Kamgang et al., 2013). Incompatible elements concentration varies with, Rb (13.2 - 13.4 ppm), Ba (294 -362 ppm), Hf (3.8 - 4.3 ppm), Zr (166 - 171 ppm), Nb (36.9 - 38.8 ppm) and Y (18.8 - 21.3 ppm). Trace elemnt ratios of K/Nb, Y/Nb and Zr/Nb range between 145.5 - 207, 0.48 - 0.58 and 4.41 - 4.5 respectively.

Amongst these compatible elements, Ni, Co, Cr, Cu and V correlate negatively with increasing SiO_2 while Sr shows a positive correlation as SiO_2 increases (Fig. 52). As for incompatible elements, positive correlation with increasing SiO_2 is observed in Rb, Ba, Yb, Hf, Zr, Nb and Y.

Table 11: Trace and rare earth elements geochemistry of Mbiame and Mayo Kila volcanic rocks.

	Mayo Kila Basanite	Basanites from Mbiame and its environs					Foidites	
SAMPLES	**MK07**	**MK 13**	**MK 17**	**MK 18**	**MK 19**	**MK 21**	**MK 14**	**MK 20**
Ba (ppm)	571	663	474	549	606	674	362	294
Cd	0.7	<0.5	1.1	0.5	0.8	0.7	0.5	0.9
Co	29	32	56	49	38	47	59	74
Cu	9	17	76	42	38	40	36	176
Cr	20	30	340	280	50	150	300	300
Cs	0.77	0.35	0.25	0.53	0.24	0.68	0.32	0.06
Ga	21.4	17.4	17.9	20.7	19.3	18.9	17.1	15.1
Hf	11.1	5.7	4.9	5.6	5.3	7.5	3.8	4.3
Li	10	10	10	10	10	10	<10	10
Mo	3	2	1	3	3	3	1	2
Nb	91.8	64.8	47.8	65	63.1	74.7	38.8	36.9
Ni	4	16	184	100	46	112	171	354
Pb	8	10	3	6	9	12	3	4
Rb	49.4	32.3	21.5	39.8	29.9	40.8	13.4	13.2
Sc	12	12	23	25	16	19	26	25
Sn	3	2	1	2	2	2	1	2
Sr	1170	2210	1065	873	1265	1080	793	929
Ta	4.9	2.2	2	3.8	2.2	3.1	1.5	1.1
Tl	<10	<10	10	<10	<10	<10	<10	10
Th	6.13	3.74	2.77	4.64	3.6	5.83	2.47	1.46
U	1.82	1.25	0.7	1.42	1.09	1.66	0.77	0.46
V	205	173	302	288	246	239	324	327
W	2	<1	<1	<1	3	<1	2	<1
Y	31.3	27.1	21.3	27.6	24.3	29.1	18.8	21.3
Zn	134	106	116	108	119	125	108	116
Zr	455	271	221	255	233	305	171	166
K	20338.19	15357.41	9878.55	12617.98	14278.24	14859.3	5644.88	7637.2
K/Nb	221.55	237	206.66	194.12	226.28	198.92	145.49	206.97
Y/Nb	0.34	0.42	0.45	0.42	0.39	0.39	0.48	0.58
Zr/Nb	4.96	4.18	4.62	3.92	3.69	4.08	4.41	4.5
La	62.5	50.2	33.5	49.1	41.8	53.8	28.1	24.2
Ce	136.5	111	71.8	92.7	89.5	110	60.5	55.4
Pr	15.65	13.65	8.19	11.05	10.65	12.85	7.3	7.16
Nd	69.1	58.1	37.7	49.4	45.8	52.8	33.5	34.4
Sm	13.35	13.05	8.99	9.36	9.36	11.4	6.84	8.42
Eu	3.54	3.97	3.15	2.64	3.13	3.22	2.58	2.24
Gd	9.65	9.32	6.78	7.13	7.93	9.82	5.72	6.84
Tb	1.19	1.24	0.87	1.03	0.88	1.23	0.83	0.81
Dy	7.32	5.93	4.73	5.62	5.01	6.54	4.75	4.64
Ho	1.28	1.15	0.68	1.02	0.9	1.1	0.9	0.83
Er	3.15	2.65	1.97	2.69	2.24	2.73	1.78	2.11
Tm	0.34	0.28	0.25	0.37	0.23	0.29	0.14	0.34
Yb	2.48	2.41	1.42	1.92	1.71	1.87	1.36	1.48
Lu	0.34	0.33	0.16	0.29	0.18	0.35	0.25	0.21
∑REE	326.39	273.28	180.19	234.32	219.32	268	154.55	149.08
(La/Yb)N	17.12	14.15	16.03	17.37	16.61	19.54	14.04	11.11
(La/Sm)N	2.92	2.4	2.33	3.28	2.79	2.95	2.57	1.79
(Ce/Yb)N	14.46	12.1	13.28	12.68	13.75	15.45	11.68	9.83
Eu/Eu*	0.95	1.1	1.23	0.99	1.11	0.93	1.26	0.9

Eu/Eu* (Eu/Eu* = $Eu_N/(Sm_N * Gd_N)^{0.5}$)

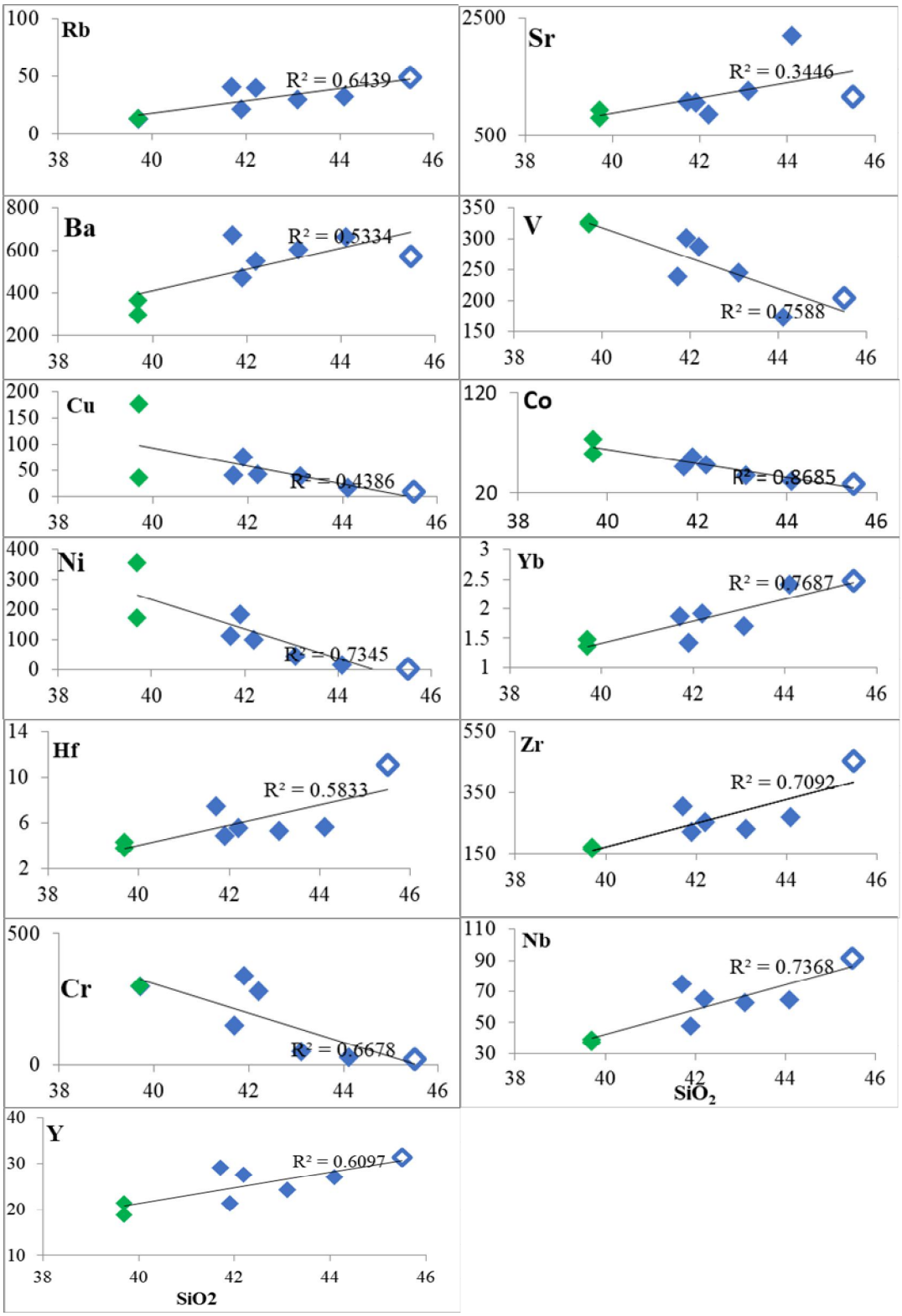

Figure 52: Variation diagrams of trace elements plotted against SiO_2 for the studied volcanic rocks. Same legend as in figure 50.

Correlation coefficients for trace elements in the lavas

Trace elements of these lavas express positive correlations between Ba and Nb (0.79), Ba and Rb (0.79), Ba and Y (0.77), Co and Cu (0.85), Co and Cr (0.88), Co and Ni (0.98), Co and V (0.91), Cu and Ni (0.93), Cr and Ni (0.79), Cr and V (0.92), Hf and Nb (0.92), Hf and Rb (0.86), Hf and Y (0.86), Hf and Yb (0.76), Hf and Zr (0.99), Nb and Rb (0.98), Nb and Y (0.96), Nb and Yb (0.76), Nb and Zr (0.95), Ni and V (0.83), Rb and Y (0.97), Rb and Yb (0.81), Rb and Zr (0.90), Y and Yb (0.88), Y and Zr (0.88), Yb and Zr (0.83) (Table 12).

Negative correlations are observed between Ba and Co (-0.84), Ba and Cu (-0.73), Ba and Cr (-0.73), Ba and Ni (-0.84), Ba and V (-0.85), Co and Nb (-0.85), Co and Rb (-0.79), Co and Y (-0.74), Co and Yb (-0.84), Co and Zr (-0.76), Cr and Nb (-0.76), Cr and Yb (-0.81), Nb and Rb (-0.80), Nb and V (-0.79), Ni and Rb (-0.76), Ni and Yb (-0.76), Rb and V (-0.72), Sr and V (-0.81), V and Y (-0.77), V and Yb (-0.90), V and Zr (-0.72) (Table 12).

Table 12: Correlation matrix between some trace elements for Mayo Kila and Mbiame volcanic rocks. Green boxes indicate negative correlation and yellow boxes indicate positive correlation.

Ba	1.00												
Co	**-0.84**	1.00											
Cu	**-0.73**	**0.85**	1.00										
Cr	**-0.73**	**0.88**	0.59	1.00									
Hf	0.52	-0.67	-0.48	-0.63	1.00								
Nb	**0.79**	**-0.85**	-0.67	**-0.76**	**0.92**	1.00							
Ni	-0.84	**0.98**	**0.93**	**0.79**	-0.59	**-0.80**	1.00						
Rb	**0.79**	**-0.79**	-0.64	-0.65	**0.86**	**0.98**	**-0.76**	1.00					
Sr	0.59	-0.62	-0.36	-0.67	0.13	0.30	-0.53	0.23	1.00				
V	**-0.85**	**0.91**	0.66	**0.92**	-0.64	**-0.79**	**0.83**	**-0.72**	**-0.81**	1.00			
Y	**0.77**	**-0.74**	-0.53	-0.69	**0.86**	**0.96**	-0.69	**0.97**	0.34	**-0.77**	1.00		
Yb	0.69	**-0.84**	-0.59	**-0.81**	**0.76**	**0.84**	**-0.76**	**0.81**	0.64	**-0.90**	**0.88**	1.00	
Zr	0.60	**-0.76**	-0.59	-0.68	**0.99**	**0.95**	-0.69	**0.90**	0.23	**-0.72**	**0.88**	**0.83**	1.00
	Ba	**Co**	**Cu**	**Cr**	**Hf**	**Nb**	**Ni**	**Rb**	**Sr**	**V**	**Y**	**Yb**	**Zr**

IV.2.2.3- Rare earth elements distribution

Basanite

The rare earth element results of basanites are presented in table 11. Total rare earth element ∑REE values are between 180.2 and 268 ppm. The ratios of normalized LREE/HREE vary slightly. The $(La/Yb)_N$ ratio have values between 14.15 and 19.54, those of $(La/Sm)_N$ vary from 2.40 to 3.28, while those of $(Ce/Yb)_N$ vary from 12.10 to 15.45. The values of europium anomaly vary from 0.93 to 1.23. Sample MK18 shows no europium anomaly with a value of 0.99. Negative Eu anomalies are observed in sample MK21 with a value of 0.93, while positive anomalies are seen in sample MK13 with a value of 1.10, sample MK17 with a value of 1.23 and sample MK19 with a value of 1.11.

Foidites

The rare earth element results of Mbiame foidites are presented in Table 11. Their total rare earth element ∑REE values range from 149.1 to 154.55 ppm. The ratios of normalized LREE/HREE slightly vary between the rocks. The values of the ratio $(La/Yb)_N$ are 11.11-14.04, those of $(La/Sm)_N$ vary from 1.79 to 2.57, while those of $(Ce/Yb)_N$ vary from 9.83 to 11.68.

The Chondrite normalised (McDonough and Sun, 1995) rare earth element (REE) patterns are parallel to sub parallel (Figure 53) and show slight enrichment of LREE (La, Ce, Nd, Sm) compared to the HREE (Gd, Dy, Er, and Yb). Primitive mantle normalized multi-element plots (Fig. 54) display negative anomalies in Th, Ta, K, Pb, and Zr while positive anomalies are seen in Ba, Nb, P, and Ti.

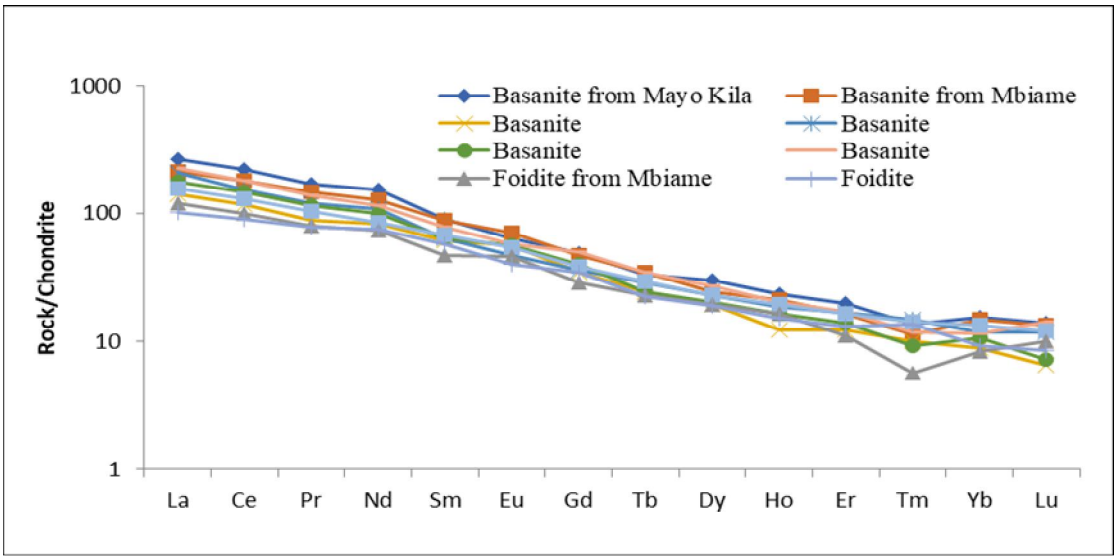

Figure 53: Chondrite normalized REE patterns of Mbiame and Mayo Kila mafic volcanic rocks, normalizing values are from McDonough and Sun (1995).

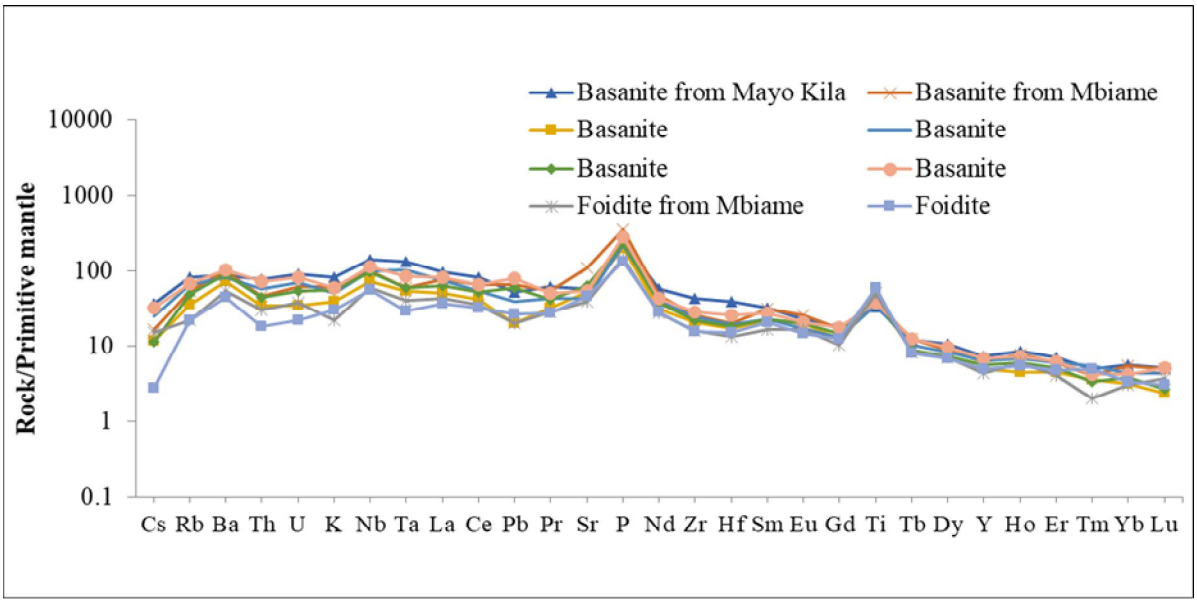

Figure 54: Primitive mantle-normalized multi-element patterns of and Mayo Kila mafic volcanic rocks, normalizing values are from Sun and McDonough (1995).

Conclusion

In the study areas, three main lithologic units were identified. In Mayo Kila, magmatic (volcanic and plutonic) units were identified and sampled while in Mbiame and its environs, only mafic volcanic rocks were sampled.

In Mayo Kila, plutonic rocks exhibit a felsic to intermediate compositions and present a high K-calc-alkaline to shoshonitic affinity. The biotite granites and two mica granites are peralumnous while the diorite and the monzonite samples are metaluminous. Most of the rocks portray ferroan character with only diorites and one biotite granite magnesian. Normative corundum occurs in the biotite granite and two mica granites but is absent in the diorite and monzonite. Trace element abundance shows high to average concentrations in LILE and transition elements. The Eu/Eu* ratio differs from one sample to another with some samples showing negative Eu anomaly while others are marked by absence in Eu anomaly.

The volcanic rock also presents alkaline affinity and plots in the K-series. Its Mg-number falls within values obtained for other alkaline mafic volcanic rocks of the Oku Volcanic Group (OVG). The rock is nepheline and diopside normative. Chondrite normalized REE show enrichment in LREE with respect to HREE. Insignificant fractionation of plagioclase is expressed by the absence of Eu anomaly.

In Mbiame and its environs, the volcanic rocks show alkaline affinity and have been identified as basanites and foidites. Most of the rocks fall in the Na_2O-series. They are nepheline and diopside normative. In this study, three samples (MK 14, MK 17 and MK20) have values of Ni, Cr and Co (Ni: 184-354 ppm, Cr: 300-340 ppm and Co: 56-74 ppm) almost similar to those proposed for primary magmas. This is an indication that the lavas were not significantly fractionated from their parental magmas and their compositions are largely controlled by mantle processes.

CHAPTER V

MORPHOLOGICAL, GEOCHEMICAL AND GEOCHRONOLOGICAL CHARACTERISTICS OF MAYO KILA AND MBIAME GEM PLACERS

This chapter presents morphological data describing alluvial profiles in Mayo Kila and Mbiame, grain size distribution parameters and heavy mineral compositions of the mineralized layers. It also presents morphological features of sapphire grains from Mayo Kila and Mbiame, trace element abundance in sapphires and its zircon inclusions as well as their ages. These characteristics have been used to decipher the difference between the magmatic dominant sapphires from the seemingly metamorphic grains.

V.1- Morphological characteristics of alluvial profiles in Mayo Kila and Mbiame

V.1.1- Alluvial profiles in Mayo Kila

In Mayo Kila, three types of alluvial profiles were described on the banks of Bewende River as follows: exposed alluvial trenches along the Bewende River, alluvial profiles in test pits dug on the banks of Bewende River and alluvial profiles in test pits dug in recent sediments in Bewende River. The mapped pits and other random sample points in Mayo Kila are plotted on the drainage maps of the area (Fig. 55).

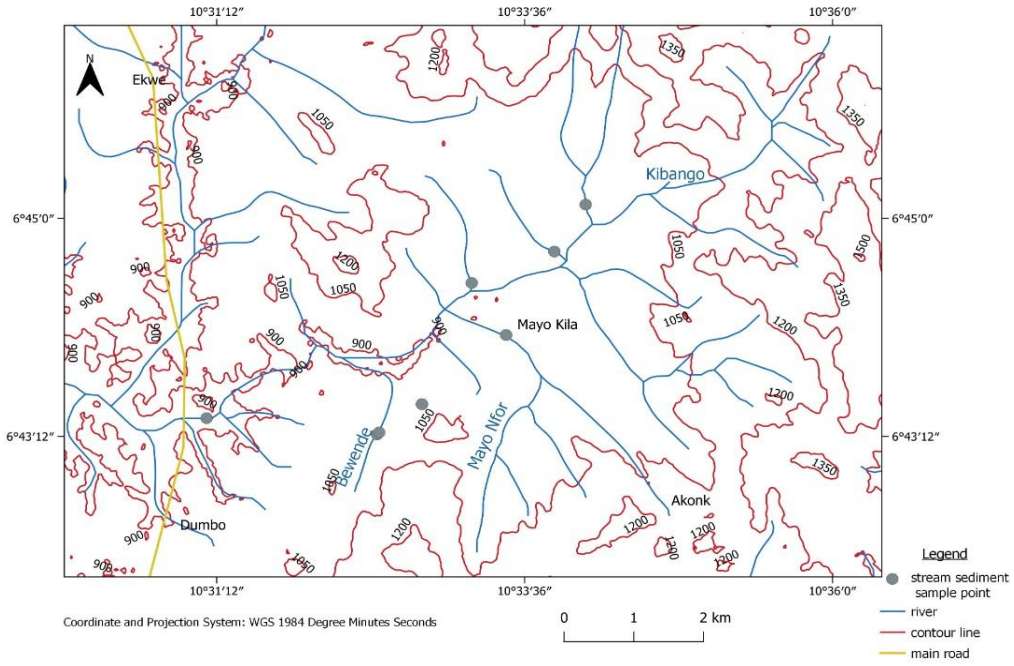

Figure 55: Alluvial prospection map of Mayo Kila.

V.1.1.1- Exposed alluvial trenches along the Bewende River

This alluvial profile (P_o) was observed along the Bewende River. It is located between latitude N06°43'282" to longitude E010°32'483", at an altitude of 940 m, and oriented SW-NE (Fig. 56). It is made up of 8 levels with variable thicknesses, composition, structure, texture and colour. From top to bottom it is made up of the following layers:

- **Level 1 (0 - 37 cm):** this level is brown, organo-mineral and mainly composed of sand and clay size particles. The thickness varies from 15 to 37 cm with its maximum thickness in the NE. It is also characterized by plant roots;
- **Level 2 (37 - 107 cm)**: this level is light brown to yellow, it is composed of sand and clay. Its thickness varies from 15 cm in its SW part, 60 cm in its NE part to 70 cm in the middle. It is also characterized by the presence of plant roots;
- **Level 3 (107 - 197 cm):** it is grey, this level is made up of fine to coarse sand and gravel. It is thicker in the NE (90 cm) and wanes to 30 cm in its middle part to 18 cm in its SW part. The sizes and content of the sand and gravel decrease in a SW - NE direction i.e. away from the active stream;
- **Level 4 (197 - 257 cm):** it is greyish white and composed mostly of sand size particles. This level varies from 60 cm in its SW part and get smaller to 50 cm in its NE;
- **level 5 (257 - 282 cm):** it is greyish white with an almost constant thickness of about 25 cm, it has a gravelly sand texture;
- **Level 6 (282 - 307 cm):** this level is mottled with reddish brown patches, composed mainly of sand. Its thickness varies from 30 cm in its SW part, 35 cm in the middle and decreases to 25 cm in its NE;
- **Level 7 (307 - 342 cm):** this level is greyish white, it is the mineralized level and it is made up of gravel and sand with disseminations of pebbles and cobbles. Its thickness varies from 30 cm in its SW part to 35 cm NE. The gravel of this layer decreases in density from the SW to the NE, i.e. away from the stream.
- **Level 8 (342 - 367 cm):** it is brown and composed mainly of sand, and has a thickness of 25 cm. This layer is underlined by highly weathered coarse grain granitic bed rock characterized by the presence of crisscrossing micas veins.

After the washing of 15 pans of gravel from the exposed gravelly level of this profile, only three (03) sapphire grains were collected although the artisans reported the collection of many sapphire grains in the area.

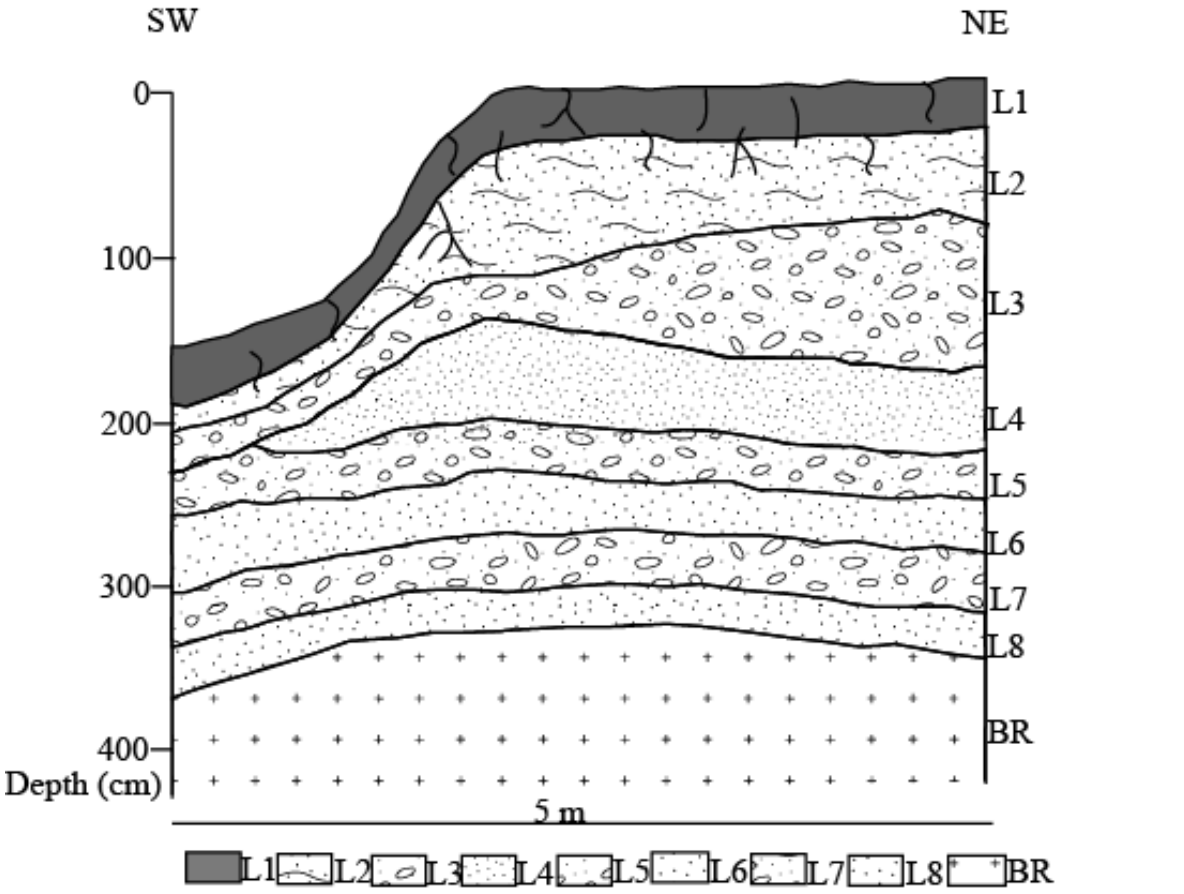

Figure 56: Exposed alluvial (P_o) trench along the Bewende River in Mayo Kila.

V.1.1.2- Alluvial profiles from a test pit on the banks of Bewende River

Pit P1

This first pit was dug about 8 m on the eastern bank of the Bewende River, at latitude N06°43'13" to longitude E010°32'27" with an altitude of 932 m. It has a width of 1 m and a 1.5 m length. Its morphological characteristics from top to bottom is as follows (Fig. 57):

- **Level 1 (0 - 30 cm):** this level has a brown colour, and represents the organo-mineral horizon with a thickness that varies from 21 to 30 cm. It is composed of clay and is also characterized by plant roots and granitic rock fragments;

- **Level 2 (30 - 85 cm):** it is a light brown level with thickness that varies from 49 to 55 cm, composed mainly of sand and clay and has a diffused boundary with the upper organo-mineral horizon;
- **Level 3 (85 - 118 cm):** it is characterized by rock fragments, scattered in a brown sand clayey soil material. The density of the rock fragments decreases downwards towards the granitic bed rock.

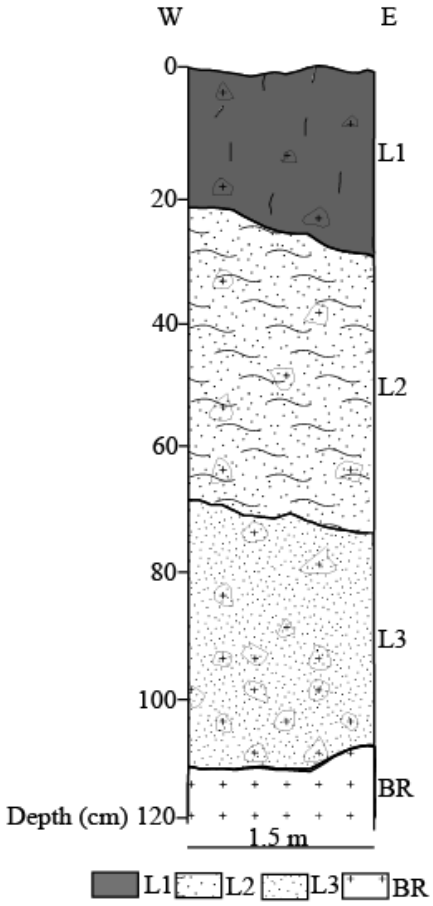

L1: dark brown clay; L2: brownish yellow sandy clay; L3: embedded rock fragments; BR: weathered porphyritic granite

Figure 57: Pit P_1 illustrating an alluvial profile on the bank of Bewende River.

Pit P_2

This pit is about 6 m on the western side of Bewende River. It has a width of 1 m and a 1.5 m length (Fig. 58). It presents the following morphological characteristics from top to bottom:

- **Level 1 (0 - 50 cm):** it is a dark brown organo-mineral horizon with a silty sand texture and the predominance of plant roots;

- **Level 2 (50 - 134 cm):** it is reddish brown, composed mainly of sand and varies from 80 to 84 cm. It also contains few plant roots. Its boundary with the upper horizon is clear;
- **Level 3 (134 - 156 cm):** it is dark grey, composed of sand and clay with thickness that varies from 20 to 22 cm. It has a clear boundary with the overlying horizon;
- **Level 4 (156 - 206 cm):** it is dark grey and portrays a sandy texture. It varies from 43 to 48 cm. Plant roots are also observed at this depth;
- **Level 5 (206 - 257 cm):** it is grey and represents the gravelly level. It is characterized by angular to rounded pebbles and coble size materials. Gravel washed from this layer yielded 1 grain from 10 pans. The bed rock of this profile is coarse grained granite.

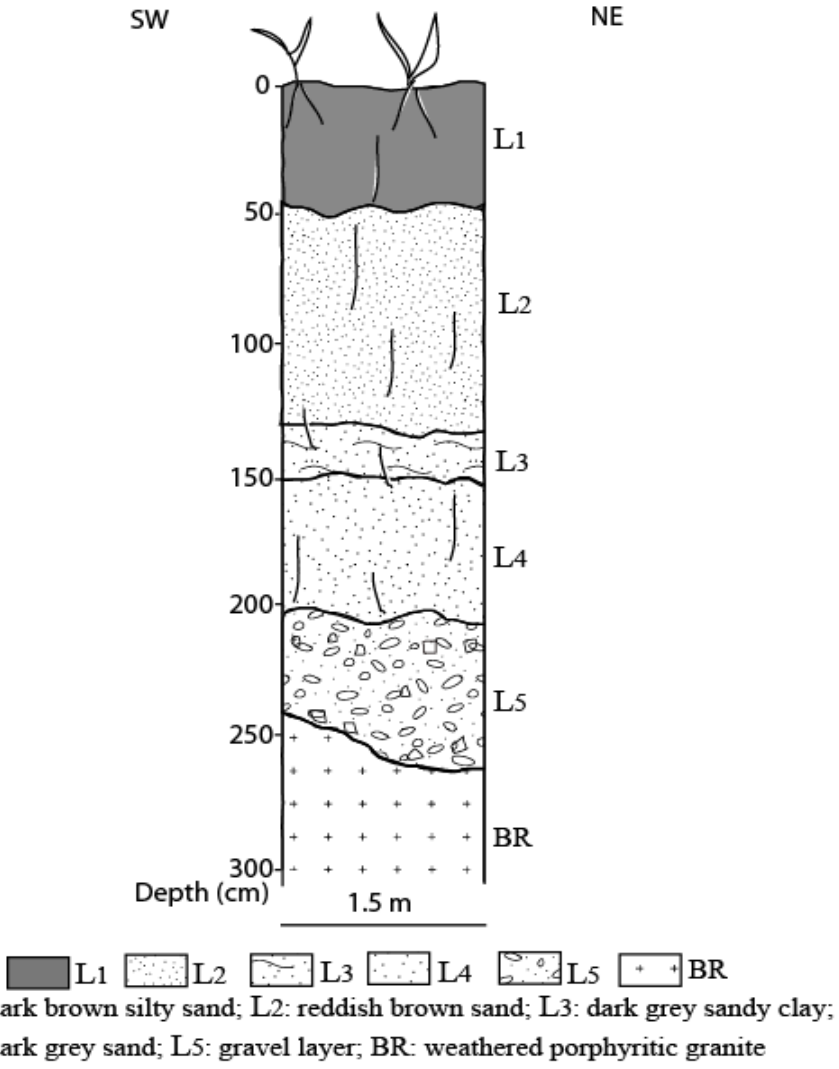

Figure 58: Pit P_2 illustrating an alluvial profile on the western flank of Bewende River.

V.1.1.3- Alluvial profiles from test pits in recent sediments

These are pits dug on the convex side of the river bed with high gravel and thin sand deposition, generally not deep. For this study, most sapphire grains were collected from these test pits.

Gravel test pit 1 (GTP1)

It is located between latitude N06°43'14" to longitude E010°32'28", on an altitude of 922 m. From top to bottom (Fig. 59a), it is characterized by a sandy and gravelly horizon as follows:

- **Level 1 (0 - 21 cm)**: it is a grey level with a medium to coarse sand composition. Its thickness can attain 21 cm. Quartz and rock fragments are also observed at this level;
- **Level 2 (21 – 76 cm)**: it is a grey gravelly level of about 55 cm thick, composed of angular to rounded pebbles. This test pit yielded 6 sapphire grains from the washing of 20 pans of gravel.

Gravel Test pit 2 (GTP2)

It is located at latitude N06°43'282" and longitude E010°32'483", about 1 km SW of pit 1, on an altitude of 925 m. From top to bottom (Fig. 59b), it is characterized by a sandy gravel horizon and a gravelly horizon as follows:

- **Level 1 (0 - 15 cm)**: it is grey, composed mostly of medium to coarse sand and has a thickness of about 15 cm;
- **Level 2 (15 - 79 cm)**: this layer is also grey and represents the gravelly level. It is about 64 cm thick and is also composed of angular and rounded pebbles and coble. From this pit, 20 pans of washed gravel yielded 4 sapphire grains.

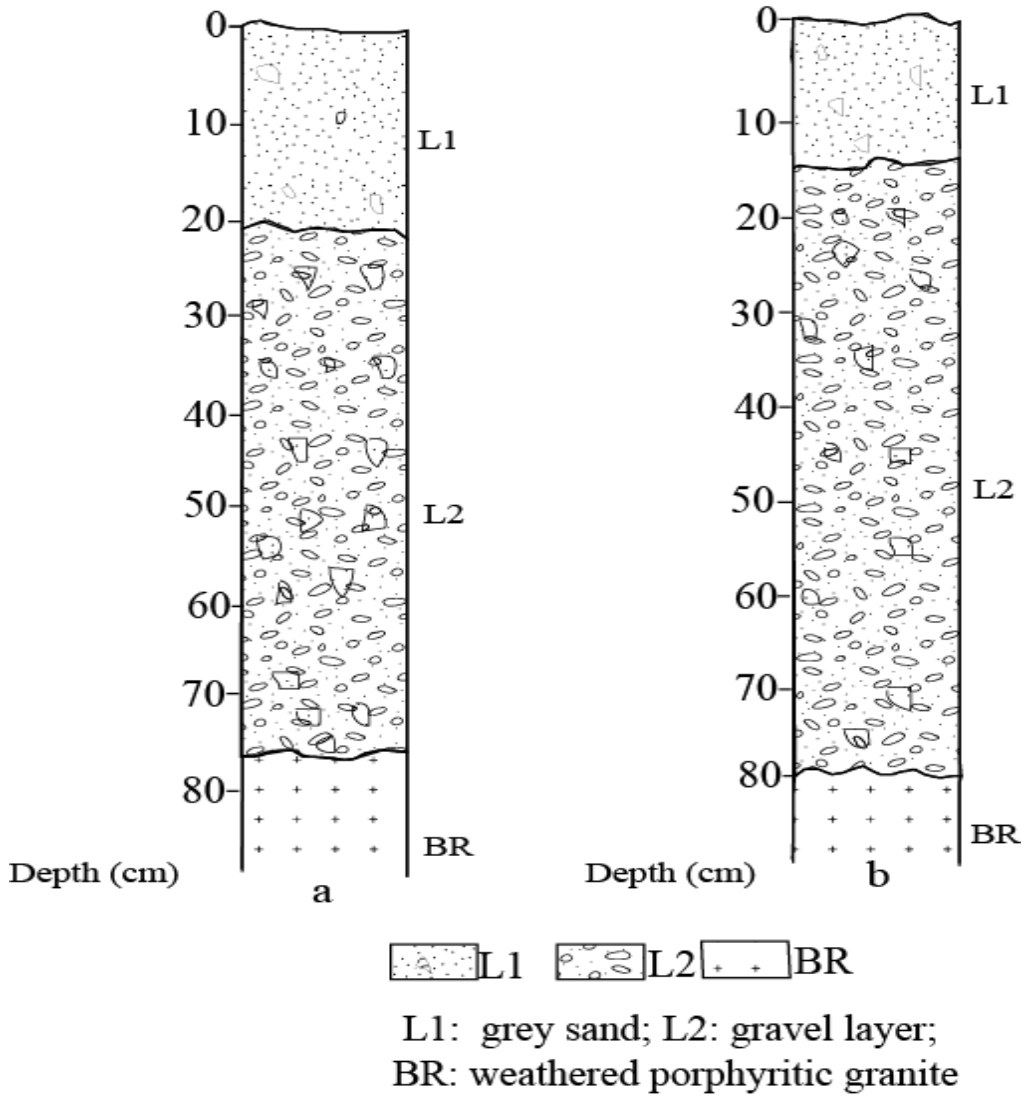

Figure 59: Alluvial profiles from test pits in recent sediments. (a) Gravel test pit 1, (b) Gravel test pit 2.

V.1.2- Alluvial profiles in Mbiame

In this area, all three pits were dug along the Mbven River at intervals of about 1 km and 600 m. The alluvial profiles rarely exceeded 1.5 m and had higher sapphire concentration than those of Mayo Kila. A total of three pits (MP1, MP2 and MP3) were dug and studied in Mbiame. The dug pits and other sample points in the area were plotted on the drainage maps (Fig. 60).

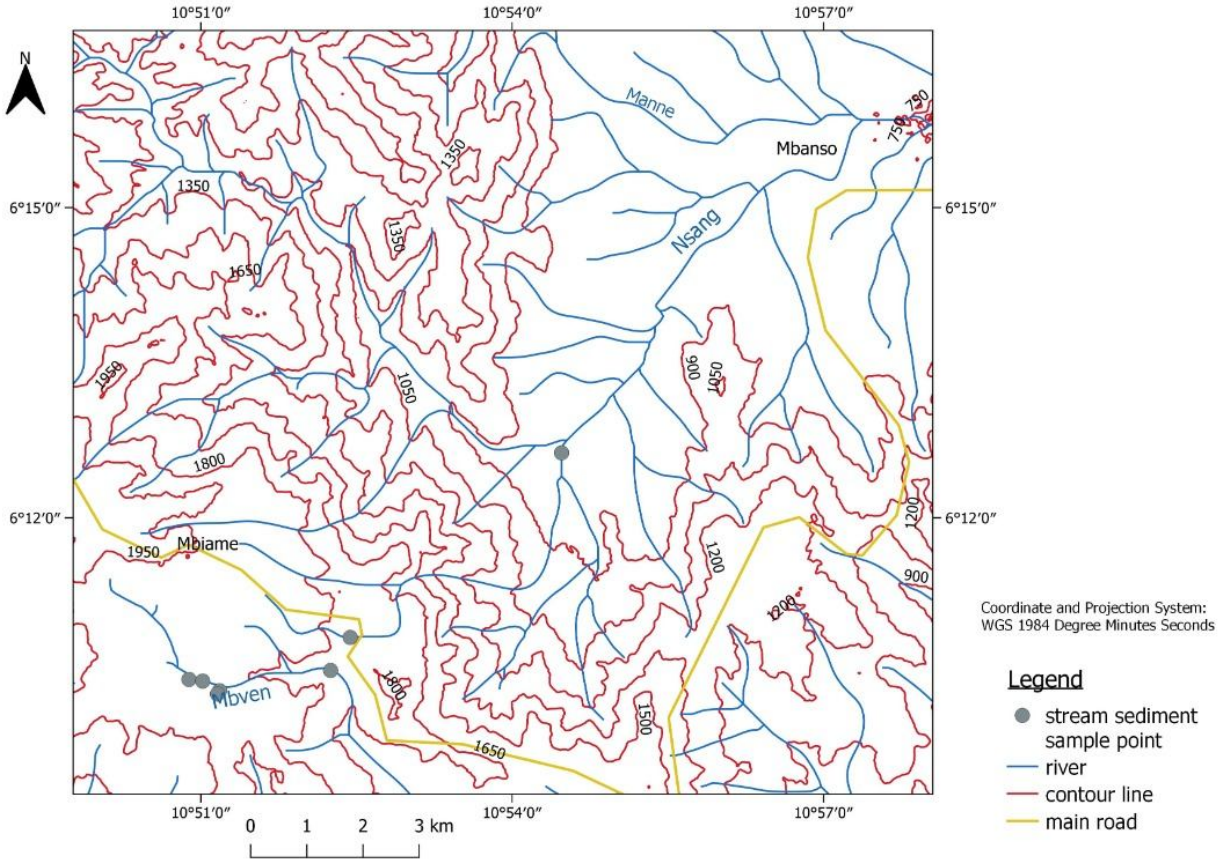

Figure 60: Alluvial prospection map of Mbiame.

Pit MP1

- **Level 1 (0 – 26 cm):** it is a black organo-mineral horizon with a silty sand texture and visible plant roots (Fig. 61). Its thickness can attain 26 cm is some places;
- **Level 2 (26 – 41 cm):** it is a yellowish brown level with thickness of about 15 cm, mainly composed of sand and observable plant roots. It has a clear boundary with the upper level;
- **Level 3 (41 - 84 cm):** It has a grey colour and composed mostly of gravel with rounded to sub rounded pebbles and cobbles. Its boundary with the overlying layer is clear. The panning of four (04) pans from this pit gave seven (07) sapphire grains.

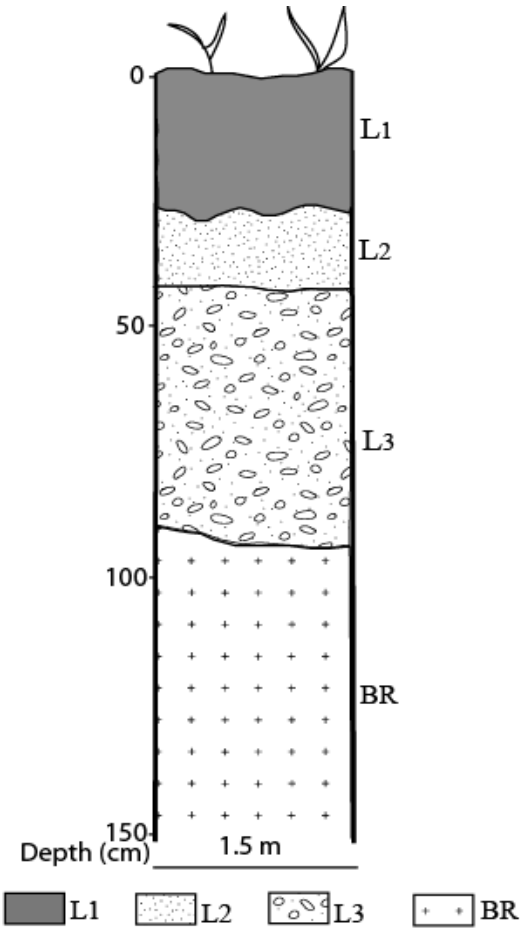

Figure 61: Pit MP1 showing alluvial profile on the Mbven River bank

Pit MP2

- **Level 1 (0 - 30 cm):** it is a black organo-mineral layer with a silty clayey texture, about 30 cm thick and observable plant roots (Fig. 62);
- **Level 2 (30 - 50 cm):** it is grey and composed mostly of silt and clay, with a thickness of about 20 cm. It has a clear boundary with the upper horizon;
- **Level 3 (50 - 82 cm):** it is a grey sandy horizon with very few rounded pebbles. It is about 32 cm thick and has diffuse boundary with the upper layer;
- **Level 4 (82 - 123 cm):** It measures about 41 cm, it is the gravel level and made up mostly of rounded pebbles and few spotted boulders. It has a diffuse limit with the upper horizon. Three pans from this pit yielded five (05) sapphire grains.

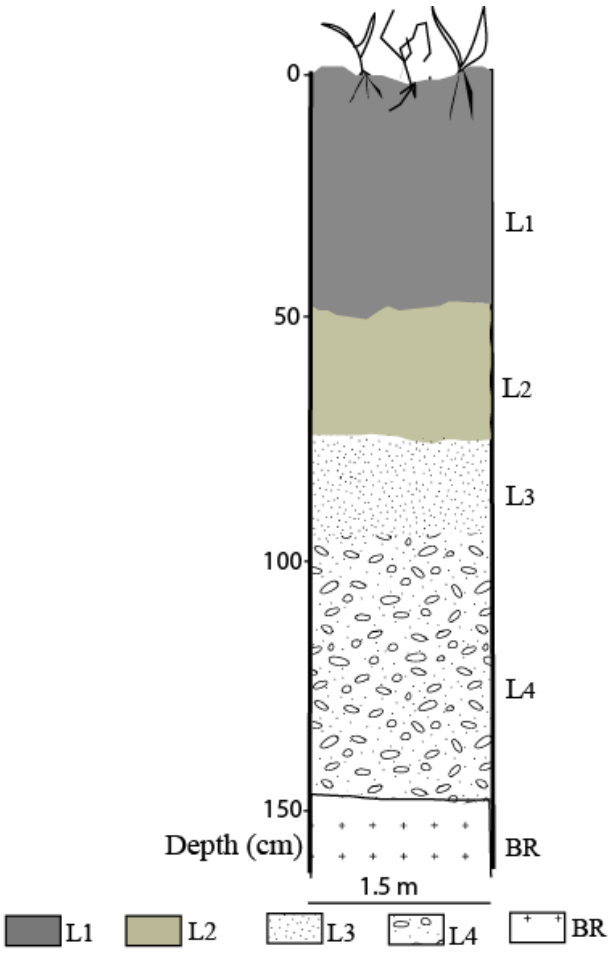

L1: black silty clay; L2: grey silty clay; L3: grey sand; L4: grey gravelly layer
BR: bed rock.

Figure 62: Pit MP2 alluvial profile on Mbven River.

Pit MP3

- **Level 1 (0 - 49 cm):** it is a black organo-mineral horizon with a silty clayey texture, it measures about 49 cm thick (Fig. 63);
- **Level 2 (52 - 77 cm):** it is a dark brown layer with a clayey texture and measures about 25 cm. It has a clear boundary with the upper horizon;
- **Level 3 (77 - 97 cm):** it is a grey sandy horizon with brown rounded nodules. It is about 20 cm thick and has clear boundary with the upper layer;
- **Level 4 (97 - 147 cm):** it is a grey layer, composed mostly of gravel and measures about 50 cm thick. It is made up of rounded pebbles and cobles. It has a diffused limit with the upper horizon. Three pans from this pit yielded eight (08) sapphire grains.

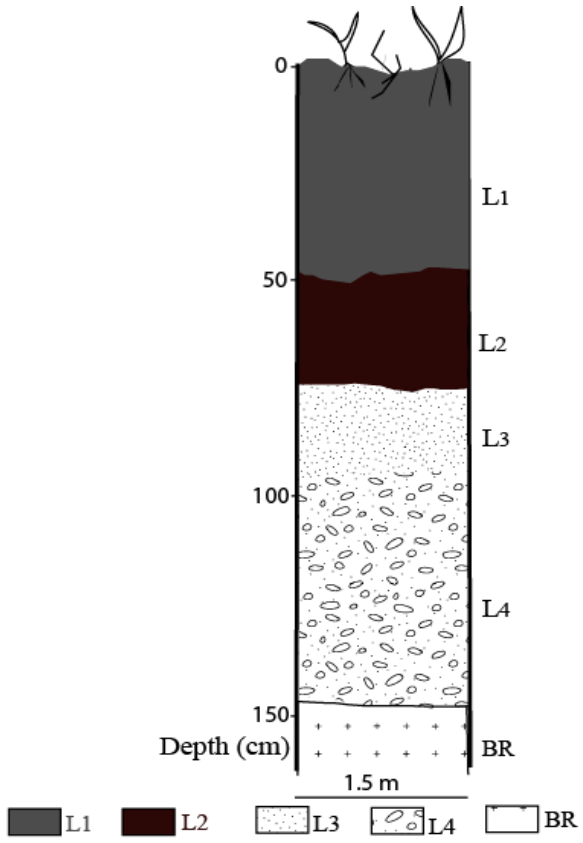

L1: black silty clay; L2: grey silty clay; L3: grey sand; L4: grey gravelly layer
BR: bed rock.

Figure 63: Pit MP3 showing alluvial profile on Mbven River.

V.2- Grain size distribution characteristics of mineralized gravelly layers of alluvial profiles in Mayo Kila and Mbiame

In this study, only the mineralized gravelly layers from the studied alluvial profiles were further analyzed for particle size distribution and ‘‘Trask Sorting Index” (S_0) deduced from Q1 (first quartile) and Q3 (third quartile) values of cumulative graphs. The particle sizes were classified according to the Wentworth (1922) sediment classification scheme (Table 13) and Trask grading scale of Folk and Ward (1957) graphical measures (Table 14).

V.2.1- Grain size characteristics of gravel layers in Mayo Kila

V.2.1.1- Grain size composition

The simple and cumulative percentages of each sieve are presented in Table 15 for Mayo Kila. Comparing these particle size distribution results (Table 15) and cumulative curves (Fig. 64), with the Wentworth sediment classification scheme, it is observed that the

materials are mostly represented by fine to coarse sand and gravels. The sand and gravel dominance of these samples is an indication of detrital materials deposited by a transfer agent, in this case river transport.

Table 13: The Wentworth sediment classification scheme (Wentworth, 1922) in Blott and Pye (2001).

Diameter (mm)	Classification	Group
>256	Boulders	Gravel
256 – 16	Cobbles	
16 – 4	Pebbles	
4 – 2	Granules	
2 – 1	Very coarse sand	Sand
1 – 0.5	Coarse sand	
0.5 – 025	Medium sand	
0.25 – 0.125	Fine sand	
0.125 – 0.063	Very fine sand	
0.063 – 0.031	Coarse silt	Mud rock
0.031 – 0.0156	Medium silt	
0.0156 – 0.0078	Fine silt	
0.0078 – 0.0039	Very fine silt	
<0.0039	clay	

Table 14: Trask grading scale $S_{o=} \sqrt{Q_3/Q_1}$ is adapted from Folk and Ward (1957) graphical measures in Blott and Pye (2001).

Sorting value (S_o)	Grading terms
$S_o < 0.35$	Very well sorted
$S_o = 0.35 – 0.50$	Well sorted
$S_o = 0.50 – 0.70$	Moderately well sorted
$S_o = 0.70 – 1.00$	Moderately sorted
$S_o = 1.00 – 2.00$	Poorly sorted
$S_o = 2.00 – 4.00$	Very poorly sorted
$S_o > 4.00$	Extremely poorly sorted

Table 15: Particle size distribution results for analyzed mineralized gravelly levels in Mayo Kila.

Profile	Samples	Sieves (mm)	40	35	30	25	20	15	10	6.5	4	2.5	2	1.6	1	0.8	0.5	0.4	0.135	0.2	0.1	Pan + Tot
P_0	L7	refuse weight	0	54	52	78	78	116	75	101	40	101	75	82	153	57	242	100	151	197	72	**9**
		Simple %	0	2.9	2.8	4.2	4.2	6.3	4.0	5.5	2.2	5.5	4.1	4.5	8.3	3.1	13.2	5.4	8.2	10.7	3.9	0.5
		Cumulative %	0	2.9	5.8	10	14.3	20.6	24.7	30.2	32.4	37.9	42.0	46.5	54.8	57.9	71.1	76.6	84.8	95.6	99.5	**100**
P_2	L5	refuse weight	0	0	27	44	45	67	40	71	20	39	91	100	184	119	392	101	135	124	58	**12**
		Simple %	0	0	1.6	2.6	2.7	4.0	2.4	4.3	1.2	2.4	5.4	6	11.0	7.1	23.5	6.1	8.1	7.4	3.5	0.7
		Cumulative %	0	0	1.6	4.2	6.9	10.9	13.3	17.6	18.8	21.1	26.6	32.5	43.6	50.7	74.2	80.3	88.4	95.8	99.3	**100**
GTP1	L2	refuse weight	133	234	93	70	131	103	58	40	14	62	63	89	184	99	103	53	159	66	38	**9**
		Simple %	7.4	13	5.2	3.8	7.3	5.7	3.2	2.24	0.7	3.4	3.5	4.9	10.2	5.5	5.7	2.9	8.8	3.6	2.1	0.5
		Cumulative %	7.4	20.4	25.5	29.4	36.7	42.4	45.6	47.8	48.6	52.1	55.6	60.5	70.7	76.2	81.9	84.9	93.7	97.3	99.5	**100**
GTP2	L2	refuse weight	0	93	107	64	128	179	64	97	61	36	57	76	126	67	172	45	52	62	35	**10**
		Simple %	0	6.1	7.0	4.3	8.4	11.7	4.8	6.3	3.9	2.3	3.7	4.9	8.2	4.4	11.2	2.9	3.4	4.1	2.3	0.6
		Cumulative %	0	6.2	13.2	17.39	25.6	37.5	41.5	47.9	51.8	54.3	57.9	62.9	71.2	75.6	86.8	89.8	93.2	97.3	99.5	**100**

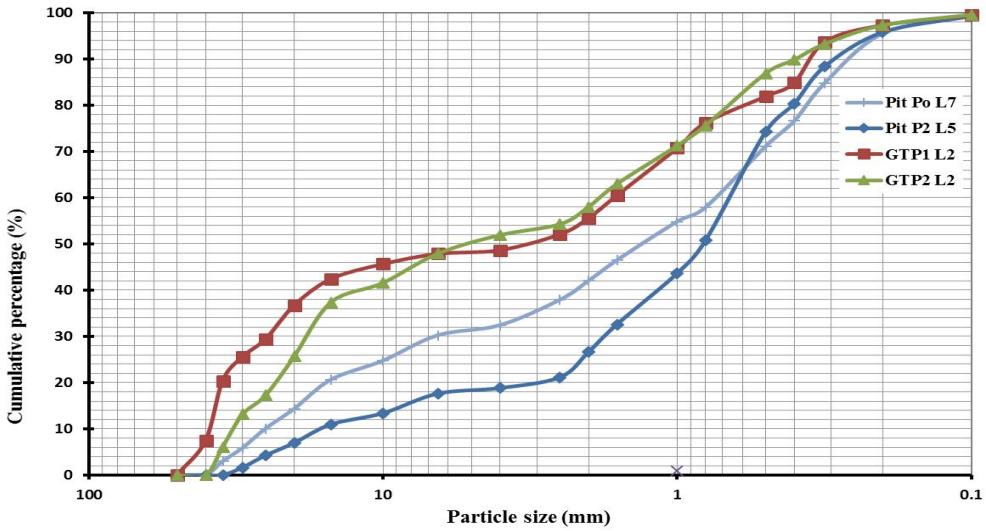

Figure 64: Cumulative curves of gravelly layers of alluvial profiles in Mayo Kila.

V.2.1.2- Trask ‘’Sorting Index’’ of gravel layers in Mayo Kila

The Trask ‘‘Sorting Index’’of the analyzed samples (Table 16) shows that the materials are poorly to very poorly sorted sediments, with the dominance of poorly sorted samples. This general poor sorting can be confirmed by the fact that most of the samples have insignificant fractions of finer grains, where coarse sand and gravel size particles are dominant. The sediment is speculated to be deposited from high-energy currents (Wan et al., 2015).

Table 16: Trask ‘‘Sorting Index” of Mayo Kila alluvial materials.

Profile	Samples	Q_1	Q_3	$S_o=\sqrt{Q_3/Q_1}$	Sorting degree
P_0	L7	22.67	73.87	1.81	Poorly sorted
P_2	L5	14.42	78.77	2.34	Very poorly sorted
GTP1	L2	40.99	82.69	1.42	Poorly sorted
GTP2	L2	39.46	88.32	1.50	Poorly sorted

V.2.2- Grain size characteristics of gravel layers in Mbiame

V.2.2.1- Grain size composition

In the Mbiame particle size distribution results (Table 17) and its cumulative curves (Fig. 65), with the Wentworth sediment classification scheme (Table 13), it can be seen that

the placer materials are also mostly represented by fine to coarse sand and gravels. This sand and gravel dominance of the samples can as well be an indication of detrital materials possibly deposited by river transport.

Table 17: Particle size distribution results for he analyzed mineralized gravelly levels in Mbiame

Profile	Samples	Sieves (mm)	40	35	30	25	20	15	10	6.5	4	2.5	2	1.6	1	0.8	0.5	0.4	0.135	0.2	0.1	Pan + Tot
MP1	L3	refuse weight	141	102	61	137	153	417	615	214	155	697	312	364	629	116	80	11	6	7	3	10
		Simple %	3.3	2.4	1.4	3.2	3.6	9.8	14.5	5.1	3.7	16.5	7.5	8.6	14.8	2.7	1.9	0.3	0.1	0.2	0.1	0.2
		Cumulative %	3.3	5.7	7.2	10.4	14	24	38.4	43.5	47.2	63.6	71	79.6	94.5	97.2	99.1	99.4	99.5	99.7	99.7	100
MP2	L4	refuse weight	0	234	107	75	449	689	449	369	135	724	260	191	445	58	83	19	9	18	6	17
		Simple %	0	5.4	2.5	1.7	10.4	15.8	10.4	8.5	3.1	16.7	6	4.4	10.3	1.3	1.9	0.4	0.2	0.4	0.1	0.4
		Cumulative %	0	5.4	7.8	9.6	20	35.8	46.2	54.7	57.8	74.5	80.5	84.9	95.2	96.5	98.4	98.8	99.1	99.5	99.6	100
MP3	L4	refuse weight	132	125	225	210	483	299	532	366	70	398	83	91	312	77	145	52	25	95	36	38
		Simple %	3.5	3.3	5.9	5.5	12.7	7.8	14	9.6	1.8	10.5	2.2	2.4	8.2	2	3.8	1.4	0.6	2.5	0.9	1.0
		Cumulative %	3.5	6.7	12.7	18.2	30.9	38.8	52.8	62.5	64.4	74.8	77	79.4	87.6	89.7	93.5	94.8	95.5	98.0	99	100

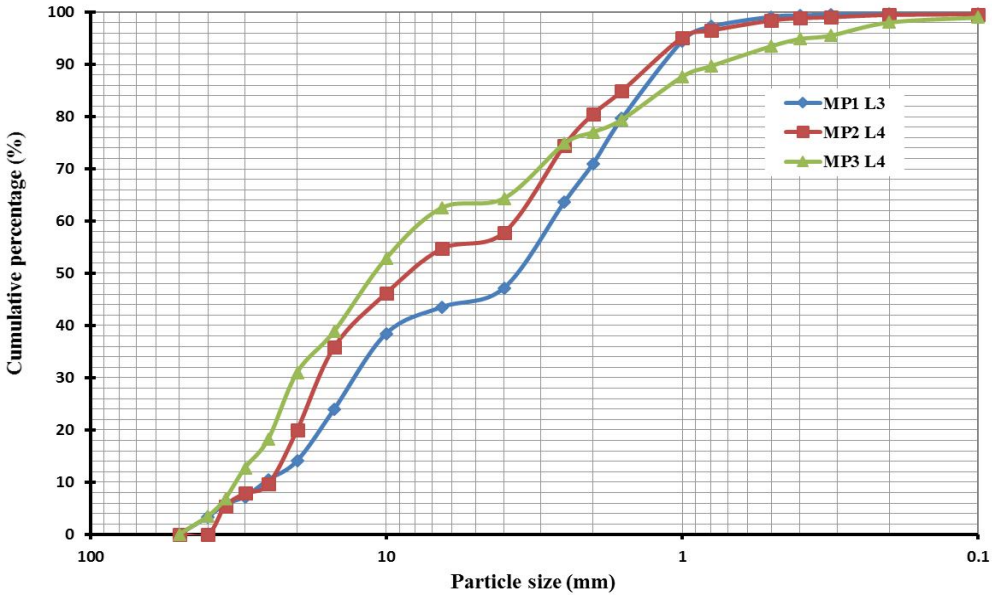

Figure 65: Cumulative curves of gravelly layers of alluvial profiles in Mbiame.

V.2.2.2- Trask ‘‘Sorting Index” of alluvial materials from Mbiame

All three samples show poorly sorted to very poorly sorted sediment distribution, with the dominance of poorly sorted samples (Table 18). This poor sorting can be confirmed by the fact that most of the samples have coarse sand and gravel size fraction. The sediments were probably deposited from high-energy currents from a close source (Wan et al., 2015).

Table 18: Trask ‘‘Sorting Index” of Mbiame (Mount Oku) alluvial materials.

Profile	samples	Q_1	Q_3	$S_o = \sqrt{Q_3/Q_1}$	Sorting degree
MP1	L3	21.44	99.19	2.15	Very poorly sorted
MP2	L4	41.01	98.63	1.55	Poorly sorted
MP3	L4	36.88	93.86	1.60	Poorly sorted

V.3- Heavy minerals in Mayo Kila and Mbiame placers

The identified heavy mineral suits in the placer deposits are grouped into two: the fine grain (with grain size <315 µm) and the medium to coarse grain (with grain size >315 µm).

V.3.1- Heavy minerals in Mayo Kila placer

V.3.1.1- Medium to coarse grained heavy minerals

This is composed of non-magnetic and magnetic fractions (Fig. 66).

The identified heavy mineral suits in the placer deposits are grouped into two: the fine grain (with grains size <315µm) and the medium to coarse grain (with grais size >315 µm).

V.3.1- Heavy minerals in Mayo Kila placer

V.3.1.1- Medium to coarse grained heavy minerals

This is composed of non-magnetic and magnetic fractions (Fig. 66).

Non-magnetic fraction

This fraction is made up of zircon, rutile, pyrite, garnet, topaz, monazite and other unidentified minerals (Fig. 66 A, C).

Zircon is euhedral to sub-hedral, up to 3 mm in size. Crystals are mostly prismatic to pyramidal. Their colours range from orange, red to brown. Most grains are sub-angular to sub-rounded, translucent to opaque and show a vitreous luster.

Topaz forms euhedral grains with sizes which do not exceed 2.5 mm. The grains are mostly colourless, transparent and display a vitreous luster.

Rutile is greyish black with euhedral to sub-hedral prismatic crystals. Rutile crystals have a sub-metallic luster and form part of the opaque minerals.

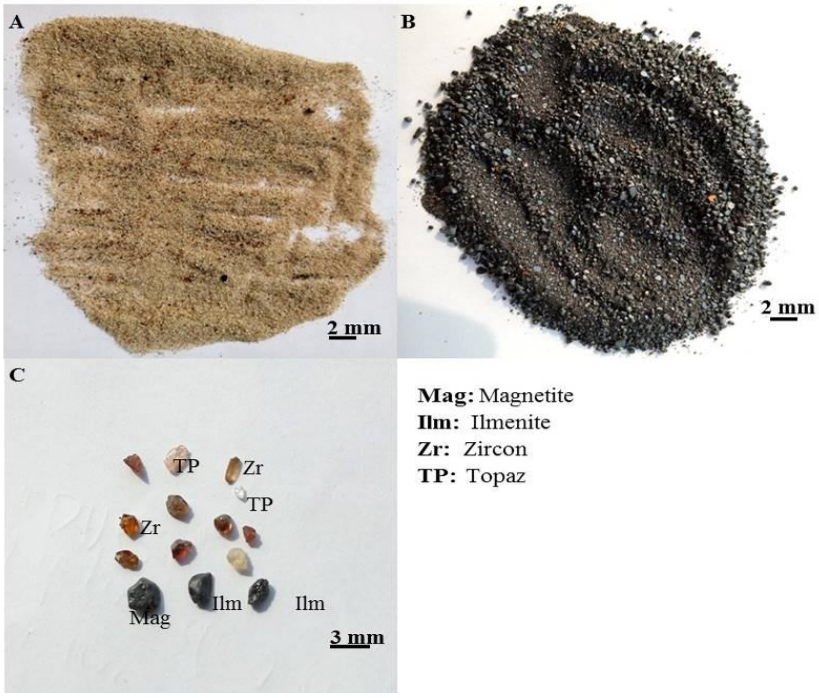

Figure 66: Pan concentrate from Mayo Kila. A: non-magnetic minerals, B: Magnetic minerals and C: Magnetic and non-magnetic minerals.

Magnetic fraction

This fraction is made up of dark colour minerals such as magnetite and ilmenite (Fig. 66 B and C).

Magnetite occurs as cubic crystals of up to 2 mm in size. They are dark grey to almost black with a sub-metallic lustre (Fig. 66 C).

Ilmenite occurs as one of the dominant opaque minerals. It is also black with sizes between 1 and 2 mm. Some crystals have striated surface, with a few displaying a sub-metallic luster (Fig. 66 C).

V.3.1.2- Fine-grained heavy minerals

A total of 14 heavy minerals from profiles and test pits in Mayo Kila were identified under the petrographic microscope (Fig. 67). These minerals include: zircon, tourmaline, disthene, epidote, pyroxene, andalusite, garnet, chlorite, ziosite, biotite, sillimanite, hornblende, apatite and opaque minerals.

Zircon

The grains show a very high relief with pink to brown portions at the middle and a predominant opaque hallo at its surroundings. The crystals are elongated and euhedral. They are mostly translucent with some crystals having inclusions. Figure 67A shows a zircon crystal identified under a Plane Polarized Light (PPL).

Tourmaline

It has dark brown prismatic crystals, display a parallel extinction and a moderate relief (Fig. 67 B).

Kyanite

The crystals are colourless under Plane Polarised Light and varies from blue, violet, yellow to grey under Crossed Polarized Light. The grains are euhedral (Fig. 67 C, D). They show high relief and are transparent. Black inclusions occur in the crystals.

Epidote

The colour is mostly green with yellow and grey shades. Its crystals are prismatic, translucent and are characterized by a fairly high relief (Fig. 67 E).

Pyroxene

Under Crossed Polarized Light, the colour is predominantly yellow with shades of blue at some edges. Its crystals also show a high relief (Fig. 67 F), and are mostly translucent.

Andalusite

The grains are sub rounded with irregular surfaces. They are colourless (Fig. 67 G) and display a moderate relief and a parallel extinction.

Garnet

Its crystals are sub rounded to rounded. The grains are pinkish brown, transparent to transluscent (Fig. 67 H) and exhibit a high relief.

Chlorite

The crystals are pale green under Plane Polariszd Light. Under crossed polarised light, the crystals display concentric rims of blue, violet and grey colour (Figs. 67 I, J).

Zoisite

The crystals are mostly short stumpy colourless to pink prisms under Plane Polarized Light, while under crossed polarised light, they display a high relief and rims of interfering colours (Figs. 67 K, L).

Biotite

The crystals show shades of brown and reddish brown colours with platy, irregular and rounded edges (Fig. 67 M). The crystals are mostly translucent.

Sillimanite

Under Plane Polarized Light, the crystals show a grey colour while under Crossed Polarised Light they display a variation of colour with blue being dominant amongst green, brown and grey. The crystals show elongated or fibrous prismatic shapes. Most of the crystals show striated surfaces with a high relief (Figs 67 N, O).

Hornblende

The crystals are pale green under Plane Polarized Light and under Crossed Polarized Light, they show colour variation from greenish blue, grey to violet. The crystals display average relief and occur as short prisms with rounded ends (Figs. 67 P, Q).

Apatite

The crystals are grey under Plane Polarized Light, and show a moderately high relief with grains that are characterized by short prismatic rounded edges (Fig. 67 R).

Opaque minerals

Opaque minerals occur in both magnetic and non-magnetic fractions. In the non-magnetic fraction, they remain unidentified and represent high percentage in most samples.

Figure 67: Microscopic features of the <315 - 200 µm non-magnetic heavy minerals from Mayo Kila. PPL: Plane Polarized Light, XPL: Cross Polarized Light.

V.3.2- Heavy minerals in Mbiame placer

V.3.2.1- Medium to coarse grained heavy minerals

This is composed of non-magnetic and magnetic fractions.

Non-magnetic fraction

This fraction is made up of zircon, sapphires, rutile and other unidentified minerals.

Zircon is made up of euhedral, up to 4 mm pyramidal crystals. Its colours range from orange, red to reddish brown. Most grains are sub-angular to sub-rounded, translucent and show a vitreous luster (Fig. 68A, C).

Sapphires form euhedral grains, with sizes exceeding 4 mm. They are mostly light blue to light green, transparent and display a vitreous luster (Fig. 68 C).

Rutile is greyish black with elongated prismatic crystals. The grains are mostly sub rounded and can attain 5 mm. Rutile crystals have a sub-metallic luster and form part of the opaque minerals with the non-magnetic mineral association.

Magnetic fraction

This fraction is mostly made up of magnetite (Fig. 68 B).

Magnetite occurs as cubic crystals that can attain up to 4 mm in size, with a dark grey to black colour and a sub-metallic luster (Figs. 68 B, C).

Mag: Magnetite, Sp: Sapphire, Zr: Zircon, Tm: Tourmaline

Figure 68: Pan concentrate from Mbiame. **A**: non-magnetic minerals, **B**: Magnetic minerals, **C**: other minerals association, **D**: hand picked tourmaline grain.

V.3.2.2- Fine grained heavy minerals

Six (06) heavy minerals were identified under the petrographic microscope (Fig. 69). These heavy minerals are: zircon, tourmaline, monazite, olivine, apatite and epidote.

Zircon: the grains have a grey to light brown colour, high relief, elongated euhedral shape with inclusions and portray rough surface (Fig. 69 A).

Tourmaline: its grains are brown to dark brown, have a moderate relief and are euhedral. It is characterized by radiating needles (Fig. 69 B).

Monazite: it is almost colourless, but small yellow and brown patches can be seen. The grains are euhedral and rounded. It is also characterized by inclusions (Fig. 69 C).

Olivine: it is colourless to very light yellow, has a high relief and spherical shape (Fig. 69 D).

Apatite: the grains are greyish-green, with dark brown overgrowths in some places and exhibit moderate relief. It is prismatic and also contains dark inclusions (Fig. 69 E).

Epidote: it is whitish in PPL (Fig. 69 F), yellowish green in XPL with shades of green and blue, and a high relief. They have broken euhedral grains and contain opaque inclusions (Fig. 69 G).

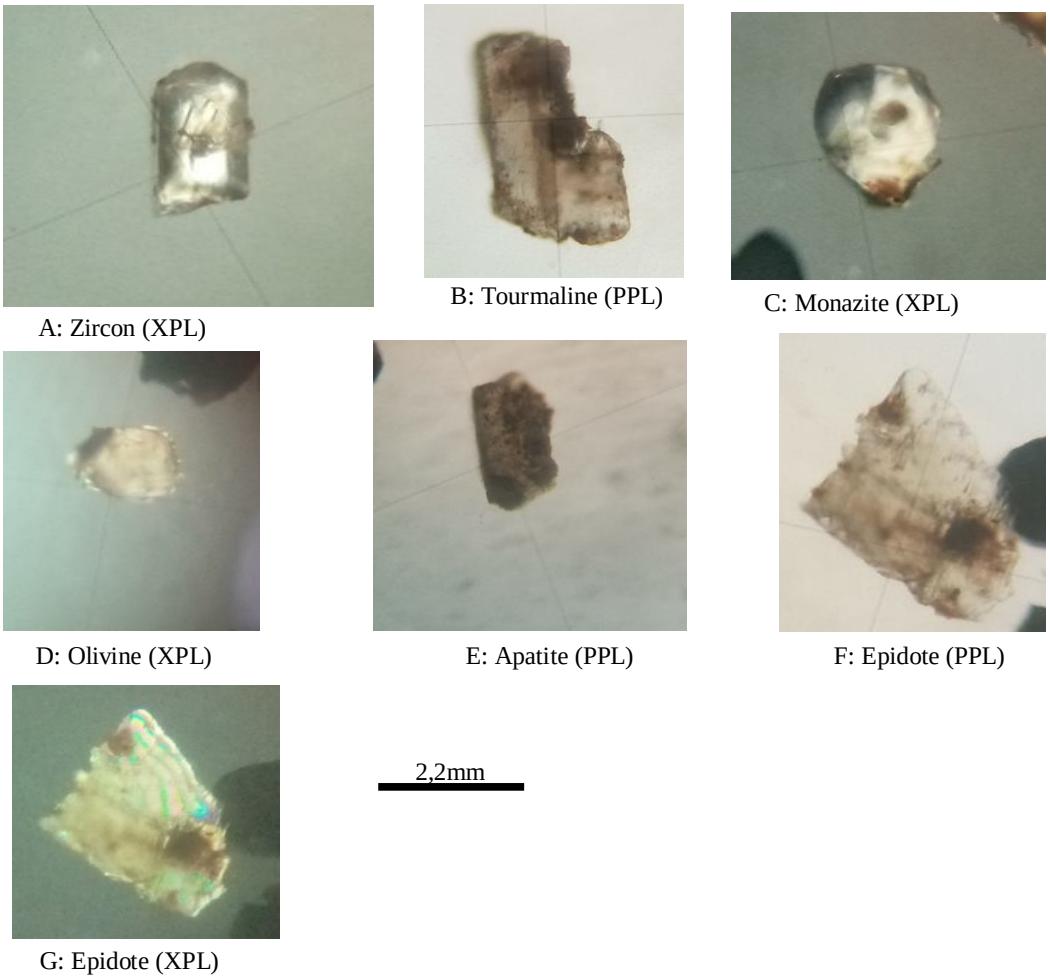

Figure 69: Microscopic feature of the <315 - 200 µm non-magnetic heavy minerals from Mbiame.

V.4- Morphological features of sapphires

Mayo Kila sapphires are pale or dark blue with tints of grey and green (Fig. 70a). The pale blue sapphires are transparent, whereas the greyish and greenish blue grains are transparent to translucent. The dark blue grains are dominantly opaque. The grain size of these sapphires varies from 2 to 5 mm with most grains being greater than 3 mm. They are mainly euhedral to sub-hedral in shape (Fig. 70a). Few are anhedral and are dominantly angular to sub-angular. Rounded or sub rounded grains are rare. Euhedral crystals form four or six sided

prisms with some of them being pyramidal showing truncated basal edges and rhombohedrons (Figs. 70b-d), or form pseudohexagonal to pinacoidal planes (Fig. 70 c). Most of the sapphires have lustrous polished surfaces. Their luster is vitreous, while their fractures are conchoidal. Corrosion and pits are found in some of the grain surfaces (Fig. 70e).

Figure 70: Morphological features of Mayo Kila sapphires. **a**: colour variation; **b**: elongated and rhombohedral sapphire grains, **c**: pseudohexagonal to pinacoid basal section of a platy sapphire grain; **d**: primary relict grain; **e**: sapphire grain with magmatic corrosion.

Mbiame sapphires range in colour from pale to dark blue with shades of grey, brown and green. They are transparent to opaque with euhedral to sub-hedral angular, sub angular and few sub rounded to rounded lustrous grains (Fig. 71a). The grains also exhibit rhombohedral and slightly elongated shapes (Fig. 71b). Magmatic corrosions are also observed on most of the grains (Figs. 71c, d).

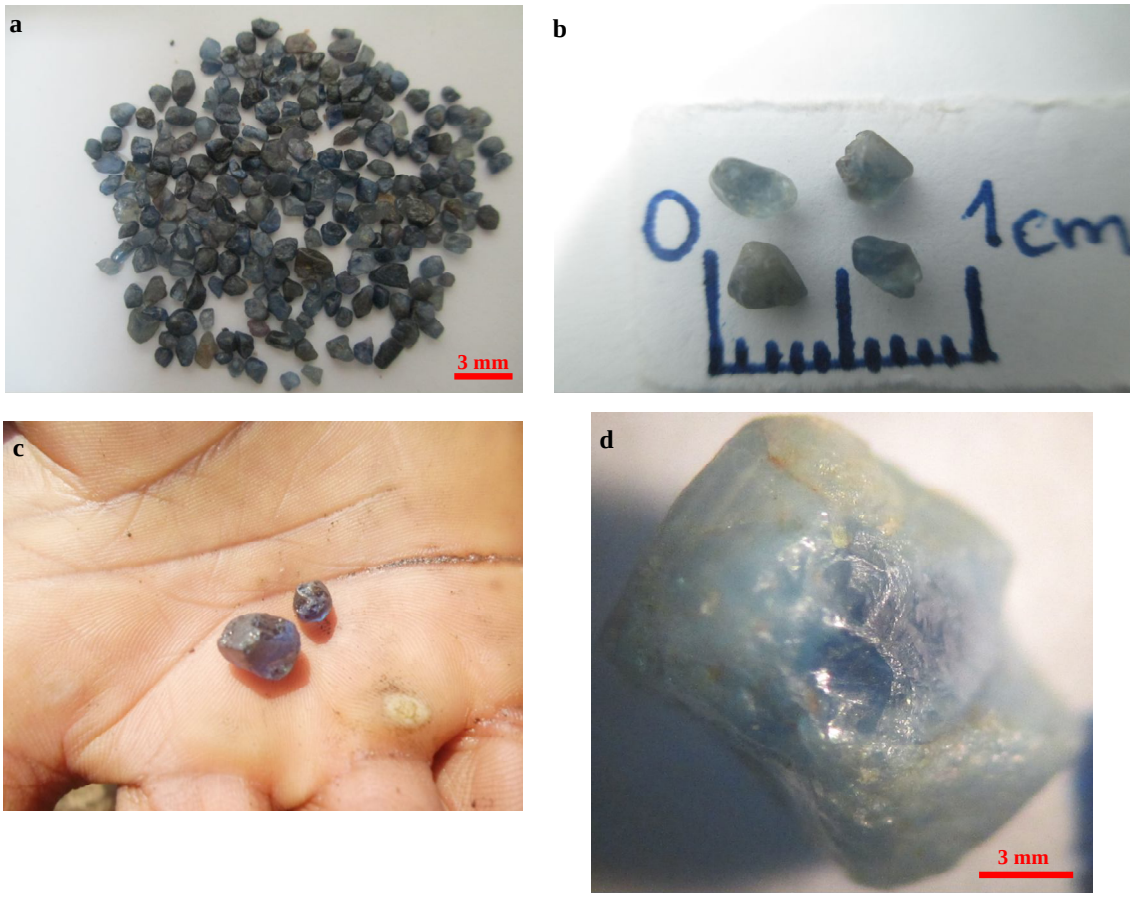

Figure 71: Morphological features of Mbiame sapphires. **a**: colour variation; **b**: elongated and rhombohedral transparent sapphire grains; **c**: transluscent rounded to sub-rounded sapphire grains with corroded surfaces; **d**: angular sapphire grain with magmatic corrosion.

V.5- Trace element of Mayo Kila sapphires

A total of thirty-four (34) chemical elements were quantified in nineteen (19) Mayo Kila sapphire grains (Table 19), with aluminum being the only major element, standardized at 529,300 ppm in this analysis. The Fe (2,208 to 14,473 ppm) and Ti (82 to1,783 ppm) contents are variable and significantly high. The Fe content is generally different in core and rim of the sapphire grains, except in grain MK17, where it is constant (3,834 ppm) in its core and rim. The Ti contents are highly variable in the core and rim of the sapphires. The Ga and Mg contents (in ppm) respectively range from 77 to 512 and 0.9 to 265. Gallium values are dominantly less than 260 ppm, whereas Mg is mostly less than 15 ppm. They are variable in core and rim of most of the grains. The V abundance ranges from 1.3 to 82 ppm. More than 60% of the grains are free of Cr. Obtained Cr values range from 1.5 to 168 ppm. Elements such as Si (up to 1,117 ppm), Sr (up to 35 ppm), Pb (up to 31 ppm), Ce (up to 30 ppm), Na (up to 18 ppm), and K (up to 14 ppm), occur in few crystals and are generally low. The Sn,

Ta, Nb, Rb, Hf, U, Th, Zr, Cu, Ni, Co, Y, Be, Mn, and Sc contents are dominantly close to or below the detection limit. The concentrations of Fe, Ti, Ga, Mg, Cr, and their ratios Fe/Mg, Fe/Ti, Ti/Mg, Ga/Mg, and Cr/Ga (Table 10) have often been used to discriminate between magmatic and metamorphic sapphires (Peucat et al., 2007; Sutherland and Abduriyim, 2009; Uher et al., 2012). In this study, the average ratios are Fe/Mg (43.8-3042), Fe/Ti (2.4-76), Ti/Mg (1.6-328), and Ga/Mg (0.4-362). The low to very low Cr and Mg abundances and dominantly high Ga/Mg ratios in most of the corundums are compatible with those found in other affiliated magmatic corundums. The dominant magmatic origin of these corundums is shown on the Fe vs. Ga/Mg, Fe/Mg vs. Ga/Mg, and Cr/Ga vs. Fe/Mg binary diagrams (Figures 72 to 74). Four zones can be distinguished in Figure 72:

- one (1) grain is plotted in the metamorphic field;
- one (1) grain is plotted between the lines separating the magmatic and metamorphic fields;
- two (2) grains are plotted on the line separating magmatic field;
- fifteen (15) grains are plotted in the magmatic field.

Table 19: Trace element abundances (in ppm) in Mayo Kila sapphire grains.

n number	Sample colour	Spots	Al	Fe	Ti	Ga	Mg	V	Sn	Ta	Nb	Zn	Th	Ce	Cr	Ni
MK1	Pale blue/ dark blue	Core	529300	4405	478	226	1.7	2	0.24	b.d.l	b.d.l	b.d.l	b.d.l	b.d.l	b.d.l	b.d.l
		Rim	529300	4418	304	244	1.2	2.3	0.17	b.d.l	b.d.l	b.d.l	b.d.l	b.d.l	b.d.l	b.d.l
MK2	Pale blue/grey	Core	529300	2859	366	294	16.5	13	b.d.l	0.23	0.8	5	b.d.l	b.d.l	b.d.l	b.d.l
		Rim	529300	2685	1028	270	9.2	14	0.12	0.14	0.11	2.2	b.d.l	b.d.l	b.d.l	b.d.l
MK3	Dark blue	Core 1	529300	3566	104	220	6.4	13	b.d.l	b.d.l	b.d.l	b.d.l	b.d.l	b.d.l	7.1	b.d.l
		Core 2	529300	3404	106	216	6.6	16	b.d.l	b.d.l	b.d.l	b.d.l	b.d.l	b.d.l	6.3	b.d.l
		Rim	529300	4603	673	231	14.4	11	0.35	0.2	0.05	1.8	0.39	30	5.8	0.3
MK4	Pale blue/ dark blue	Core	529300	7879	1776	281	4.1	2.5	1.76	1.67	0.86	1.1	0.02	0.08	b.d.l	b.d.l
		Rim	529300	7037	553	213	3	3.1	0.55	0.06	b.d.l	b.d.l	0.26	12.9	5.9	b.d.l
MK5	Greenish blue	Core	529300	14473	191	224	40.3	30	0.33	1.48	2.68	1	0.04	0.03	3.2	1.29
		Rim	529300	9950	131	188	21.6	24	b.d.l	b.d.l	b.d.l	b.d.l	b.d.l	0.04	b.d.l	0.53
MK6	Dark blue	Core	529300	6070	481	241	3.6	3	0.2	0.2	0.10	1.6	0.04	27	12	0.31
		Rim	529300	5106	333	223	4.3	5.5	0.19	0.04	0.09	0.9	0.02	b.d.l	9.2	0.38
MK7	Grey	Core	529300	3244	161	431	1.7	1.5	0.36	0.5	0.09	b.d.l	b.d.l	b.d.l	1.5	b.d.l
		Rim	529300	2975	143	512	0.9	1.9	0.26	2.08	0.31	b.d.l	b.d.l	0.36	1.9	b.d.l
MK8	Pale blue	Core	529300	3549	378	207	21.2	32	b.d.l	0.06	0.05	1.6	0.08	19	155	1.15
		Rim	529300	3672	160	232	32.1	30	0.09	14	16	3.9	0.23	0.1	20	1.08
MK9	Pale blue/ dark blue	Core	529300	3881	306	402	1.5	2.2	0.64	1.6	0.87	0.6	0.03	b.d.l	b.d.l	b.d.l
		Rim	529300	4617	578	434	6.5	3.4	1.28	84	76	2.8	0.91	0.25	b.d.l	b.d.l
MK10	Pale blue	Core	529300	3625	387	252	5.5	14	0.11	0.01	0.04	1.2	b.d.l	b.d.l	b.d.l	b.d.l
		Rim	529300	3615	436	231	5.6	13	0.14	0.01	b.d.l	1.5	b.d.l	b.d.l	b.d.l	b.d.l
MK11	Pale blue	Core	529300	3983	359	300	29.4	8.1	1.71	421	475	4.9	3.79	1.28	b.d.l	b.d.l
		Rim	529300	4834	356	250	2.6	1.3	0.47	0.09	0.05	b.d.l	b.d.l	b.d.l	b.d.l	b.d.l
MK12	Pale blue	Core	529300	4922	680	321	5.5	1.8	1.68	1.92	0.73	262.2	0.03	0.02	b.d.l	b.d.l
		Rim	529300	4678	503	337	4	2.3	1.18	1.36	0.5	b.d.l	b.d.l	0.07	b.d.l	b.d.l
MK13	Dark blue	Core	529300	8001	325	215	10.9	7.4	0.11	0.02	b.d.l	0.9	b.d.l	b.d.l	b.d.l	b.d.l
		Rim	529300	6347	196	206	21	8.7	b.d.l	0.03	b.d.l	1	b.d.l	b.d.l	b.d.l	0.26
MK14	Dark blue	Core	529300	4591	229	350	3.9	2.3	1.27	132	61	1.9	0.68	0.2	b.d.l	b.d.l
		Rim	529300	5100	698	355	7	2.6	1.32	80	12	3.1	0.1	5.59	b.d.l	0.86
MK15	Greyish blue with brown spots	Core	529300	4145	287	213	47.7	29	b.d.l	0.35	0.28	2.6	0.05	0.13	b.d.l	0.57
		Rim	529300	4365	382	228	64.2	34	0.1	3	2.21	2.9	0.06	0.22	13	0.55
MK16	Pale blue/ dark blue	Core	529300	2208	82	284	14	44	b.d.l	b.d.l	b.d.l	b.d.l	b.d.l	b.d.l	83	b.d.l
		Rim	529300	2866	557	292	19.9	39	0.39	0.08	0.04	1	b.d.l	b.d.l	9.4	0.52
MK17	Pale blue/ dark blue	Core	529300	3834	1783	260	26.3	16	0.54	7.94	4.07	3.2	0.13	b.d.l	b.d.l	b.d.l
		Rim	529300	3834	1408	254	20.3	19	0.35	0.51	0.29	b.d.l	b.d.l	0.04	b.d.l	0.46
MK18	Greyish blue/ dark blue	Core	529300	4859	860	193	11.2	3	0.44	0.08	0.03	b.d.l	b.d.l	b.d.l	b.d.l	b.d.l
		Rim	529300	4699	745	201	10.1	3.4	0.51	0.12	0.03	b.d.l	b.d.l	b.d.l	b.d.l	b.d.l
MK19	Dark blue	Core	529300	9699	295	110	179.3	82	0.11	b.d.l	b.d.l	b.d.l	0.01	b.d.l	168	1.5
		Rim	529300	9747	423	77	264.9	69	0.22	b.d.l	b.d.l	b.d.l	0.01	b.d.l	115	1.67

***Table 19**: Continued*

Grain number	Spots	Hf	Sr	Pb	Zr	Cu	U	Y	W	Be	Gd	Co	Rb	Si	Yb
MK1	Core	b.d.l	b.d.l	b.d.l	b.d.l	b.d.l	b.d.l	b.d.l	b.d.l	b.d.l	b.d.l	b.d.l	0.04	b.d.l	b.d.l
	Rim	b.d.l	b.d.l	0.04	b.d.l	b.d.l	b.d.l	b.d.l	b.d.l	b.d.l	b.d.l	b.d.l	b.d.l	b.d.l	b.d.l
MK2	Core	b.d.l	b.d.l	b.d.l	b.d.l	b.d.l	b.d.l	b.d.l	b.d.l	b.d.l	b.d.l	b.d.l	b.d.l	b.d.l	b.d.l
	Rim	0.03	b.d.l	b.d.l	b.d.l	b.d.l	b.d.l	b.d.l	b.d.l	b.d.l	b.d.l	b.d.l	0.04	b.d.l	b.d.l
MK3	Core 1	b.d.l	b.d.l	b.d.l	b.d.l	135	b.d.l	b.d.l	b.d.l	b.d.l	b.d.l	b.d.l	b.d.l	1117	b.d.l
	Core 2	b.d.l	b.d.l	b.d.l	b.d.l	b.d.l	b.d.l	b.d.l	b.d.l	b.d.l	b.d.l	b.d.l	b.d.l	b.d.l	b.d.l
	Rim	b.d.l	0.69	31	0.06	0.29	0.03	0.69	b.d.l	b.d.l	0.55	0.08	b.d.l	b.d.l	0.05
MK4	Core	0.15	b.d.l	b.d.l	0.28	b.d.l	b.d.l	b.d.l	b.d.l	b.d.l	b.d.l	0.09	b.d.l	b.d.l	b.d.l
	Rim	0.03	8.21	15	b.d.l	0.49	0.01	0.60	b.d.l	b.d.l	0.31	b.d.l	b.d.l	b.d.l	0.05
MK5	Core	0.02	0.16	b.d.l	b.d.l	b.d.l	b.d.l	b.d.l	b.d.l	b.d.l	b.d.l	b.d.l	b.d.l	b.d.l	b.d.l
	Rim	b.d.l	1.71	0.32	b.d.l	b.d.l	b.d.l	b.d.l	b.d.l	b.d.l	b.d.l	b.d.l	b.d.l	b.d.l	b.d.l
MK6	Core	b.d.l	35	18.78	b.d.l	b.d.l	0.02	0.93	b.d.l	b.d.l	0.43	b.d.l	b.d.l	b.d.l	0.04
	Rim	0.02	0.65	b.d.l	b.d.l	b.d.l	0.01	b.d.l	b.d.l	b.d.l	b.d.l	b.d.l	b.d.l	b.d.l	b.d.l
MK7	Core	b.d.l	b.d.l	b.d.l	b.d.l	b.d.l	b.d.l	b.d.l	b.d.l	b.d.l	b.d.l	b.d.l	b.d.l	b.d.l	b.d.l
	Rim	b.d.l	0.23	0.47	b.d.l	b.d.l	b.d.l	0.02	b.d.l	b.d.l	b.d.l	b.d.l	b.d.l	b.d.l	b.d.l
MK8	Core	b.d.l	22.2	19	b.d.l	0.74	0.03	1.66	0.11	b.d.l	0.73	0.12	b.d.l	966	0.04
	Rim	b.d.l	0.02	b.d.l	b.d.l	1.97	b.d.l	b.d.l	0.45	b.d.l	b.d.l	0.08	0.09	b.d.l	b.d.l
MK9	Core	0.04	b.d.l	b.d.l	0.04	b.d.l	b.d.l	b.d.l	b.d.l	0.94	b.d.l	b.d.l	b.d.l	b.d.l	b.d.l
	Rim	0.04	b.d.l	0.04	0.18	b.d.l	b.d.l	b.d.l	1.31	4.08	b.d.l	b.d.l	b.d.l	b.d.l	b.d.l
MK10	Core	b.d.l	b.d.l	b.d.l	b.d.l	b.d.l	b.d.l	b.d.l	b.d.l	b.d.l	b.d.l	b.d.l	b.d.l	b.d.l	b.d.l
	Rim	b.d.l	b.d.l	b.d.l	b.d.l	0.33	b.d.l	b.d.l	b.d.l	b.d.l	b.d.l	b.d.l	b.d.l	b.d.l	b.d.l
MK11	Core	0.29	b.d.l	b.d.l	1.41	0.29	0.03	0.1	4.86	2.79	b.d.l	b.d.l	b.d.l	b.d.l	b.d.l
	Rim	b.d.l	b.d.l	b.d.l	b.d.l	b.d.l	b.d.l	b.d.l	b.d.l	b.d.l	b.d.l	b.d.l	b.d.l	b.d.l	b.d.l
MK12	Core	0.05	b.d.l	b.d.l	0.13	b.d.l	b.d.l	b.d.l	b.d.l	1.29	b.d.l	b.d.l	b.d.l	b.d.l	b.d.l
	Rim	b.d.l	b.d.l	b.d.l	0.12	b.d.l	b.d.l	b.d.l	b.d.l	b.d.l	b.d.l	b.d.l	b.d.l	b.d.l	b.d.l
MK13	Core	b.d.l	0.38	2.28	b.d.l	b.d.l	b.d.l	b.d.l	b.d.l	b.d.l	b.d.l	b.d.l	b.d.l	b.d.l	b.d.l
	Rim	b.d.l	0.11	b.d.l	b.d.l	b.d.l	b.d.l	b.d.l	b.d.l	b.d.l	b.d.l	b.d.l	b.d.l	b.d.l	b.d.l
MK14	Core	0.04	b.d.l	0.07	0.19	3.12	b.d.l	b.d.l	3.31	2.49	b.d.l	b.d.l	b.d.l	b.d.l	b.d.l
	Rim	0.04	8.95	10	0.06	0.36	0.02	0.21	0.07	3.11	b.d.l	b.d.l	0.06	b.d.l	b.d.l
MK15	Core	b.d.l	b.d.l	b.d.l	0.06	b.d.l	0.08	0.05	b.d.l	b.d.l	b.d.l	b.d.l	b.d.l	963	b.d.l
	Rim	b.d.l	0.05	b.d.l	0.05	b.d.l	0.16	0.06	0.14	b.d.l	0.11	b.d.l	b.d.l	b.d.l	b.d.l
MK16	Core	b.d.l	b.d.l	b.d.l	b.d.l	0.3	b.d.l	b.d.l	b.d.l	b.d.l	b.d.l	b.d.l	b.d.l	b.d.l	b.d.l
	Rim	b.d.l	b.d.l	0.29	b.d.l	b.d.l	b.d.l	b.d.l	b.d.l	b.d.l	b.d.l	b.d.l	b.d.l	b.d.l	b.d.l
MK17	Core	0.09	b.d.l	0.09	0.09	0.72	b.d.l	b.d.l	0.15	b.d.l	b.d.l	b.d.l	0.10	b.d.l	b.d.l
	Rim	0.03	b.d.l	b.d.l	0.04	b.d.l	b.d.l	b.d.l	b.d.l	b.d.l	b.d.l	b.d.l	b.d.l	b.d.l	b.d.l
MK18	Core	0.03	b.d.l	b.d.l	b.d.l	b.d.l	b.d.l	b.d.l	b.d.l	b.d.l	b.d.l	b.d.l	b.d.l	b.d.l	b.d.l
	Rim	0.02	b.d.l	0.11	b.d.l	0.5	b.d.l	b.d.l	b.d.l	b.d.l	b.d.l	b.d.l	b.d.l	b.d.l	b.d.l
MK19	Core	b.d.l	b.d.l	b.d.l	b.d.l	b.d.l	b.d.l	b.d.l	b.d.l	b.d.l	b.d.l	b.d.l	b.d.l	b.d.l	b.d.l
	Rim	b.d.l	b.d.l	b.d.l	0.04	b.d.l	b.d.l	b.d.l	b.d.l	b.d.l	b.d.l	0.09	b.d.l	b.d.l	b.d.l

Table 19: *Continued*

Grain number	Spots	Mn	Na	K	Sc	Fe/Mg Average	Fe/Ti Average	Ti/Mg Average	Ga/Mg Average	Fe/Ga Average	Cr/Ga Average
MK1	Core	b.d.l	b.d.l	b.d.l	b.d.l	3042.4	11.3	269.6	162	18.7	00
	Rim	b.d.l	b.d.l	b.d.l	b.d.l						
MK2	Core	b.d.l	b.d.l	b.d.l	b.d.l	215.7	3.9	54.2	21.9	9.8	00
	Rim	b.d.l	b.d.l	b.d.l	b.d.l						
MK3	Core 1	b.d.l	b.d.l	b.d.l	b.d.l	422.5	13.1	32.2	24.3	17.3	0.03
	Core 2	b.d.l	b.d.l	b.d.l	b.d.l						
	Rim	b.d.l	b.d.l	b.d.l	b.d.l						
MK4	Core	b.d.l	b.d.l	b.d.l	b.d.l	2100.8	6.4	327.9	69.6	30.2	0.01
	Rim	b.d.l	b.d.l	b.d.l	b.d.l						
MK5	Core	b.d.l	b.d.l	b.d.l	b.d.l	394.5	75.8	5.2	6.6	59.3	0.01
	Rim	b.d.l	b.d.l	b.d.l	b.d.l						
MK6	Core	b.d.l	b.d.l	b.d.l	b.d.l	1414.7	13.7	103	58.7	24.1	0.01
	Rim	b.d.l	b.d.l	b.d.l	b.d.l						
MK7	Core	b.d.l	b.d.l	b.d.l	b.d.l	2391.9	20.5	116.9	362.7	6.6	0.05
	Rim	b.d.l	b.d.l	b.d.l	b.d.l						
MK8	Core	b.d.l	b.d.l	14	b.d.l	135.5	13.4	10.1	8.2	16.4	0.01
	Rim	b.d.l	b.d.l	b.d.l	b.d.l						
MK9	Core	b.d.l	b.d.l	b.d.l	b.d.l	1062.2	9.6	110.5	104.5	10.2	0.4
	Rim	b.d.l	b.d.l	b.d.l	b.d.l						
MK10	Core	b.d.l	b.d.l	b.d.l	b.d.l	652.2	8.8	74.1	43.5	14.9	00
	Rim	b.d.l	b.d.l	b.d.l	b.d.l						
MK11	Core	11.95	b.d.l	b.d.l	b.d.l	275.5	12.3	22.3	17.2	16	00
	Rim	b.d.l	b.d.l	b.d.l	b.d.l						
MK12	Core	b.d.l	b.d.l	b.d.l	b.d.l	1010.5	8.1	124.5	69.3	14.6	00
	Rim	b.d.l	b.d.l	b.d.l	b.d.l						
MK13	Core	b.d.l	b.d.l	b.d.l	b.d.l	224.9	27.5	8.2	6.6	34.1	00
	Rim	b.d.l	b.d.l	b.d.l	b.d.l						
MK14	Core	b.d.l	b.d.l	b.d.l	b.d.l	654.8	10.5	62.6	47.6	13.7	00
	Rim	b.d.l	b.d.l	b.d.l	b.d.l						
MK15	Core	b.d.l	b.d.l	b.d.l	b.d.l	76	12.7	5.9	3.9	19.3	00
	Rim	6.87	b.d.l	b.d.l	b.d.l						
MK16	Core	b.d.l	b.d.l	b.d.l	b.d.l	149.7	7.9	18.8	16.9	8.8	0.03
	Rim	b.d.l	b.d.l	b.d.l	b.d.l						
MK17	Core	b.d.l	17.83	b.d.l	b.d.l	162.5	2.4	68.5	11	14.7	0.2
	Rim	b.d.l	b.d.l	b.d.l	b.d.l						
MK18	Core	b.d.l	b.d.l	b.d.l	b.d.l	448.7	5.9	75.3	18.5	24.3	00
	Rim	b.d.l	b.d.l	b.d.l	b.d.l						
MK19	Core	b.d.l	b.d.l	b.d.l	b.d.l	43.8	27	1.6	0.4	103.9	1.51

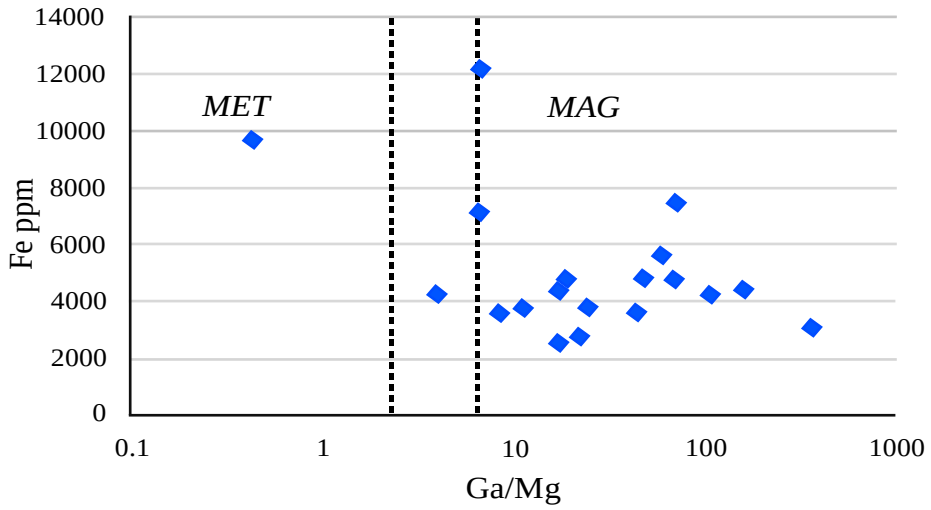

Figure 72: Fe versus Ga/Mg plot diagram for the Mayo Kila sapphires, NW Cameroon (MAG: Magmatic field; MET: Metamorphic field), adapted from Peucat et al. (2007).

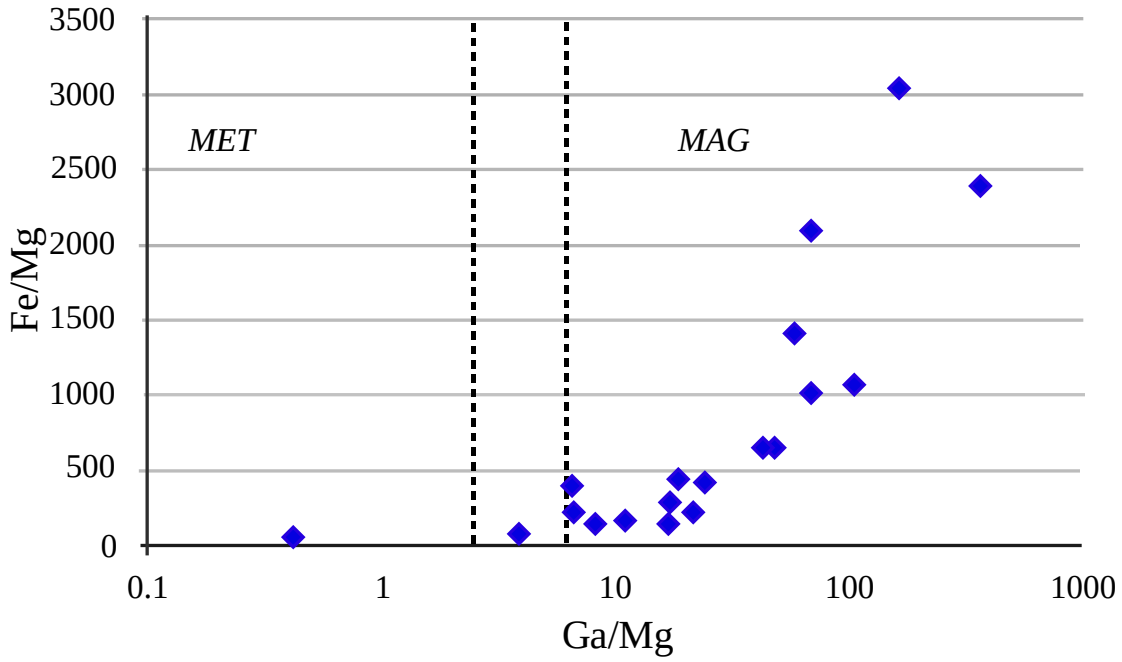

Figure 73: Fe/Mg versus Ga/Mg plot diagram for the Mayo Kila sapphires, NW Cameroon (MAG: Magmatic field; MET: Metamorphic field), adapted from Peucat et al. (2007).

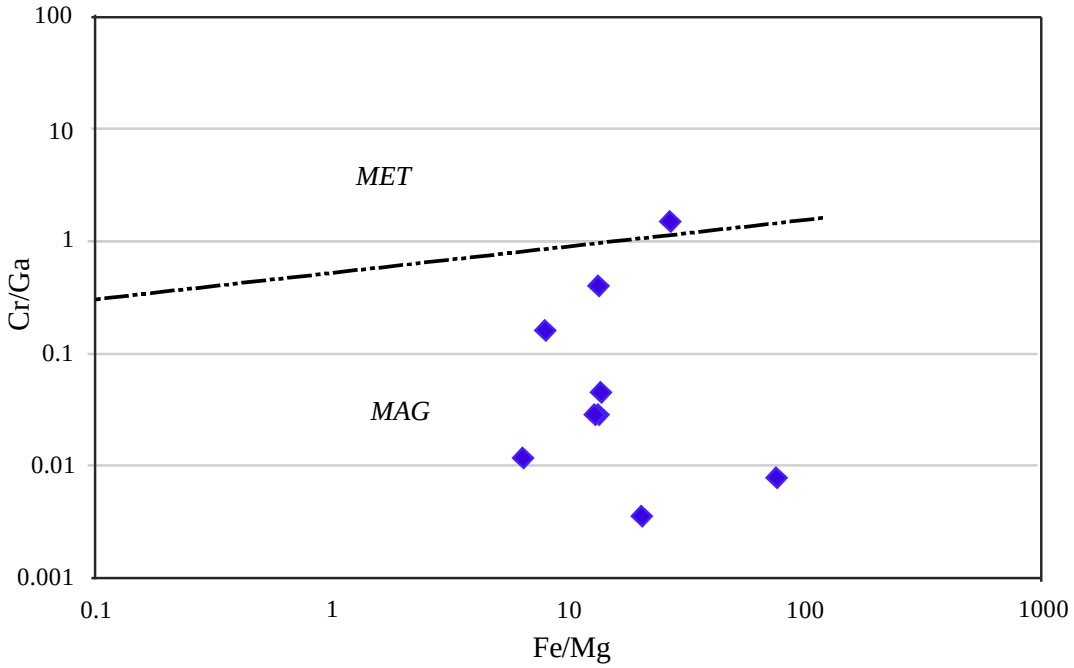

Figure 74: Cr/Ga versus Fe/Mg plot diagram for the Mayo Kila sapphires, NW Cameroon (MAG: Magmatic field; MET: Metamorphic field), adapted from Peucat et al. (2007).

V.6- Trace element geochemistry and U-Pb dating of zircon inclusions

Six trace elements (Hf, Ti, Fe, Pb, Th, and U) were quantified in zircon inclusions within two Mayo Kila samples (MK6 and MK10). The variable concentration of these elements is shown in Table 20. Within these elementary suites, Hf is dominant with significantly high contents that range from 13,354 to 26,238. The Hf value is generally below 17,500 ppm (mostly in MK6) with the highest value (26,238 ppm) found in MK11. It clearly distinguishes this inclusion from others. Thorium concentration ranges from 4,018 to 45,584 ppm with the lowest value found in MK11. The U content ranges from 7,025 to 17,175 ppm with most values being greater than 7,825 ppm. The calculated Th/U ratios range from 0.39 to 2.65 with a mean value of 1.35 is within the range limit in some magmatic crystallized zircons described by Konzett et al. (1998), Belousova et al. (2002) and Hoskin and Schaltegger (2003). The Fe, Pb, and Ti contents (in ppm) range from 25 to 468, 12 to 38 and 4 to 13 respectively. The calculated core age for the zircon inclusions found in the Mayo Kila corundums ranges from 30.0 to 31.8 Ma with a mean of 30.78 ± 0.28 Ma and a 95% confidence level (Fig. 75).

Table 20: Trace element abundances (in ppm) and U-Pb age for zircon inclusions in Mayo Kila corundum grains.

Grain number	Spot number	Hf	Th	U	Fe	Pb	Ti	Th/U	^{207}Pb cor ^{206}Pb/^{238}U age	± 1 ster	^{206}Pb/^{238}U ratio	± 1RSE	^{207}Pb/^{206}Pb ratio ±1 RSE		^{208}Pb/^{232}Th ratio	± 1RSE
MK6	SE10A006	13354	14491	9400	468	17.21	8	1.541	30.82	0.35	0.0049	1.1%	0.0580	3.3%	0.0015	1.9%
MK6	SE10A007	15743	9941	7825	145	13.43	8	1.270	30.74	0.33	0.0048	1.1%	0.0478	1.7%	0.0015	1.6%
MK6	SE10A008	16126	10246	8849	171	14.92	5	1.158	30.45	0.39	0.0048	1.2%	0.0618	3.9%	0.0016	2.5%
MK6	SE10A009	16645	7398	7052	25	12.26	7	1.049	30.72	0.44	0.0048	1.4%	0.0482	3.3%	0.0016	1.8%
MK6	SE10A010	17291	12820	9399	205	22.19	8	1.364	31.07	0.42	0.0055	1.3%	0.1451	1.7%	0.0025	1.8%
MK6	SE10A011	14766	45584	17175	117	37.23	13	2.654	30.77	0.30	0.0048	1.0%	0.0460	1.7%	0.0014	1.5%
MK11	SE10A013	26238	4018	10156	248	21.89	4	0.395	31.00	0.48	0.0056	1.3%	0.1607	1.7%	0.0058	3.8%

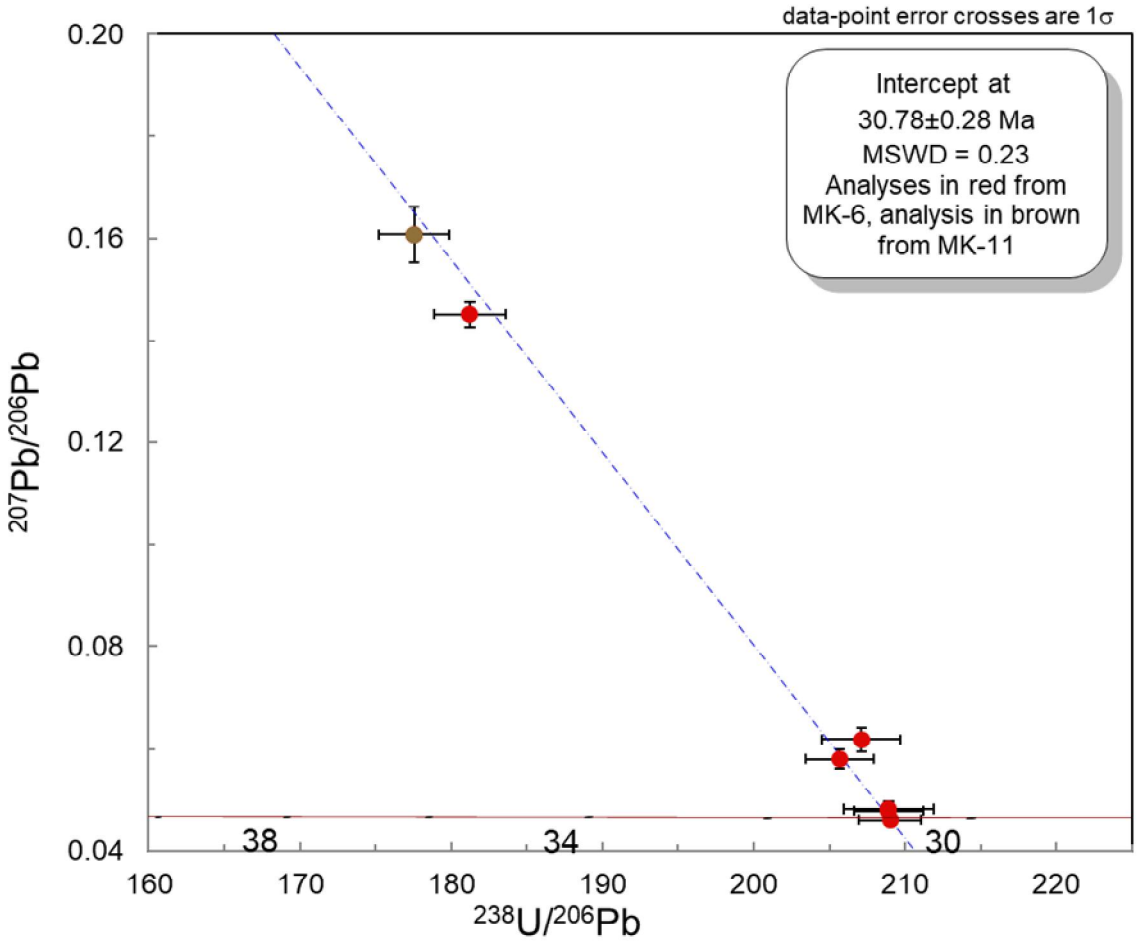

Figure 75: Concordia plot diagram for zircon inclusions found in some Mayo Kila sapphires (MK6 and MK11).

Conclusion

In Mayo Kila and Mbiame, alluvial prospection of sapphire occurrences was done in placers and meandering river valleys. Particle size analysis reveals that the placer materials are mostly represented by fine to coarse sand and gravels. The calculation of Trask Sorting Index of the samples shows that all samples are poorly to very poorly sorted. Heavy minerals analysis of the placers was dominated by zircon, tourmaline and rutile. Sapphire grains from Mayo Kila placers are pale to dark blue with grains of up to 5 mm. Sapphire grains in these two localities are mainly euhedral.

Trace element concentration (in ppm) obtained from Mayo Kila grains are suggestive to a dominantly magmatic origin for the sapphires. The calculated core ages for zircon inclusions ranges from 30.0 to 31.8 Ma, with a mean of 30.78 ± 0.28 Ma and a 95% confidence level. The chapter that follows will present the petrography and the geochemical signature of the surrounding rocks in the study areas.

PART III

DISCUSSION

CHAPTER VI

CHARACTERISTICS AND PROVENANCE OF CLASTIC MATERIALS FORMING THE MAYO-KILA AND MBIAME GEM-BEARING PLACERS AND ROCKS OF THE SURROUNDING

In this chapter, the main results from field investigation and laboratory analysis are discussed. This includes the interpretation of sedimentological data obtained from alluvial material analysis as well as geochemical, geochronological and gemological aspects of obtained sapphire grains. Also, the petrography and geochemistry of the surrounding rocks are discussed in order to propose the origin of the sapphire occurrences.

VI.1- Characteristics and origin of alluvial materials

VI.1.1- Characteristics of alluvial material

Field investigations show that clastic materials are made up of cobble to pebble size gravel and sand materials observed in almost all river beds. In Mayo kila, these clastic materials are made up of quartz fragments, granite, gneiss and very few basaltic rock fragments. While in Mbiame, the fragments are mostly made up of mafic volcanic clasts, followed by granitic fragments, rhyolite and quartz fragments. In some places, the clasts have been cemented to conglomerates.

The rock fragments from Mayo Kila have various shapes from angular, sub-angular to sub-rounded while those from Mbiame are angular to well rounded. The angular shaped materials could be indicative of short distance transport and the well-rounded materials signify a distant origin or from very high velocity of the transporting rivers. With the exception of quartz fragments, most of the rock fragments show deeply weathered surfaces. Particle size distribution results reveal that the placer materials are mostly represented by fine to coarse sand and gravels. The sand and gravel dominance of these samples is an indication of detrital materials deposited by a transfer agent. In this case, river transport is the most likely means.

All the samples show poorly sorted to very poorly sorted sediment distribution, with the dominance of poorly sorted samples. This poor sorting can be confirmed by the fact that most of the samples have fewer fine grain fractions, whereas the coarse sand and gravel are dominant. The sediments are assumed to be deposited from high-energy currents (Wan et al.,

2015). This poor sorting can also be attributed to a short distance transport from a proximal source.

VI.1.2- Heavy mineral occurrence and their significance

Heavy minerals occur in a wide range of magmatic and metamorphic rocks as accessory minerals. They are known to be of different degrees of resistance to weathering and abrasion, and have been proven to be useful tools in the analysis of provenance of stream sediments (Morton, 1985; Mange and Maurer, 1992). The heavy mineral assemblage presented in this study are from the Mayo Kila and Mbiame placers.

The heavy minerals obtained from alluvial profiles and test pits were identified under the petrographic microscope. These minerals include: zircon, tourmaline, disthene, epidote, pyroxene, andalusite, garnet, chlorite, zoisite, biotite, sillimanite, hornblende, apatite, opaque minerals and other unidentified minerals. This mineral association is similar to those observed in the Nsanaragati (Kanouo et al., 2012c), Mayo Kewol placers (Boaka et al., 2010) and those of other secondary magmatic sapphire deposits around the world (Coenraads et al., 1990; Garnier et al., 2005). The abundance of these heavy minerals in the placers is conditioned by the existing different rock types in the area as well as their weathering, transport and depositional history. Minerals like epidote, zoisite, disthene, andalusite and sillimanite are indicative of medium to high grade metamorphic source while minerals such as zircon, tourmaline, apatite, garnet, hornblende and pyroxenes occur both in magmatic and metamorphic rocks. These minerals are not considered as good tracers and in the study areas, they clearly express the granito-gneissic nature of the basement rock. However, tourmaline often occurs in pegmatite veins and is indicative of hydrothermal alteration in the study areas. In addition, the presence of easily weathered minerals like pyroxene and amphibole suggests high erosion rates, rapid transport and short grain residence time in the river (Kao and Milliman, 2008), implying a proximal source of these sediments.

VI.2- Corundum characteristics and occurrence

The mineralogy and chemistry of sapphire grains coupled with U-Pb dating of zircon inclusions permitted to discuss the characteristics and geological origin of the Mayo Kila blue sapphires.

VI.2.1- Sapphire morphology

The morphology of the Mayo Kila and Mbiame placer sapphires has been used to constrain their source parameters. The sapphires are mostly euhedral but few anhedral grains

do exist. They are generally angular, typifying short distance transportation from their source area and dominantly represent nearby source accumulated clasts. The sub-angular to sub-rounded shapes of some of the sapphires may be due to their mechanical abrasion during moderate distance transportation in water, or could represent post depositional features acquired by constant reworking of accumulated clasts (Kanouo et al., 2012a). Some of the sapphires show irregular corrosion patterns, which could have resulted from corundum-magma interaction owing to disequilibrium with the carrier magma during its ascent to the surface (Coenraads et al., 1990; Guo et al., 1996; Sutherland et al., 2008).

Blue, green, and yellow are the most represented colours in magmatic secondary sapphires, and are commonly referred to as Blue-Green-Yellow or BGY sapphires (Sutherland et al., 1998). These are the main colours of Mayo Kila and Mbiame sapphires and those of Mamfe and Mayo Kewol placers (Kanouo et al 2012a; Boaka et al., 2010).

VI.2.2- Sapphire trace element chemistry

The Fe, Ti, Cr, Ga, Mg contents and chemical ratios such as Ga/Mg, Fe/Ti, Fe/Mg and Cr/Ga of corundum xenocrysts carried by continental alkali basalts are used to distinguish their magmatic versus metamorphic origin (e.g. Sutherland et al., 2002, 2009, 2015a; Garnier et al., 2005; Zaw et al., 2006; Peucat et al., 2007; Kanouo et al., 2012a; Boaka et al., 2011; Uher et al., 2012). Generally, Fe and Ga reveal higher concentrations in magmatic sapphires with values from 1,800 to 13,000 ppm and 70 to 570 ppm respectively, while in metamorphic ones these values are lower with contents of less than 3,000 and 75 ppm for Fe and Ga respectively. In contrast, low Cr and Mg contents are typical of magmatic sapphires with both values usually less than 40 ppm, whereas gem corundums of metamorphic origin are enriched in these elements with both values generally greater than 60 ppm. Consequently, the Ga/Mg ratio is commonly >6 in magmatic sapphires and <3 in metamorphic ones. Conversely, the Cr/Ga ratio is <0.1 for magmatic sapphires and >1 for metamorphic sapphires. The Fe/Ti ratio is generally higher in magmatic than metamorphic sapphires. The Fe/Mg ratio is significantly higher for magmatic sapphires (Fe/Mg >>100) and lower for metamorphic and metasomatic ones (Fe/Mg <100; Peucat et al., 2007).

In this study, Trace element analysis of sapphires shows significant concentration (in ppm) in some elements: Fe (2,208 to 14,473), Ti (82 to 1783), Ga (77 to 512), Mg (0.9 to 264.9) and Cr (≤168). Calculated ratios show extreme variations, with Fe/Mg (43 to 3043), Fe/Ti (2 to 76), Ti/Mg (1 to 328), Ga/Mg (0.4 to 363) and Cr/Ga (≤ 1.5). From this data, these sapphires dominantly crystallized in alkaline magmas with few grains pointing towards a

metamorphic/metasomatic source. These values are consistence to those obtained for other Cameroonian magmatic sapphires from Mayo Kewol and Nsanaragati (Kanouo et al 2012a; Boaka et al., 2011), and are within values obtained by Peucat et al. (2007) for magmatic sapphire deposits around the world.

The colour of Mayo Kila sapphires varies from pale, grayish to greenish and dark blue. The colour variation may be due to different concentrations of Fe, Ti, V and Cr (Emmett et al., 2003; Sutherland et al., 2009; Kanouo et al., 2012a, 2016). Fe and Ti are the major chromophore agents, and their substitution and pairing effect are responsible for the dominant blue colour (Emmett et al., 2003; Kanouo et al., 2012a) of Mayo Kila sapphires. Their variation in concentration, as well as other substituting elements can affect the final colour of sapphire crystals (Emmett et al., 2003), as pale, grayish, greenish and dark blue colours are observed in the studied sapphire grains.

Gallium, Mg and colouring agents described above often substitute Al in corundum lattice, and their substitution highly depends on the availability of these elements in the crystallization solution (Peucat et al., 2007; Kanouo et al., 2012a, 2016; Sutherland et al., 2015a). The significantly high Ga (up to 512 ppm) and relative high Fe (up to 14,473 ppm) suggest, they mainly crystallized in Ga-Fe-enriched environment with some alkali to alkaline affinities or silica enrichment, as Si content in one grain is up to 1117 ppm. The alkali to alkaline nature of crystallized melt (s) is favored by the significant presence of Na (up to 17.8 ppm), K (up to 14 ppm), and Sr (up to 35 ppm) in some of the sapphire grains. The relative Na, K and Si enrichment in some of the grains is not due to feldspathic inclusions as found in Bo Phio sapphires (Khamloet et al., 2014), but is favored by lattice substitution, as no feldspar inclusion was found in spotted zones. The magmatic origin is shown in Figure 76, where all grains are plotted in the magmatic field. In the Fe-Mg-Ti ternary diagram, grains plot in the magmatic field and are clustered on the high Fe-Ti axis due to their enrichment in these elements.

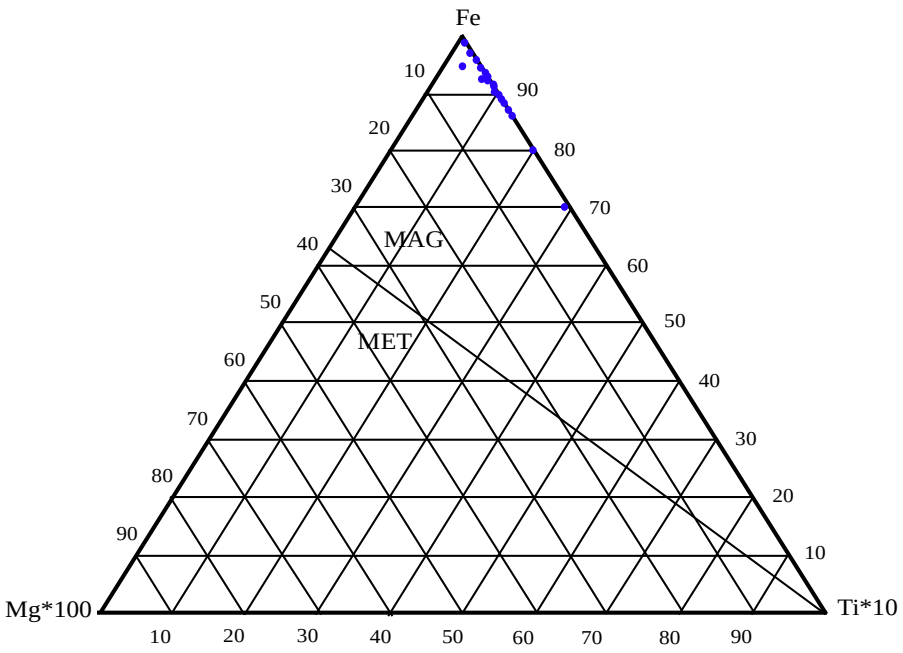

Figure 76: Fe-Ti*10-Mg*100 ternary diagram (Peucat et al., 2007) for Mayo Kila sapphires MAG: Magmatic field, MET: Metamorphic fields.

The Ti (82 -1,783 ppm) content in the magmatic corundums is highly heterogeneous with some being greater than others. They may represent corundums from two different magmatic environments: a Ti enriched source (e.g. MK4: Ti up to 1,776 ppm) and Ti depleted source (e.g. MK16: Ti less than 83 ppm). The very high Ti content in the rim of some of these corundums (e.g. MK2: Ti = 1,028 ppm) is not due to Ti mineral inclusion (e.g. ilmenite: Khamloet et al., 2014; rutile: Sutherland et al., 1998), as this was not found in spotted rim. Other magmatic corundums have significantly low Mg and V contents (e.g. MK15: Mg up to 64 ppm, V up to 34 ppm; MK13: Mg up to 21 ppm, V: 8 ppm; and MK5: Mg up to 40 ppm, V up to 30 ppm). They may be intermediate type, as the V content is less than 35 ppm in this corundum (Zaw et al., 2014). The clear difference between these corundum grains and other grains is shown in their Fe versus Ga/M and Fe/Mg versus Ga/Mg ratios as most grains occur within the values of magmatic fields. Samples MK13 and MK5 occur slightly out of the values for magmatic sapphires and may be transitional corundums (Peucat et al., 2007; Kanouo et al., 2012a, 2016) crystallized during metasomatism (Sutherland et al., 2015b).

Niobium and Ta abundance in some of the magmatic corundums are relatively high (e.g. MK14: Nb up to 61 ppm, Ta up to 132 ppm and MK11: Nb up to 475 ppm, Ta: up to 421 ppm). Niobium and Ta do not easily substitute Al in corundum structure; the relatively

high Nb and Ta contents in some Mayo Kila corundums may be due to their crystallization in primary Nb-Ta ore deposits (Kanouo et al., 2016). The high Zn content in one of the corundums (MK12: Zn up to 262 ppm) may be due to elementary substitution as a result of crystallization in Zn-enriched environment (Peucat et al., 2007). Also, the high Ce content (19 to 30 ppm) in some of the corundums may be associated to their crystallization in Ce-enriched melts rather than monazite [(Ce, La, Th) PO_4] inclusion (Khamloet et al., 2014), as these grains have very low Th (≤0.39 ppm).

The metamorphic affiliated corundum (MK19 with Mg > Ga, relative high Cr content up to 168 ppm) could have grown in a Fe-Mg-Cr enriched metamorphic rock. The presence of an unanalyzed rutile inclusion in MK19 suggests a crystallization in a metapelitic rock rather than an eclogitic rock as eclogite is absent within the local and regional geological settings (Tetsopgang et al., 2008; Fozing et al., 2013). Alternatively, some sapphires may have grown in syenitic magmas and interacted with Mg-rich sources, allowing some sapphires to incorporate Mg and spread the Ga/Mg ratios (Peucat et al., 2007).

A comparative plot for Mayo Kila sapphires in Fe vs. Ga/Mg diagram with those studied in Eastern Australia, Southeast Asia, China and Africa (Figure 77), places these sapphires in the same field together with those from another deposit in Cameroon; Barrington 2; Australia; Cudgegong-Gulgong 2, Australia; Yarrowitch 2, Australia; Chantaburi, Thailand; Hainan, Fudjian and Shandong, China; Sam Sai, Laos; Pailin, Cambodia; Jos Plateau, Nigeria; Analafady, Madagascar and Gaba Tula, Kenya. The data for this comparative corundum plots are from Peucat et al. (2007), Sutherland et al. (2009b), and Kanouo et al. (2012a).

In figure 78, they also plot in the magmatic field and overlap with the syenitic type magmatic deposite of Ilmen (Russia) and Garba Tula (Kenya). This is due to their high iron content and Ga/Mg ratios above 6. Cameroonian sapphire defines a new domain of magmatic type deposits (Figure 79), close to the basaltic type deposit of Southern Vietnam (Pham Van et al., 2004).

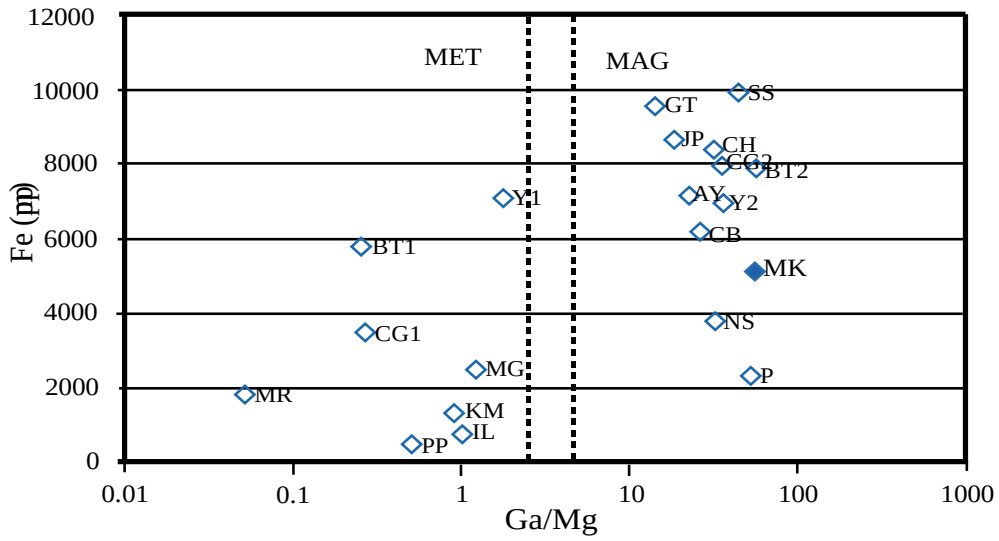

Figure 77: Fe vs. Ga/Mg comparative plot diagram for the Mayo Kila sapphires and other studied corundums from Africa, eastern Australia, Asia, and Colombia (MAG: Magmatic field; MET: Metamorphic field): MK: Mayo Kila; NS: Nsanaragati, Cameroon; BT: Barrington; CG: Cudgegong-Gulgong; MR: Macquarie River; Y: Yarrowitch, Australia; CH:Hainan, Fudjian and Shandong, China; CT: Chanthuburi, Thailand; SS: Sam Sai, Laos; P: Pailin, PP: Pailin Pastel, Cambodia; MG: Mogok, Myanmar; Kashmir, India; JP: Jos Plateau, Nigeria; AY: Analafady, IL Ilakaka, Madagascar; GT: Gaba Tula, Kenya. Corundum plots from other localities are based on Peucat et al. (2007), Sutherland et al. (2009b), and Kanouo et al. (2012a).

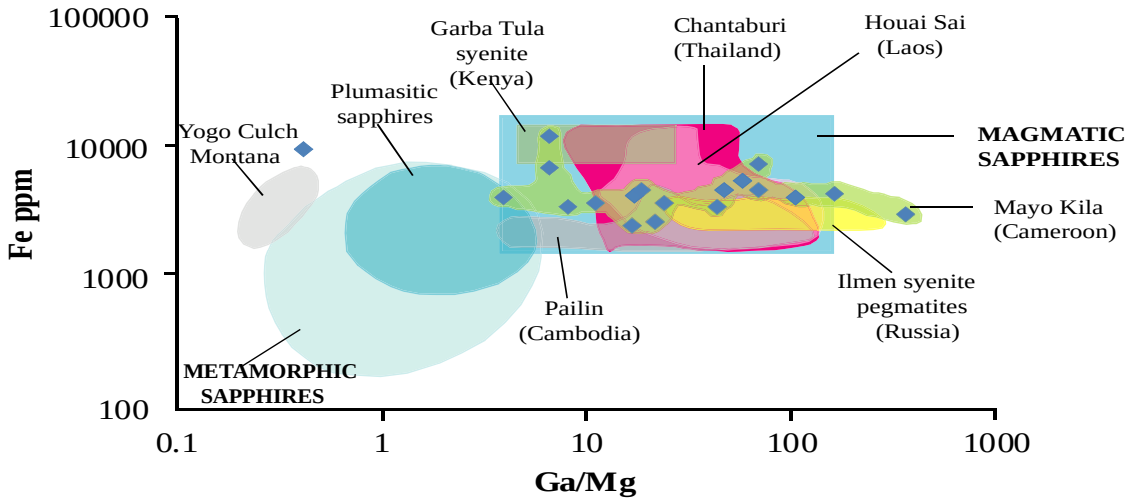

Figure 78: Fe versus Ga/Mg discrimination diagram (after Peucat et al., 2007; Voudouris et al., 2019), demonstrating the position of Mayo Kila sapphires and other magmatic sapphires around the world.

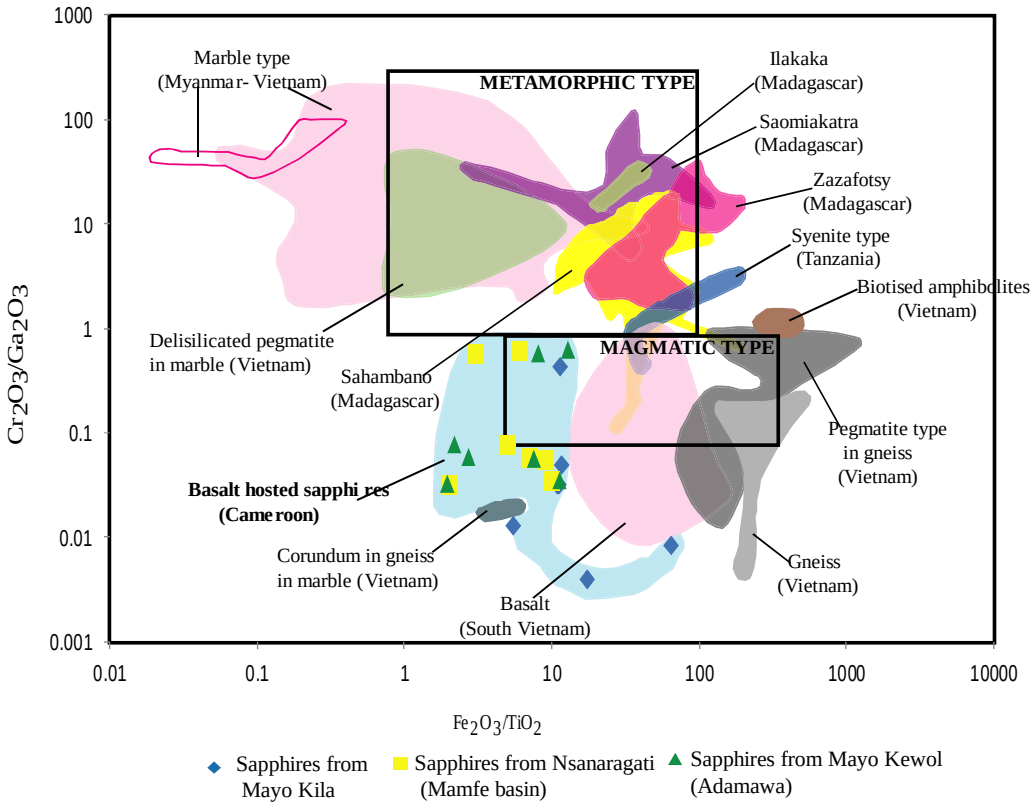

Figure 79: Cr_2O_3/Ga_2O_3 versus Fe_2O_3/TiO_2 (after Rakotondrazafy et al., 2008) plot demonstrating the new domain of magmatic type deposite defined by Cameroonian sapphires with resepct to deposits around the world.

VI.2.3- Zircon trace element chemistry and geochronology

Trace elements contents in zircon found in some Mayo Kila sapphires are significantly high; Hf (13,354 -26,238 ppm), Th (4018 - 45,584 ppm), and U (7,052-17,175 ppm). These data are in the range obtianed in zircons from magmatic terrains in association with alkali basalts (Sutherland et al., 2002, 2009b). The U and Th concentrations are higher than those published by Sutherland et al. (2002, 2015b) for zircon inclusions in Ban Huai Sai and Lava Plains corundums. They are also higher than the typical U (<30 ppm) and Th (<10 ppm) proposed by Heaman et al. (1990) and Belousova et al. (2002) for mantle zircons. The high U and Th contents indicate their enrichment in the hosting source rocks. These U-Th rich zircon inclusions probably crystallized in a Th-U ore body. The high concentration of Th, U, and Hf in these zircon inclusions are similar to those crystallized in highly evolved melts, displaying peralkaline syenitic or granitic compositions (Guo et al., 1996a). However, their Th/U ratios, generally not far from 1, are in the range of igneous crustal zircons values (Belousova et al., 2002; Kirkland et al., 2015).

The Hf value in these inclusions is greater than 9000 ppm, implying that they were crystallized in the absence of rifting, as Hf contents in zircon grew during continental rifting is less than 9000 ppm (Heaman et al., 1990). With their very high Hf contents, they are inclusions grown in highly fractionated Hf-enriched melts (Guo et al., 1996; Sutherland et al., 1998). The Hf contents are within the range limit (10,000 - 28,000 ppm) in zircon associated with corundum in syenitic xenocrysts found in basalts (Guo et al., 1996), but more than most values found in coarse-grained zircons (generally ≤ 9000 ppm) in the Western Mamfe corundum gem placers (dominantly from granitoids cooled within continental rift system: Kanouo et al., 2012b, 2015, 2016). They may be zircons crystallized in nepheline-syenite pegmatite, as the Hf contents in zircons from this rock range from 1.1 to 2.8 wt.% (Belousova et al., 2002). The syenitic pegmatite origin of these zircons is supported by their significantly high Th and low Pb content which are largely within range in zircon from this rock type (Belousova et al., 2002). The iron contents in the inclusions are more than those in Belousova et al. (2002) nepheline-syenite pegmatite zircon. These inclusions were probably crystallized in an Fe-enriched environment.

U-Pb dating of zircon inclusions has shown that the apparent ages of the zircons are almost identical to the age of the basalt from which corundum is recovered (Coenraads et al. 1990). However, Guo et al. (1996a) showed that at the high temperature of basaltic magmas, the zircon inclusion U-Pb chronometer can be reset within the time of a magma's eruption-cooling cycle due to Pb diffusion. As a result, the real timing of zircon crystallization, and thus the timing of corundum formation, could have been before the volcanism represented by the host basalts (Guo et al.,1996b).

The geochronological data point to a mean age of 30.78 ± 0.28 Ma (Lower Cenozoic: Oligocene), for the magmatic crystallization of the zircon inclusions. This shows that rocks of this age provided part of the clasts forming the Mayo Kila gem placer. The depositional period of these Lower Cenozoic detritus is assumed to be post-Oligocene. The mean age of these zircon inclusions is more than that of the youngest Western Mamfe zircon grains (27-11 Ma) whose source areas are assumed to be around the Mount Bambouto and Mount Bamenda (part of the CL) (Kanouo et al., 2012b, 2015). This shows that the Mayo Kila zircon inclusions and these zircon grains were not crystallized in the same environment.

The source rocks of the Oligocene zircon inclusions can be found within rocks of the Cameroon Line, made up of young anorogenic syenitic to granitic plutons (Njonfang and Moreau, 1996; Njonfang et al., 2011) with their ages ranging from Lower Paleocene to

Lower Oligocene (Rankenburg et al., 2005; Kanouo et al., 2015), and much younger and older felsic and mafic volcanic to sub volcanic rocks (Lee et al., 1994; Marzoli et al., 2000; Mileli et al., 2012; Kamgang et al., 2013; Kanouo et al., 2015). The obtained mean age (30.78 ± 0.28 Ma) is closer to those of some rocks found in Mount Oku (31-22 Ma: Rankenburg et al., 2005), but largely below obtained ages for igneous basement rocks (530 - 510 Ma: Tetsopgang et al., 1999; 569 to 420 Ma: Tetsopgang et al., 2008) within the local geological settings. They were not crystallized in these Precambrian rocks, but in more felsic syenitic young plutons with similar age as some rocks found in Mount Oku. These sapphires likely crystalized from the Ntumbaw syenitic pluton with mostly peraluminous magmas and some compatible element contents closer to crustal values.

On the FeO - Cr_2O_3 - MgO - V_2O_3 versus FeO + TiO_2 + Ga_2O_3 diagram of Guiliani et al. (2010, 2014), most of the Mayo Kila sapphires crosscut the domains of metasomatic sapphires and sapphires as xenocrysts in alkali-basalt while three samples crosscut the domains of sapphires in alkali basalts and syenite (Figure 80), probably due to their high concentrations in Fe, Ti and Ga. When compared to other studied sapphire occurences in Cameroon from Nsanaragati (Kanouo et al., 2012a) and Mayo Kewol (Boaka et al., 2011), sapphires crosscut the domains of metasomatic and alkali-basalt sapphires with highest number of samples in the metasomatic domain (Fig. 80), except for two samples from Nsanaragati, which are completely out of the defined domains, probably due to their much higher Ti levels (6,919–7,069 ppm), as well as their excesses in Fe levels (Kanouo et al., 2012). From these diagrams, it is confirmed that Mayo Kila sapphires as well as the other studied sapphires in Cameroon are of a magmatic and/or metasomatic origin.

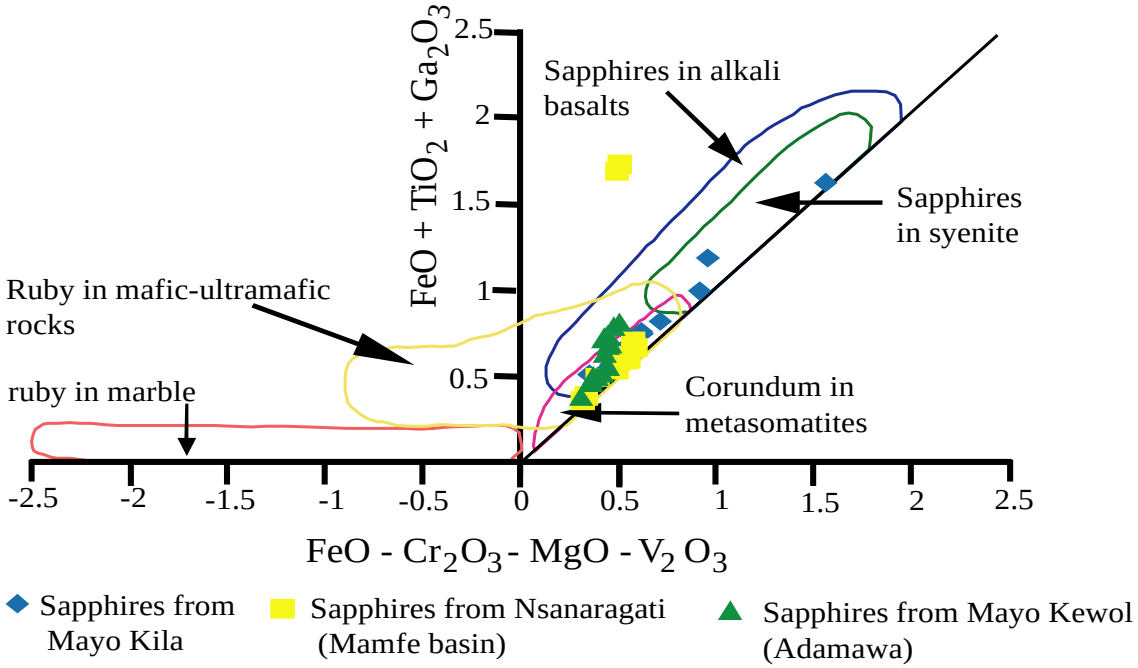

Figure 80: Position of Mayo Kila sapphires and other Cameroonian sapphires on the FeO - Cr_2O_3 - MgO - V_2O_3 versus FeO + TiO_2 + Ga_2O_3 diagram (in wt.%) used for the geological classification of the corundum deposits (after Guiliani et al., 2010).

Similarities in Cameroonian sapphire deposits

Cameroonian sapphire deposits are principally magmatic and are related to Cenozoic intraplate alkaline basalt volcanism of the Cameroon Line. The trace element contents of their zircon inclusions show that they represent magmatic crystallized zircons sourced from syenogranitic or syenitic rocks.

The trace element contents of saphires from Nsanaragati Fe (2496 - 4643 ppm), Ti (49 - 7069 ppm), Ca (360 - 976 ppm), Si (485 - 687 ppm), Ga (149 - 307 ppm), V (4 - 41 ppm) and Mg (2 - 42 ppm) (Kanouo et al., 2012c), Mayo Kewol Fe (up to 4140 ppm), Ga (up to 420 ppm), Ti (1960 ppm), Mg (0 – 80 ppm), V (0 – 90 ppm) and Cr (0 - 130 ppm) (Baoka à Koul et al., 2011) and Mayo Kila Fe (2208 to 14473), Ti (82 to 1783), Ga (77 to 512), Mg (0.9 to 264.9) and Cr (≤168) (Mbih et al., 2016). These values show strong overlapping with those of other magmatic sapphires from basaltic fields around the world.

The colours blue, green, and yellow are mostly abundant amongst the magmatic secondary sapphires. These types of sapphires are commonly referred to as ‘Blue-Green-Yellow’ or ‘BGY’ sapphires in the literature (e.g., Sutherland et al., 1998). These are the main colours of studied Cameroounian sapphires (Kanouo et al 2012a; Boaka et al., 2010 and information herein).

All studied sapphire deposits in Cameroon show some similarity in the heavy mineral associations. Those of Mayo Kewol are made up of magnetite, ferrocolumbite, cassiterite, monazite, beryl, topaz, zircon and corundum (Boaka et al., 2010), those of Nsanaragati are rutile, sapphires, apatite, magnetite and zircon (Kanouo et al., 2012a). In mayo Kila and Mbiame, the most represented heavy minerals are magnetite, rutile, tourmaline, zircon, apatite and monazite.

Sapphire grains from the three localities are secondary magmatic sapphires with evidence of chemical corrosion, indicating disequilibrium with the basaltic carrier magma. This feature suggests a non-cogenetic origin of the corundum and their assumed host basalt (Coenraads et al., 1990).

VI.3.5- Potential sapphire sources

The geologic and geotectonic context in which sapphires occur is predominantly that of alkaline basalt from intracontinental rift settings, and never in basalts from other geotectonic settings (Irving and Price, 1981; Baldwin et al., 2017). Examples of such sapphire occurrences are sapphires from Cenozoic volcanism of the French Massif Central (Gaillou, 2003; Giuliani et al., 2009; Medard et al., 2012), sapphire from alkali-basaltoid volcanism from Central Vietnam (Izokh et al., 2010) and the in situ sapphire occurrences from the Siebengebirge Volcanic Field, Germany (Baldwin et al., 2017).

The French Massif Central is an example of continental intraplate alkaline magmatism and is spatially related to the West-European Rift-System (Woodland and Jugo, 2007). The French massif is made up of the Aubrac, Velay, Devès, Coiron, Cantal, Ceallier, Bas-Vivrais and des Chaine des Puys. The Tertiary to recent volcanism of this massif occurred in three phases (Michon and Merle, 2001) and is associated to the magmatism that let to rifting and the formation of the limagne graben (Woodland and Jugo, 2007). On this massif, alluvial sapphire deposits are associated with basaltic volcanism and syenitic enclaves within trachyte. Sapphire formation occurs at various times, from 19.9 ± 0.4 Ma in the Limagne to 956 ± 11 ka in the Velay. These ages are consistent with those of the local volcanism. They contain inclusions of feldspars, zircons, ilmenite, and Nb-rich oxides. Most of the sapphires were brought to the surface by basaltic magmas with clear evidence of disequilibrium textures such as dissolution features on the sapphire surfaces. They probably originated from the crystallization of a water-rich trachytic melt, derived either by fractional crystallization of a basaltic mantle melt, or by direct low-degree melting of the mantle (Medard et al., 2012).

Sapphire from alkali-basaltoid volcanism from Central Vietnam (Izokh et al., 2010) occur in Neogene-Quaternary intraplate basaltoid magmatism that led to the formation of vast basaltic plateaux. The basaltic plateaux are predominantly tholeiitic basalts in the basaltic sequences, and subordinate alkaline rocks (Hoang and Flower, 1998; Izokh et al., 2010). The placer is localized in eluvial laterites developed from alkali basalt flow. Other placer minerals associated with sapphires are zircon, tourmaline and garnet. The placer sapphires in this area are shown to have crystallized from a more fractionated iron-rich syenitic melt with the participation of CO_2 and CO_2-H_2O fluids in shallower crustal horizons and the subsequent eruptions of alkali basalts favored the transport of garnet and pyroxene megacrysts as well as sapphire and zircon xenocrysts to the surface (Izokh et al., 2010).

The Siebengebirge Volcanic Field is part of the Central European Volcanic Province (CEVP) which forms a 200-300 km broad Cenozoic intra-continental volcanic belt north of the Alpine Orogen (Baldwin et al., 2017). The most primitive mafic volcanics are basanites to alkali basalts; more felsic volcanics are SiO_2 saturated latites to trachytes and SiO_2 undersaturated phonotephrites to tephriphonolites (Kolb et al., 2012, Baldwin et al., 2017). The mafic alkaline rocks have been known to host sapphire megacrysts (Baldwin et al., 2017). According to this author, sapphire mineralization took place in four stages of magmatic differentiation as follow: (i) the initiation of alkaline basaltic volcanism in the Siebengebirge Volcanic Field, (ii) the differentiation of alkaline mafic magmas leading to the formation of highly evolved phonolites which was accompanied by a build-up of CO_2 in the melt, (iii) carbonatitic melt exsolved from highly evolved phonolite saturated in CO_2 and separates from the phonolite. Sapphires then precipitated from the carbonatite after physical separation, (iv) the fresh pulses of alkaline mafic melts while on its path to the surface encounters the carbonatite lenses, this encounter leads to the dissolution of the carbonatite lenses and subsequent incorporation of the sapphires by the alkaline mafic melt which carried them to the surface.

On the African continent, the Benue Trough (BT) represents a tectono-magmatic structure characterized by horsts and grabens, whose individual dispositions are mostly controlled by north-south trending normal faults and northeast-southwest strike-slip faults (Suh et al., 2000). Its magmatic province constitutes a spatial link between the alkaline to peralkaline province of Nigeria to the North and the CL to the South (Ngako et al., 2006). On the Benue Trough, the origin of sapphire deposits has been linked to the emplacement of some large Cenozoic intraplate alkaline basalt-basanite-trachyte-phonolite (Girei et al., 2016). The Guroji sapphire deposit on the Mambilla Plateau in the northeast of the Beneu Trough

occurs within placers spatially and temporally associated with intraplate alkaline basaltic flows and plugs. The weathering of these Cenozoic alkaline intraplate basaltic rocks and subsequent alluvial processes led to the formation of economically viable sapphire deposits. The main inclusions found in these crystals are feldspar, uranopyrochlo and zircon.

In Kenya, the Dusi sapphire is associated to the Mozambique Belt. Sapphires are recovered from a N-S vertical monzonite dyke of up to 5 meters thick. The monzonite is composed of microcline, plagioclase, corundum, biotite, muscovite and sericite, zircon, magnetite and apatite (Simonet et al., 2004). The 579 ±6 Ma age obtained from zircon inclusions in corundum, dates the beginning of the monzonitic magma crystallization and coincides with the age range of a major N-S shearing event in the Dusi area.

Corundum occurrence in Cameroon has been attributed to two mega structures; the Central Cameroon Shear Zone and the Cameroon Line (Boaka et al., 2011; Kanouo et al., 2012a). The two studied sapphire deposits in Cameroon are those of Nsanaragati in the Mamfe basin (Kanouo et al., 2012a) and Mayo Kewol in the Adamawa plateau (Boaka et al., 2011). In these deposits, sappire crystals are extracted from alluvial placers and are associated to other heavy minerals such as topaz, beryl, zircon, monazite, cassiterite, magnetite ferrocolumbite for the Mayo Kewol placers (Boaka et al., 2010) and Zircon, tourmaline, kyanite, spinel and garnet for the Mamfe placers (Kanouo et al., 2012a). Their trace element contents point to a magmatic origine with Fe contents far higher than 2000 ppm, Ga contents higher thatn 140 ppm and Ga/Mg ratios are mostly higher than 10. Mineral inclusions in Mayo Kewol sapphires are zircons, ilmenorutile and ilmenite (Boaka et al., 2011). Mean age from zircon inclusion from Mamfe sapphires gave 12.39 ±0.55 Ma, thus, attaching the sapphires to upper Cenozoic magmatic event of Mount Bambouto basaltic and alkaline lavas of the CL (Kanouo et al., 2012a). Both authors propose the crystallization of sapphires from deep seated syenitic melts and were transported to the surface by alkaline basalts of the CL.

VI.3.5.1- Magma sources for the Mayo Kila plutonic rocks

The major, trace and rare element contents of the surrounding rocks have been used to propose their magma sources and tectonic setting.

Mantle and crust are two end member sources of granitoids. While most granitic rocks originate by contribution from both sources, some are derived purely from one end member source (Pearce, 1996). Results from this study are in concordance with detailed works on the

Nkambe granitoids by Tetsopgang et al. (2006; 2008 and 2011). These rocks display chemical compositions typical of high - K calc-alkaline to shoshonitic with peraluminous and metaluminous affinities. The peraluminous types are biotite and two mica granites while diorite and monzonite are metaluminouse. These variations suggest that these rocks were derived from different protoliths. The peraluminous S-type rock could have been derived from the partial melting of metasedimentary protolith or supracrustal deposition (Chappell and White, 2001), while the metaluminous I-type rocks were derived from a metaigneous protolith (Pearce, 1996; Frost et al., 2001; Nédélec and Bouchez, 2015). On the Patino-Douce (1999) diagram for the discrimination of the sources of granitic rocks (Figure 81), two biotite granite samples plot in the peraluminouse granite domain, the other two samples plot in the domain of metagreywackes together with two mica granite from this study and those from Tetsopgang et al. (2006) and monzogranite from Tetsopgang et al. (2011). The diorite and monzonite from this study and quartz monzonite from Tetsopgang et al. (2011) plot in the domain of amphibolite derived melt.

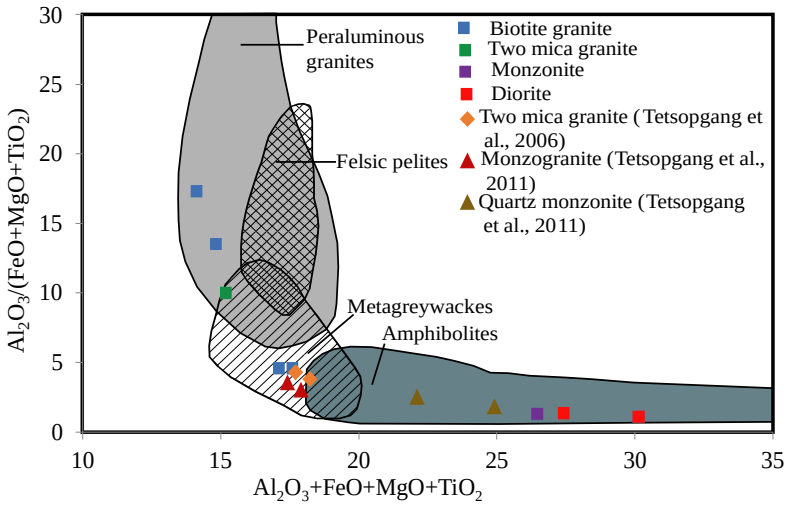

Figure 81: Discrimination diagram of $Al_2O_3/(FeO + MgO + TiO_2)$ versus $Al_2O_3 + FeO + MgO + TiO_2$ of Patino-Douce (1999) for the different sources of granitic rocks.

However, Tetsopgang et al. (2006) argue that, the high Na_2O in the two mica granites could suggest the I-type origin of the source rock, since fractional crystallization of metaluminous magmas can derive peraluminous granites. Thus, the peraluminousity of these two-mica granites can be as a result of differentiation of an I-type source melt.

VI.3.5.2-Geotectonic setting of Mayo Kila plutonic rocks

It is observed that, High-K calc-alkaline granitoids in continental collisional setting evolve to shoshonitic compositions during the late stages of orogeny, where crustal delamination operates (Liegeois et al., 1994). Coupled with data in this study, petrographic and geochemical data from Tetsopgang et al. (2008), situates the emplacement of the studied plutonic rocks in a syn- to post-collisional tectonic setting. On the Rb against Y + Nb tectonic discrimination diagram of Pearce et al. (1984), the diorite and one biotite granite samples plot in the volcanic arc granite domains, three biotite granite samples plot on the line separating the syn-collitional granites and Volcanic arc granites. The two-mica granite and monzonite samples plot in the within-plate granite domain. With comparative samples from Tetsopgang et al. (2006; 2008), selected samples of two mica granite and magnetite-rich two mica granites all plot in the domain of syn-collitional granites. Those of foliated biotite monzogranite mostly plot in the domaine of volcanic arc granite with few samples in the syn-collitional domain. The same trend is observed for the massive biotite monzogranite. On the domain of within plate granites, both foliated and massive biotite monzogranite have one sample each. Most of the samples are clustered within the triple point between volcanic arc granite, within-plate granite and syn-collitional granites, defined as the domain of post-collision granitoids (Fig. 82).

However, conferring to Tetsopgang et al. (2006; 2008), these rocks were put in place in a syn- to post- collitional tectonic setting, with the foliated biotite monzogranite, representing syn- to late-collision conditions, as its CHIME zircon age range from 569±12–558±24Ma, whereas the post-collision massive biotite monzogranite gives CHIME zircon ages of 533±12–524±28 Ma (Tetsopgang et al., 2008). Also, two-mica granites represent syn- to late collisional intrusions materialized by emplacement of elongate NE-SW trending plutons and N-S trending stocks of magnetite-rich two-mica granite of syn- and late-collisional tectonic setting (Tetsopgang et al., 2006).

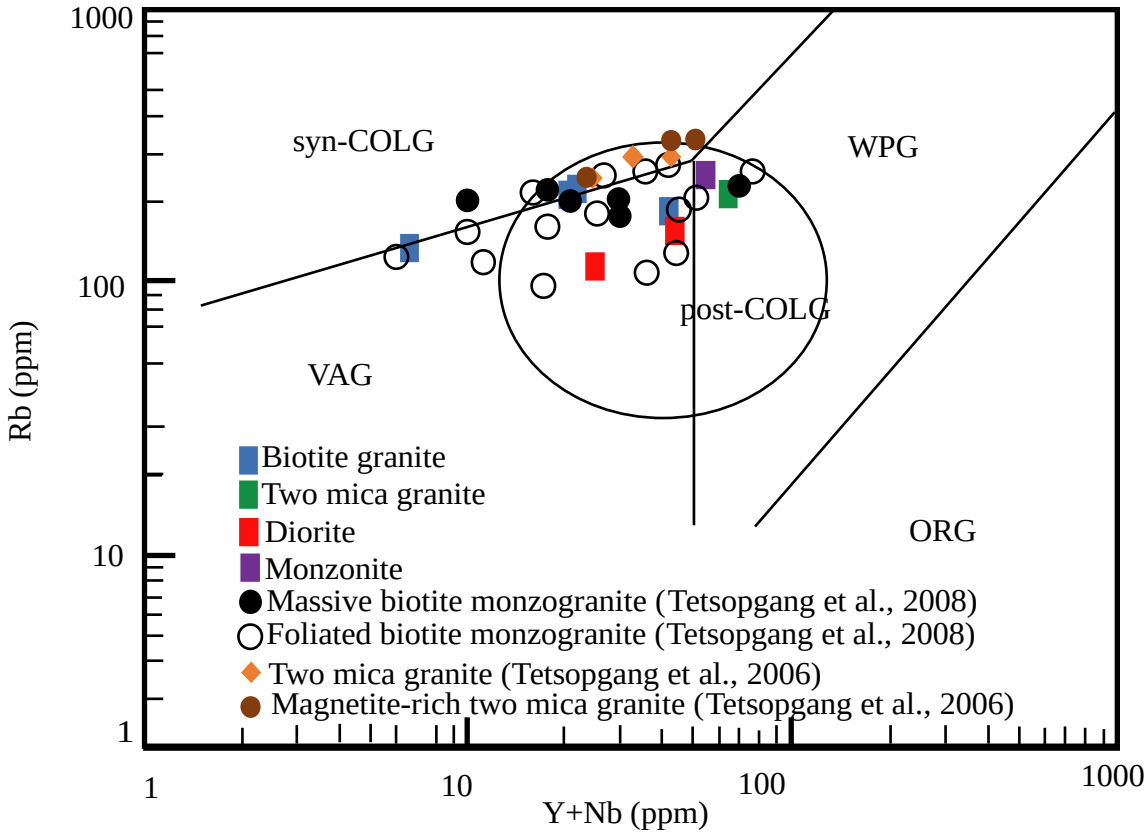

Figure 82: Tectonic discrimination diagrams of (a) Rb vs. (Y + Nb) (after Pearce et al., 1984), showing the geotectonic domains of Mayo Kila plutonic rocks: ORG-ocean ridge granite; VAG- volcanic arc granite; syn-COLG-syn-collision granite; post-COLG- post-collision granite; WPG- within-plate granite.

VI.3.5.3-Magma sources of Mayo Kila and Mbiame mafic volcanic rocks

According to the total Alkali silica diagram of Le Maitre et al. (2002), all the studied lavas show alkaline affinity and plot in the domains of basanite and foidite. Harker plots show negative correlation of silica with Fe_2O_3, MgO and CaO, suggesting a progressive fractional crystallization of mafic minerals such as olivine, clinopyroxenes and basic plagioclase. These rocks also show important concentrations in CaO (7.77 - 11.1 wt.%), indicating fractionation of calcium rich minerals (plagioclase and clinopyroxenes). On the other hand, positive correlation of Al_2O_3, K_2O and Na_2O suggests the crystallization of alkaline minerals.

Primary magmas are usually characterized by concentration of compatible elements such as Ni, Cr and Co with concentrations of (Ni: 300-400 ppm; Cr: 300-500 ppm; Co: 50-70 ppm; e.g., Frey et al., 1978; Jung and Masberg, 1998). In this study, the range of Ni, Cr and

Co (Ni: 4-354 ppm, Cr: 20-340 ppm and Co: 29-74 ppm) show lower to overlapping values, compared to those assumed for primary magmas, thus, indicating crystal fractionation with the removal of olivine + pyroxene ± spinel assemblage (Kamgang et al., 2013). The overlapping values of most of these compatible elements (Ni, Co and Cr) are observed mostly in the two foidite samples (MK14 and MK20), indicating that these lavas were not significantly fractionated from their primary magmas (Kamgang et al., 2013; Tchuimegnie et al., 2015; Dedzo et al., 2019) and their extensive fractionation took place in a higher level of the magma chambers. Thus, contamination by country rocks was not important and the composition was largely controlled by mantle processes (Jung and Masberg, 1998).

As demonstrated on the Sr versus Ba diagram (Fig. 83) of Franz et al. (1999), the principal differentiation mechanism of these lavas is fractional crystallization, marked principally by fractionation phases like ferro-titano oxide, olivine, clinopyroxene and plagioclases. The same trends are observed for other Mount Oku lavas from Wainama area (Wotchoko et al., 2017), Bafmeng area (Chenyi et al., 2017) and other parts of Mount Oku (Njilah et al., 2013).

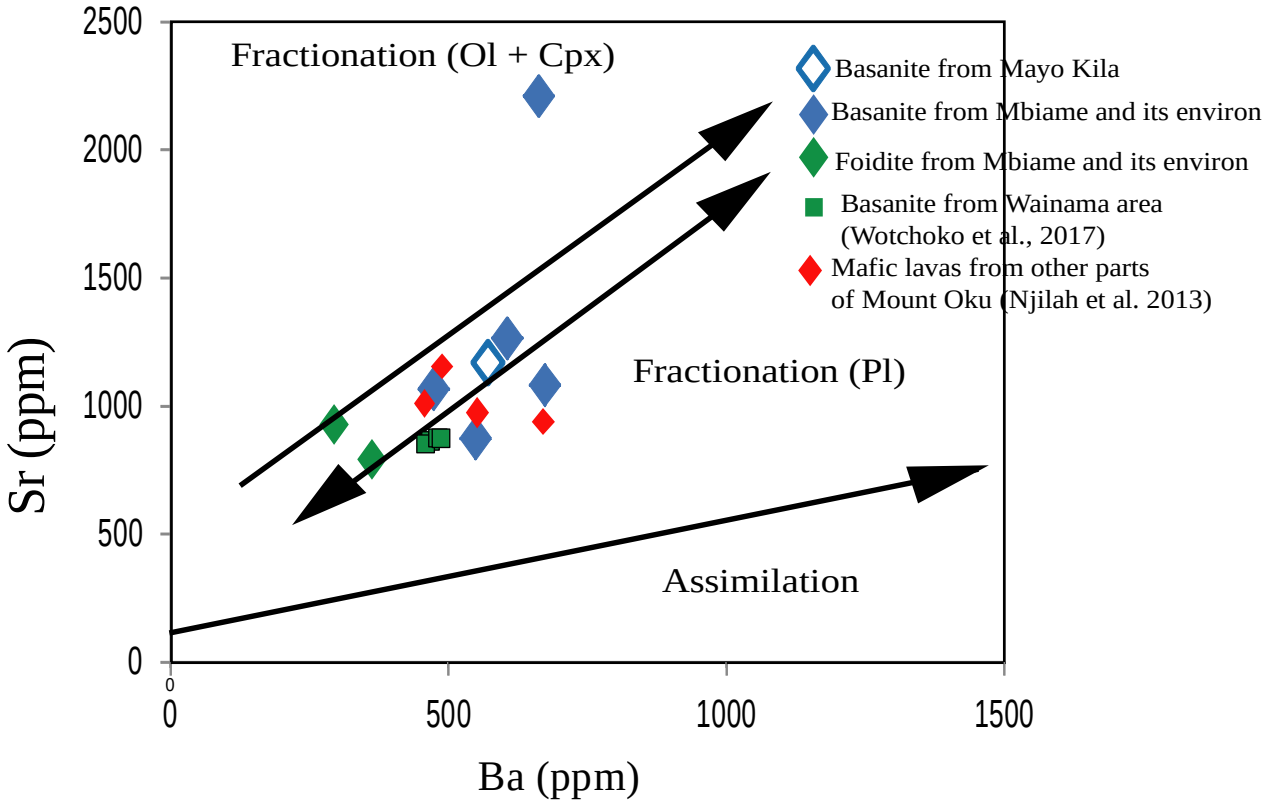

Figure 83: Sr versus Ba diagram for studied mafic rocks (after Franz et al., 1999).

The Zr/Nb versus Zr diagram (Figure 84) of Franz et al. (1999), indicates a mantle source of the studied mafic lavas, those of Wainama area (Wotchoko et al., 2017), and other parts of Mount Oku (Njilah et al., 2013). However, the occurrence of the basanite sample (MK07) in the space between the mantle source and assimilation domains could be due to contamination by partial assimilation of the granito-gneissic basement (Franz et al., 1999).

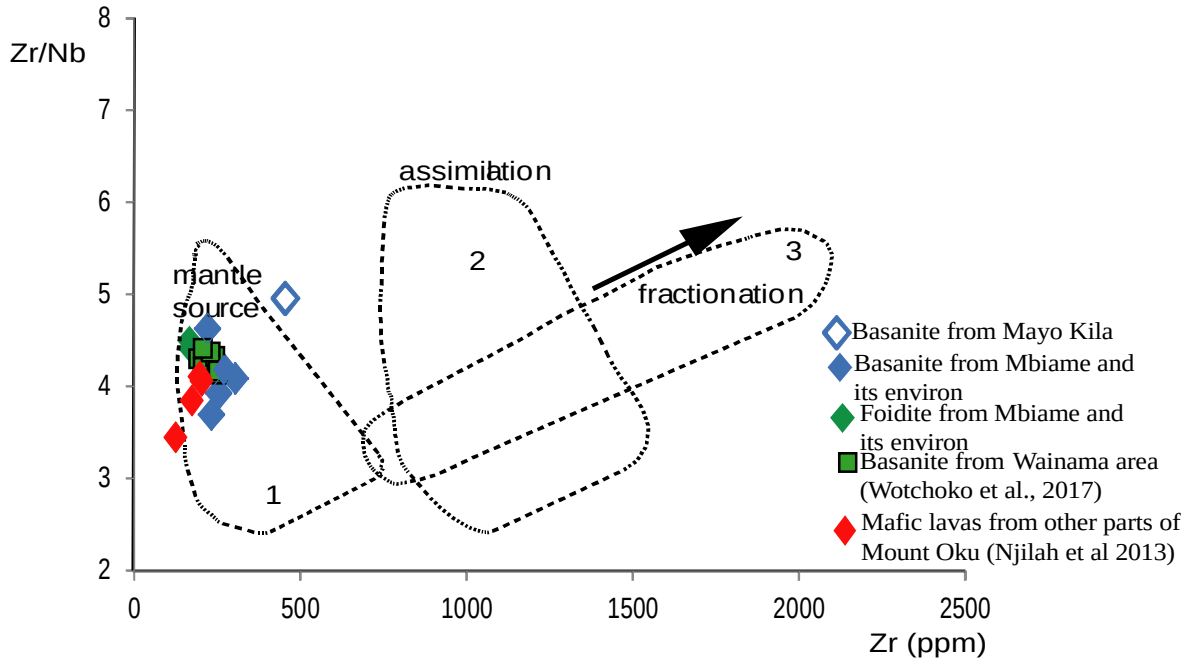

Figure 84: Zr/Nb versus Zr diagram indicating the mantle source of the studied mafic rocks. Dashed lines show fields of rocks of Meidob Hills, Sudan (after, Franz et al., 1999).

Garnet retention in magmas is often used to decipher their mantle sources, as garnet retention in these magmas is usually expressed by HREE depletion relative to LREE (Green et al., 1989). Mafic lavas of Mount Oku are characterized by an enrichment in LREE compared to HREE with high fractionation indexes $(La/Yb)_N$, with values from 11.11 to 19.54. This indicates the presence of garnet as residual phase in the source during partial melting (Kamgang et al., 2013). In addition, the high $(Tb/Yb)_N$ ratios (2.2 -2.9) of the studied lavas overlap with values considered to be characteristic of the presence of residual mantle source (Wang et al., 2002). These values are also consistent with those obtained for mantle sourced garnet magmas of some mafic lavas of the CL (Kamgang et al., 2013; Tchuimegnie et al., 2015) and similar to other mantle derived magmas of the CL sourced from the garnet stability field (Asaah et al., 2015; Chenyi et al., 2017; Wotchoko et al., 2017; Dedzo et al., 2019).

The Dy/Yb versus La/Yb diagram (Bogard and Wörner, 2003) (Figure 85) show the melting of garnet and spinel peridotite, based on the compatibility of Yb and incompatibility of La in garnet. Moreover, the different rate and fraction of La/Yb and Dy/Yb ratios during the melting stages plot in the garnet stability field (Wotchoko et al., 2017). In this study, the discrimination diagram between garnet and spinel peridotite melting indicates that the magmas of the study areas were formed from the partial melting of garnet peridotite with trends that fall within high degrees (9-13%).

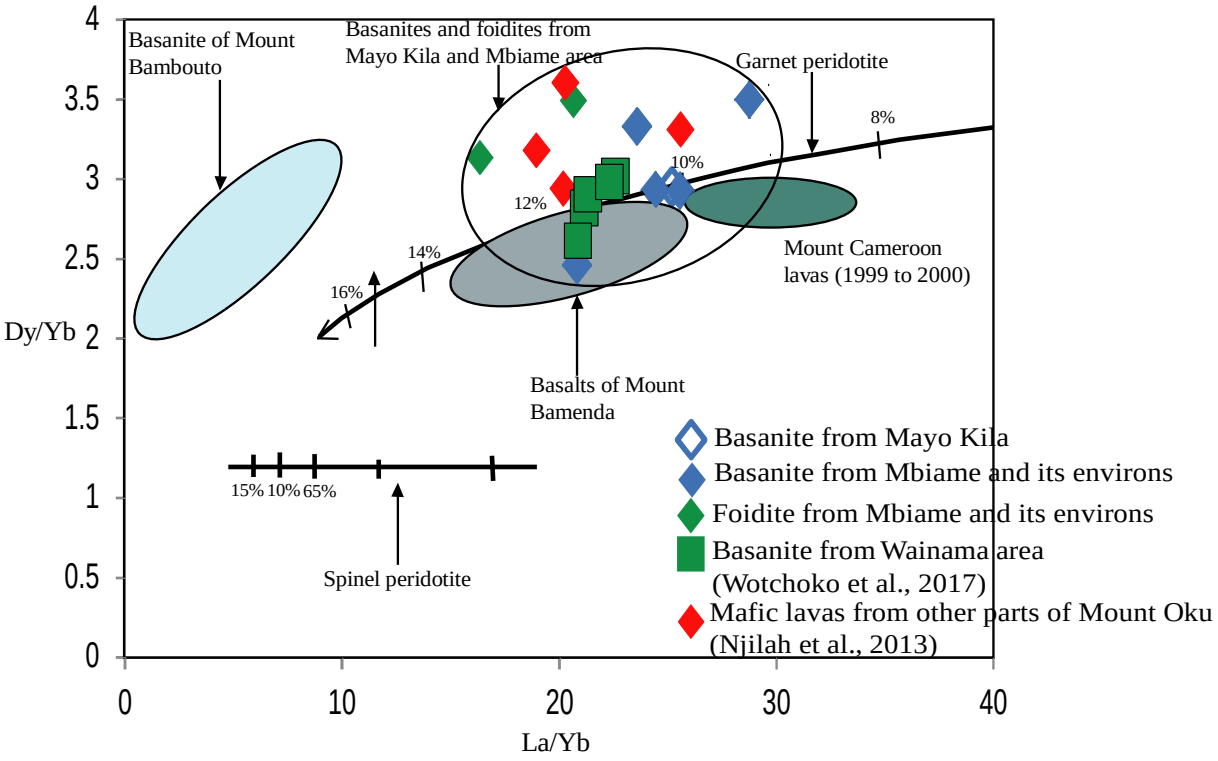

Figure 85: Dy/Yb versus La/Yb discrimination diagram (after Bogard and Wörner, 2003). Melt curves for garnet peridotite and spinel peridotite are from Bogard and Wörner (2003), Mount Bambouto from Nkouathio (2006) in (Wotchoko et al., 2017), Mount Bamenda from Kamgang et al. (2013) and Mount Cameroun from Suh et al. (2003).

REE spectra of studied lavas normalized with Chondrite values from McDonough and Sun (1995), all the lava samples are above those of N-MORB and E-MORB and strongly resemble that of OIB (Fig 86). These curves are similar to those observed in most mantle derived lavas of the CL (Kamgang et al., 2013; Tchuimegnie et al., 2015; Asaah et al., 2015; Chenyi et al., 2017; Wotchoko et al., 2017).

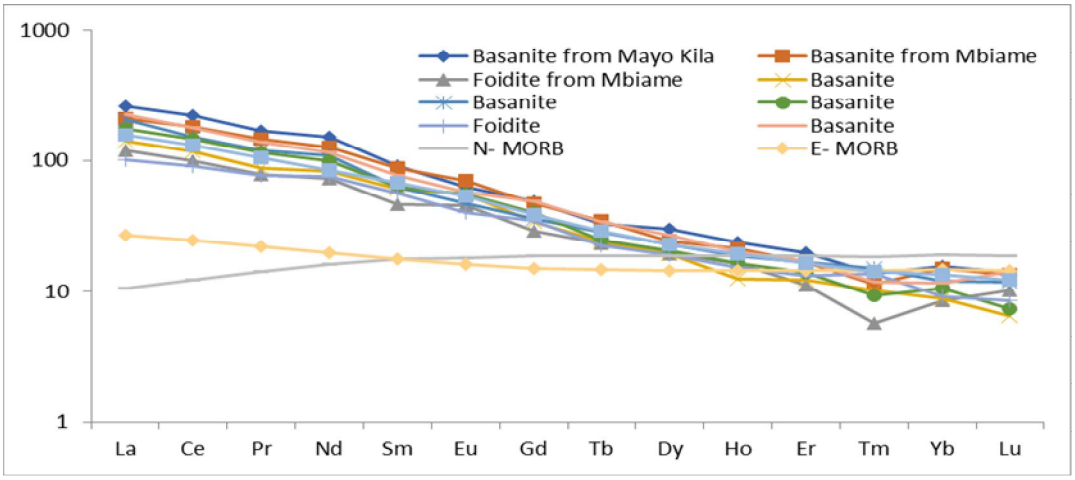

Figure 86: REE spectra of studied lavas normalized with Chondrite values from McDonough and Sun (1995), the values for OIB, N-MORB and E-MORB are from Sun and McDonough (1989). (OIB= Ocean Island Basalt, N-MORB= normalized-mid ocean ridge basalt, E-MORB= enriched-mid ocean ridge basalt.

VI.3.5.4- Geotectonic setting of Mayo Kila and Mbiame mafic volcanic rocks

The distribution of samples in the geotectonic discrimination diagram of Ta/Hf versus Th/Hf of Schandl and Gorton (2002) indicates that the rocks fall in the Within Plate Volcanic Zone (WPVZ) (Fig. 87) and on the Y/15-La/10-Nb/8 discrimination diagram of Cabanis and Lecolle (1989), the rocks fall in the domain of alkaline basalts from intracontinental rift (Fig 88).

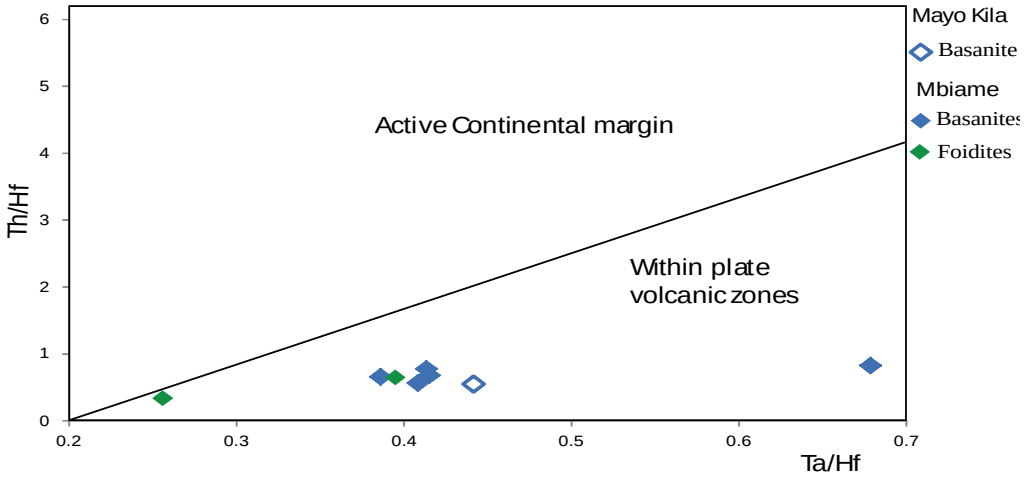

Figure 87: Ta/Hf versus Th/Hf discrimination diagram showing the geotectonic context of Mbiame and Mayo Kila lavas (after, Schandl and Gorton, 2002).

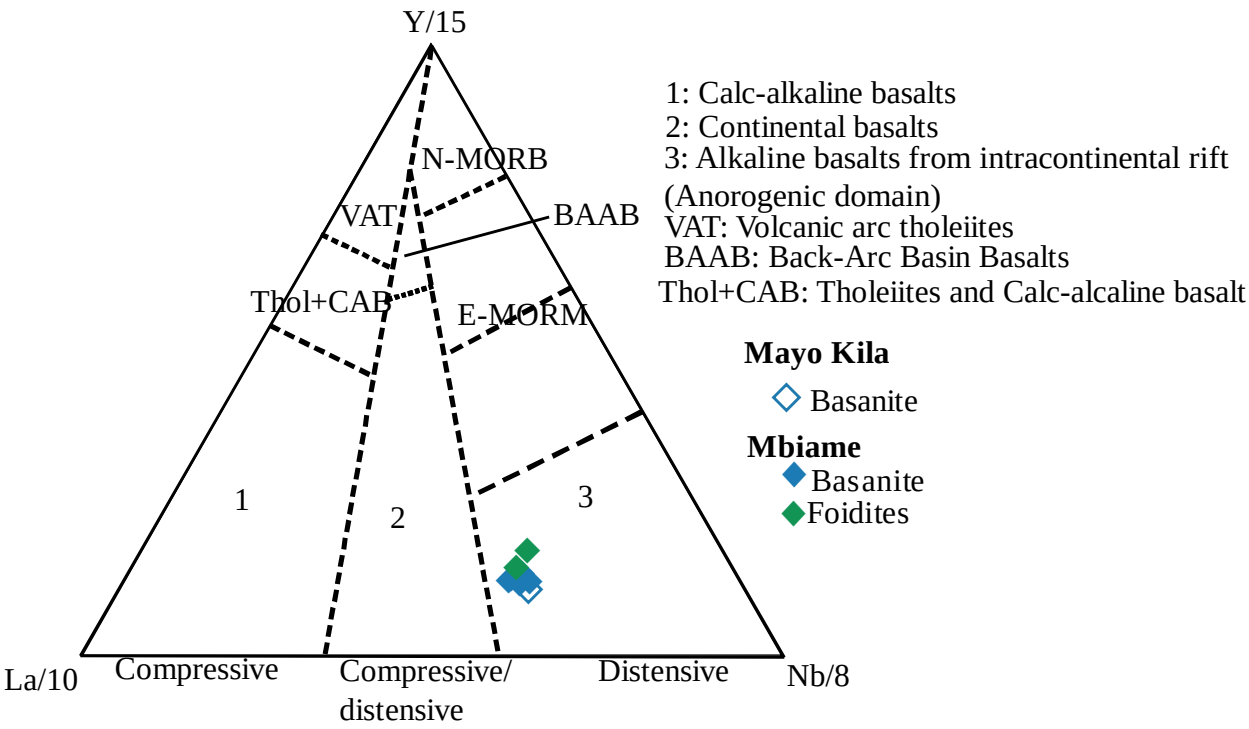

Figure 88: Y/15-La/10-Nb/8 discrimination diagram showing the domains of Mbiame and Mayo Kila lavas (after, Cabanis and Lecolle, 1989).

The identifation of the different lithologies and the establishment of their geotectonic settings have made it possible to identify two major environments within the study areas: a calc-alkaline to shoshonitic plutonic domain marked by syn- to post- collisional orogeny, and an alkaline intraplate volcanism. The plutonic environment is represented by the granite-gneissic basement made up of Pan-African granitoids (Njilah et al., 2007, 2013) with ages of about 530-510 Ma (Tetsopgang et al., 1999), 569 to 420 Ma (Tetsopgang et al., 2008). These lithologies are partially covered by Cenozoic volcanic rocks which represent the alkaline intraplate volcanism, characterized by alkaline mafic rocks like basalts, basanite, nephelinite and trachy-basalts (Njilah et al., 2007, 2013; Chenyi et al., 2017; Wotchoko et al., 2017). The petrography, mineralogy and chemistry of the studied rocks as well as the entire Cameroon Line are similar to those of alkaline intraplate series (Njilah et al., 2007, 2013; Kamgang et al., 2013; Wotchoko et al., 2017). Their trace and REE data are consistent with those of mantle sourced magmas, obtained within the garnet stability field similar to mantle generated OIB (Kamgang et al., 2013; Tchuimegnie et al., 2015; Asaah et al., 2015; Chenyi et al., 2017; Wotchoko et al., 2017; Dedzo et al., 2019) and show variable degree of crustal contamination and assimilation of sub-continental lithospheric mantle (SCLM) (Rankenburg et al., 2005). Their ages generally vary between Cenozoic to recent (Rankenburg et al., 2005).

The Central Cameroon Shear Zone corresponds to the SW extension of the Central African Shear Zone (Fairhead, 1988) which is outlined by a broad mylonite belt oriented N70^{o}E and extends from Cameroon to Sudan (Cornachia and Dars, 1983), and was dextrally activated during the Pan-African tectonic evolution (Ngako et al., 1991). The CL is oriented N30^{o}E and its continental sector is segmented by several N70^{o}E shear zones of Pan-African age. It has also been described as the unique example on Earth, of an active intraplate alkaline tectono-magmatic alignment (Deruelle et al., 2007). Structurally, it is believed to be a succession of echelon-form mega-tension gashes, resulting from reworking during Aptian-Albian times of the N70^{o}E shear zones at the beginning of the opening of the Central Atlantic Ocean (Deruelle et al., 2007). The reworking of these fracture zones could be related to the occurrence of hot lines in the asthenospheric mantle (Bonatti and Harrison, 1976), and a subsequent pathway for the ascension of magma to the earth surface.

The similarity in structure between the BT with the CL and the East African Rift System with its extension in South Africa (Figure 89), has been suggested a mechanism of episodic emplacement of alkaline magmas through the entire African continent. The alignment of magmatic complexes resulted from a complex interaction between hot spots (mantle plumes acting in succession) and lithospheric fractures (including Precambrian faults) during African plate motion (Njonfang et al., 2011).

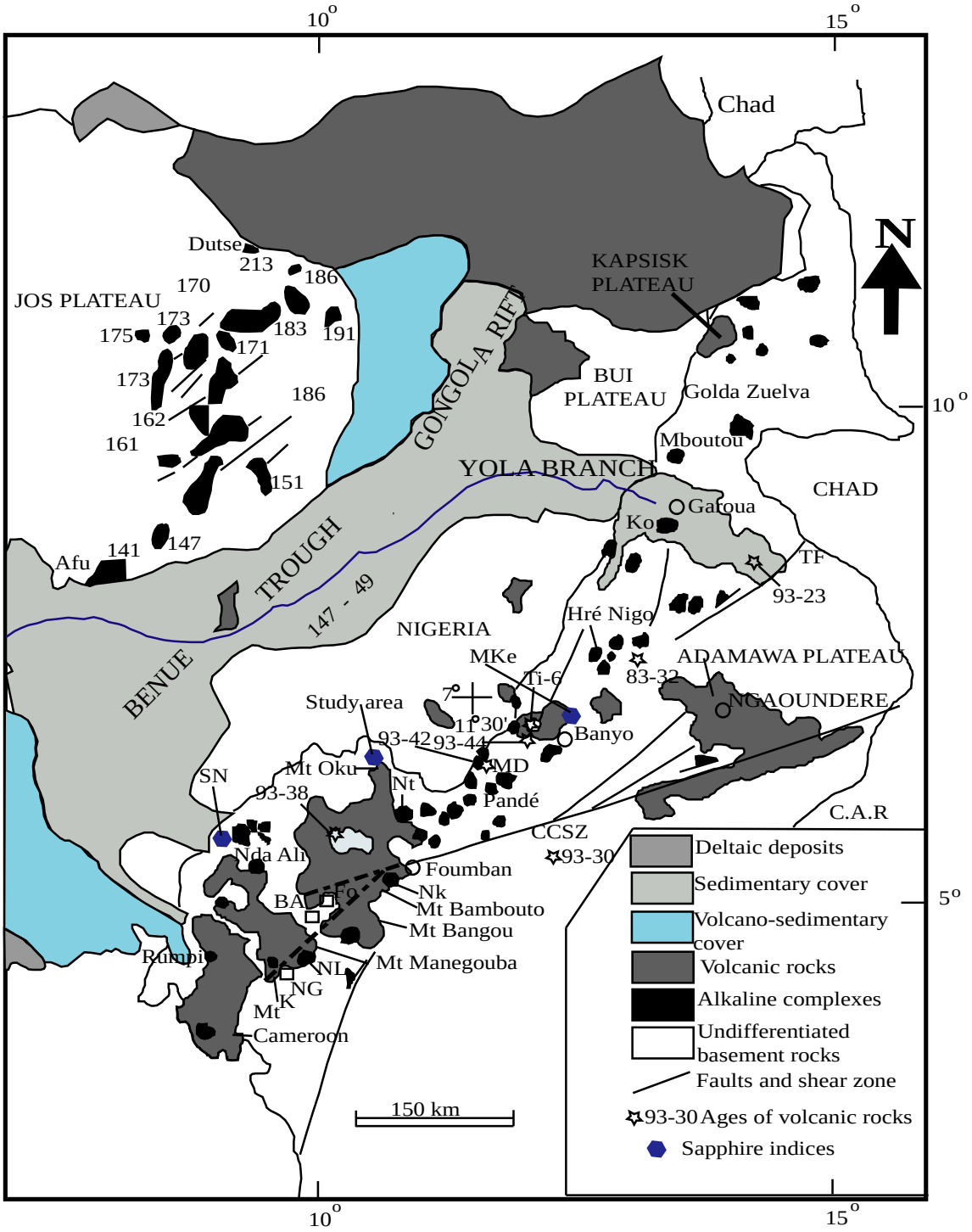

Figure 89: A compilation of Cameroon and Nigeria geological maps showing the location of the Benue Trough, the Cameroon Line and the Central Cameroonian Shear Zone (Ngako et al., 2006). The sapphire indices of Nsanaragati (SN) and Mayo Kewol (MKe) are from Kanouo et al. (2012a) and Boaka et al. (2010) respectively.

VI.4- Genetic models of corundum crystallisation

Although corundum from secondary magmatic deposits often occurs in alluvial or eluvial placer deposits, they are generally thought to be carried to the surface by ascending basaltic melts (Garnier et al., 2005; Uher et al., 2012; Baldwin et al., 2017). This observation is strongly supported by rare in-situ occurrences of corundum in alkaline mafic rocks (Livenson and Cook, 1994). Meanwhile, basaltic magmas are unable to crystallize corundum due to the facts that alkali basalts are undersaturated with respect to corundum, and alkali basalts are too rich in FeO and MgO for corundum to be stable (Baldwin and Ballhaus, 2018). The occurrence of these sapphires in basalts could implies that the generation of corundum has occured at a level higher than that of the magma generation probably within magma/metamorphic aluminous rich melts. The calculated ratios of some selected trace elements like Fe/Mg (43-3043), Fe/Ti (2-76), Ti/Mg (1-328), and Ga/Mg (0.4-363) as proposed by Peucat et al. (2007) show that the sapphires in this study are dominantly magmatic.

According to Limtrakun et al. (2001, 2003), corundum genesis involving magmatic processes can be divided into two groups as follows:

- plutonic crystallization at high pressures and;
- magma mixing at mid-crustal depths.

VI.4.1- Proposed genetic models of corundum crystallisation

From the two groups proposed by Limtrakun et al. (2001, 2003) for magmatic corundum genesis, four models are currently proposed that involve plutonic crystallization and a single model for magma mixing at mid-crustal depths.

VI.4.1.1- Plutonic crystallisation of corundum at high pressures

These models have been well illustrated by Irving (1986), Aspen et al. (1990), Sutherland et al. (1998) and Upton et al. (1999).

The Irving (1986) model: According to this model, the plutonic crystallization of corundum from highly evolved alkali melts formed by the fractional crystallization of intraplate magmas (e.g., nephelinites, basanites) at mantle and lower crustal pressures.

The Aspen et al. (1990) model: the plutonic crystallization of corundum from syenitic melts that are produced from high temperature crystallization of anhydrous trachytic magmas at deep crustal levels or in the upper mantle.

The Sutherland et al. (1998) model: Plutonic crystallization from primary alkali melts which are produced by low-moderate degrees of partial melting of amphibole-metasomatised mantle, or alternatively by partial melting of a lower crustal amphibole-bearing assemblage (e.g., amphibole pyroxenite). This model also suggests that corundum can crystallize directly from volatile-rich saturated felsic melts that are generated and fractionated largely under mantle/lower crust conditions.

The Upton et al. (1999) model: Plutonic crystallization from syenitic melts possibly originating from partial melting of metasomatised mantle, but with aluminous character, developed by loss of alkalis and carbonatitic fractions.

VI.4.1.2- Generation of corundum by magma mixing at mid-crustal levels

This model applied studies of mineral inclusions in corundum (Guo et al., 1996) and suggests that at least two melt components (carbonatitic and felsic melts) combine to produce the corundum. Based on the mineral inclusions observed in corundum, a single source is not adequate to explain all the inclusion data. At least two components must be involved in the source of corundum to explain the bimodal mineral inclusion suites, which indicate both an evolved alkaline-peralkaline felsic composition and another of carbonatitic affinity. This suggests that mixing and/or interaction between alkaline granite or syenitic pegmatite composition (magma or rock) and carbonatitic magma may be responsible for the formation of corundum. Such a hybridisation process is likely to be restricted to the intracontinental rifting regimes, where most carbonatitic magmas occur, and is also constrained to take place at mid-crustal level according to the inclusion mineral-based temperature estimate. During the interaction between granitic magmas and interfering carbonatitic magma, Al-rich phases crystallize in the hybrid zone. Then, subsequent basaltic magmatism rich in alkalis and volatiles, ascended rapidly to carry pre-formed corundums to the surface. This model has recently been used by Baldwin et al. (2017) to account for the formation of the in situ sapphire occurrences in the Siebengebirge Volcanic Field in Germany.

VI.4.2- Proposed genetic model for the Mayo Kila and Mbiame sapphires

The high Fe and Ga values coupled with low Mg and Cr values and calculated ratios of Fe/Mg (43-3043), Fe/Ti (2-76), Ti/Mg (1-328), and Ga/Mg (0.4-363) as proposed by Peucat et al. (2007) suggest a dominantly magmatic origin for the studied sapphires, possibly xenocrysts from alkaline basaltic magmas. Also, trace element concentrations (Hf, Th and U) and Th/U ratios obtained from zircon inclusions in the sapphires are compatible with quantified values in magmatic crystallized zircons. They are also consistent with those

crystallized in highly evolved melts, similar to syenitic or granitic compositions (Guo et al., 1996). The crystallisation of corundum from fractionated syenitic melt has been reported as one of the models proposed for the formation of sapphires in basaltic terrains (Irving, 1986; Aspen et al., 1990; Coenraads et al., 1990, 1995; Guo et al., 1996; Sutherland et al., 1998; and Upton et al., 1999). Based on the high Hf, U, and Th contents in the zircon inclusions found in the studied sapphires, the silicate parental melts are considered to be highly fractionated (Guo et al., 1996a). Also, the high Th and low Pb contents are consistent with those obtained from zircons from syenitic pegmatites (Belousova et al., 2002). This is based on the fact that trace element data from zircon inclusions in these sapphires point to a nepheline syenitic pegmatite melt (Belousova et al., 2002), crystallized at the crustal level as their U and Th content are far higher than values (U:<30 ppm and Th:<10 ppm) obtained in mantle zircons (Heaman et al.,1990; Belousova et al., 2002). From these data, it can be acknowledged that Mayo Kila sapphire xenocryst crystallized in a nepheline syenitic pegmatite melt, probably from the Ntumbaw syenite, in a crustal environment and was only channeled to the surface by the Cenozoic alkaline basalts from the Mount Oku volcanism, with magmas formed at mantle level (Njilah et al; 2007, 2013). The ascension of these magmas must have been favoured by the complex interaction between hot spots (mantle plumes acting in succession) and the existing lithospheric fractures and faults of the African plate motion (Deruelle et al., 2007; Njonfang et al., 2011; Asaah et al., 2015). This hypothesis is demonstrated by the parallel alignment of the CL and the central Cameroon Shear Zone of De Plaen et al. (2014), figure 90.

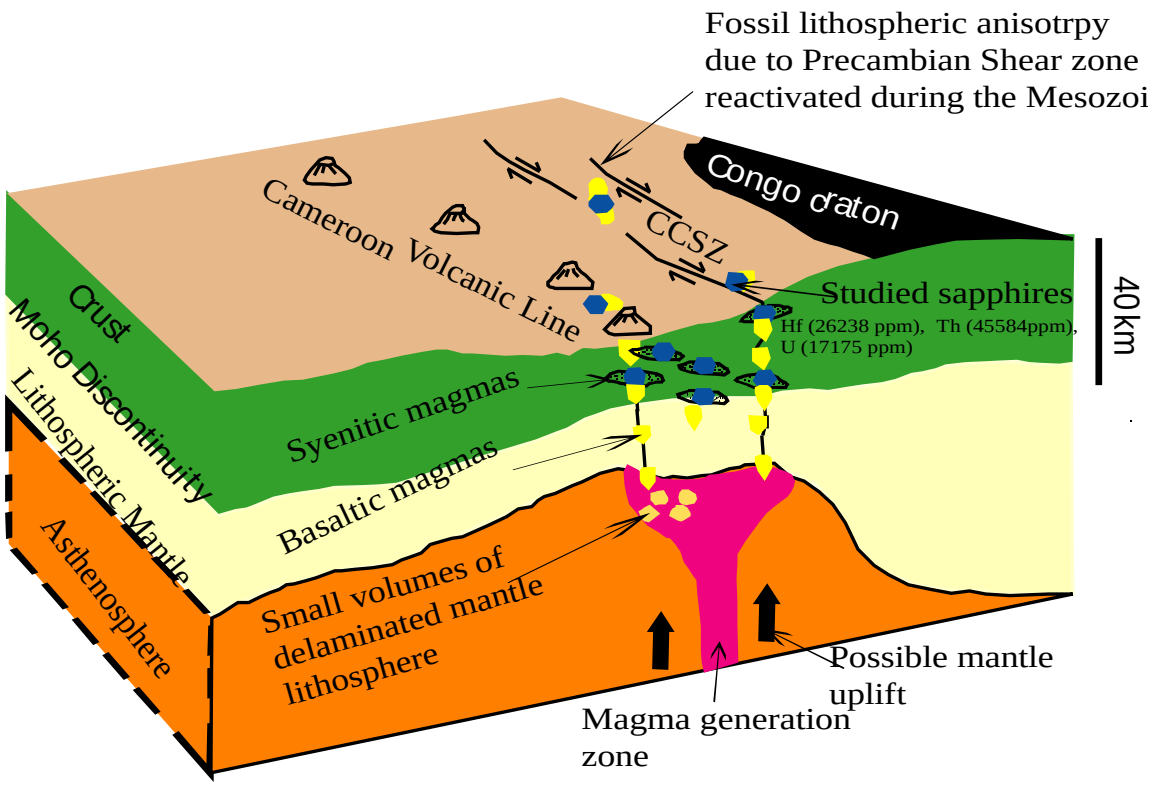

Figure 90: An illustration of the genetic model of the studied sapphires showing the formation of sapphire in syenitic magmas at crustal level, basaltic magmas and the basement structures. A summary conceptual cartoon for the Cameroon crust and mantle after De Plaen et al. (2014). CCSZ (Central Cameroon Shear Zone).

This hypothesis can be supported by the following geological and petrogenetic facts:

- the placer in Mayo kila occurs within a dominantly granitoid out crop area, with most samples being paraluminous and corundum normative;

- alumina could have been sourced from highly evolved melts of syenitic to syenogranitic compositions as supported by zircon trace element contents. The syenitic melts could have been produced from high temperature crystallization of anhydrous trachytic magmas at deep crustal levels as proposed by Aspen et al. (1990). This can be supported by the fact that Mount Oku area is made up of numerous trachyte outcrops with few syenitic plutons such as that of the Ntumbaw complex. This complex is made made up of peraluminous (A/CNK = 1.1 - 1.3) intermediate rocks, with some samples showing highly fractionated values of compatible elements (Ni (<10 - 15 ppm), Cr (12-72 ppm) and Co (10 - 43 ppm)). These values are indicative of a crustal origin.

- only zircon and rutile, typical of accessory granitoid were observed as mineral inclusions in the sapphire grains (Pakhomova et al., 2006); this is an indication that these sapphires crystallized in a felsic melt. Zircon and rutile also occur as accessory minerals in most intermediate rocks of the Ntumbaw complex.

- the lack of olivine, pyroxene and other minerals that are typical of basalts (Coenraads et al., 1990; Pakhomova et al., 2006) amongst the sapphire mineral inclusions is an indication that the sapphires did not crystallize in the mantle derived basaltic magmas;

- the alkali basalt samples from the study areas are not corundum-normative and could not concentrate sapphire;

- the sapphire megacrysts show corroded surfaces, suggesting disequilibrium with the carrier magma (Coenraads et al., 1990);

- The upstream location of the tumbaw synite could probably be the source of the Mbiame placer materials.

Conclusion

The combination of field data and literature review has been used to decipher sapphire mineralization in the study areas. Sedimentological studies show that the detritic materials are poorly to very poorly sorted. These are evidence that the sediments were deposited from high-energy currents from a short distance transport from a proximal source. The proximal nature of these source rocks is further confirmed by the presence of easily weathered minerals like pyroxene and amphibole. The sub angular to sub rounded nature of some of the sapphires has been attributed to mechanical abrasion of these grains during moderate distance transport in water. The irregular corrosion patterns show corundum-magma interaction, owing to disequilibrium with the carrier magma during its ascent to the surface. Data from trace element analysis show that sapphires dominantly crystallized in alkaline magmas with few grains pointing towards a metamorphic/metasomatic source. Dated zircon inclusions from these sapphires show very high concentrations in U and Th which signifies crystallization in a crustal environment and are consistence with those crystallized in highly evolved melts, similar to peralkaline syenitic or granitic compositions.

In Mayo Kila, petrographic and geochemical analyses show that the plutonic rocks are formed by partial melting from different protoliths in a syn- to post-collisional tectonic setting. The mafic volcanic rocks were formed in the garnet stability field and resemble the

mantle generated OIB. Their geochemical signatures also indicate their affinity to alkaline basalts from an intracontinental rift.

These analyses guided us towards the hypothesis that the sapphires of these areas are magmatic, with a parent rock of syenitic composition within the Ntumbaw complex, formed at crustal level and were transported to the surface by mantle basaltic magma through the numerous fractures that characterize the Cameroon line and the Central Cameroon Shear Zone.

GENERAL CONCLUSION AND PERSPECTIVES

This work is focused on the occurence of sapphire mineralization in Mayo Kila and Mbiame, with objective to establish a genetic model as well as to locate the primary source of these sapphires. Conclusion obtained from each chapter are briefly summarised below, followed by the perspectives proposed for the work.

Characteristics of Mayo Kila and Mbiame alluvial deposits

Mayo Kila and Mbiame alluvial deposits are made up of cobble to pebble size gravel and sand materials observed on river beds and banks in the study areas. The materials are poorly sorted. This poor sorting is attributed to the fact that the sediments were deposited from high-energy currents. It can also be attributed to a short distance transport from a proximal source.

Sapphire mineralization is mostly observed in the gravelly and coarse sand levels and is accompanied by other heavy minerals such as zircon, tourmaline, disthene, epidote, pyroxene, andalusite, garnet, chlorite, zoisite, biotite, sillimanite, hornblende, apatite, opaque minerals and other unidentified minerals. The sapphires are mainly blue in colour with no colourless, pure green or yellow grains. The grains are mostly euhedral but few anhedral grains do occur. They are generally angular, sub-angular to sub-rounded, typifying short distance transportation from their source area. Some of the sapphires show irregular corrosion patterns, probably owing to disequilibrium between the sapphire grains and the carrier magma during its ascent to the surface. The primary relict structure of the sapphires is shown by elongated and rhombohedral sapphire grains, pseudo-hexagonal to pinacoidal basal section of a platy sapphire grain.

Analysed sapphire grains from Mayo Kila are characterized by trace element such as iron (2,208 - 14,473 ppm), titaniun (82 – 1,783 ppm), galium (77- 512 ppm), magnesium (up to 264.9 ppm), chromium (up to 168 ppm) and vanadium (up to 82 ppm). Elements such as tin, nobium, tantalium and nickel are minor components in the studied sapphires.

Solid inclusions in these sapphires are limited to rutile and zircon. The zircon inclusions are characterized by hafnium (13,354 - 26,238 ppm), thurium (4,018 - 45,584 ppm) and uranium (7,825 - 17,175 ppm), and Th/U ratio between 0.39 and 2.65. The dated zircon inclusions give a Cenozoic age (mean of 30.78 ± 0.28 Ma) to the Mayo Kila sapphires.

Characteristics of the surrounding rocks

In the study areas, two main lithologic units were identified. In Mayo Kila, magmatic (volcanic and plutonic) units were identified and sampled while in Mbiame and other areas of Mount Oku, only mafic volcanic rocks were sampled.

In Mayo Kila, petrographic and geochemical studies show that the rock samples collected are mainly of plutonic and volcanic units. The plutonic unit is made up of biotite granites, two mica granites, diorites and monzonite, while the volcanic unit is made up of basanites. The plutonic present a high K-calc-alkaline to shoshonitic affinity with the dominance of alkaline-calc to alkaline series. They show contrasts in their origins, the felsic rocks (biotite granite and two-mica granite) are peraluminous and exhibit characteristics of magmas formed by partial melting at a crustal level, while the intermediate samples (monzonite and diorite) are mostly metaluminous and I-type, and show features of mantle-derived mafic magmas. Normative corundum occurs in the biotite granite and two mica granites and is absent in the diorites and monzonite. All samples are formed by partial melting from different protoliths. The two mica granites have a metapelitic source, two biotite granites from a metagreywacke source while the diorites and monzonite are from a metatonalitic to meta amphibolitic source. These rocks are formed in a syn- to post-collisional tectonic setting. The mafic volcanic rock on its part expresses an alkaline affinity with a mantle source similar, to alkaline basalts from an intracontinental rift.

In Mbiame and other areas of Mount Oku, the mafic volcanic rocks show alkaline affinity and were identified as basanite and foidites. Most of the rocks fall in the Na_2O-series and are nepheline, leucite and diopside normative. The magmas of these areas portray a residual mantle source and were formed from the partial melting of garnet peridotite with trends that fall within high degrees (9-13%). Their geochemical signatures also indicate their affinity to alkaline basalts from an intracontinental rift.

Evaluation of the primary source of sapphire

In this study, no sapphire grain was found in either of the host rocks or their associated clastic fragments. Thus, the present-day location of the primary source points to the syenitic rocks from the Ntumbaw anorogenic complex with peraluminous character and crustal origin. Nevertheless, data from this study and literature review has been used to point out some genetic implications of these sapphires as follow:

- the sapphire grains are predominantly blue, and are similar to sapphires derived from basaltic terrains with desilicated pegmatitic and syenitic origins;

- the sapphires have corroded surfaces, which is an indication that the sapphires occurred as xenocryts and were not in equilibrium with their host magma. This is a major characteristic of sapphires sourced from magmatic rocks;

- the zircon and rutile solid inclusions are typical of accessory granitoid greisen and is an indication that these sapphires crystallized in a highly evolved melt. Also, the Ti-Nb-Ta-enrichment in some grains is an indication that the melt was rich in incompatible elements;

- Fe versus Ga/Mg discrimination diagram plots the studied sapphires in the same domain with basalt hosted sapphires from Asia and other parts of the world;

- from Fe/M versus Cr/Ga and Fe - Ti*10 - Mg*100 discrimination diagrams, sapphires are mostly similar to corundum from weathered alkali basalts, Al-rich diorite and syenitic gneiss;

- zircon inclusions in sapphires have a U-Pb age of 30.78 ± 0.28 Ma. These zircon inclusions are within tertiary ages proposed for the Ntumbaw anorogenic complex, and most likely brought to surface by the Mount Oku mafic alkaline lavas with an age range of 31 - 22 Ma.

Evaluation of sapphire genetic models

Proposing a genetic model for corundum is often difficult, but from literature review, there is a general consensus that corundum genesis must involve at least two main stages. An early stage where corundum is formed as a magmatic or metamorphic phase at upper mantle or lower crustal depths and a second stage where corundum is incorporated and transported to the surface via a magmatic event.

The presence of magmatic corrosion on the Mayo Kila sapphires suggests they are not in equilibrium with the host magma. This indicates that they are xenocrysts in the magmas.

Trace element concentrations and calculated ratios for some of the selected elements show Fe/Mg, Fe/Ti, Ti/Mg, and Ga/Mg, a dominantly corundum crystallization in alkaline magma and thus supports both models.

Their U and Th content are far higher than values (U:<30 ppm and Th:<10 ppm) obtained in mantle zircons. This indicates that they probably crystallized at a crustal level. Also, the high Th and low Pb contents are consistent with those obtained in zircons from syenitic pegmatites.

Perspectives

With the aim to provide complete information on the origin of sapphire mineralization in these areas, further analyses are needed in order to confirm and complete the results obtained from this study.

1- Mineral and fluid inclusions analysis of both Mayo Kila and Mbiame sapphires. Fluid, melt and mineral inclusions have potential to preserve valuable information about the chemical environment, physical conditions and the geological processes that affect the host mineral at the time of its deposition. Primary mineral inclusions can provide information on the melt composition of the parental magma of the host mineral, as they are potential samples of the parental magma. While fluid inclusion studies on its part can provide critical information on the composition of the melt that crystallized the host minerals, pressure, and thus the depth of mineral crystallization.

2- Oxyen isotope analysis of both Mayo Kila and Mbiame sapphires. Oxygen isotopes are useful to determine the origin of corundum because of the distinct O-isotope difference between mantle and crustal rocks. This will confirm if the Mayo Kila and Mount Oku sapphires crystallized in the mantle or crustal environment.

3- Detailed prospection of placer sapphires in Mbiame and other areas of Mount Oku which seem to have higher sapphire concentration.

REFERENCES

Abdulrahman, A. A. 2017. Origin and economic importance of corundum. BSc. thesis, Kafrelsheikh University, Egypt, p. 107.

Ajonina, H.N. 2016. Evolution of Cretaceous sediments in the Mamfe Basin, SW Cameroon: Depositional environments, Palynostratigraphy, and Paleogeography. PhD. Thesis, University of Hamberg, Germany, p. 202.

Aka, F.T., Kusakabe, M.K., Nagao, K., Tanyileke, G. 2001. Noble gas isotopic compositions and water/gas chemistry of soda springs from the islands of Bioko, SaõTomé and Annobon, along the Cameroon Line, West Africa. Applied Geochemistry, 16, 323–338.

Aka, F.T., Nagao, K., Kusakabe, M., Sumino, H., Tanyileke, G., Ateba, B., Hell, J. 2004. Symmetrical helium isotope distribution on the Cameroon Line, West Africa. Chemical Geology, 203, 205–223.

Altherr, R., Holl, A., Hegner, E., Langer, C., Kreuzer, H. 2000. High-potassium, calc-alkaline I-type plutonism in the European Variscides: northern Vosges (France) and northern Schwarzwald (Germany). Lithos, 50, 51–73.

Asaah, A. E. N., Yokoyama, T., Aka, F. T., Usui, T., Wirmvem, J. M., Chako Tchamabe, B., Ohba, T., Tanyileke, G. & Hell, J. V. 2014. A comparative review of petrogenetic processes beneath the Cameroon Line: Geochemical constraints. Geoscience Frontiers, doi:10.1016/j.gsf.2014.04.012.

Asaah, A. N. E., Yokoyama, T., Aka, F. T., Usui, T., Kuritani, T., Wirmvem, M. J., Iwamori, H., Fozing, E. M., Tamen, J., Mofor, G. Z., Ohba, T., Tanyileke G. & Hell, J. V. 2015. Geochemistry of lavas from maar–bearing volcanoes in the Oku Volcanic Group of the Cameroon Line. Chemical Geology, 406, 55–69.

Aspen, P., Upton, B.G.J., Dicken, A.P. 1990. Anorthoclase, sanidine and associated megacrysts in Scottish alkali basalts: high pressure syenitic debris from upper mantle sources? European Journal of Mineralogy, 2, 503-517.

Ateba, B., Dorbath, C., Dorbath, L., Ntepe, N., Frogneux, M., Aka, F.T., Hell, J.V., Delmond, J.C., Manguelle, D. 2009. Eruptive and earthquake activities related to the 2000 eruption of Mount Cameroon volcano (West Africa). Journal of Volcanology and Geothermal Research, 179, 206–216.

Aydogan, S.M and Moazzen, M. 2012. Origin and metamorphism of corundum-rich metabauxites at Mt Ismail in the southern Menderes Massif, SW Turkey. Resource Geology, 62, 243-262.

Baker, J., Peate, D., Waight, T., Meyzen, C. 2004. Pb isotopic analysis of standards and samples using a Pb-207-Pb-204 double spike and thallium to correct for mass bias with a double-focusing MC-ICP-MS. Chemical Geology, 211, 275-303.

Baldwine, L.C. 2016. Petrogenesis of basalt-hosted sapphires from the Siebengebirge Volcanic Field (SVF) In Western Germany. Ph.D thesis, Bonn University Germany. p. 201.

Baldwin, L. C., Tomaschek, F., Ballhaus, C., Gerdes, A., Fonseca, R. O. C., Wirth, R., Geisler, T., Nagel, T. 2017. Petrogenesis of alkaline basalt-hosted sapphire megacrysts. Petrological and geochemical investigations of in situ sapphire occurrences from the Siebengebirge Volcanic Field, Germany. Contributions in Mineralogy and Petrology, 172, 43, doi:10.1007/s00410-017-1362-0.

Baldwin, L. C and Ballhaus, C. 2018. Experimental investigation of the reaction between corundum xenocrysts and alkaline basaltic host magma: Constraints on magma residence times of basalt-hosted sapphires. Lithos, 302–303, 447–454.

Barfod. D.N and Fitton, J.G. 2014. Pleistocene volcanism on São Tomé, Gulf of Guinea, West Africa. Quaternary Geochronology, 21, 77-89.

Belousova, E.A., Griffin, W.L., Fisher, N.I. 2002. Igneous zircon: trace element composition as an indicator of source rock type. Contributions in Mineralogy Petrology, 143, 602–622.

Black, L.P and Gulson, B.L. 1978. The age of the Mud Tank carbonatite, Strangways Range, Northern Territory. BMR Journal of Australian Geology and Geophysics 3, 227–232.

Black, L. P., Kamos, L., Allen, C.M., Aleinikoff, J.N., Davis, D.W., Korsch, R.J., Foudoulis, C. 2003. TEMORA 1: a new zircon standard for Phanerozoic U–Pb geochronology. Chemical Geology, 200, 155– 170.

Black, L.P., Kamo, S.L., Allen, C.M., Davis, D.W., Aleninikoff, J.N., Valley, J.W., Mundil, R., Campbell, I.H., Korsch, R.J., Williams, I.S., Foudoulis, C. 2004. Improved $^{206}Pb/^{238}U$ microprobe geochronology by the monitoring of a trace-element related matrix effect; SHRIMP, ID-TIMS, ELA-ICP-MS, and oxygen isotope documentation for a series of zircon standards. Chemical Geology, 205, 115-140.

Blott, S. J and Pye K. 2001. Gradistat: A Grain Size Distribution and Statistics Package for the Analysis of Unconsolidated Sediments. Earth Surface Processes and Landforms, 26, 1237–1248.

Boaka, L. 0M., Yongue, F.R., Ndjigui, D.P. 2010. The alluvial sapphire profiles of Mayo Kewol placer in Adamawa region (North-Cameroon): granulometry and mineralogical features. Journal of African Earth Sciences, 56, 121–126.

Boaka, L. M., Yongue, F.R., Giuliani, G. 2011. Mineralogical features and geological origin of the sapphires from Mayo Kewol paleoplacers in Adamawa Region North Cameroon). Advances in Material Science Research, 2, 125-142.

Boaka, L. M. 2018. Genèse, contexte géotectonique et évolution supergène de la minéralisation de saphir du secteur de Marma (Région de l'Adamaoua-Cameroun). Thèse de Doctorat, Université de Yaoundé, p. 185.

Bogard, P.J.F and Wörner, G. 2003. Petrogenesis of basanitic to tholeiitic volcanic rocks from the Miocene Vogelsberg, Central Germany. Journal of Petrology, 44, 569-602.

Bonatti, E and Harrison, C.G.A. 1976. Hot lines in the Earth's mantle, Nature, 263, 402–404.

Bottrill, R. S. (1996). Corundum and sapphire in Tasmania. Tasmanian Geological Survey, Record 1996/05.

Bouyo Houketchang, M., Toteu, S.F., Deloule, E., Penaye, J., Van Schmus, W.R. 2009. U–Pb and Sm–Nd dating of high-pressure granulites from Tcholliré and Banyo regions: evidence for a Pan-African granulite facies metamorphism in northcentral Cameroon. Journal of African Earth Sciences, 54, 144–154.

Burke, K. 2001. Origin of the Cameroon Line of volcano-capped swells. The Journal of Geology, 109, 349-362.

Canabis, B and Lecolle, M. 1989. Le diagramme La/10-Y/15-Nb/8: un outil pour la discrimination des series volcanique et la mise en évidence des processus de melange et/ou de contamination crustale. Compte Rendude l'Academie des Sciences, Series II, 309, 2023-2029.

Chappell, B. W and White, A. J. R. 1992. I- and S-type granites in the Lachlan Fold Belt. Transactions of the Royal Society of Edinburgh: Earth Sciences, 83, 1-26.

Chappell, B.W. 1999. Aluminium saturation in I- and S-type granites and the characterization of fractionated haplogranites. Lithos, 46, 535–551.

Chappell, B.W., White, A.J.R. 2001. Two contrasting granite types: 25 years later. Australian Journal of Earth Sciences, 48, 489–499.

Chenyi, M. L.V., Nkouathio, D. G., Wotchoko, P., Kouankap Nono, G.D., Zénon, I., Guedjeo, C.S., Seuwui, D. T. 2017. Volcanology and geochemical study of the volcanic rocks of the Bafmeng area (Mount Oku, Cameroon Line). International Journal of Biological and Chemical Sciences, 11, 841-864.

Coenraads, R.R., Sutherland, F.L., Kinny, P.D. 1990. The origin of sapphire: U-Pb dating of zircon inclusions sheds new light. Mineralogical Magazine, 54, 113-122.

Compton, R.R. 2016. Geology in the field. Published by Earthspun Books 2016 1b Achilles Ways, Pinelands 7405, Cap Town, South Africa.

Cornachia, M and Dars, R. 1983. Un trait structural majeur du continent africain: les linéaments centrafricains du Cameroun au golfe d'Aden. Bulletin de la Société Géologique de France, 25, 101–109.

Cornen, R and Maury, R. C. 1980. Petrology of the volcanic island of Annobon, Gulf of Guinea. Marine Geology, 36, 253-67.

Cox, K.G., Bell, J.D., Pankhurst, R.J. 1979. The interpretation of igneous rocks (1st edition): Springer Netherlands, p. 450.

De Plaen, R.S.M., Bastow, I. D., Chambers, E. L., Keir, D.R. Gallacher, J., Keane, J. 2014. The development of magmatism along the Cameroon Line: Evidence from seismicity and seismic anisotropy. Journal of Geophysical Research: Solid Earth, 119, 5, 4233-4252.

Dedzo, M.G., Asaah, A. N. E., Eric Martial Fozing, E. M., Tchamabé, B.C., Zangmo, G.T., Dagwai, N., Seuwui, D.T., Kamgang, P., Festus Tongwa Aka, F.T., Ohba, T. 2019. Petrology and geochemistry of lavas from Gawar, Minawao and Zamay volcanoes of the northern segment of the Cameroon Line (Central Africa): constraints on mantle source and geochemical evolution. Journal of African Earth Sciences, 153, 31-41.

Delaunay, A. 2004. Détermination d'un gradient de température de formation des Saphirs du Cachemire. Maîtrise de Sciences de la Terre et de l'Univers. Université de Nantes, France, p. 32.

Déruelle, B., N'ni, J., Kambou, R. 1987. Mount Cameroon: an active volcano of the Cameroon Line. Journal of African Earth Sciences, 6, 197–214.

Deruelle, B., Moreau, C., Nkoumbou, C., Kambou, R., Lissom, J., Njonfang, E., Ghogumu, R. T., Nono, A. 1991. The Cameroon Line: a review. **In Kampunzu, A. B., and Lubala, R. T., eds**. Magmatism in extension structure settings: the Phanerozoic. African Plate. Berlin, Springer, 275-327.

Déruelle, B., Ngounouno, I., Demiffe, D. 2007. The 'Cameroon Hot Line' (CHL): A unique example of active alkaline intraplate structure in both ocean and continental lithospheres. C.R. Geoscience, 339, 589-600.

Dissanayake, C.B., Chandrajith, R., Tobschall, H.J. 2000. The geology, mineralogy and rare element geochemistry of the gem deposits of sri lanka. Bulletin of the Geological Society of Finland, 72, Parts 1–2, 5–20. Dissertation Johannes Gutenberg-Universität Mainz.

Dumort, J.C. 1968. Carte géologique de reconnaissance et note explicative sur la feuille Douala-Ouest (1 : 500000). République Fédérale du Cameroun, Direction des Mines et de la Géologie du Cameroun, p. 69.

Emmett, J.L., Scarratt, K., McClure, S.F., Moses, T., Douthit, T.R., Hughes, R., Novak, S., Shigley, J.E., Wang, W., Bordelon, O., Kane, R.E. 2003. Beryllium diffusion of ruby and sapphire. Gems and Gemology, 39, 84–135.

Eyong, J. T., Ngueutchoua, G., Bessong, M., Hell, V. J., Bokanda, E. E., Wignall, Paul., Best. 2019. Sedimentologic and palaeoenvironmental evolution of the Mamfe Cretaceous Basin (SW Cameroon): Evidence from lithofacies analysis, tectonics and evaporite minerals suite. Journal of African Earth Sciences, 149, 19–41.

Fairhead, J. 1988. Mesozoic plate tectonic reconstructions of the Central South Atlantic Ocean: The role of the West and Central African rift system, Tectonophysics, 155, 181–191.

Fanka, A. and Sutthirat, C. 2018. Petrochemistry, Mineral Chemistry, and Pressure-Temperature Model of Corundum-Bearing Amphibolite from Montepuez, Mozambique. Arabian Journal for Science and Engineering, 43, 3751–3767.

Fitton, J.G and Hughes, D.J. 1977. Petrochemistry of volcanic rocks of the island of Principe, Gulf of Guinea. Contributions to Mineralogy and Petrology, 64, 247-272.

Fitton, J.G., 1980. The Benue trough and Cameroon line – a migrating rift system in West Africa. Earth Planet and Sciences. Letters, 51, 132–138.

Fitton, J.G and Dunlop, H.M. 1985. The Cameroon line, West Africa, and its bearing on the origin of oceanic and continental alkali basalt. Earth and Planetary Science Letters, 72, 23-38.

Fléchet, G. 2007. Understanding the origin of rubies and sapphires to improve prospecting strategies. Actualité Scientifique. Sheet number 278.

Forestier, F and Lasnier, B. 1969. Découverte de niveaux d'amphibolite à pargasite, anorthite, corindon et sapphirine dans les schistes cristallins de la vallée du Haut Allier Existence du faciès granulite dans le Massif Central Francais. Contributions to Mineralogy and Petrology, 23, 194–235

Fozing, E. M., Njanko T., Kwékam M., Séta N., Yakeu Sandjo A. F., Njonfang E. 2013. Sub magmatic and solid-state deformations during the emplacement of the Misajé Pan-African Pluton (Northwestern Cameroon): constraints from field observations, microstructures and anisotropy of magnetic susceptibility. International Research Journal of Geology and Mining, 3, 40-56.

Fozing, E. M., Kwékam, M., Njanko, Th., Njonfang, E., Séta, Naba., Yakeu, S.A.F., Sawadogo, S. 2014. Structural evolution of the Pan-African Misajé pluton (Northwestern Cameroon). Syllabus Review, Science. Series, 5, 12 – 26.

Franz, G., Steiner, G., Volker, F., Pudlo, D., hammerschmidt, K. 1999. Plume related alkaline magmatism in Central Africa- the Meidob hills (W Sudan). Chemical Geology, 157, 27-47.

Frey, F.A., Green, D.H., Roy, S.D. 1978. Integrated models of basalt petrogenesis: a study of quartz tholeiites to olivine melilitites from South Eastern Australia utilizing geochemical and experimental petrological data. Journal of Petrology, 19, 463-513.

Frost, B.R., Barnes, C.G., Collins, W.J., Arculus, R.J., Ellis, D.J., Frost, C.D. 2001. A geochemical classification of granitic rocks. Journal of Petrology, 42, 2033–2048.

Fu, J., Liu, S., Cawood, P.A., Wang, M., Hu, F., Sun, G., Gao, L., Hu, Y. 2018. Neoarchean magmatic arc in the western Liaoning Province, northern North China Craton: geochemical and isotopic constraints from sanukitoids and associated granitoids. Lithos, 322, 296–311.

Gaillou, E. 2003. Les saphirs du Massif Central : etude mineralogique des saphirs du Sioulot, du Mont Coupet et du Menoyre. Determination de leur origin. Diplôme de DEA, Universite Blaise Pascal, Clermont-Ferrand, France. p. 45.

Garnier, V., Giuliani, G., Maluski, H., Deloule, E., Phan Trong, T., Pham Van, L., Hoang Quang, V. 2005. Age and significance of ruby-bearing marble from the Red River shear zone, Northern Vietnam. Canadian Mineralogist, 43, 1315-1329.

Garnier, V., Giuliani, G., Ohnenstetter, D., Anthony, E. F., Dubessy, J., Banks D., Hoàng Q. V., Thérèse. L, Maluski, H., Pêcher A., Bakhsh K. A., Long P.V., Trinh P. T., Schwarz, D. 2008. Marble-hosted ruby deposits from Central and Southeast Asia: Towards a new genetic model. Ore Geology Reviews, 34, 169–191.

Garnier, V., Giuliani, G., Ohnenstetter, D., Schwardz, D. 2004. Les gisements de corindon: classification et genèse. Les placers à corindon gemme. Le Règne Minèrale, 55, 7-47.

Gerhard, E., Pat, E. 2006. Placer formation and placer minerals. Ore Geology Reviews, 28, 373 – 375.

Ghogomu, R.T., Moreau, C., Brown, W., Rocci, G. 1989. The Ntumbaw Complex, NW Cameroon: An atypical anorogenic ring-complex of intermediate composition: Journal of African Earth Sciences, 8, 1-9.

Girei, M.B., Solomon A.R., Magaji S.S. 2016. Nigerian Gem Quality Sapphire Occurrences: A Review.

Giuliani, G., Ohnenstetter, D., Garnier, V., Fallick, A.E., Rakotondrazafy, M., Schwarz, D. 2007. The Geology and Genesis of Gem Corundum Deposits. Mineralogical Association of Canada, Short Course 37, Yellowknife, Northwest Territories, p. 23–78.

Giuliani, G., Fallick, A., Ohnestetter, D., Pegere, G. 2009. Oxygen isotopes composition of sapphires from the French Massif Central: implications for the origin of gem corundum in basaltic fields. Mineralium Deposita, 44, 221–231.

Giuliani, G., Lasnier, B., Ohnenstetter, D., Fallick, A.E. and Pégère, G. 2010. Les gisements de corindon de France. Le Règne Minéral 93, 5–22.

Giuliani, G., Ohnenstetter, D., Fallick, A E., Groat, L., Fagan, A. J. 2014. The Geology and Genesis of Gem Corundum Deposits. Mineralogical Association of Canada Short Course 44, Tucson AZ, February 2014, p. 29-112.

Godwill, T. N. 2019. Productivity challenge of soils along the slopes of Mount Oku in Cameroon. Fluid Mechanics, 5, 1-7.

Graham, I.T., Khin Zaw., Cook, N.J. 2008. The genesis of gem deposits. Ore Geology Reviews, 34, 1-2.

Graham, I, Sutherland, L, Khin Zaw, Nechaev, V, Khanchuk, A. 2008. Advances in our understanding of the gem corundum deposits of the West Pacific continental margins intraplate basaltic fields. Ore Geology Reviews, 34, 200–215.

Green, T.H., Sie, S.H., Ryan, C.G., Cousens, D.R. 1989. Proton microprobe determined partitioning of Nb, Ta, Zr, Sr and Y between garnet, clinopyroxene and basaltic magma at high pressure and temperature. Chemical Geology, 74, 201–216.

Groat, L. A., Turner, D. J., Evans, R.J. 2014. Gem deposits. Treatise on Geochemistry 2nd Edition. **http://dx.doi.org/10.1016/B978-0-08-095975-7.01126-8**. University of British Columbia, Vancouver, BC, Canada.

Guo, J. F. 1993. Origin and distribution of corundum from basaltic terrains. Unpublished PhD. thesis, Macquarie University, Sydney, Australia, 326 pp. In Limtrakun, P. 2003. Origin and distribution of corundum from an intraplate alkali basaltic province in Thailand: evidence from field and inclusion studies. Ph.D thesis, University of Tasmania. p. 293.

Guo, J., O' Reilly, S. Y., Griffin, W. L. 1996a. Zircon inclusions in corundum megacrysts: I. Trace element geochemistry and clues to the origin of corundum megacrysts in alkali basalts. Geochimica et Cosmochimica Acta, 60, 2347-2363.

Guo, J., O' Reilly, S. Y., Griffin, W. L. 1996b. Corundum from basaltic terrains: a mineral inclusion approach to the enigma. Contributions to Mineralogy and Petrology, 122, 368–386.

Haimeur, J., Chabane, A., El Amrani, E.I. 2003. Analyse petro-mineralogique des interaction calco-alcalins de Zaer (Maroc Centre) : Modele petrogenetique. Bulletine de l'Institut Scientifique de Rabat 26, Section Science de la Terre, 27-48.

Halliday, A. N., Davidson, J. P., Holden, P., DeWolf, C. P., Lee, D.C., Fitton, J. G. 1990. Trace element fractionation in plumes and the origin of HIMU mantle beneath the Cameroon Line. Nature, 347, 523-528.

Hapuarachchi, D. J. A.C. 1998. Corundum in the Gem Gravels of Sri Lanka. Gondwana Research, Vl, Nos, 314, p. 415-416.

Harris, N.B.W, Pearce, J.A, Tindle, A.G. 1986. Geochemical characteristics of collision-zone magmatism. Journal Geological Society, London, Special Publication 19, 67-81.

Hauzenberger, C. A., Häger, T., Hofmeister, W., Quang, V.X., Fernando, R. G.W.A. 2003. Origin and formation of gem quality corundum from Vietnam. "Geo- and Material-Science on Gem-Minerals of Vietnam" Proceedings of the International Workshop, Hanoi, October 1 – 8 - 2003.

Heaman, L. M.. Bowins, R., Crocket, J. 1990. The chemical composition of igneous zircon suites: Implications for geochemical tracer studies. Geochimica Cosmochimica Acta, 54, 1597- 1607.

Hoang, N and Flower, M. 1998. Petrogenesis of Cenozoic basalts from Vietnam: implication for origins of a 'Diffuse igneous province'. Journal of Petrology, 39, 369–395.

Hoskin, P.W.O and Schaltegger, U. 2003. The Composition of Zircon and Igneous and Metamorphic Petrogenesis. Reviews in Mineralogy and Geochemistry, 53, 27 – 62.

Hughes, R. W. 1997. Ruby and sapphire. Introduction and Overview. Boulder, CO, RWH Publishing, p. 512.

Ibe, C. U and Obiora, S.C. 2019. Geochemical characterization of Granitoids in Katchuan Irruan area: further evidence for peraluminous and shoshonitic compositions and post-collisional setting of granitic rocks in the Precambrian Basement Complex of Nigeria. Acta Geochimica. doi.org/10.1007/s11631-019-00318-0.

Directive 2007/2/EC of the European Parliament and of the Council of 14 March 2007 establishing an Infrastructure for Spatial Information in the European Community (INSPIRE).

Irving A. J., Price R. C. 1981. Geochemistry and evolution of lherzolite-bearing phonolitic lavas from Nigeria, Australia, East Germany and New Zealand. Geochimica et Cosmochimica Acta, 45, 1309-1320.

Irving, A. J. 1986. Polybaric magma mixing in alkali basalts and kimberlites: evidence from corundum, zircon and ilmenite megacrysts. 4th International Kimberlite Conference, Perth, Geological Society of Australia Abstract Series. Blackwell Scientific, Oxford, 16, 262–264.

Izokh, A.E., Smirnov, S.Z., Egorova, V.V., Anh, T.T., Kovyazin, S.V., Phuong, N.T., Kalinina, V.V. 2010. The conditions of formation of sapphire and zircon in the areas of alkali-basaltoid volcanism in Central Vietnam. Russian Geology and Geophysics, 51, 719–733.

Jackson, S.E., Pearson, N.J., Griffin, W.L., Belousova, E.A. 2004. The application of laser ablation-inductively coupled plasma-mass spectrometry to in situ U–Pb zircon geochronology. Chemical Geology, 211, 47-69.

Jung, S. and Masberg, P. 1998. Major-and-trace element systematics and isotope geochemistry of Cenozoic mafic volcanic rocks from the Vogelsberg (Central Germany) - constraints on the origin of continental alkaline and tholeiitic basalts and their mantle sources. Journal of Volcanology and Geothermal Research 86, 151 - 177.

Kagou Dongmo, A., Wandji, P., Pouclet, A., Vicat, J.-P., Cheilletz, A., Nkouathio, D.G., Alexandrov, P., Tchoua, F. 2001. Evolution volcanologique du mont Manengouba (Ligne du Cameroun), nouvelles données pétrographiques, géochimiques et géochronologiques. C. R. Acad. Sci. Paris, Sér IIa 333, 155-162.

Kagou, D.A., Nkouathio, D., Pouclet, A., Bardintzeff, J.M., Wandji, P., Nono, A., Guillou, H., 2010. The discovery of late Quaternary basalt on Mount Bambouto: implications for recent widespread volcanic activity in the southern Cameroon Line. Journal of African Earth Sciences, 57, 96-108.

Kamdem, J. B., Kraml, M., Keller, J., Henjes-Kunst. F. 2002. Cameroon Line magmatism: conventional K/Ar and single-crystal laser $^{40}Ar/^{39}Ar$ ages of rocks and minerals from the Hossere Nigo anorogenic complex, Cameroon. Journal of African Earth Sciences, 35, 99-105.

Kamgang P, Njonfang E, Nono A, Gountie D, Tchoua M.F. 2010. Petrogenesis of a silicic magma system: Geochemical evidence from Bamenda Mountains, NW Cameroon, Cameroon Line. Journal of African Earth Sciences, 58, 285-304.

Kamgang, P., Chazot, G., Njonfang, E., Ngongang Tchuimegnie, N.B., Tchoua, F. 2013. Mantle sources and magma evolution beneath the Cameroon Line: Geochemistry of mafic rocks from the Bamenda Mountains (NW Cameroon). Gondwana Research 24, 727-741.

Kampunzu, A.B and Popoff, M. 1991. Distribution of the main Phanerooic rifts and associated magmatism. Introductory notes in Kampunzu, A.B and Lubala, R.T. (Eds). Magmatism in extensional structural setting. The Phanerooic African Plate, Berlin, New York, Heidelberg, p. 2-10.

Kanouo, N.S. 2008. Etude géologique des indices de minéralisation de saphir dans la partie Sud du bassin sédimentaire de Mamfe. Mémoire de D.E.A, en Science de la Terre. Univ de Yaoundé I, p. 91.

Kanouo, N.S., Khin Zaw, Yongue, F.R., Sutherland, F.L., Meffre, S., Njonfang, E., Ma, C. 2012a. Detrital mineral morphology and geochemistry: Methods to characterize and

constrain the origin of the Nsanaragati blue sapphires, South-western region of Cameroon. Journal of African Earth Sciences 70, 18–23.

Kanouo, S.N., Zaw Khin., Yongue, F.R., Sutherland, L.F., Meffre, S., Njonfang, E., Ma, C., Tchouatcha, S.T. 2012b. U–Pb zircon age constraining the source and provenance of gem-bearing late Cenozoic detrital deposit, Mamfe Basin, SW Cameroon. Journal of Resource Geology, 3, 316-324.

Kanouo, S.N., Yongue, F.R., Shouyu, C., Njonfang, E., Ma, C. 2012c. Greyishblack rutile megaclasts from the Nsanaragati Gem Placer, SWCameroon: Geochemical features and genesis. Journal of Geography and Geology 3, 134-146.

Kanouo, S.N. 2014. Geology of the Western Mamfe Corundum Deposits, SW Region Cameroon: Petrography, Geochemistry, Geochronology, Genesis, and Origin. Unpublished Ph.D Thesis. University of Yaoundé I, p. 225.

Kanouo, S.N., Yongue, F.R., Ekomane, E., Njonfang, E., Ma, C., Lentz, D.R., She, Z., Zaw, K., Venkatesh, S.A. 2015. U-Pb ages for zircon grains from Nsanaragati Alluvial Gem Placers: its correlation to the source rocks. Resource Geology 65, 103-121.

Kanouo S.N, Ekomane E, Yongue F.R, Njonfang E, Zaw K. 2016. Trace elements in corundum, chrysoberyl, and zircon: Application to mineral exploration and provenance study of the western Mamfe gem clastic deposits (SW Cameroon, Central Africa). Journal of African Earth Science, 113, 35-50.

Kao, S.J and Milliman, J.D. 2008. Water and sediment discharge from small mountainous rivers, Tawain: The role of lithology, episodic events and human activities. Journal of Geology, 116, 431 -448.

Khamloet, P., Pisutha-Arnond, V., Sutthirat, C. 2014. Mineral inclusions in sapphire from the basalt-related deposit in Bo Phloi, Kanchanaburi, western Thailand: indication of their genesis. Russian journal of Geology and Geophysics, 55, 1087–1102.

King, S. D and Ritsema, J. 2000. African hot spot volcanism: Small-scale convection in the upper mantle beneath cratons, Science, 290, 1137–1140.

Kirkland, C.L., Smithies, R.H., Taylor, R.J.M., Evans, N., McDonald, B. 2015. Zircon Th/U ratios in magmatic environs. Lithos, 212, 397–414.

Kolb, M., Paulik, H., Kirchenbaur, M., Münker, C. 2012. Petrogenesis of mafic to felsic lavas from the Oligocene Siebengebirge Volcanic Field (Germany): implications for the origin of intracontinental volcanism in Central Europe. Journal Petrology, 53, 2349–2379.

Konzett, J., Armstrong, R.A., Sweeny, R.J., Compston, W. 1998. The timing of Marid suite metasomatism in the Kaapvaal mantle: an ion probe study of zircons from Marid xenoliths. Earth Planetary Science Letters, 160, 133-145.

Kosler, J. 2001. Laser-ablation ICPMS study of metamorphic minerals and processes. In: Sylvester P. J. ed. Laser-ablation-ICPMS in the earth sciences; principles and applications Mineralogical Association of Canada Short Course Handbook, 29, 185-202.

Kosler, J and Sylvester, P.J. 2003. Present trends and the future of zircon in geochronology; laser ablation ICPMS. Review in Mineralogy Geochemistry, 53, 243-275.

Kouske, A.P., Suh, C.E., Ghogomu, R.T., Ngako, V. 2012. Na-Metasomatism and Uranium Mineralization during a Two-Stage Albitization at Kitongo, Northern Cameroon: Structural and Geochemical Evidence. International Journal of Geosciences, 3, 258-279.

Kündig, R., Bühler, C., Surbeck, H. 2012. Aluminium oxide (corundum, emery, sapphire /ruby). Applied Mineralogy and Non-Metallic Resources I.

Kwékam, M., Liégeois, J.-P., Njonfang, E., Affaton, P., Hartmann, G., and Tchoua, F. 2010. Nature, origin and significance of the Fomopéa Pan-African high-K calc-alkaline plutonic complex in the Central African fold belt (Cameroon): Journal of African Earth Sciences, 57, 79–95.

Laplaine, L and Soba, D. 1967. Rapport du service géologique pour les années 1965–1966–1967, prospection de saphirs dans le bassin crétacé de Mamfé. Archives BRGM/DMG/MINMEE.

Laplaine, L. 1969. Indices minéraux et ressources minérales du Cameroun et synthèse simplifiée des connaissances sur la géologie du Cameroun. Paris, p.139–141.

Lapworth, D.J., Knights, K.V., Key, R.M., Johnson, C.C., Ayoade, E., Adekanmid, M.A., Arisekola, T.M., Okunlola, O.A., Backman, B., Eklund, M., Everett, P.A., Lister, R.T., Ridgway, J., Watts, M.J., Kemp, S.J., Pitfield, P.J. 2012. Geochemical mapping using stream sediments in west-central Nigeria: Implications for environmental studies and mineral exploration in West Africa. Journal of Applied Geochemistry, 27, 1035–1052.

Le Maitre, R.W. (Editor), Streckeisen, A., Zanettin, B., Le Bas, M.J., Bonin, B., Bateman, P., Bellieni, G., Dudek, A., Efremova, S., Keller, J., Lameyre, J., Sabine, P.A., Schmid, R., Sørensen, H., Woolley A.R. 2002. Igneous rocks: A Classification and Glossary of Terms. Recommendations of the International Union of Geological Sciences Sub commission on the Systematics of Igneous Rocks. Cambridge University Press, p. 254.

Lee, D. C., Halliday, A. N., Fitton, J. G. & Poli, G. 1994. Isotopic variations with distance and time in the volcanic islands of the Cameroon line: evidence for a mantle plume origin. Earth and Planetary Science Letters, 123, 119-138.

Levinson, A.A and Cook, F.A. 1994. Gem corundum in alkali basalt: origin and occurrence. Gems and Gemology, 30, 253-62.

Li, X., Long, W.G., Li, Q.L., Liu, Y., Zheng, Y.F., Yang, Y.H., Chamberlain, K.R., Wan, D.F., Guo, C.H., Wang, X.C., Tao, H. 2010. Penglai Zircon Megacrysts: A Potential New Working Reference Material for Micro beam Determination of Hf-O Isotopes and U-Pb Age. Geostandards Geoanalytical Research, 34, 117-134.

Li, Y., Yang, Y., Liu, Y. C., Groppo, C., Franco Rolfo, F. 2020. MuscoviteDehydrationMelting in Silica-Undersaturated Systems: A Case Study fromCorundum-Bearing Anatectic Rocks in the Dabie Orogen. Minerals, 10, 213. doi:10.3390/min10030213.

Liégeois, J.P., Black, R., Navez, J., Latouche, L. 1994. Early and late Pan-African orogenies in the Aır assembly of terranes (Tuareg shield, Niger). Precambrian Research, 67, 59–88.

Liégeois, J.-P., Navez, J., Hertogen, J., and Black, R. 1998. Contrasting origin of post-collisional high-K calc-alkaline and shoshonitic versus alkaline and peralkaline granitoids. The use of sliding normalization: Lithos, 45, 1–28.

Limtrakun P, Zaw K, Ryan C.G, Mernagh T.P. 2001. Formation of the Denchai gem sapphires, northern Thailand: evidence from mineral chemistry and fuid/melt inclusion characteristics. Mineralogical Magazine, 65,725–735.

Limtrakun, P. 2003. Origin and distribution of corundum from an intraplate alkali basaltic province in Thailand: evidence from field and inclusion studies. Ph.D thesis, University of Tasmania. p. 293.

Liu, L., Qiu, J.S., Zhao, J.L., and Yang, Z.L. 2014. Geochronological, geochemical, and Sr–Nd–Hf isotopic characteristics of Cretaceous monzonitic plutons in western Zhejiang Province, Southeast China: New insights into the petrogenesis of intermediate rocks: Lithos, 196, 242–260.

Mange, M.A., Maurer, H.F.W. 1992. Heavy Minerals in Colour. Chapman and Hall, London. p. 147.

Maniar, P.D and Piccoli, P.M. 1989. Tectonic discrimination of granitoids. Geological Society of America Bulletin, 101, 635-643.

Martin, D and Segalen, P. 1966. Notice explicative de la Carte pédologique du Cameroun oriental au 1/1,000.000. ORSTOM, Centre de Yaoundé, p. 80-93.

Marzoli, A., Renne, P.R., Peccirillo, E.M., Castorina, F., Bellieni, G., Melfi, A.G., Nyobe, J.B., N'ni, J. 1999. Silicic magmas from the continental Cameroon Line (Oku, Bambouto

and Ngaoundere): 40Ar-39Ar dates, petrology, Sr-Nd-O isotopes and their petrogenetic significance. Contributions to Mineralogy and Petrology, 135, 133-150.

Marzoli, A., Peccirillo, E.M., Renne, P.R., Bellieni, G., Iacumin, M., Nyobe, J.B., Tongwa, A.T. 2000. The Cameroon Line revisited: petrogenesis of continental basaltic magmas from lithospheric and asthenospheric mantle sources. Journal of Petrology, 41, 87-109.

Mbih P.K, Meffre, S, Yongue, F.R, Kanouo, S.N, Thomson, J. 2016. Chemistry and origin of the Mayo Kila sapphires, NW region Cameroon (Central Africa): Their possible relationship with the Cameroon Line. Journal of African Earth Science 118, 263-273.

McDonough, W. F. and Sun, S. S. 1995. The composition of the Earth. Chemical Geology, 120, 223-253.

McGee, B.M. 2005. Characteristics and origin of the Weldborough sapphire, NE Tasmania. (Unpublished BSc thesis): University of Tasmania, School of Earth Science, Hobart, Australia.

Medard, E., Paquette, J.L., Devouard, B., Ricci., J., Boivin, P., Gaillou, E. Rochault, J., Hardiagon, M. 2012. Gem sapphires and zircons from Cenozoic volcanism of the French Massif Central. Conference paper, First volcandark meeting. Olot, Spaine. January 2012.

Meffre, S., Large, R.R., Scott, R., Woodhead, J., Chang, Z., Gilbert, S.E., Danyushevsky, L. V., Maslennikov, V., and Hergt, J.M. 2008. Age and pyrite Pb-isotopic composition of the giant Sukhoi Log sediment-hosted gold deposit, Russia. Geochimica et Cosmochimica Acta, 72, 2377-2391.

Mercier, A., Debat, P., Saul M.J. 1999. Exotic origin of the ruby deposits of the Mangari area in SE Kenya. Ore Geology Reviews, 14, 83–104.

Mercier, A., Debat, P., Saul, J.M. 2007. Exotic origin of the ruby deposits of the Mangari area in SE Kenya. Ore Geology Reviews, 14, 83–104.

Michon, L and Merle, O. 2001. The formation of the West European rift: a new model as exemplified by the Massif Central area. Bulletin de la Société Géologique de France, 172, 213 - 221.

Merle, R., Marzoli, A., Aka, F.T., Chiaradia, J. M., Reisberg, L., Castorina, F., Jourdan, F., Renne, P. R., N'ni, J., Nyobe, J. B. 2017. Mt Bambouto Volcano, Cameroon Line: Mantle Source and Differentiation of Within-plate Alkaline Rocks. Journal of Petrology, 58, 933-962.

Meyer, H.O.A and Mitchelle, R.H. 1988. Sapphire-bearing ultramafic lamprophyres from Yogo, Montana: A Ouachitite. The Canadian Mineralogist, 26, 81-88.

Meyers, J.B., Rosendahl, B.R., Harrison, C.G.A., Ding, Z.D. 1998. Deep-imaging seismic and gravity results from the offshore Cameroon Line, and speculation of African hotlines. Tectonophysics, 284, 31-63.

Middlemost, E.A.K. 1975. The Basalt Clan. Earth Science Reviews, 11, 337-364.

Milelli, L., Fourel, L., Jaupart, C. 2012. A lithospheric instability origin for the Cameroon Line. Earth and Planetary Sciences Letters, 335-336, 80-87.

Moreau, C., Regnoult, J. M., Deruelle, B. & Robineau, B. 1987. A new tectonic model for the Cameroon line, Central Africa. Tectonophysics, 139, 317-334.

Morton, A.C. 1985. Heavy-minerals in provenance studies. In: Zuffa, G.G. (Ed.), Provenance of Arenites. NATO Advanced Study Institute Series C, 148, 249–277.

Ndip, E.Y, Agyingyi, C.M, Nton, M.E. 2018. Review of the geology of mamfe sedimentary basin, SW Cameroon, Central Africa. Journal of Oil Gas Petrochemical Science, 1, 35-40. DOI: 10.30881/jogps.00008.

Nédélec, A., Bouchez, J.L. 2015. Granites: Petrology, Structure, Geological Setting and Metallogeny. Oxford University Press, p. 335.

Nédélec, A., Nsifa, E.N., Martin, H. 1990. Major and trace element geochemistry of the Archaean Ntem plutonic complex (South Cameroon): petrogenesis and crustal evolution. Precambrian Research, 47, 35–50.

Neh Fru, E.M. 2014. Exploration of sapphire indices in Mayo Kila Donga Mantung Division NW Region Cameroon. Master II Thesis, University of Yaoundé I, Cameroon, p. 74.

New South Wales Department of Primary Industries 2003. Sapphire and ruby.

Ngako, V., Jégouzo, P., Nzenti, J.P. 1991. Le Cisaillement Centre Camerounais. Rôle structural et géodynamique dans l'orogenèse panafricaine. Comptes Rendus de l'Académie des Sciences, Paris 313, 457–463.

Ngako, V., Affaton, P., Nnange, J.M., Njanko, Th. 2003. Pan-African tectonic evolution in central and Southern Cameroon: transpression and transtension during sinistral shear movements, Journal of African Earth Sciences, 36, 207-214.

Ngako, V., Njonfang, E., Aka, F. T., Affaton, P., Joseph Metuk Nnange, J.M. 2006. The North–South Paleozoic to Quaternary trend of alkaline magmatism from Niger–Nigeria to Cameroon: Complex interaction between hotspots and Precambrian faults. Journal of African Earth Sciences 45, 241–256.

Ngako, V., Affaton, P., Njonfang, E. 2008. Pan-African tectonics in northwestern Cameroon: implications for the history of western Gondwana. International Association of Gondwana Research, 14, 509-522.

Ngounouno, I., Moreau, C., Deruelle, B., Demaiffe, D., Montigny, R. 2001. Petrology of the alkaline undersaturated complex of Kokoumi (Cameroon). Bulletin de la Société Géologique de France, 172, 675-686.

Njanko, T., Nédélec, A. & Affaton, P. 2006. Synkinematic high-K calc-alkaline plutons associated with the Pan-African Central Cameroon Shear Zone (W-Tibati area): petrology and geodynamic significance, Journal of African Earth Sciences, 44, 494-310.

Njel, U. O. 1986. "Paléogéographie d'un Segment de l'Orogenèse Panafricaine, la Ceinture Volcano-Sédimentaire de Poli (Nord Cameroun)," Compte Rendu de l'Académie des Sciences, 30, 1737-1742.

Njilah, K., Temdjim, R., Nzolang, C., Tchuitchou, R., Ajonina, H. 2007. Geochemistry of Tertiary-Quartenary lavas of Mt. Oku, Northwest Cameroon, 040. Revisita facultad de ingeenieria Univeridad de Antioquia, Junio. p. 59 - 75.

Njilah, I. K., Moundi A., Temdjim R., Ntieche B. 2013. Sr-Nd-Pb isotopic studies of lavas of Mt. Oku volcano, North West Cameroon: A case involving HIMU, depleted and enriched mantle sources. Journal of Geology and Mining Research, 5, 124 - 135.

Njonfang, E and Moreau, C. 1996. The mineralogy and geochemistry of a subvolcanic alkaline complex from the Cameroon Line: the Nda Ali Massif, Southwest Cameroon. Journal of African Sciences, 22, 113-132.

Njonfang, E and Moreau, C. 2000. The mafic mineralogy of the Pandé massif, Tikar plain, Cameroon: Implications for a peralkaline affinity and emplacement from highly evolved alkaline magma. Mineralogical Magazine, 64, 525–537.

Njonfang, E., Nono, A., Kamgang, P., Ngako, V., and Tchoua, F.M. 2011. Cameroon Line alkaline magmatism (central Africa): A reappraisal, *in* Beccaluva, L., Bianchini, G., and Wilson, M., eds., Volcanism and Evolution of the African Lithosphere: Geological Society of America Special Paper, 478, 173–191.

Njonfang, E., Tchuenté Tchoneng, G., Cozzupoli, D., Lucci, F. 2013. Petrogenesis of the Sabongari alkaline complex, Cameroon line (central Africa): Preliminary petrological and geochemical constraints. Journal of African Earth Sciences, 83, 25–54.

Nkouathio, D.G., Kagou Dongmo, A., Bardintzeff, J.-M., Wandji, P., Bellon, H., Pouclet, A. 2008. Evolution of volcanism in graben and horst structures along the Cenozoic Cameroon Line (Africa): implications for tectonic evolution and mantle source composition. Mineralogy and Petrology, 94, 287-303.

Nkoumbou, C., Njopwouo, D., Villieras, F., Njoya, A., Yonta Ngoune, C., Ngo Njock, L., Tchoua, F.M., Yvon, J. 2006. Talc indices from Boumnyebel (Central Cameroon), physico-chemical characteristics and geochemistry. Journal of African Earth Sciences, 45, 61–73.

Nono, A., Njonfang, E., Kagou Dongmo, A., Nkouathio, D.G., and Tchoua, F.M. 2004. Pyroclastic deposits of the Bambouto volcano (Cameroon Line, Central Africa): Evidence of a Strombolian initial phase: Journal of African Earth Sciences, 39, 409–414.

Nzenti, J. P., Barbey, P., Jegouzo, P, Moreau, C. 1984. Un nouvel exemple de ceinture granulitique dans une chaîne protérozoïque de collision : les migmatites de Yaoundé au Cameroun. Compte Rendu. Académie des Sciences Paris 299, 1197-1199.

Nzenti J. P., Barbey P., Macaudiere J., and Soba D. 1988. Origin and evolution of the late precambrian high-grade Yaounde gneisses (Cameroon). Precambrian Research, 38, 91-109.

Nzenti, J.P. 1998. Neoproterozoic alkaline meta-igneous rocks from the Pan-African North Equatorial Fold belt (Yaoundé, Cameroon): biotites and magnetite-rich pyroxenites, Jouran of African Earth Sciences, 26, 37-47.

Olivry, J.C. 1986. Fleuves et rivières du Cameroun. MESRES-ORSTOM, ISBN2-7099-0804-2. 733p.

Pakhomova, V.A., Zalishchak, B.L., Odarichenko, E.G., Lapinab, M.I., Karmanov, N.S. 2006. Study of melt inclusions in the Nezametnoye corundum deposit, Primorsky region of the Russian Far East: Petrogenetic consequences. Journal of Geochemical Exploration, 89, 302–305.

Patiño Douce A.E. 1999. What do experiments tell us about relative contributions of crust and mantle to the origin of granitic magma? In: Castro A., Fernandez C., Vigneress J.L. (Eds.), Understanding Granites: Integrating New and Classification Techniques. Geological Society, London, Special Publications, 168, 55-75.

Paton, C., Woodhead, J.D., Hellstrom, J. C., Hergt, J.M., Greig, A., Maas, R. 2010. Improved laser ablation U-Pb zircon geochronology through robust down-hole fractionation correction. Geochemistry, Geophysics, Geosystems, 11, 1525-2027.

Pearce, J.A., Harris, N.B.W., and Tindle, A.G. 1984. Trace element discrimination diagrams for the tectonic interpretation of granitic rocks: Journal of Petrology 25, 956–983.

Pearce, J.A. 1996. Sources and settings of granitic rocks: Episodes19, 120–125.

Peccerillo, A and Taylor, S. 1976. Rare earth elements in East Carpathian volcanic rocks. Earth and Planetary Science Letters, 32, 121 - 126.

Pêcher, A., Giuliani, G., Garnier, V., Maluski, H., Kausar, A.B., Malikf, R.H., Muntazf, H.R. 2002. Geology, geochemistry and Ar–Ar geochronology of the Nangimali ruby deposit, Nanga Parbat Himalaya (Azad Kashmir, Pakistan). Journal of Asian Earth Sciences, 21, 265–282.

Penaye, J., Toteu, S.F., Michard, A., Bertrand, J.M., Dautel, D. 1989. Reliques granulitiques d'âge Protérozoïque inférieur dans la zone mobile panafricaine d'Afrique

Centrale au Cameroun; géochronologie U–Pb sur zircons. Compte Rendu. Académie des Sciences. Paris 309, 315-318.

Penaye J., Toteu S. F., Tchameni R., Van Schmus W. R., Tchakounte J., Ganwa A., Minyem D., and Nsifa E. N. 2004. The 2.1 Ga West Central African Belt in Cameroon: extension and evolution. Journal of African Earth Sciences, 39, 159-164.

Penaye, J., Kroner., A., Toteu, S.F., Van Schmus., W. R., Doumnang J.C. 2006. Evolution of the Mayo Kebbi region as revealed by zircon dating: An early (ca.740 Ma) Pan-African magmatic arc in southwestern Chad. Journal of African Earth Sciences, 44, 530-542.

Penaye, J., Toteu, S.F., Van Schmus, W.R., Nzenti, J.P. 1993. U–Pb and Sm–Nd preliminary geochronologic data on the Yaoundé series, Cameroon: reinterpretation of the granulitic rocks as the suture of a collision in the "Centrafrican belt". Compte Rendu. Académie des Sciences Paris, 317, 789-794.

Peronne. 1969. Notice explicative sur la feuille Wum-Banyo. Direction des Mines et de la Géologie du Cameroun, 49p.

Peucat, J.J., Ruffaut, P., Fritsch, E., Bouhnik-Le, E., Simonet, C., Lasnier, B. 2007. Ga/Mg ratio as a new geochemical tool to differentiate magmatic from metamorphic blue sapphire. Lithos, 98, 261–271.

Pham Van, L., Hoáng Quang, V., Garnier, V., Giuliani, G., Ohnenstetter, D., Lhomme, T., Schwarz, D., Fallick, A.E., Dubessy, J., Phan Trong, T., 2004. Gem corundum deposits in Vietnam. Journal of Gemmology, 29, 129–147.

Pouclet, A., Dongmo, A. K., Bardintzeff, J. M., Wandji, P., Tagheu, P. C., Nkouathio, D., Bellon, H., Ruffet, G. 2014. The Mount Manengouba, a complex volcano of the Cameroon line: volcanic history, petrological and geochemical features. Journal of African Earth Sciences, 97, 297-321.

Rakotondrazafy, A. F. M, Giuliani, G, Ohnenstetter, D, Fallick, A.E, Rakotosamizanany, S, Andriamamonjy, A, Ralantoarison, T, Razanatsehenoa, M, Offant, Y, Garnier, V, Maluski, H, Dunaigre, C, Schwarz, D, Ratrimo, V. 2008. Gem corundum deposits of Madagascar: A review. Ore Geology Reviews, 34, 134–154.

Ranasinghe, P.N, Dissanayake, C.B, Rupasinghe M.S. 2005. Application of geochemical ratios for delineating gem-bearing areas in high grade metamorphic terrains. Applied Geochemistry, 20, 1489–1495.

Rankenburg, K., Lassiter, J. C. & Brey, G. 2004. Origin of megacrysts in volcanic rocks of the Cameroon volcanic chain-constraints on magma genesis and crustal contamination. Contributions to Mineralogy and Petrology, 147, 129–144.

Rankenburg, K., Lassister, J.C., Brey, G. 2005. The role of continental crust and lithospheric mantle in the genesis of Cameroon Line lavas: constraints from isotopic variations in lavas and megacrysts from the Biu and Jos Plateau. Journal of Petrology, 46, 169–190.

Reusch, A. M., Nyblade, A. A., Wiens, D. A., Shore, P. J., Ateba, B., Tabod, C. T. & Nnange, J. M. 2010. Upper mantle structure beneath Cameroon from body wave tomography and the origin of the Cameroon Line. Geochemistry, Geophysics, Geosystems, 11, Q10W07. doi:10.1029/2010GC003200.

Rohan Fernando, G.W.A. 2001. Genesis of Metasomatic Sapphirine-Corundum-Spinel-bearing Granulites in Sri Lanka. An Integrated Field, Petrological and Geochemical Study. Ph.D thesis, University of Mainz, Germany, p. 184.

Sack, P.J., Berry, R.F., Meffre, S., Falloon, T.J., Gemmell, J.B., Friedman, R.M. 2011. In situ location and U-Pb dating of small zircon grains in igneous rocks using laser ablation-inductively coupled plasma-quadrupole mass spectrometry. Geochemistry, Geophysics, Geosystems, 12. Q0AA14, doi:10.1029/2010GC003405.

Schandl, E. S and Gorton, M. P. 2002. Applications of high field strength elements to discriminate tectonic setting in VMS environments. Economic geology, 97, 629-642.

Shor, R and Weldon, R. 2009. Ruby and sapphire production and distribution: a quarter century of change. Gems and Gemology, 45, 236–259.

Simonet, v., Paquette, J.L., Pin, C., Lasnier, B., Fritsch, E. 2004. The Dusi (Garba Tula) sapphire deposit, Central Kenya - a unique Pan-African corundum-bearing monzonite. Journal of African Earth Sciences, 38, 401–410.

Sighomnou, D., 2004. Analyse et redefinition des regimes climatiques et hydrologiques du cameroun : perspectives d'evaluation des resources en eau. These de Doctorat d'Etat ès Sciences, Université de Yaounde I, Cameroun, 290p.

Simonet, C. Fritsch, E. Lasnier, B. 2008. A classification of gem corundum deposits aimed towards gem exploration. Ore Geology Reviews, 34, 127–133.

Slama, J., Kosler, J., Condon, D.J., Crowley, J.L., Gerdes, A., Hanchar, J.M., Horstwood, M.S.A., Morris, G.A., Nasdala, L., Norberg, N., Schaltegger, U., Schoene, B., Tubrett, M.N., Whitehouse, M.J. 2008. Plesovice zircon - A new natural reference material for U-Pb and Hf isotopic micro analysis. Chemical Geology, 249, 1-35.

Suh, C.E., Sparks, R.S.J., Fitton, J.G., Ayonghe, S.N., Annen, C., Nana, R., Luckman, A. 2003. The 1999 and 2000 eruptions of Mount Cameroon: eruption behaviour and petrochemistry of lava. Bulletin of Volcanology, 65, 267–281.

Suh, C.E., Luhr, J.F., Njome, M.S. 2008. Olivine-hosted glass inclusions from Scoriae erupted in 1954–2000 at Mount Cameroon volcano, West Africa. Journal of Volcanology Geothermal Research, 169, 1–33.

Sun, G., Liu, S., Gao, L., Hu, Y., Guo, R., Fu, J., Wang, M., Ma, C., Hu, F. 2019. Neoarchean sanukitoids and associated rocks from the Tengzhou-Pingyi intrusive complex, North China Craton: insights into petrogenesis and crust–mantle interactions. Gondwana Research, 68, 50–68.

Sun, S.S. and McDonough, W.F. 1989. Chemical and isotopic systematics of oceanic basalts: implications for mantle composition and processes. Journal of Geological Society, London, Special Publications, 42, 313–345.

Sutherland, F.L., Hoskin, O.W.P., Fanning, M.C. and Coenraads, R.R. 1998. Models of corundum origin from alkali basaltic terrains: a reappraisal. Contributions to Mineralogy and Petrology, 133, 356-372.

Sutherland, F.L., Bosshart, G., Fanning, C.M., Hoskin, P.W.O., Coenraad, R.R. 2002. Sapphire crystallization, age and origin, Ban Huai Sai, Loais: age based on zircon inclusion. Journal of African Earth Sciences, 20, 841-849.

Sutherland, F.L., and Abduriyim, A. 2009. Geographic typing of gem corundum: a test case from Australia. The Journal of Gemmology, 31, 5–8.

Sutherland, F.L., Zaw, K., Meffre, S., Giuliani, G, Fallick, A.E., Graham, I.T., Webb, G.B. 2009. Gem corundum megacrysts from East Australia basalt fields: Trace elements, O isotopes and origins. Australian Journal of Earth Sciences, 56, 1003–1020.

Sutherland. L.F and Meffre, S. 2009. Zircon megacryst ages and chemistry, from a placer, Dunedin volcanic area, eastern Otago, New Zealand. New Zealand Journal of Geology and Geophysics, 52, 185-194.

Sutherland, F. L., Zaw, K., Meffre, S., Yui, T-F., Thu, K. 2015a. Advances in Trace Element "Fingerprinting" of Gem Corundum, Ruby and Sapphire, Mogok Area, Myanmar. Minerals, 5, 61-79.

Sutherland, F. L., Coenraads, R.R., Abduryim, A., Meffre, S., Hoskin, O.W.P., Giuliani, G., Beattie, R., Wuhrer., R., Sutherland, B.G. 2015b. Corundum (sapphire) and zircon relationships, Lava Plains gem fields, NE Australia: Integrated mineralogy, geochemistry, age determination, genesis and geographical typing. Mineralogical Magazine, 79, 545–581.

Tchameni R., Pouclet A., Penaye J., Ganwa A. A., and Toteu S. F. 2006. Petrography and geochemistry of the Ngaoundere Pan-African granitoids in Central North Cameroon: Implications for their sources and geological setting. Journal of African Earth Sciences, 44, 511-529.

Tchameni, R., Sun, F., Dawaï, D., Danra, G., Tékoum, L., Negue, N.E., Vanderhaeghe, O., Nzolang, C., Dagwaï, N. 2016. Zircon dating and mineralogy of the Mokong Pan-African magmatic epidote-bearing granite (North Cameroon). International Journal Earth Sciences,105, 1811-183.

Tchuimegnie Ngongang, N. B., Kamgang, P., Chazot, G., Agranier, A., Bellon, H., Nonnotte, P. 2015. Age, geochemical characteristics and petrogenesis of Cenozoic intraplate alkaline volcanic rocks in the Bafang region, West Cameroon. Journal of African Earth Science, 102, 218–232.

Tchunte, P.M.F., Tchameni, R., André-Mayer, A.S., Dakoure, H.S., Turlin, F., Marc Poujol, M., Nomo, E.N., Fouotsa, A.N.S., Rouer, O. 2018. Evidence for Nb-Ta Occurrences in the Syn-Tectonic Pan-African Mayo Salah Leucogranite (Northern Cameroon): Constraints from Nb-Ta Oxide Mineralogy, Geochemistry and U-Pb LA-ICP-MS Geochronology on Columbite and Monazite. Minerals, 8, 188. doi:10.3390/min8050188.

Tedonkenfack, S.S.T., Tamena, J., Nkouathioa, D.G., Asaah A N.E., Gountié-Dedzoedzoc, M., Akad, F.T. 2019. Petrography and geochemistry of mantle xenoliths from Ibal-Oku region (North-West region, Cameroon): Preliminary evidence of mantle heterogeneities. Journal of African Earth Sciences, 154, 70–79.

Tetsopgang, S., Suzuki, K., Adachi, M. 1999. Preliminary CHIME dating of granites from the Nkambe area, northwestern Cameroon, Africa. Journal of Earth Planetary Sciences, Nagoya University, 46, 57–70.

Tetsopgang, S., Enami, M., Njonfang, E. 2006. Petrology of highly evolved Pan-African two-mica granitesfrom the Nkambe area, West Cameroon. Journal of African Earth Sciences 46, 305–317.

Tetsopgang, S., Suzuki, K., Njonfang, E. 2008. Petrology and CHIME geochronology of Pan-African high K and Sr/Y granitoids in the Nkambe area, Cameroon. Gondwana Research, 14, 686–699.

Tetsopgang, S., Enami, M., Njonfang, E. 2011. Emplacement P-T conditions of Pan-African biotite-amphibole granitoids in the Nkambe area. Cameroon. Journal of mineralogical and petrological Sciences, 106, 306-319.

Toteu, S.F., Van Schmus, W.R., Penaye, J., Michard, A. 2001. New U–Pb and Sm–Nd datafrom north-central Cameroon and its bearing on the pre-Pan African history of central Africa. Precambrian Research, 108, 45–73.

Toteu, S.F., Penaye, J., Poudjom Djomani, Y. 2004. Geodynamic evolution of the Pan-African belt in central Africa with special reference to Cameroon. Canadian Journal of Earth Science, 41, 73-85.

Toteu S. F., Fouateu R. Y., Penaye J., Tchakounte J., Mouangue A. C. S., Van Schmus W. R., Deloule E., and Stendal H. 2006. U-Pb dating of plutonic rocks involved in the nappe tectonic in southern Cameroon: consequence for the Pan-African orogenic evolution of the central African fold belt. Journal of African Earth Sciences, 44, 479-493.

Tsafack, J.P.F., Wandji, P., Bardintzeff, J.M., Bellon, H., Hervé Guillou, H. 2009. The Mount Cameroon stratovolcano (Cameroon Line, Central Africa): Petrology, geochemistry, isotope and age data. Geochemistry, Mineralogy and Petrology, 47, 65-78.

Uher, P., Giuliani, G., Szakáll, S., Fallick, A., Strunga, V., Vaculovič, T., Ozdín, D., Gregáňová, M. 2012. Sapphires related to alkali basalts from the Cerová Highlands, Western Carpathians (southern Slovakia): composition and origin. Geologica Carpathica, 63, 1, 71—82.

Upton, B.G.J., Hinton, R.W., Aspen, P., Finch, A., Valley, J.W. 1999. Megacrysts and associated xenoliths: evidence for migration of geochemically enriched melts in the upper mantle beneath Scotland. Journal of Petrology, 40, 935-956.

Van Schmus W. R., Oliveira E. P., da Silva Filho A. F., Toteu S. F., Penaye J., and Guimaraes I. P. 2008. Proterozoic links between the Borborema Province, NE Brazil, and the Central African Fold Belt. Geological Society, London, Special Publications, 294, 69-99.

Voudouris, P., Mavrogonatos, C., Graham, I., Giuliani, G., Melfos, V., Karampelas, S., Karantoni, V., Wang, K., Tarantola, A., Zaw, K., Meffre, S., Klemme, S., Berndt, J., Heidrich, S., Zaccarini, F., Fallick, A., Tsortanidis, M., Lampridis, A. 2019. Gem Corundum Deposits of Greece: Geology, Mineralogy and Genesis. Minerals, 9, 49. doi:10.3390/min9010049.

Walton, L. 2004. Exploration criteria for coloured gemstone deposits in the Yukon. Energy, Mines and resources. Yukon Geological Survey. Open file 2004–10.

Wan, H., M., W., M., Siti, A., B., N., Mojtaba, P. 2015. Statistical Characterisation of Grain-Size Distribution in Fluvial Sediment of Kelantan Rivers. Jurnal Teknologi (Sciences and Engineering) 74, 3, 103–109.

Wang, K., Plank, T., Walker, J.D., Smith, E.I. 2002. A mantle melting profile across the Basin and Range, SW USA. Journal of Geophysical Research, 107. doi.org/10.1029/2001JB000209.

Wentworth, C.K. 1922. A scale of grade and class terms for clastic sediments. *Journal of Geology* **30**: 377–392, In Blott, S. J. and Pye, K., 2001. GRADISTAT: A Grain Size Distribution and Statistics package for the analysis of unconsolidated Sediments. Earth surface processes and landforms, 26, 1237 - 1248.

Wiedenbeck, M., Alle, P., Corfu, F., Griffin W.L., Meier, M., Oberli, F., Vonquadt A., Roddick, J.C., Speigel W. 1995. Three Natural Zircon Standards for U-Th-Pb, Lu-Hf, Trace-Element and REE Analyses. Geostandards Newsletter, 19, 1-23.

Whalen, J.B., Currie, K.L., Chappell, B.W. 1987. A-type granites: geochemical characteristics, discrimination and petrogenesis. Contributions to Mineralogy and Petrology, 95, 407–419.

Woodland, A. B and Jugo, P. J. 2007. A complex magmatic system beneath the Devès volcanic field, Massif Central, France: evidence from clinopyroxene megacrysts. Contributions in Mineralogy and Petrology, 153, 719–731.

Wotchoko, P., Nkouathio, D., Kouankap, N., Chenyi, M., Guedjeo, C., Bulam, A., Tchokona, S., Seplong, Y. 2017. Petrogenesis of lava from wainama west, Mount Oku (CL): source characterization and magma evolution. Journal of Geosciences and Geomatics, 4, 91–101.

Yager, T. R., Menzie, W. D., Olson, D W. 2008. Weight of Production of Emeralds, Rubies, Sapphires, and Tanzanite from 1995 through 2005. Open-File Report 2008–1013. U.S. Department of the Interior U.S. Geological Survey. p. 12.

Yakymchuk, C and Szilas, K. 2018. Corundum formation by metasomatic reactions in Archeanmetapelite, SW Greenland: Exploration vectors for ruby deposits within high-grade greenstone belts. Geoscience Frontiers, 9,727-749.

Yamgouot, F.N., Déruelle, B., Mbowou, I.B.G., Ngounouno, I., Demaiffe, D. 2016. Geochemistry of the volcanic rocks from Bioko Island “Cameroon Hot Line”: Evidence for plume-lithosphere interaction. Geoscience Frontiers, 7, 743-757.

Yui, T.F., Wu, C.M., Limtrakum, P., Sricharn, W., Boonsoong, A. 2006. Oxygen isotope studies on placer sapphire and ruby in the Chantaburi-Trat alkali basaltic gem field, Thailand. Lithos, 86, 197–211.

Zaw, K., Sutherland F. L., Della Pasqua, F., Ryan, C. G., Yui, T. Z., Mernagh, T. P., Duncan, D. 2006. Contrasts in gem corundum characteristics eastern Australian basalt fields: trace elements, fluid/melt inclusions and oxygen isotopes. Mineralogical Magazine, 70, 669–687.

Zaw, K., Sutherland, F.L., Yui, Tzen-Fu, Meffre, S., Thu, K. 2014. Vanadium-rich ruby and sapphire within Mogok Gemfield, Myanmar: implications for gem colour and genesis. Mineralium Deposita, 50, 200-215.

ANNEX